ANALYSIS OF THE NONLINEAR BEHAVIOR OF CANTILEVER SHEETPILE RETAINING WALLS IN SATURATED CLAY

By

MICHEL I. NAJJAR

Bachelor of Science in Civil Engineering
Oklahoma State University
Stillwater, Oklahoma
1979

Master of Science
Oklahoma State University
Stillwater, Oklahoma
1980

Submitted to the Faculty of the
Graduate College of the
Oklahoma State University
in partial fulfillment of
the requirements for
the Degree of
DOCTOR OF PHILOSOPHY
May, 1989

ANALYSIS OF THE NONLINEAR BEHAVIOR OF

CANTILEVER SHEETPILE RETAINING

WALLS IN SATURATED CLAY

Thesis Approved:

Thesis Adviser

Dean of the Graduate College

ACKNOWLEDGEMENTS

I would like to express my thanks and appreciation to my advisor, Dr. William P. Dawkins, for his encouragement, guidance and support during the course of this study. I would also like to thank the other members of my supervising committee. Furthermore, I would like to offer special thanks to Dr. Mete Oner for his help and useful suggestions.

I cannot offer enough thanks to my entire family for their unwavering patience and unlimited support. That is a debt to them that I will always owe.

Special thanks are due to two dear friends: Dr. Issam Hallal who was incredibly helpful in all phases of this work, both on the personal level as an encouraging and motivating friend, and on the technical level as well; and thanks to his brother Mr. Afif Hallal, manager of the CAD lab, for opening an account for me on the Harris 800 computer and for giving me very useful technical advice in the computer area in general.

TABLE OF CONTENTS

Chapter Page

LIST OF TABLES

LIST OF FIGURES

Figure Page

CHAPTER I

INTRODUCTION

The design of a sheetpile retaining wall is usually based on the assumption that the soil pressures exerted on the piling are at the limiting states of active or passive equilibrium at every point on the wall. The limiting soil pressure state is then coupled with an assumed displacement configuration to establish the required depth of penetration of the piling. Subsequently, the displacements of the wall are estimated from other assumed displacement conditions. The classical design procedure does not address the compatibility of the wall displacements with soil pressures.

Because the classical design is based on a typical unit strip of the wall-soil system, the strip of wall is sometimes analyzed as a beam-on-foundation where the soil on either side of the wall is replaced by springs. This latter approach (subsequently referred to as the soil-structure interaction (SSI) method) enforces compatibility of wall displacements and soil pressures and does not require any prior assumptions regarding displacement configurations or wall support conditions. While the SSI method is attractive, there is only limited information regarding the characteristics of springs which are used to represent the soil.

The most complete analytical model of the wall soil system would be obtained by the use of nonlinear finite elements to represent the soil.

This procedure, subsequently referred to as FEM, has been applied successfully to the analysis of a variety of earth retaining systems. However, the finite element analysis is much too cumbersome for use in an iterative design environment.

Because so many simplifying assumptions are inherent in the classical design theory and the SSI method, the current study was needed as a starting point to clarify the behavior.

Statement of Purpose

The purpose of this study is to use the finite element method to study the behavior of cantilever sheetpile walls embedded in soft, saturated clay ($\phi = 0$), and to use the results to investigate the soil spring characteristics which are used with the SSI method.

Furthermore, the values of the soil modulus, Es, given by Terzaghi (Ref. 39) were not supported by any experimental or theoretical corroboration. Hence, this study will attempt to investigate their validity and to elucidate the overall behavior.

Scope

In this study, three types of analyses for cantilever sheetpile retaining walls in saturated clay were carried out: (1) analysis based on the classical design method; (2) SSI analysis using the programs "CSHTSSI" and "CBEAMC" (Refs. 11, 12); and, (3) finite element analysis using the program "SIMULATE" (Refs. 20, 21). The results from the three methods were compared. The finite element solutions were used to point out the pros and cons of the classical and SSI procedures.

CHAPTER II

LITERATURE SURVEY

The solution of soil-structure interaction problems started in 1776, with the work of Coulomb (Ref. 9) whose theory provided a means of evaluating earth pressures for soils against retaining walls. Coulomb's theory assumes that the structure can displace by an amount sufficient to mobilize full-active and full-passive pressures; thus, the theory is basically useful to calculate maximum pressures on rigid retaining structures. However, this theory is convenient only for evaluating extreme failure cases but provides no valid information about the behavior at intermediate working stress levels.

Winkler (Ref. 43) developed a soil model based on direct proportionality between soil pressure and structural deflection at any particular point along the structure. This assumption obviously does not treat the soil medium as a continuum and hence has some limitations.

Biot (Ref. 1) extended Winkler's hypothesis to the analysis of infinite beams on two or three dimensional elastic foundations subject to concentrated loads.

Vesic (Ref. 41) extended Biot's work to include beams with finite length and subject to moments. He also investigated the validity of Winkler's hypothesis and drew the conclusion that it is only truly valid for infinite beams on a semi-infinite elastic subgrade. Vesic also

stated that using Winkler's hypothesis gives rise to higher moments and leads to underestimation of displacements and pressures. Vesic also recommended correction procedures for the analysis of finite length beams.

Reese and Matlock (Ref. 35) used nonlinear elasto-plastic soil response curves for the analysis of laterally loaded piles for offshore structures. The pile was modelled with beam-column elements.

Haliburton (Ref. 18) extended the procedure used by Matlock and Reese for the analysis of flexible sheetwall retaining structures. He discussed methods for calculating soil response curves and compared some SSI solutions with the corresponding classical solutions.

Dawkins (Refs. 11, 12) used a finite element representation for the wall and an elasto-plastic nonlinear representation for the soil. The programs "CBEAMC" and "CSHTSSI" developed in these references were used in this study for comparison. This work automated the application of water loads, distributed loads, and distributed linear and nonlinear springs.

Because of the deficiency of the Winkler model in accounting for the continuous behavior of the soil, two-parameter models were introduced. The two-parameter models added a continuous layer between the soil springs and the structure. For example, the Filonenko-Borodich model (Ref. 15) uses a membrane under tension between the structure and the soil springs. Hetenyi's model (Ref. 22) adds an elastic beam to model the two-dimensional behavior. Pasternak's model (Ref. 31) uses a shear layer between the Winkler springs and the structure which, in a way, couples adjacent layers together. Also, Vlasov and Leont'ev (Ref. 42) developed a two-parameter continuous

foundation model. Two-parameter models are, in general, represented by the following differential equation:

$$P(x) = K.V(x) - Ds.d^{(4)}V(x)/dx^4 \qquad (2.1)$$

where P(x) = soil pressure

K = modulus of subgrade reaction

V(x) = structural displacement

Ds = second soil parameter

As can be readily seen, if Ds = 0, the model reduces to Winkler's.

The shortcoming of two-parameter models lies in the lack of extensive field tests for evaluating the two soil parameters.

Elastic continuum models were used to describe the behavior of soils beneath structures as well as the displacements of the soil at a distance away from the structure. Bousinesq (Ref. 2) and Cheung (Ref. 4) evaluated a flexibility matrix for the soil-structure interface. This flexibility matrix can be inverted and added to the beam-column stiffness matrix. FEM analysis reveals that the above mentioned approach produces accurate moments and rotations but erroneous absolute displacements.

The finite element method has been used to study problems involving soil-structure interaction, particularly flexible earth-retaining walls. The work done in the FE field is extensive. A few of the publications pertinent to this study are mentioned below. Goodman, Taylor and Brekke (Ref. 17) developed an interface finite element between the soil and the wall. R.W. Clough and Woodward (Ref. 7) analyzed embankment stresses and deformations using the FEM. R.W.

Clough also developed three-dimensional finite elements for general soil problems (Ref. 8). Chang and Duncan (Ref. 13) developed a nonlinear model for soil to be used in the FEM. Girijavallabham and Reese (Ref. 16) analyzed settlements under circular footings as well as the behavior of retaining walls. Ruser and Dawkins (Ref. 37) performed a nonlinear three-dimensional analysis of laterally loaded piles in saturated clay. Clough and Duncan (Refs. 5, 6) used the FEM for the analysis of sheetpile walls and U-frame structures that were a part of the Port Allen and Old River locks. The close agreement between the results obtained from the FEM analysis and actual measurements helped establish the FEM as a valuable analysis tool; however, its high cost and relative complexity renders it impractical for design purposes.

CHAPTER III

CLASSICAL AND SSI METHODS

In this Chapter, a brief review of the Classical and the SSI methods is given.

Classical Design Theory

In the analysis and design of cantilever sheetpile walls using the classical method, some assumptions are made in order to simplify the problem into a determinate one that can be solved with the common tools of structural analysis. These assumptions are:

1. The wall is assumed to rotate counterclockwise about a point in the embedded depth. By doing so, the wall will induce active and passive soil responses on either side.

2. The wall is assumed to rotate as a rigid body through a displacement sufficient to mobilize full-active as well as full-passive pressures on either side of the wall.

3. The wall derives its support solely from passive pressures on either side.

The active and passive pressures are calculated using Coulomb earth pressure coefficients along the wall on either side giving rise to net-active and net-passive pressures. These pressures are treated as loads acting on the wall and are used for analysis and design. In the design phase, the main objective is to find the penetration depth, D′,

and the transition distance, Z (Fig. 1) that will satisfy moment and force equilibrium (Σ Fx = 0, Σ Mt = 0). An example of the design procedure by the classical method is shown in Appendix A. With the depth of penetration established or already known, the analysis phase is carried on by assuming that the wall acts as a cantilever supported at the bottom. The net pressures are then applied as loads on the wall and the shears, moments, and deflections are calculated.

It can be observed that limit analysis and ultimate soil resistance criteria do not always lead to accurate analyses of flexible sheetpile retaining walls. The basic premise underlying this method is that the structure displaces sufficiently to develop ultimate soil resistance. For example, in Terzaghi's paper (Ref. 39), the soil is assumed to be a plastic material where full-active and full-passive pressures develop as a result of some wall displacements. In particular, full-active pressure is reached for V/H = 0.0014 and 0.0084 for dense and loose sand respectively; V is the lateral deflection and H is the height of the wall. These theories consider the structure to be extremely rigid compared to the soil. This assumption is inaccurate for flexible retaining walls and results in very high estimates for the depth of penetration. Furthermore, such flexible structures can fail from local excessive stresses long before they deform enough to mobilize full-active and passive pressures.

SSI Method

It is clear from the above discussion that a method is needed to permit the soil pressures to assume values intermediate to the ultimate cases and to be dependent on the deflection of the structure. Such a

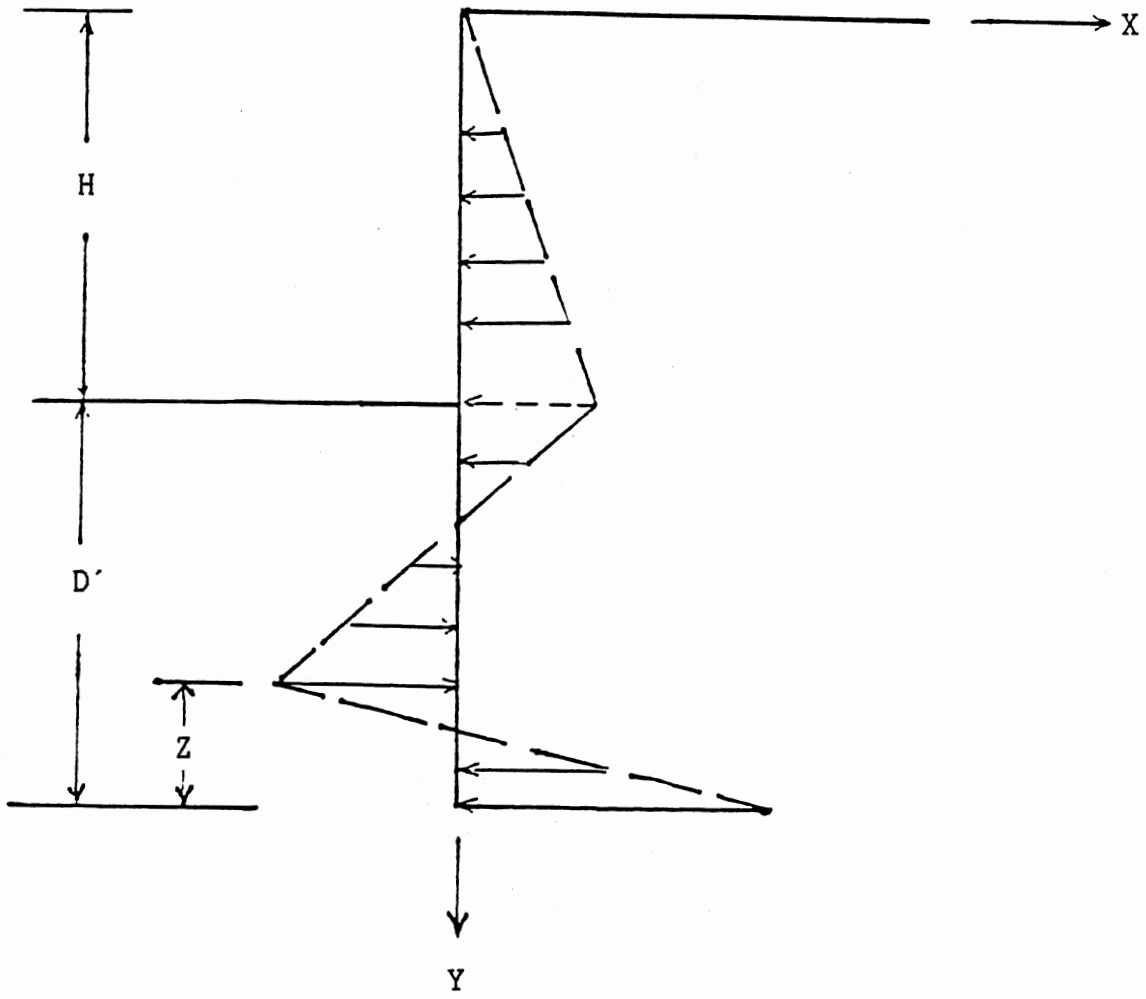

Figure 1. Net pressure variation with depth.

method was developed based on a combination of Winkler's hypothesis and limit equilibrium and it is commonly referred to as the SSI method.

The SSI method treats a flexible retaining wall as a linearly elastic structure which derives its supports from nonlinear springs that represent the soil on each side of the wall. Nonlinear soil force-displacement curves are found on either side of the wall and a gravity-turn-on solution is carried out. The solution requires iterative solutions of the following differential equation:

$$E.I.d^{(4)}V/dx^4 + K.V = 0 \qquad (3.1)$$

where E, I, and V are Young's Modulus, the moment of inertia, and the deflection of the wall respectively. K is the soil modulus and is a function of the displacement V.

In this study, computer programs "CBEAMC" (Ref. 11) and "CSHTSSI" (Ref. 12) were used. Both of these programs use beam-column finite elements to model the wall.

Limit Pressures

A typical soil response curve which has been used in SSI analyses is shown in Fig. 2. The soil pressures are assumed to vary linearly between the limit-active and limit-passive pressures.

Limit-Active Pressure. The active condition arises when the wall is moving away from the soil.

$$Pa = Ka.\sigma_v - 2Cu.\sqrt{Ka} \qquad (3.2)$$

In the above equation,

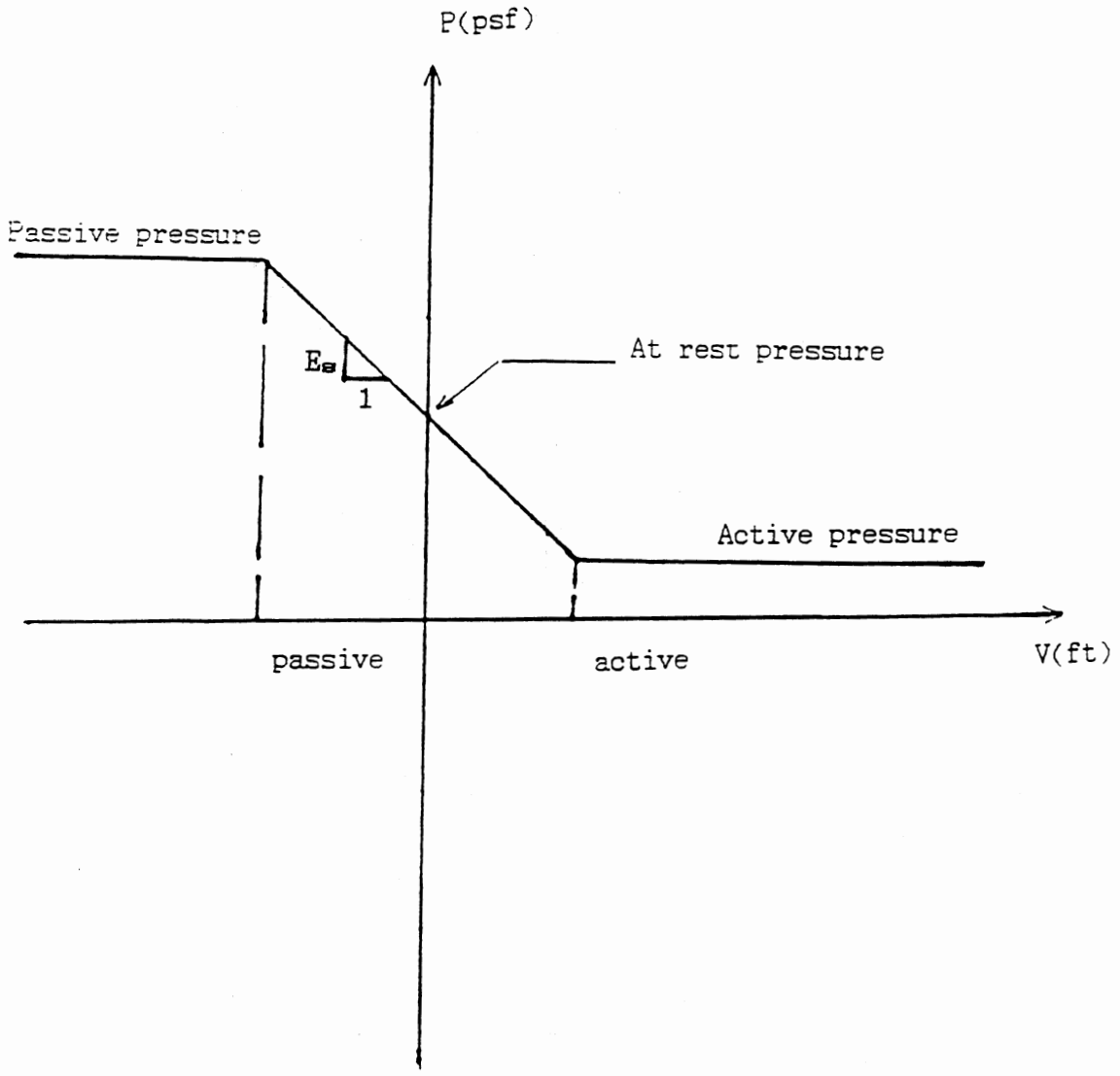

Figure 2. Nonlinear Soil Response Curve.

σ_v = vertical soil pressure

Cu = soil cohesion

Ka = active pressure coefficient.

The above equation for Pa can result in negative values for soil pressure. Whenever this happens, the value of Pa is set to zero.

Limit-Passive Pressure. The passive condition occurs when the wall is moving into the soil.

$$Pp = Kp.\sigma_v + 2Cu.\sqrt{Kp} \qquad (3.3)$$

In the above equation,

Kp = passive pressure coefficient.

In the present study, the soil under consideration was saturated clay under (ϕ = 0) conditions. Also, the wall was assumed to be smooth. Under the above conditions, the following new equalities are obtained:

$$Ka = Kp = 1 \qquad (3.4)$$

$$Pa = \sigma_v - 2.Cu \qquad (3.5)$$

$$Pp = \sigma_v + 2.Cu \qquad (3.6)$$

The at-rest pressure (wall does not move) is also given by:

$$Po = Ko.\sigma_v \qquad (3.7)$$

where Ko is the at-rest pressure coefficient.

For saturated undrained clay under plane strain conditions, $\phi = 0$ and Poisson's ratio, $v = 0.5$.

$$K_o = v / (1-v) = 1 \qquad (3.8)$$

Therefore,

$$P_o = \sigma_v \qquad (3.9)$$

Soil Pressure-Displacement Variation

The two following assumptions dictate the variation of soil pressures with wall displacements:

(a) The soil pressure at any point on the wall depends on the horizontal movement of the wall at that point and is independent of all adjacent points (Winkler's hypothesis).

(b) As mentioned earlier, the pressure varies linearly between the active and passive limits, passing through the at-rest value.

Soil pressure-displacement curves to the left and to the right are obtained at regular intervals along the height/depth of the sheetpile. Typical curves are shown in Fig. 3. The following soil behavior is observed for the soil on either side of the wall:

1. At zero wall displacement ($V = 0$), the soil pressure value for the soil on both sides is the at-rest value. These pressures correspond to point Po in Figs. 3b, and 3c.

2. If the wall moves to the left, the pressure due to the right side soil decreases until it reaches the limit active value P_{AR} after which it remains constant. At the same time, the left side soil pressure increases as the wall displaces to the left until it reaches the limit passive value P_{PL} after which it remains constant with further displacement.

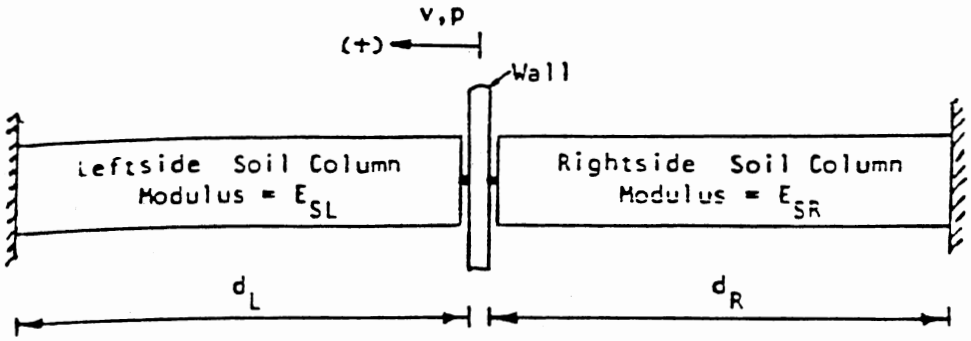

a. Typical soil columns

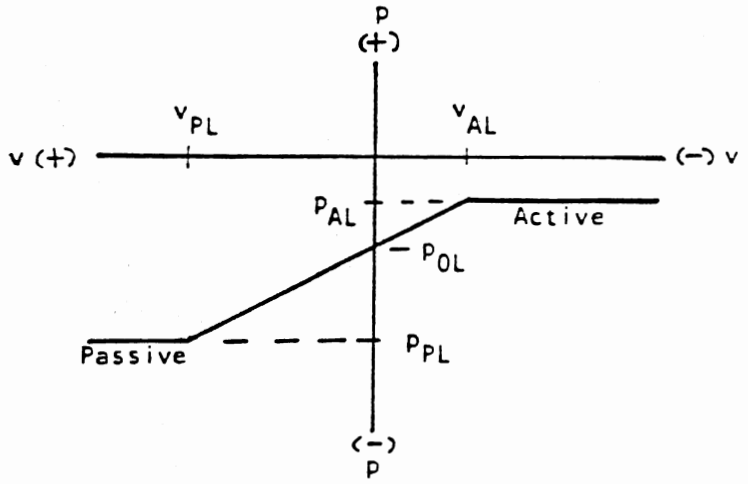

b. Leftside soil

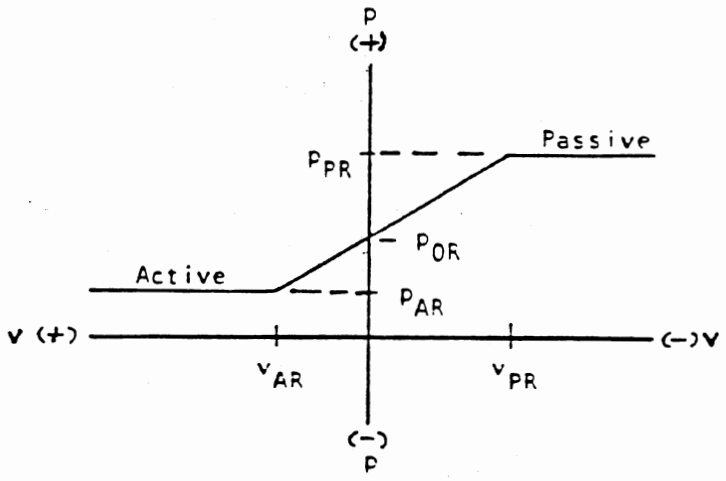

c. Rightside soil

Figure 3. Soil pressure-displacement variations.

3. If the wall displaces to the right, the right side soil pressure increases until P_{PR} is reached after which it stays constant. At the same time, the left side soil pressure on the wall decreases until a minimum value PAL is reached.

The displacements corresponding to limit values of pressures are found as follows (Ref. 12):

$$Va = \frac{(Po-Pa).D}{Es} \tag{3.10}$$

$$Vp = \frac{(Po-Pp).D}{Es} \tag{3.11}$$

where D is an interaction distance (discussed subsequently), and Es is the soil modulus.

The soil modulus value used in the equations above depends on the type of soil. For saturated undrained clays, the values of Es can be determined by one of two ways:

1. For stiff clays, the following equation was proposed by Terzaghi (Ref. 40):

$$Es = 0.67\ Es1/D \tag{3.12}$$

where Es1 is obtained from load bearing tests on 1ft x 1ft square plates.

2. For soft clays, Skempton's method may be used (Ref. 38). Skempton observed that the shape of the laboratory soil triaxial test is similar to that of the load deformation curve for a loaded soil mass. He also noticed that about 50% of the ultimate soil resistance is

developed at a structural deflection of:

$$V = 2.5\ \epsilon_{50}.\ B \qquad (3.13)$$

where ϵ_{50} is the strain at 50% of ultimate strength (qu) for the clay when tested in unconfined compression, and B is the beam width which corresponds to the interaction distance, D, mentioned earlier.

For most clays ϵ_{50} is about 0.01 (1%) but is smaller for stiff clays (about 0.005) and is larger for softer clays (about 0.02). Therefore, if the ultimate soil resistance for a plate bearing test can be determined, the following equation may be used to evaluate Es:

$$Es = \frac{Pult/2}{2.5.\epsilon_{50}.B} = \frac{Pult}{5.\epsilon_{50}.B} \qquad (3.14)$$

The final, and perhaps the most difficult step in the SSI method, is the estimation of the interaction distance for the soil on both sides of the wall. The interaction distance is approximately the distance away from the wall through which the soil is significantly stressed. The role of D is obtained by analogy to the "pressure bulb" depth beneath a strip footing as shown in Fig. 4.

Originally, it was thought that D is most critical in passive zones and not as critical where active behavior is manifest. The validity of this assumption will be discussed later in this study.

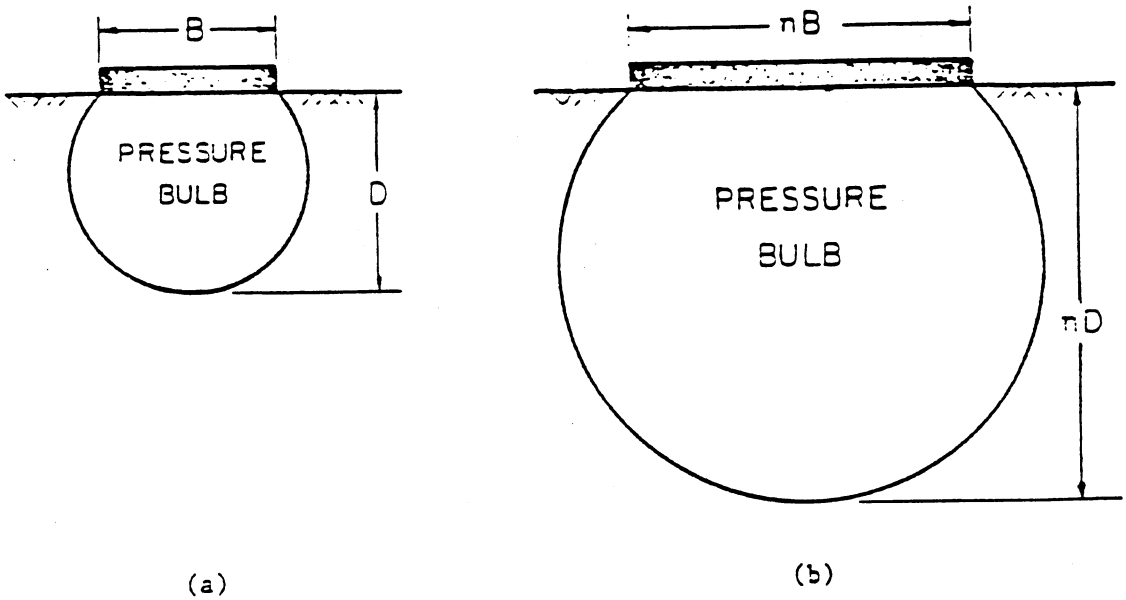

Figure 4. Pressure Bulbs for Beams of Width B and nB

CHAPTER IV

COMPUTER PROGRAM AND METHODOLOGY

The original intent of this study was to perform a gravity-turn-on nonlinear finite element analysis of cantilever sheetpiles in undrained saturated clay. For that purpose, a computer program was developed utilizing the following finite elements:

1. Isoparametric quadrilateral elements to model the soil medium.
2. Beam-column elements for the wall which is assumed to be linear and elastic.
3. Goodman elements for the soil-wall interface.

Furthermore, the hyperbolic model was used to model the stress-strain behavior of the soil. This model was developed by Duncan and Chang (Ref. 13) and involves the evaluation of the initial soil modulus, E_i , the tangent modulus, E_t , and Poisson's ratio, v, in terms of the principal stresses and some soil parameters. Specifically, the following equations are used:

i) The initial soil modulus is given by:

$$E_i = K P_a (\sigma_3/P_a)^n \qquad (4.1)$$

in which E_i is the initial modulus, 'P_a' is the atmospheric pressure

expressed in the same units as σ_3 and 'K' and 'n' are dimensionless numbers that may be determined by running a series of tests and plotting the values of E_i vs. σ_3 on a log-log scale and then fitting a straight line to the data.

ii) The instantaneous tangent soil modulus is given by (Ref. 13):

$$E_t=\left[1 - \frac{R_f(1-\sin(\phi))(\sigma_1-\sigma_3)}{2.Cu.\cos(\phi)+2.\sigma_3.\sin(\phi)}\right]^2 K.P_a(\sigma_3/P_a)^n \qquad (4.2)$$

where R_f is a factor representing the failure ratio which is a number less than one.

This expression for (E_t) is very powerful for incremental stress analysis. First, elastic modulii are assumed from which FEM values for (σ_1) and (σ_3) are calculated at the centroid of each element. From Eq.4.2, the value of (E_t) can be calculated for each element and that value is used for the next load increment.The same process is carried on until the full load is applied.

iii) The instantaneous Poisson's ratio is given by (Ref. 13):

$$v = \frac{G-F.\mathrm{Log}(\sigma_3/P_a)}{1 - \left[\frac{d(\sigma_1-\sigma_3)}{K.Pa(\sigma_3/P_a)^n \left| 1 - \frac{R_f(\sigma_1-\sigma_3)(1-\sin(\phi)}{2.Cu.\cos(\phi) + 2.\sigma_3.\sin(\phi)}\right|}\right]^2} \qquad (4.3)$$

All of the parameters involved in the above expression can be

determined from a series of triaxial tests with volume change measurements. Furthermore, equations 4.1, 4.2, and 4.3 become much simpler when $\phi = 0$ conditions are implemented. In that case, Poisson's ratio, v, reduces to ≈ 0.5 and 'n' becomes zero.

Another finite element program "SIMULATE" was developed by Dr. Issam Hallal and Dr. Mete Oner for the analysis of floodwalls (Ref.20). This program had within its scope the desired capability to perform gravity-turn-on analysis in addition to many other features. Using this program, the effect of the stress-path can be investigated by performing a gradual buildup analysis (i.e., by adding the retained soil in layers). Also, the program "SIMULATE" uses a modified version of the f-model (Ref. 20) to represent the stress-strain behavior of the soil. In comparison to the hyperbolic model, the f-model has increased capabilities for simulating unloading or stress reversal. Whereas the hyperbolic model assumes that the soil unloads and reloads along a straight line of higher stiffness than the original loading curve, the f-model uses a curve similar to the original loading curve for unloading and reloading. This makes the f-model more accurate especially when some of the soil elements undergo unloading or reloading. Furthermore, a postprocessor was developed for the program "SIMULATE" thus facilitating tremendously the analysis of results. For the reasons mentioned above, the program "SIMULATE" was used exclusively in the current study.

In this program, isoparametric quadrilateral elements are used for the soil and beam-column elements are used for the wall. The wall-soil interface is modelled using nonlinear springs which permit the wall to separate from the adjacent soil. This interface consists of two nodes,

occupying the same location (Fig. 5), connected by nonlinear springs, which in general, have stiffness in both the tangential and normal directions (Fig. 6). In this study, the stiffness in the tangential direction was set to zero to reflect a smooth wall-soil interface.

When a tension stress is encountered for the interface element, separation occurs and the normal stiffness is set to zero. In the case of compression, a large value for Kn is used to assure that no intrusion occurs from the adjacent soil nodes into the wall.

Features of the Program "SIMULATE"

The Incremental Approach

In the incremental approach (Fig. 7), the total load is applied in a series of increments. An initial modulus value is chosen for each element and a small increment of load is applied. The resulting displacements, stresses and strains are then calculated. At the beginning of each new increment of load, a new value for modulus, usually tangent modulus, is chosen for each element. These new values depend on the stresses and strains found from the previous load increment. Thus, the nonlinear stress-strain relationship will be approximated by a series of straight lines as shown in Fig. 7. This procedure is repeated until the total desired load is applied. The final state of stress and strain will be obtained by summing up the results for all the increments.

The main advantage of the incremental approach is that no iterations are required if small steps are used and that initial conditions can be easily included in the model. Another advantage of this method is that the load can be applied in very small increments,

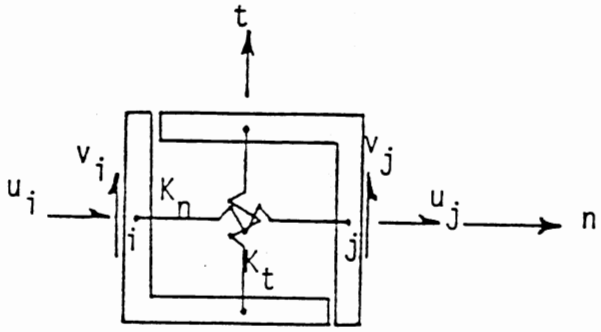

Figure 5. Typical Interface (linkage) Element.

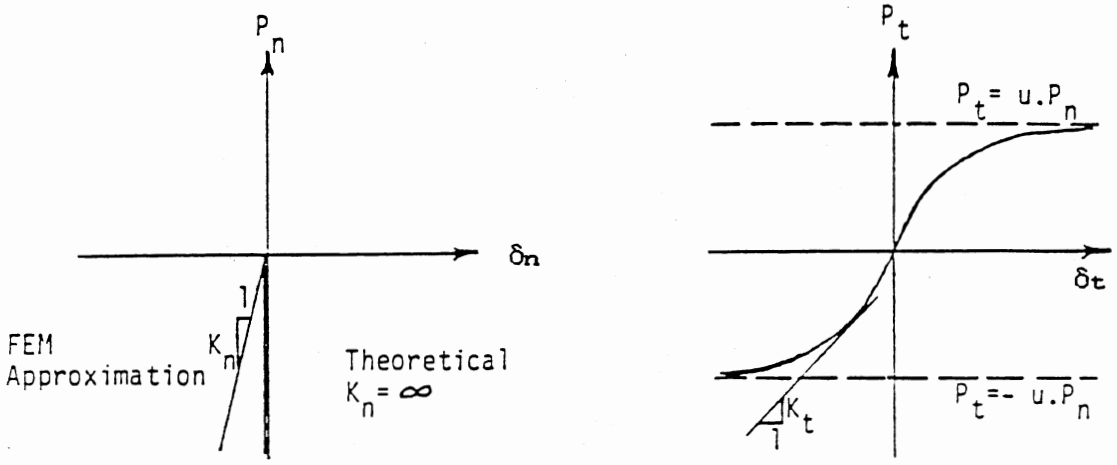

Case I. $\delta_n < 0$ ($\delta_n = u_j - u_i$, compression)

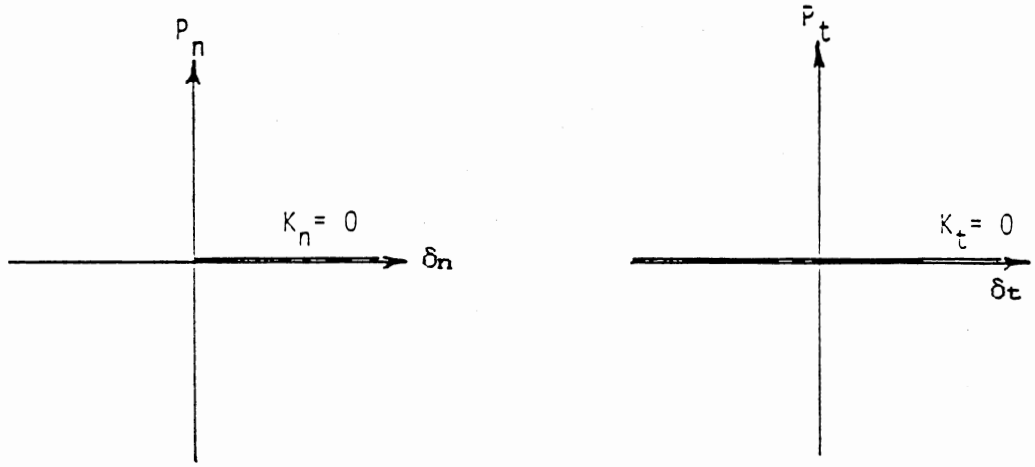

Case II. $\delta_n > 0$ (separation, tension)

Figure 6. Various load-displacement relations for the interface.

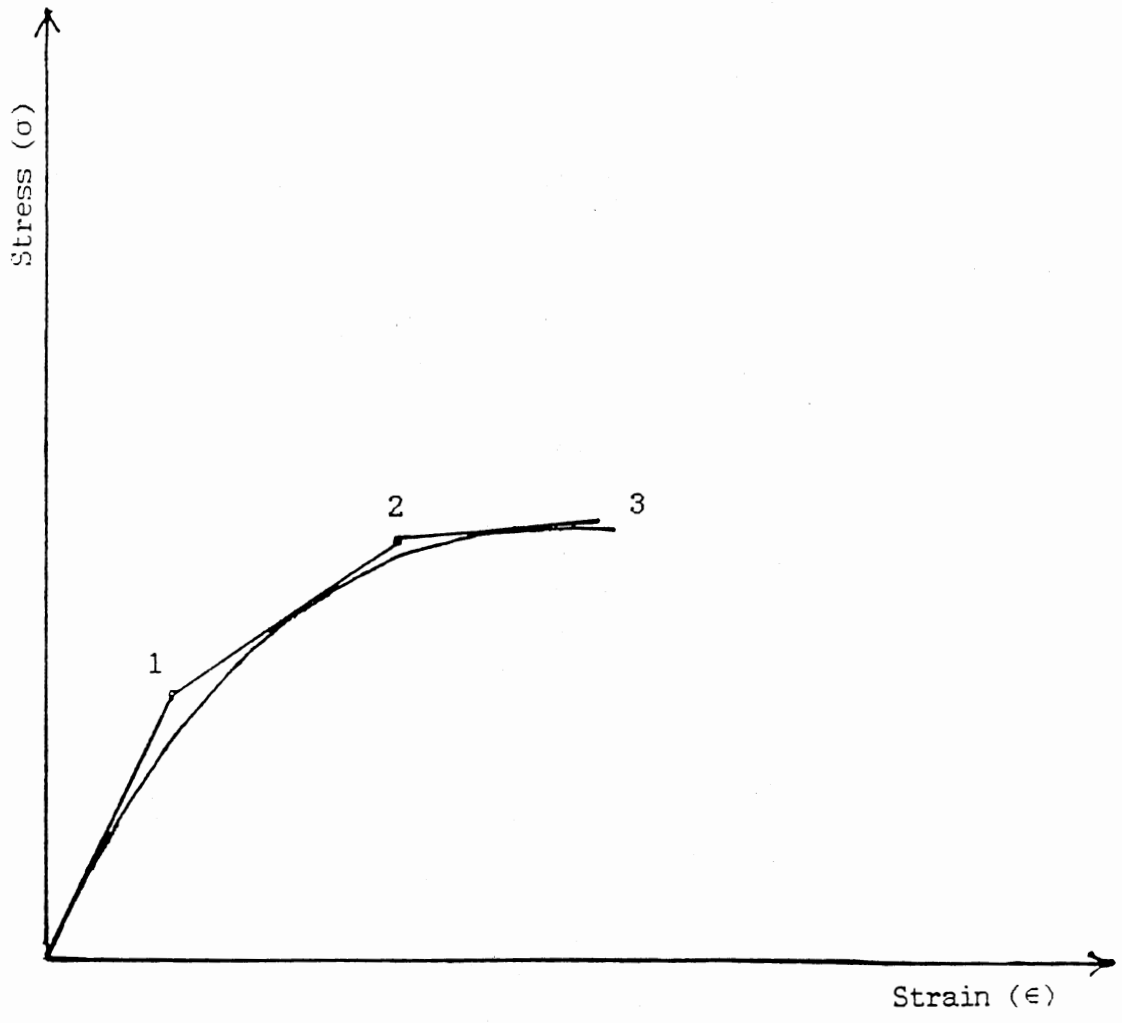

Figure 7. Stress vs. strain for nonlinear incremental analysis

thus, improving the accuracy to within any desirable tolerance. At the same time, this approach gives an idea about the gradual buildup of stresses and strains with the increase in load. This could be utilized to simulate the actual construction process and trace the stress paths very closely.

In the program "SIMULATE", the incremental approach is used in conjunction with an acceleration scheme to improve convergence as discussed in Appendix A (Ref. 20).

Simulation of Incompressibility Condition

In the past, flexible retaining walls have been successfully modelled assuming plane strain conditions. This is because the wall extends a long distance in the lateral direction. For plane strain conditions, the constitutive matrix [D] is:

$$[D] = \frac{E(1-v)}{(1+v)(1-2v)} \begin{bmatrix} 1 & v/1-v & 0 \\ v/1-v & 1 & 0 \\ 0 & 0 & (1-2v)/2(1-v) \end{bmatrix} \qquad (4.4)$$

Originally, in the case of local failure or in the event of tension stresses, the value of E was set to a small number. This caused the values of normal stresses to remain constant. However, for saturated undrained normally consolidated clay ($\phi = 0$, $v \approx 0.5$) the above behavior is inadequate. This is because such soils are almost incompressible, i.e., they act as a very viscous liquid, and continue to pick up normal stress even after local failure. The inadequacy of Eq. 4.4 was demonstrated by Duncan et. al. (Ref. 5). In that study, the mode of

post-failure behavior resulting from Eq. 4.4 was found to differ considerably from the real behavior. Even after failure, soils continue to carry additional normal stresses and subsequently an additional small amount of shear stress.

To remedy the afore-mentioned shortcoming for post-failure behavior, the program "SIMULATE" is based on an alternate stress-strain formulation obtained by rearranging Eq. 4.4 in the form:

$$\{\sigma\} = \begin{bmatrix} M & M-2G & 0 \\ M-2G & M & 0 \\ 0 & 0 & 2G \end{bmatrix} \{\epsilon\} \qquad (4.5)$$

where M is the constrained modulus given by:

$$M = \frac{E(1-v)}{(1-2v)(1+v)} \qquad (4.6)$$

and G is the shear modulus given by:

$$G = \frac{E}{2(1+v)} \qquad (4.7)$$

After failure, G is set to a small value while M is kept at its value for the step prior to failure. This approach permits very accurate simulation of the soil behavior before and after failure.

f-Model

The f-model used by the program "SIMULATE" conforms to the

following important aspects of behavior of flexible retaining walls in normally consolidated undrained clay:

(a) The soil stiffness should decrease as the loading progresses.

(b) The stiffness of the soil should increase with increasing confining pressure.

(c) Under non-monotonic loading, the soil should be allowed to unload or reload along a different curve with higher stiffness.

(d) Active and passive stress paths should be recognized and modelled properly.

In particular, the program "SIMULATE" utilizes a modified version of the f-model. For that reason, it was thought convenient to mention some of the basics of this method. The original f-model was modified (Ref. 20) to account for reversal in loading direction from active to passive and vice-versa. The stress-strain relationship used in the f-model is derived later in this chapter and is given by Eq. 4.15. The constrained modulus, M, and the shear modulus, G, are related to Young's modulus, E, and Poisson's ratio, v, as follows:

$$M = \frac{E.(1-v)}{(1-2v)(1+v)} \tag{4.8}$$

The constrained modulus at geostatic conditions, Mo, is calculated from the following relationship :

$$Mo = mPa\ (\sigma_1/P_a)^n \tag{4.9}$$

where σ_1 is the major principal stress, P_a is the atmospheric pressure, and m and n are empirical constants to be determined.

Referring to Fig. 8, The degree of mobilization "f" in the hyperbolic model is given by the following relationship:

$$f = \tau_{max}/Cu=(\sigma_{1m}-\sigma_{3m})/(\sigma_{1f}-\sigma_{3f}) \qquad \text{for } \phi = 0 \qquad (4.10)$$

where,

τ_{max} is the maximum mobilized shear stress

σ_{1m} and σ_{3m} are the mobilized principal stresses

σ_{1f} and σ_{3f} are the principal stresses at failure

f=1 corresponds to a state of failure according to the Mohr-Coulomb failure criterion, whereas f=0 corresponds to an isotropic state of loading with $\tau_{max} = 0$.

At any intermediate level of stress, the shear modulus is given by:

$$G = Go(1-f)/(1-fo) \qquad (4.11)$$

where fo and Go is the degree of mobilization and shear modulus at Ko condition, respectively. From the definition of f and Go, Eq.4.11 can also be written as follows:

$$G = G_i(1-f) \qquad (4.12)$$

in which G_i is the initial shear modulus at f=0 (isotropic state) which corresponds to E_i in the hyperbolic model.

Eq. 4.12 shows that as f increases to 1 at failure, the value of shear modulus, G , decreases to zero. Under drained conditions, M is kept constant at its initial value. In an undrained situation, M and G

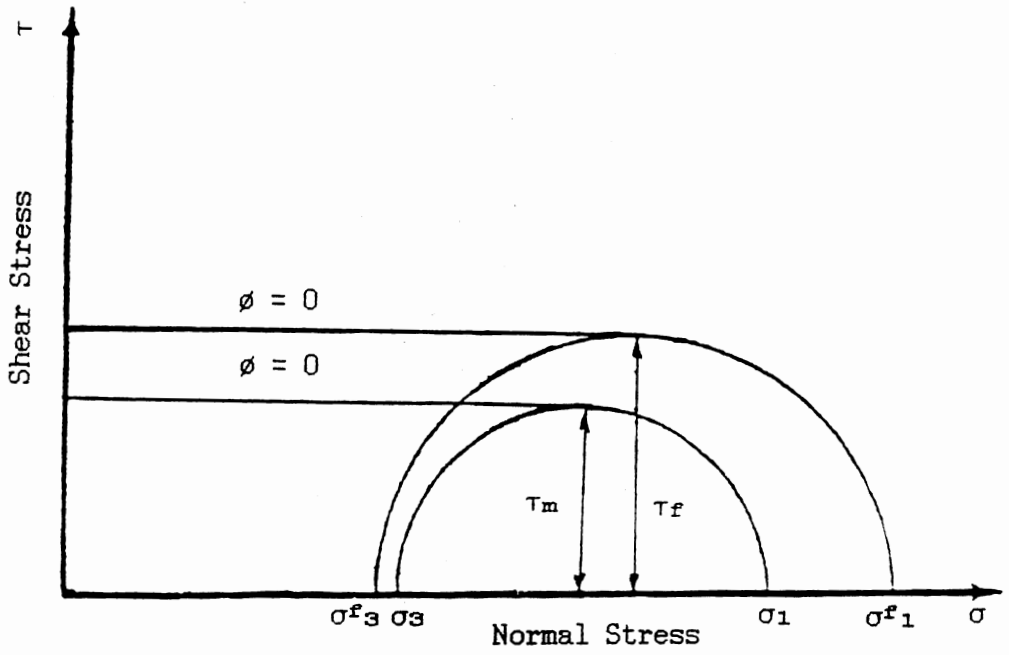

Figure 8. Mohr-coulomb failure envelope for soft saturated clay

both vary while Poisson's ratio is kept at approximately 0.5.

In its original form, only the loading branch of the degree of mobilization (f) vs. axial strain (ϵ) curve was formulated. This branch starts at f=0 and becomes asymptotic to the horizontal line at f=1 (Fig. 9). In reference (20), the original f-model was modified to take into account unloading and reloading as shown in Fig. 10. Another variable f' was introduced that takes into account both the loading direction and the closeness of the state of stress to the failure envelope. This model was used successfully in the study of floodwalls (Ref. 20). In that regard, the f-model is superior to the hyperbolic model that assumes linear unloading behavior. In the case of undrained stress-strain behavior Eq. (4.12) remains valid. However, f is calculated as the ratio of maximum shear stress to the undrained shear strength (Eq. 4.10). Since in triaxial tests the major principal stress σ_1 , is usually increased and then the axial strain , ϵ , in that direction is recorded, it is very convenient to determine E_i first and then to calculate G_i from the theory of elasticity. Keeping in mind that v = 0.5 for undrained conditions, G_i can be found as follows:

$$G_i = E_i/2(1+v_i) = E_i/3 \qquad (4.13)$$

where E_i is Young's modulus at initial isotropic conditions.

Eq. 4.13 can be integrated in the (ϕ = 0) case to obtain the following relationship:

$$\epsilon = A \ln (1-\tau/Cu) = A \ln (1-f) \qquad (4.14)$$

where $A = -2.Cu/E_i$

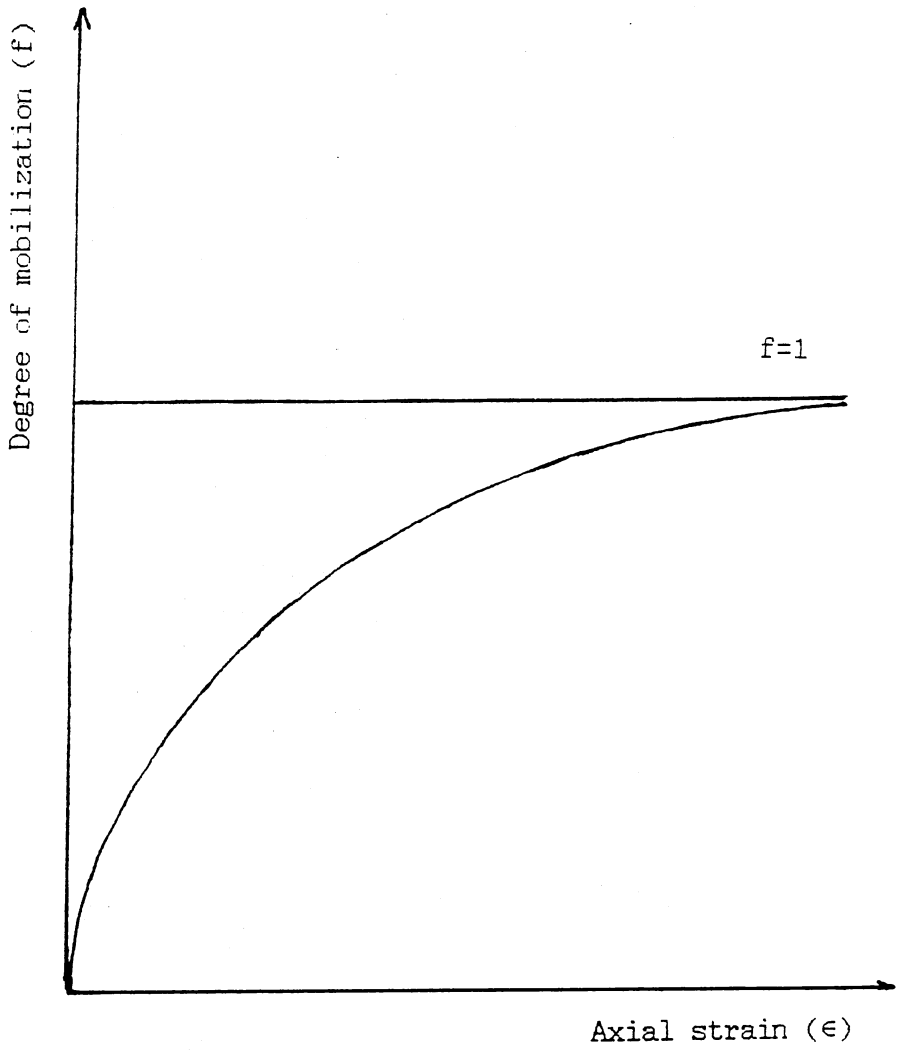

Figure 9. General virgin curve of the f-model.

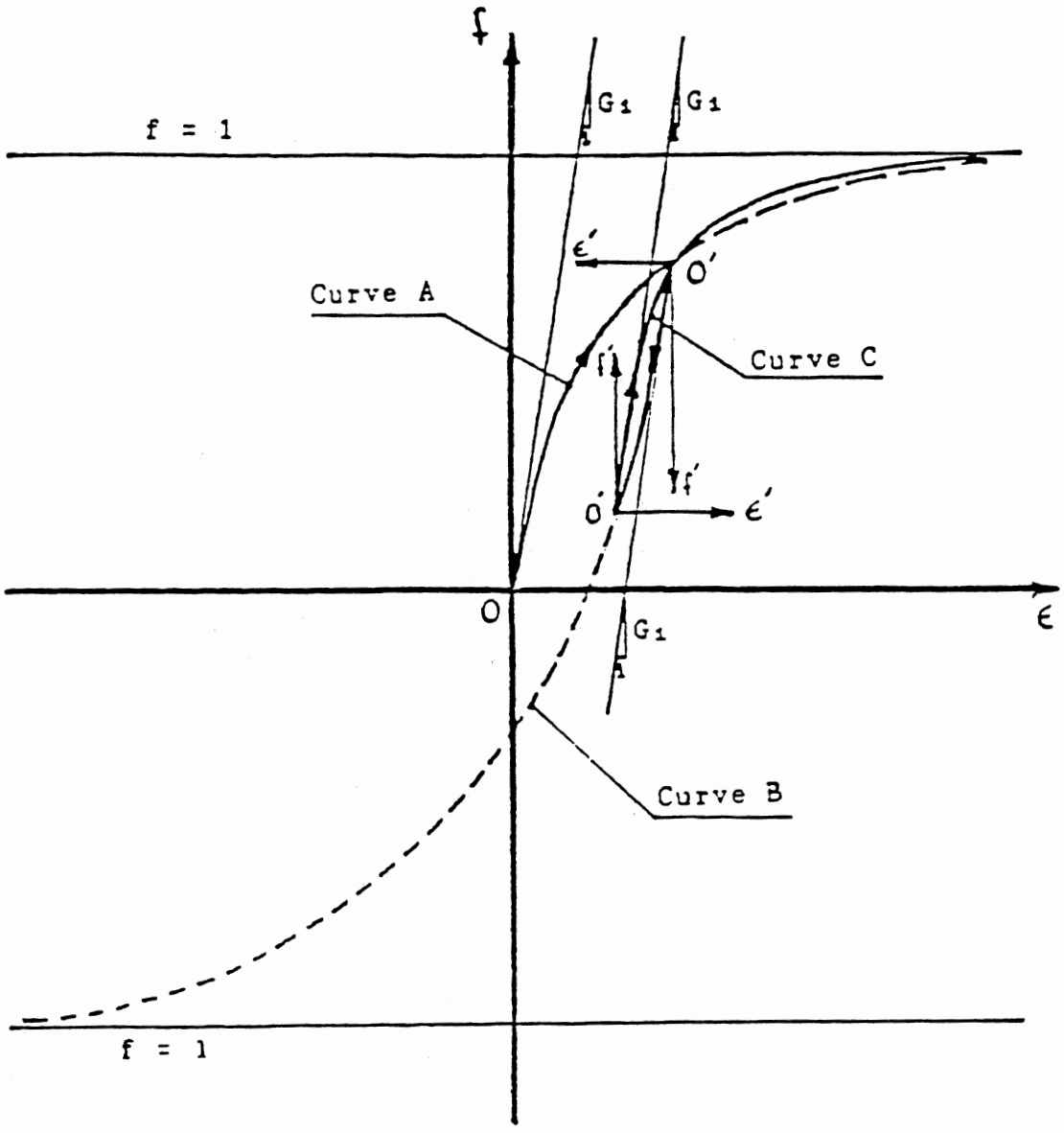

Figure 10. Generalization of the f-model for unloading and reloading on different paths.

The experimental stress-strain curve can now be used and any point in the range of interest can be substituted into equation (4.14) to find the value of E_i. A very common procedure is to measure the axial strain at mid-height, i.e., for f=1/2. The secant modulus obtained at that point is known as " E_{50} " in the literature. Furthermore, E_i can be easily related to E_{50}. It has been observed that the initial curvature of the model affects this inter-dependence. For (ϕ = 0) conditions, the following equation can be easily verified (Eq. B.20 in Appendix B):

$$(E_i/E_{50}) = -2\ln(1/2) = 1.386 \qquad (4.15)$$

The parameters needed for the f-model can be easily obtained by a simple correlation with the hyperbolic model for which a wide data base already exists. Appendix B establishes the correlation between the parameters of the two models for the ϕ = 0 case.

CHAPTER V

SOIL TYPE AND PARAMETERS

The purpose of the study was to establish a benchmark for the evaluation of the SSI approach in comparison to the finite element method. As discussed previously, the stress-strain characteristics of soils are quite complicated. Many parameters may be needed to represent their behavior such as, K, N, Rf, m for E_t (Eq. 4.2), and F, d, G for v (Eq. 4.3). The current state of the SSI method does not have within its purview the flexibility to take all of these parameters into consideration. However, the selected soil (saturated undrained normally consolidated clay) requires very few parameters to describe its behavior. This selection simplifies the situation considerably and makes it much easier to correlate the SSI and the finite element parameters. The advantages of these soils are:

1. Independence of the initial modulus, E_i, of the confining stress, σ_3.
2. Constant Poisson's ratio.
3. A one to one correspondence between SSI and finite element parameters.

Due to the constant nature of the Mohr-Coulomb failure envelope ($\phi = 0$), it is evident that regardless of the value of the confining stress, σ_3, the deviatoric stress at failure, $(\sigma_1-\sigma_3)_f$, is constant and is equal to 2Cu. Therefore, the value of E_i is independent of σ_3.

This is also apparent from Eq. B.20 in Appendix (B), $E_i = 1.386\ E_{50}$, where E_{50} is constant for clay soil under $\phi = 0$ condition. Furthermore, it follows from Eq. B.1 that n = 0, thus reducing the number of parameters needed.

As discussed in Chapter Five, the Poisson's ratio, v, depends on the parameters F,d, G (Eq. 4.3). These parameters were found to affect the behavior of the soil. The current SSI approach does not have a provision to incorporate the effect of poisson's ratio directly. However, for unconsolidated undrained condition such a provision is not needed since Poisson's ratio is constant (approximately 0.5). This is because the soil is almost incompressible. In the present study, v = 0.49 was used for numerical stability reasons.

For $\phi = 0$ soil, both the f and the hyperbolic models reduce to a one parameter model. This parameter is given in Eqs. 5.1 and 5.2 (Appendix B):

$$E_{50}/Cu = 1/\epsilon_{50} = m \qquad (5.1)$$

$$k = (1.386\ Cu/Pa).m \qquad (5.2)$$

The above equations simplify the correlation of the parameters used in the FEM with those used in SSI analyses. Once a value for m or k is chosen, an equivalent ϵ_{50} is calculated to be used in the SSI analysis in one of two ways.

1. If Skempton's method (Ref. 38) is used to evaluate the soil stiffness, ϵ_{50} fits directly in the following relation:

$$E_s = (5.7\ Cu)/(5.\epsilon_{50}.D) \qquad (5.3)$$

2. If Terzaghi's formula (Ref.17) is used,

$$E_s = 0.67\ Es_1\ (1\ ft)/(D\ ft) \qquad (5.4)$$

ϵ_{50} is accounted for indirectly since it is determined from the clay consistency. For stiff clays, ϵ_{50} is about 0.010 (1%), but is lowered to 0.005 for very stiff clays or raised to 0.02 for very soft clays.

The soil considered in all the case studies reported here is stiff according to Terzaghi's criteria ($q_u = 2.Cu \geq 1$ tsf). Therefore, ϵ_{50} = 0.01 was used. From Eq. 5.1, the corresponding value of m was 100.

Analyzed Cases

The section of the wall used in this analysis is a PZ-27 sheet-pile. Initially, a 30 ft wall with a 30 ft depth of penetration was analyzed. The soil density was 110 pcf. The cohesion of the soil, Cu, was varied (1000, 1300, 1600 psf) to study its effect on the behavior. Also, different values of embedment depths (15', 20') were analyzed to study the corresponding behavior. The reasons for these selections are as follows:

1. A value of Cu = 1000 psf corresponds to qu = 2000 psf. This coincides exactly with the lower limit for stiff clays in Terzaghi's tables (Ref. 40). It was desirable to stay within that range so that Terzaghi's method could be used.

2. Using the classical method (Appendix A), the following height for a tension crack is obtained:

for Cu = 1000 psf,

$$h_c = 2Cu/\gamma = 2(1000)/110 = 18.18 \text{ ft}$$

for Cu = 1300 psf,

$$h_c = 2(1300)/110 = 23.63 \text{ ft}$$

for Cu = 1600 psf,

$$h_c = 2(1600)/110 = 29 \text{ ft}$$

From these calculations, a height of retained soil equal to 30 feet was chosen.

3. For Cu = 1000 psf, calculations for embeddment depth based on the classical theory are shown in Appendix A. A value of about 27 feet was found, and for that reason a starting embeddment of 30 feet was used. Subsequently, embeddment depths of 20 feet and 15 feet were studied.

4. Further runs were carried out to determine the cutoff value of Cu for which the FEM predicts failure by instability. Similar SSI analyses were performed for the same purpose.

The analysis was done on a cantilever sheetpile in homogeneous soil. This was deemed to be a good starting point that provides a springboard to more complex situations such as anchored bulk heads, layered systems, etc...

Since undrained saturated clay was studied, the total stress approach was adopted.

Fig. 11 is a schematic representation of the pile-soil system. The top soil surface is chosen as zero elevation. Other elevations are measured from that datum positive upward. The elevation at the original ground surface is -30′ since the height of retained soil is 30 ft for

all the analyzed cases. However, the elevation at the bottom of the wall varies with the depth of penetration (-45′,-50′,-60′ for the 15′, 20′, and 30′ penetration depths respectively). Also, some critical locations (A-I) are shown in Fig. 11. These points will be referred to in the discussion of results.

The mesh used for the finite element solution is shown in Fig. 12. It consists of a total of 635 nodes and 524 soil elements. The lateral and vertical dimensions were varied to ensure that the boundaries do not affect the solution in the vicinity of the wall. In the lateral direction, a distance of 150 ft on either side was found to be sufficient. This can be seen from the stress contours (Figs. 13-16). Since these contour lines become horizontal, any additional lateral extension will not affect the final solution. On the other hand, an increase in the vertical extension, will continue to affect the final solution due to the incompressibility of the soil. However, the stresses in the soil and the moments in the pile were found to stabilize when 200 ft was reached and this value was used for all analyses.

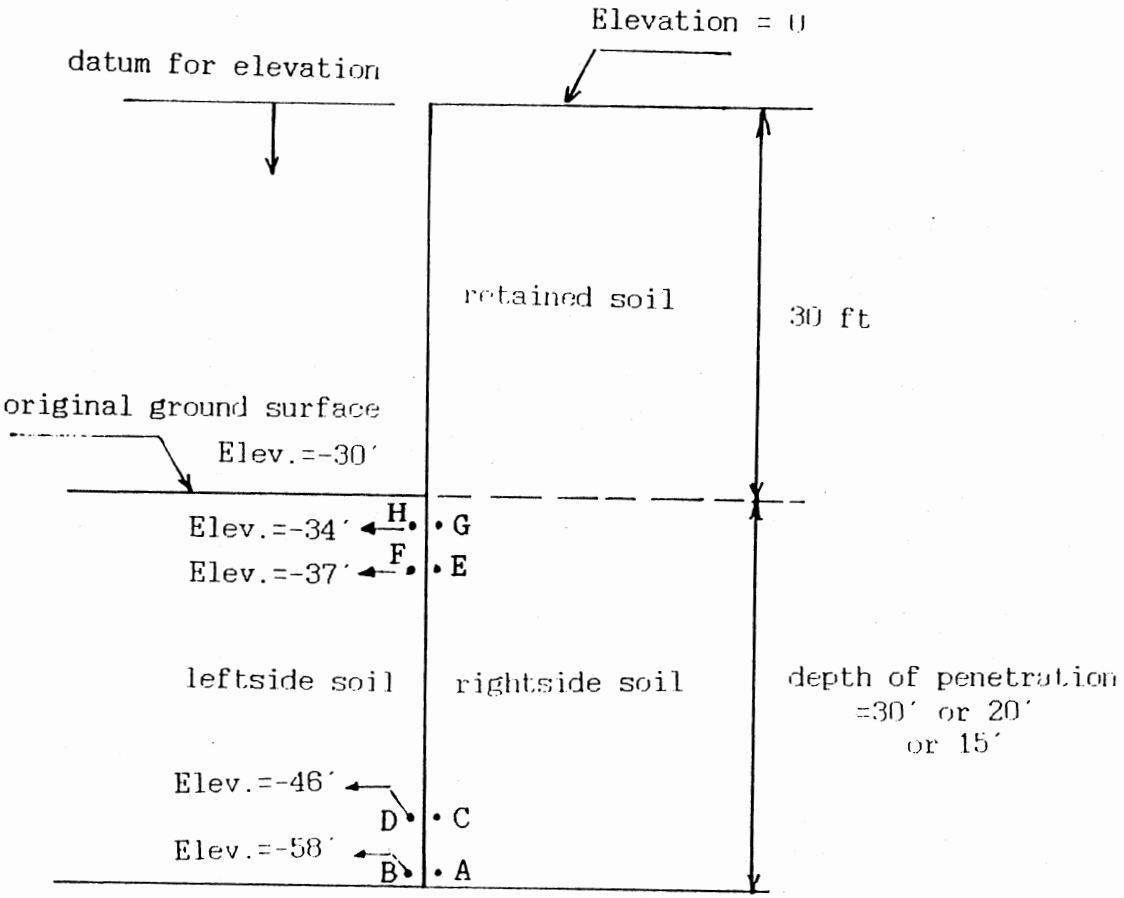

Figure 11. Schematic representation of the wall-soil system.

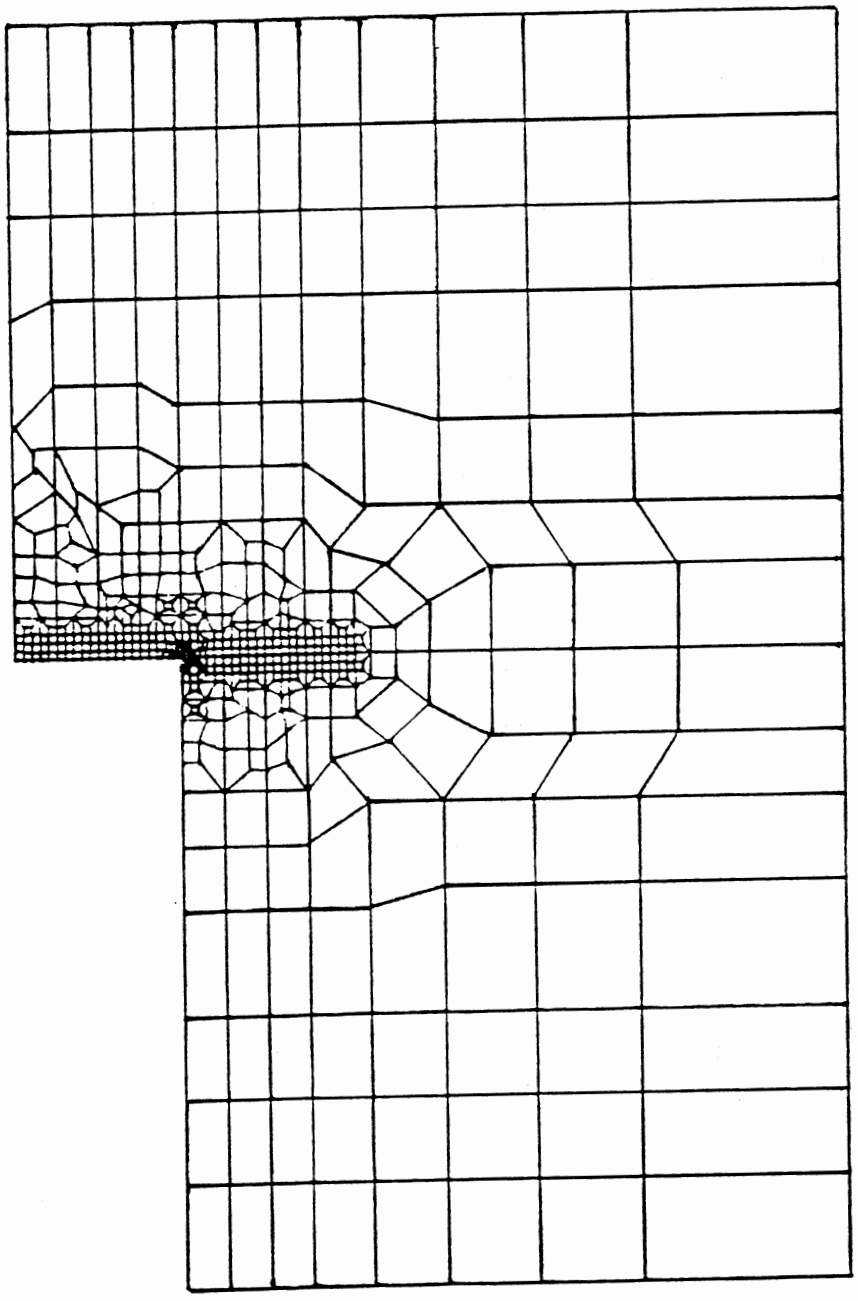

Figure 12. Grid for typical finite element analyses.

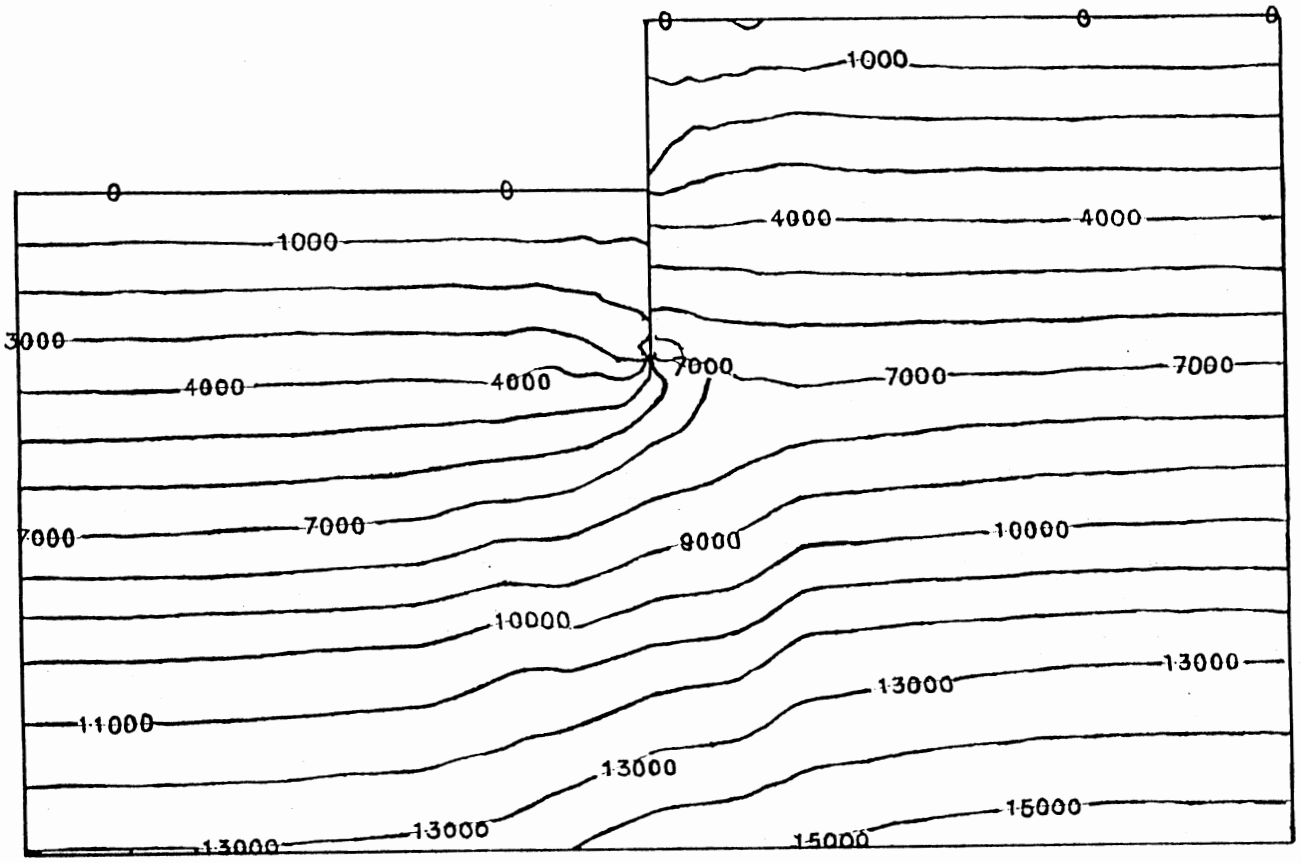

Figure 13. Vertical stress contours from gravity-turn-on analysis.
Cu = 1300 psf; depth of penetration = 30 ft.

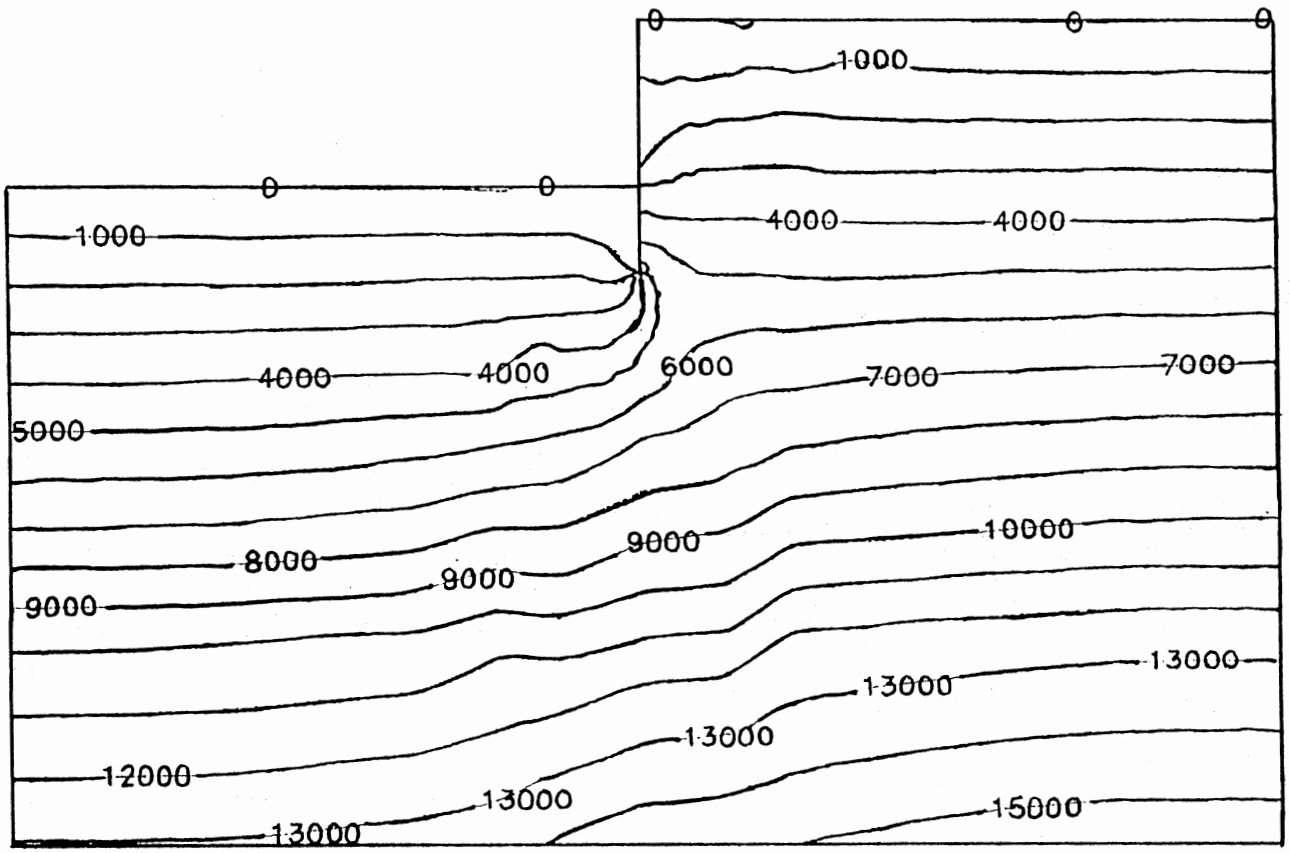

Figure 14. Vertical stress contours from gravity-turn-on analysis.
Cu = 1300 psf; depth of penetration = 15 ft.

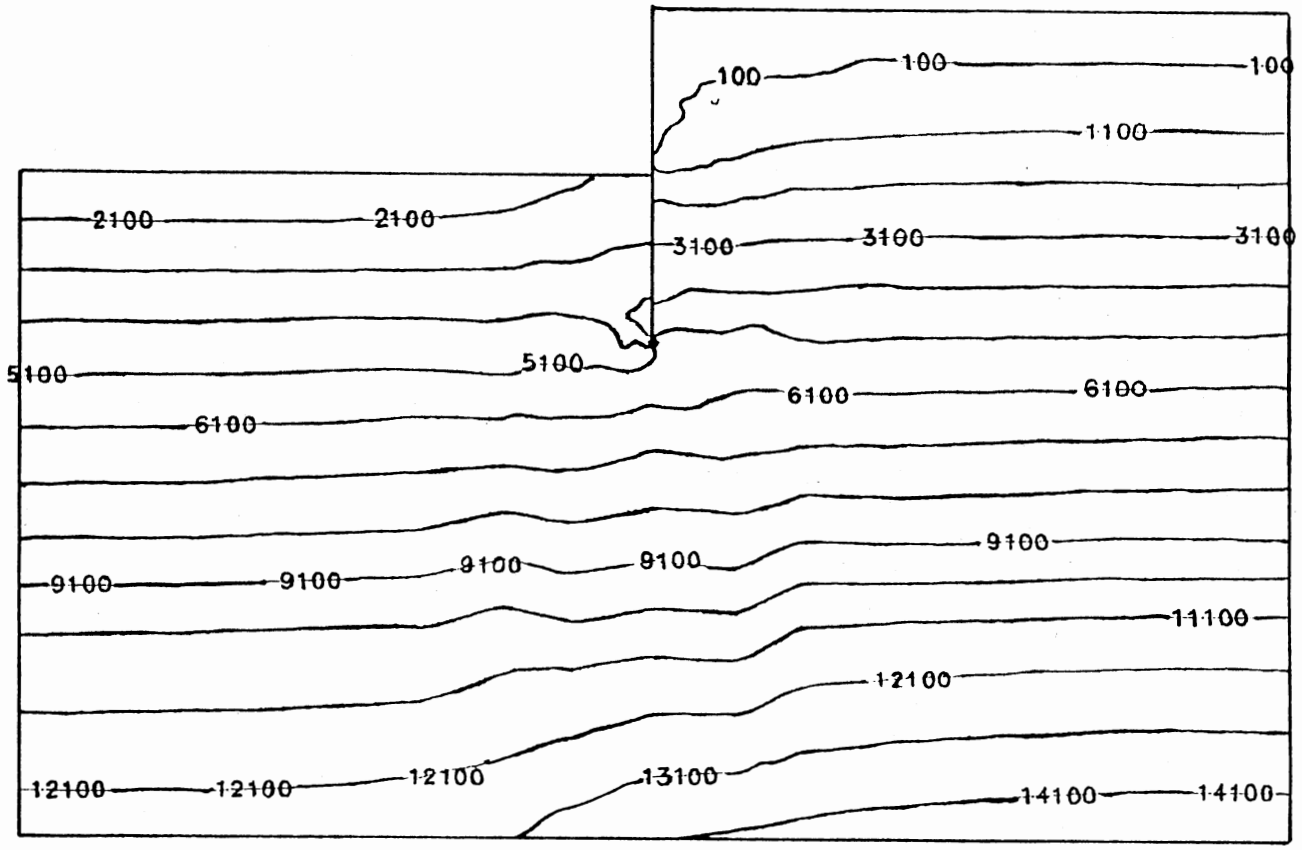

Figure 15. Horizontal stress contours from gravity-turn-on analysis. Cu = 1300 psf; depth of penetration = 30 ft.

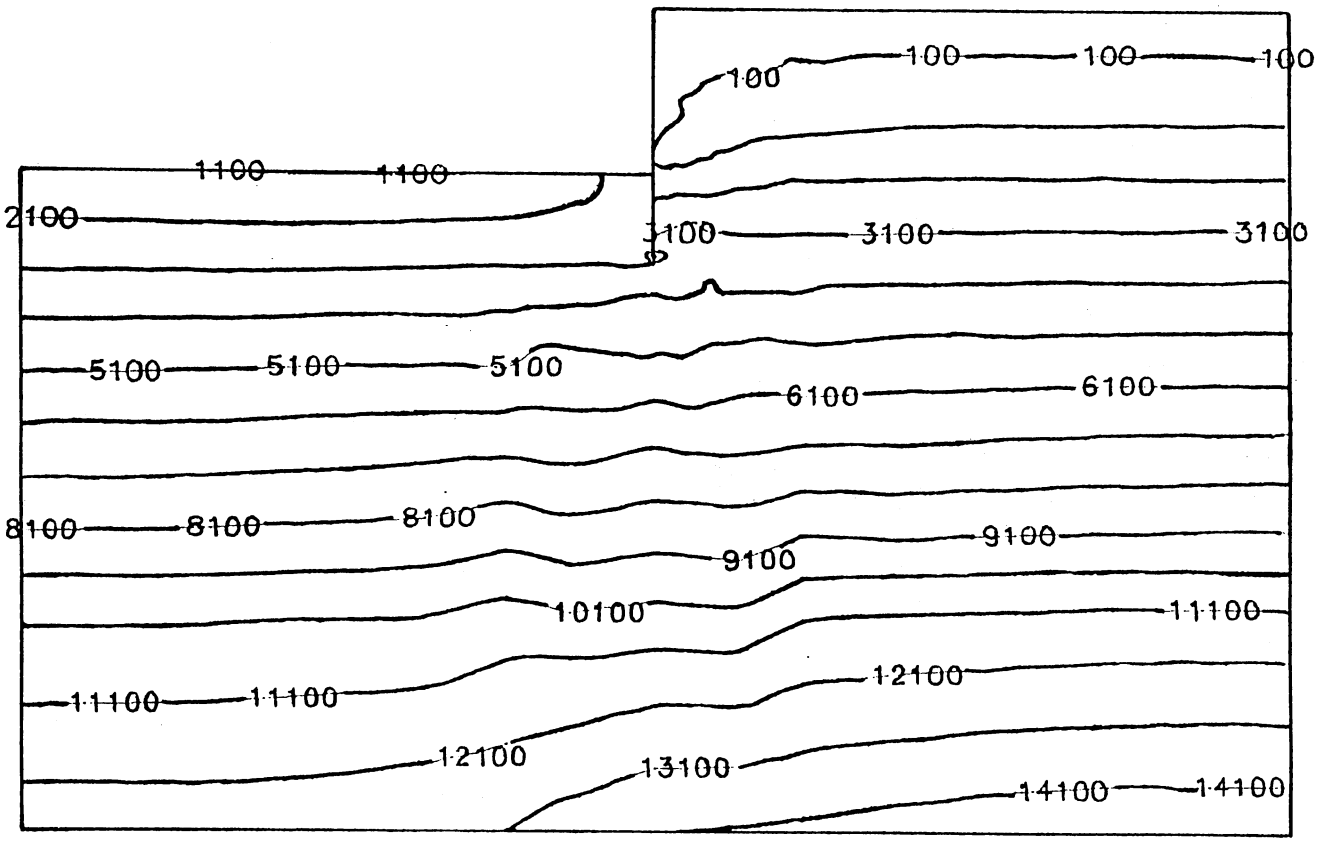

Figure 16. Horizontal stress contours from buildup analysis.
Cu = 1300 psf; depth of penetration = 15 ft.

CHAPTER VI

DISCUSSION OF RESULTS

The stress-strain behavior of soils is stress-path dependent. Therefore, the construction procedure of the wall is expected to have an important influence on stresses and displacements. Hence, it is necessary to understand the effect of the construction sequence before any meaningful analysis and comparison with the SSI method can be done. For that reason, two types of finite element analyses were carried out namely: gravity-turn-on and sequential construction (buildup) solutions.

Gravity-Turn-On Method

The gravity-turn-on method assumes that the soil-wall system exists in its final configuration from the beginning. The weight of the soil is applied gradually. At the end of each load increment, the overall stiffness matrix is modified based on the state of stress from the previous increment.

Buildup Method

In this approach, the wall is initially inserted in a level soil layer where geostatic conditions prevail (Fig. 17). For this initial layer, a gravity-turn-on analysis is carried out to initialize the stresses. The displacements obtained from this step are discarded to simulate in-situ conditions. In the subsequent steps, the retained soil

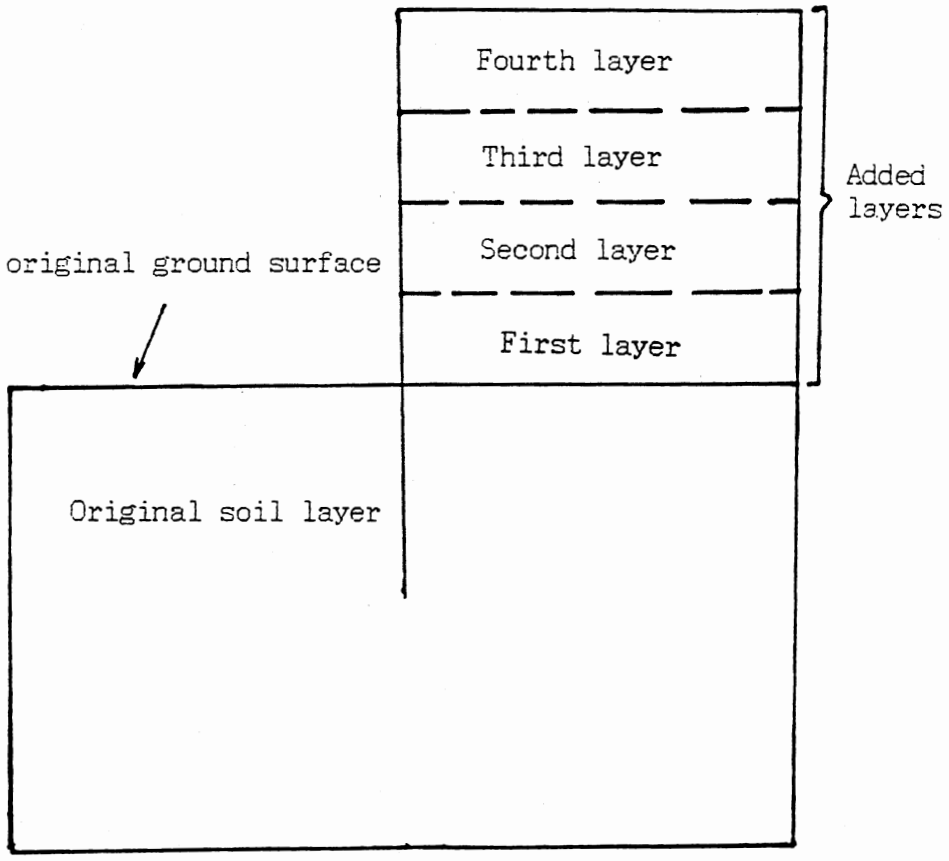

Figure 17. Simulation of Sequential Construction.

is added in layers. In this study, four such layers were used. Each layer is analyzed in substeps in order to improve the accuracy of the solution. The global stiffness matrix is updated for each increment in a manner similar to the gravity-turn-on case.

Comparison between Buildup and Gravity-Turn-On

The comparison of the behavior of the buildup and gravity-turn-on solutions includes soil modulus (E_s), moments, displacements, and net pressure profiles.

Soil Modulus (E_s)

Figs. 18-21 show stress vs. displacement curves for a typical analyzed case; namely: Cu = 1600 psf, and 30 ft depth of penetration (Figs. 18-19 for buildup and Figs. 20-21 for gravity-turn-on). Each curve represents the variation of stress (on the leftside and rightside of the wall) with the displacement of the particular point on the wall. A suitable measure of the soil modulus (E_s) values on either side of the wall is the secant modulus; i.e., the slope of the line connecting the initial and final points on the curves.(e.g., the slope of the line joining points P & P'in Fig. 18). For the Cu = 1600 psf and 30 ft penetration case, values of E_s were calculated for several locations along the pile for both the gravity-turn-on and buildup solutions. The results are shown in Table I.

It is clear from Table I that the values of E_s are lower in the buildup case. This is because the geostatic stresses in the original configuration (before the erection of the wall and the filling process) do not correspond to any deformation. For example, for Cu = 1600 psf,

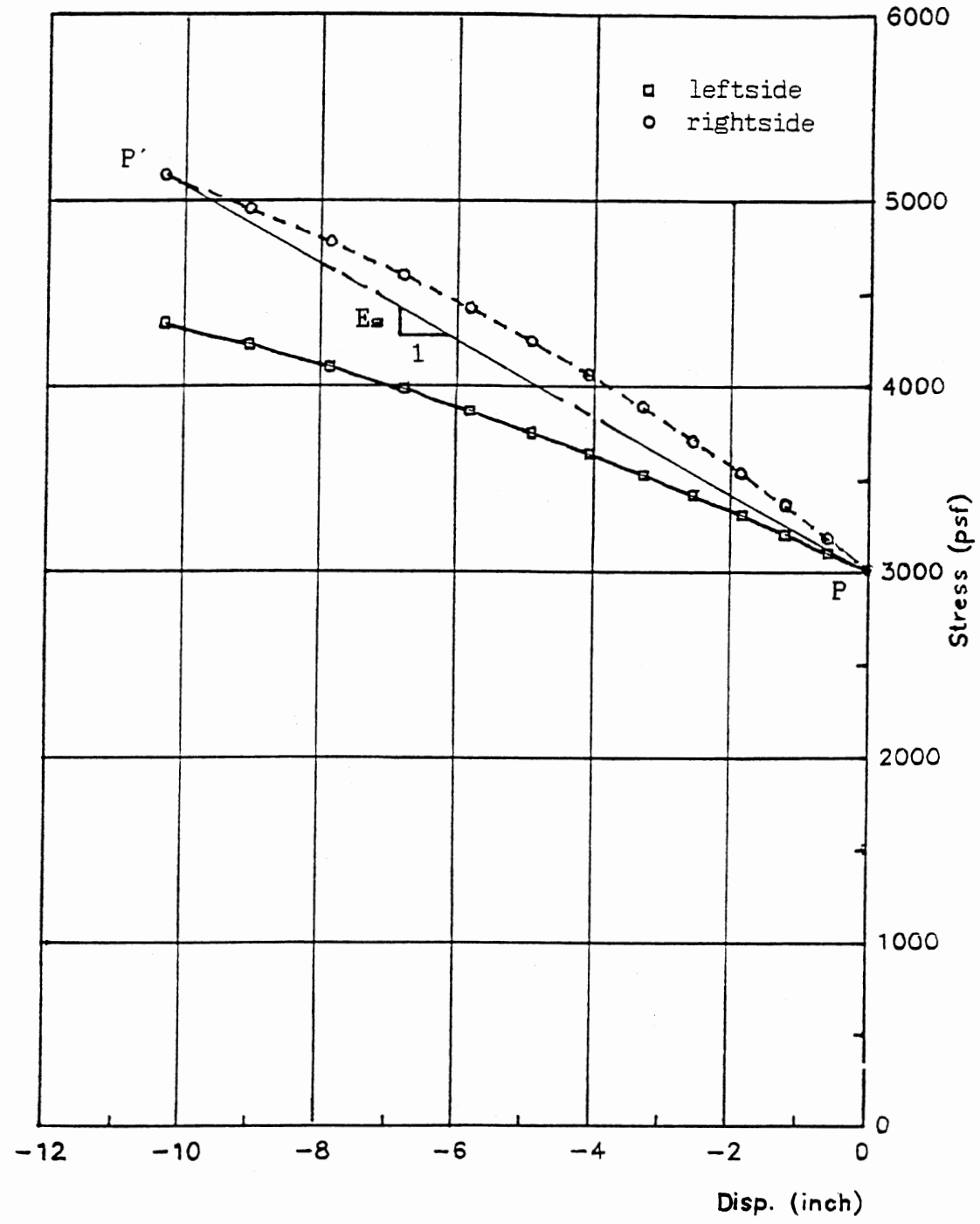

Figure 18. Soil-Response curve for points A & B (elevation = - 58 ft) Buildup analysis; Cu = 1600 psf; 30 ft pile penetration.

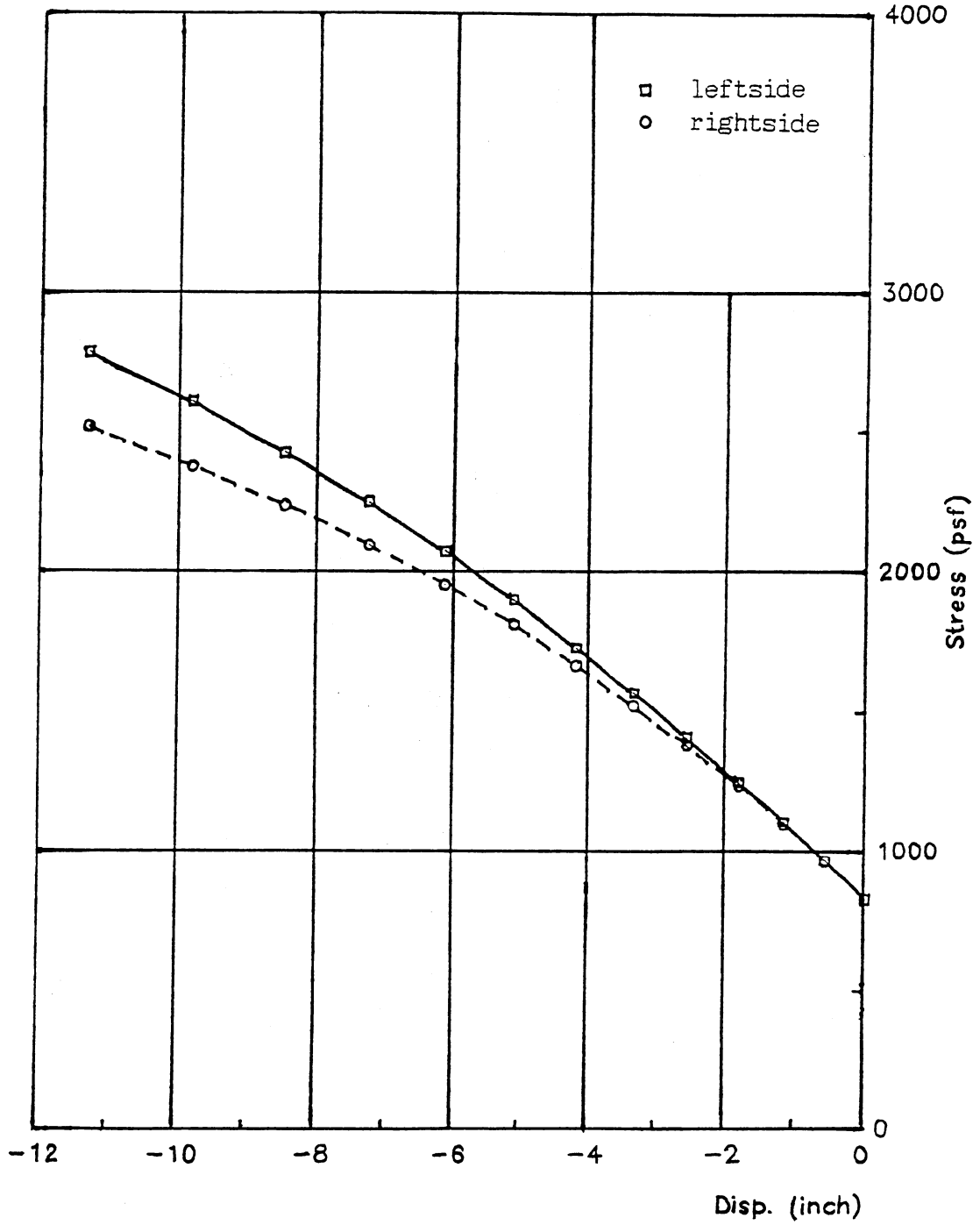

Figure 19. Soil-Response curve for points E & F (elevation = - 37 ft) Buildup analysis; Cu = 1600 psf; 30 ft pile penetration.

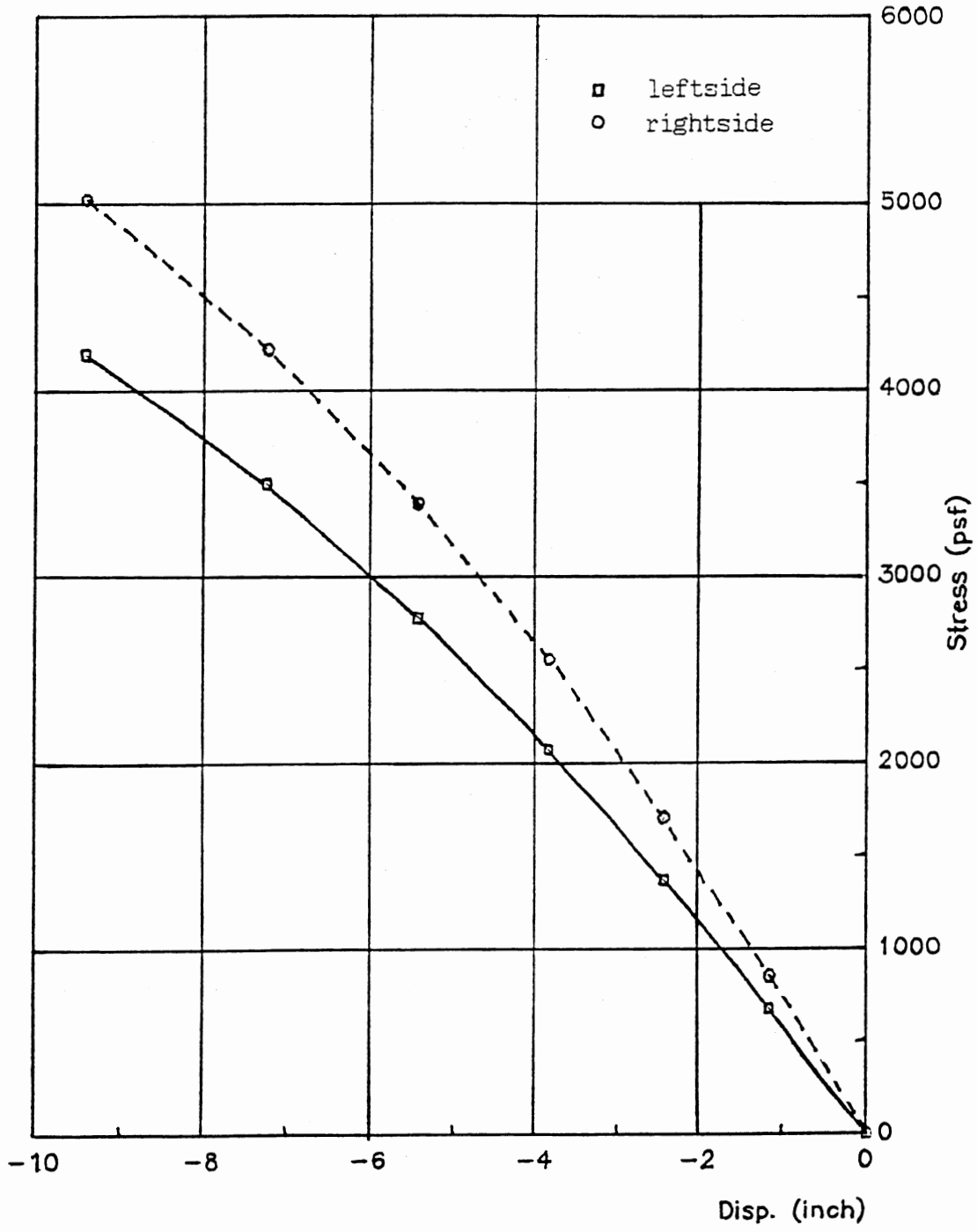

Figure 20. Soil-Response curve for points A & B (elevation = - 58 ft) Gravity-turn-on; Cu=1600 psf; 30 ft pile penetration.

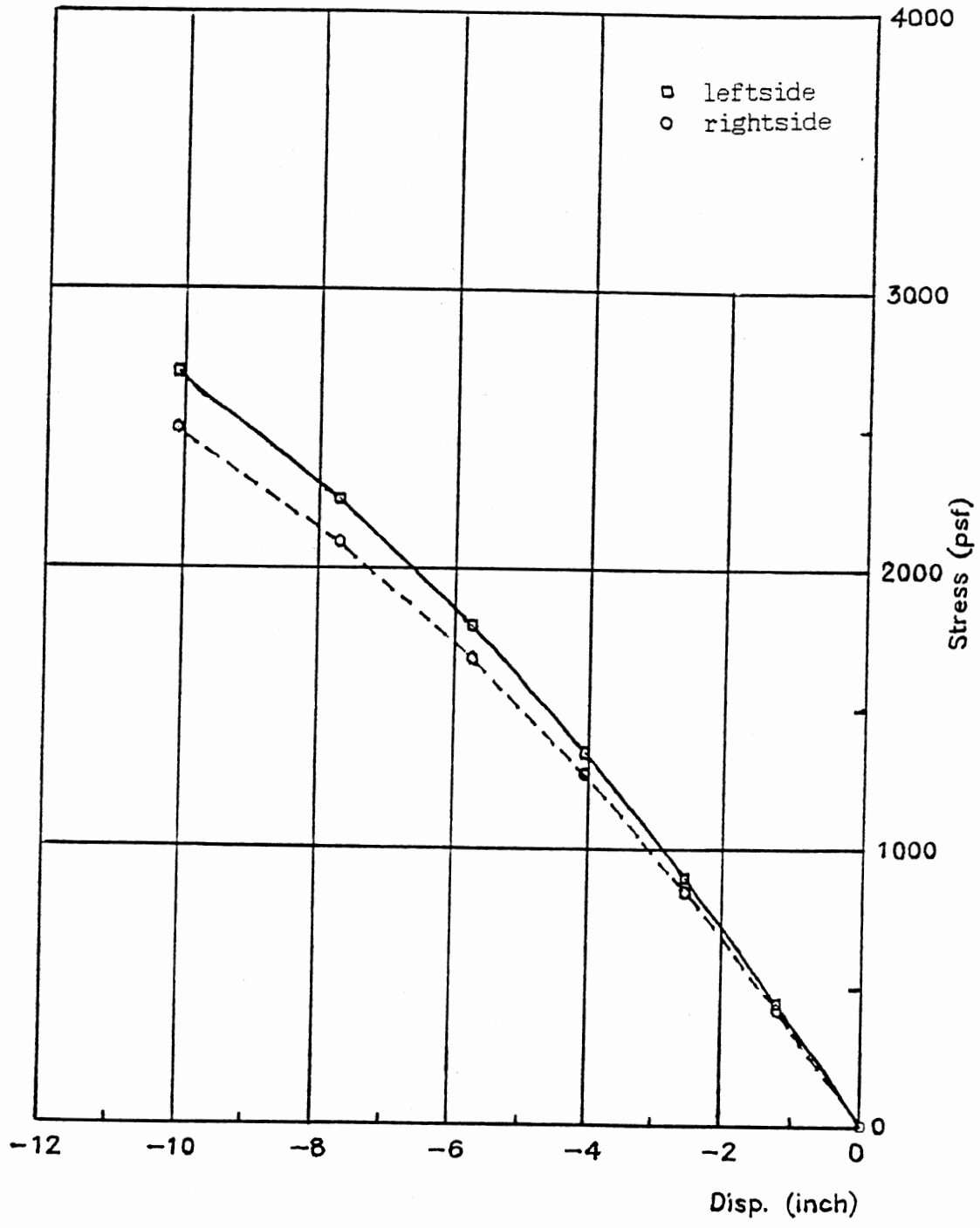

Figure 21. Soil-Response curve for points E & F (elevation = - 37 ft) Gravity-turn-on; Cu=1600 psf;30 ft pile penetration.

TABLE I

COMPARISON OF E_s FOR GRAVITY-TURN-ON & BUILDUP
FOR Cu=1600 PSF & 30′ PENETRATION

Elev.(ft)	Soil Modulus (E_s), pci			
	Leftside		Rightside	
	Gravity-Turn-on	Buildup	Gravity-turn-on	Buildup
-58.5	3.10	.82	3.7	1.41
-55.5	3.12	.91	3.2	1.08
-52.5	2.97	1.02	2.94	1.04
-49.5	2.73	1.12	2.73	1.01
-46.5	2.47	1.10	2.47	0.97
-43.5	2.22	1.07	2.22	0.94
-40.5	2.05	0.97	1.98	0.90

and 30 ft penetration depth, this corresponds to the points located on the vertical (stress) axis (e.g., point P in Fig. 18). For more illustration, stress vs. displacement plots are shown at the same location from both gravity-turn-on and buildup analyses (Figs. 22,23). The final state of the system (e.g., points M & M'in Fig. 22 is relatively close for the two cases in terms of both stresses and displacements. However, when the secant modulus was calculated in the buildup case (E_{s2} in Fig. 23), the value of in-situ geostatic stress ($\approx$ 500 psf) was subtracted from the final stress resulting in smaller values of E_s in comparison to the gravity-turn-on case ($E_{s1} > E_{s2}$ in Fig. 23).

Bending Moments

Table II shows the maximum negative moment values obtained from the buildup and gravity-turn-on analyses for different values of Cu. The convention used in this study is that negative moment produces compression on the leftside of the wall. It is clear that for any value of Cu, the maximum moment is larger for the buildup case than for the corresponding gravity-turn-on case. However, the location of the maximum moment is almost the same for the two cases. This is best illustrated in Fig. 24 for the Cu = 1600 psf and 30 ft depth of penetration and is equally valid for all the other cases. The reason for this difference in maximum moment magnitudes is that the system is stiffer in the gravity-turn-on case because all the soil is present throughout all the load increments. Therefore, each element contributes to the global stiffness of the system from the beginning. Also, as discussed before, the soil stiffness (E_s) is higher for the

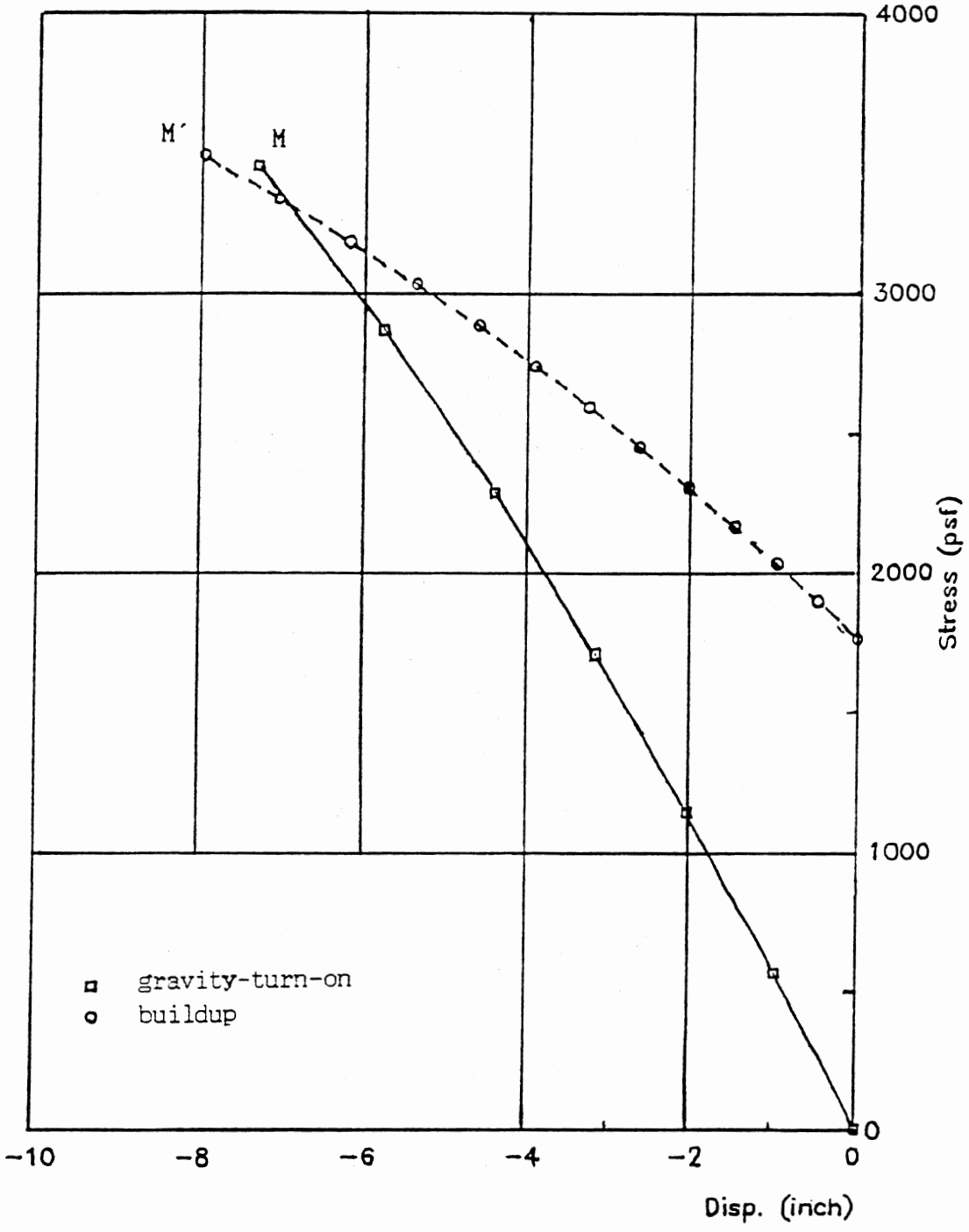

Figure 22. Soil-Response curve for point C (elevation = - 46 ft) Cu = 1600 psf; 30 ft pile penetration.

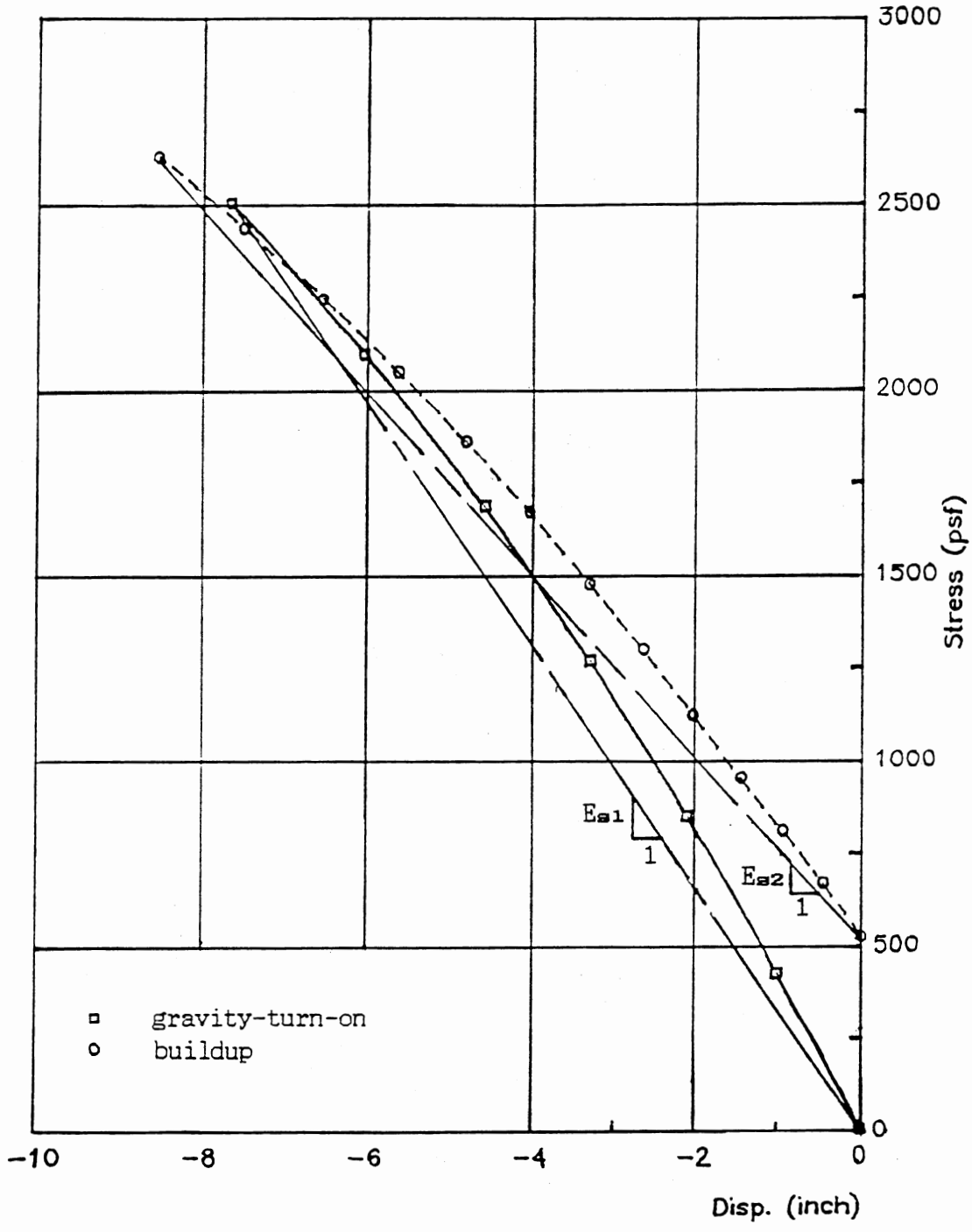

Figure 23. Soil-Response curve for point H (elevation = - 34 ft)
Cu = 1600 psf; 30 ft pile penetration.

TABLE II

MAXIMUM BENDING MOMENTS & THEIR LOCATIONS

Description	maximum -ve moment(k-ft)	Elev.(ft)
grav-turn-on cu=1000 psf 30′penetration	13.2	-37.5
buildup cu=1000 psf 30′penetration	18.2	-38.0
grav-turn-on cu=1300 psf 30′penetration	10.8	-35.2
buildup cu=1300 psf 30′penetraion	15.9	-35.2
grav-turn-on cu=1600 psf 30′penetration	9.5	-34.9
buildup cu=1600 psf 30′penetration	14.0	-35.0
grav-turn-on cu=1300 psf 20′penetration	12.8	-36.0
grav-turn-on cu=1300 psf 15′penetration	13.0	-35.0

* Maximum negative bending moments and their locations for the different cases.

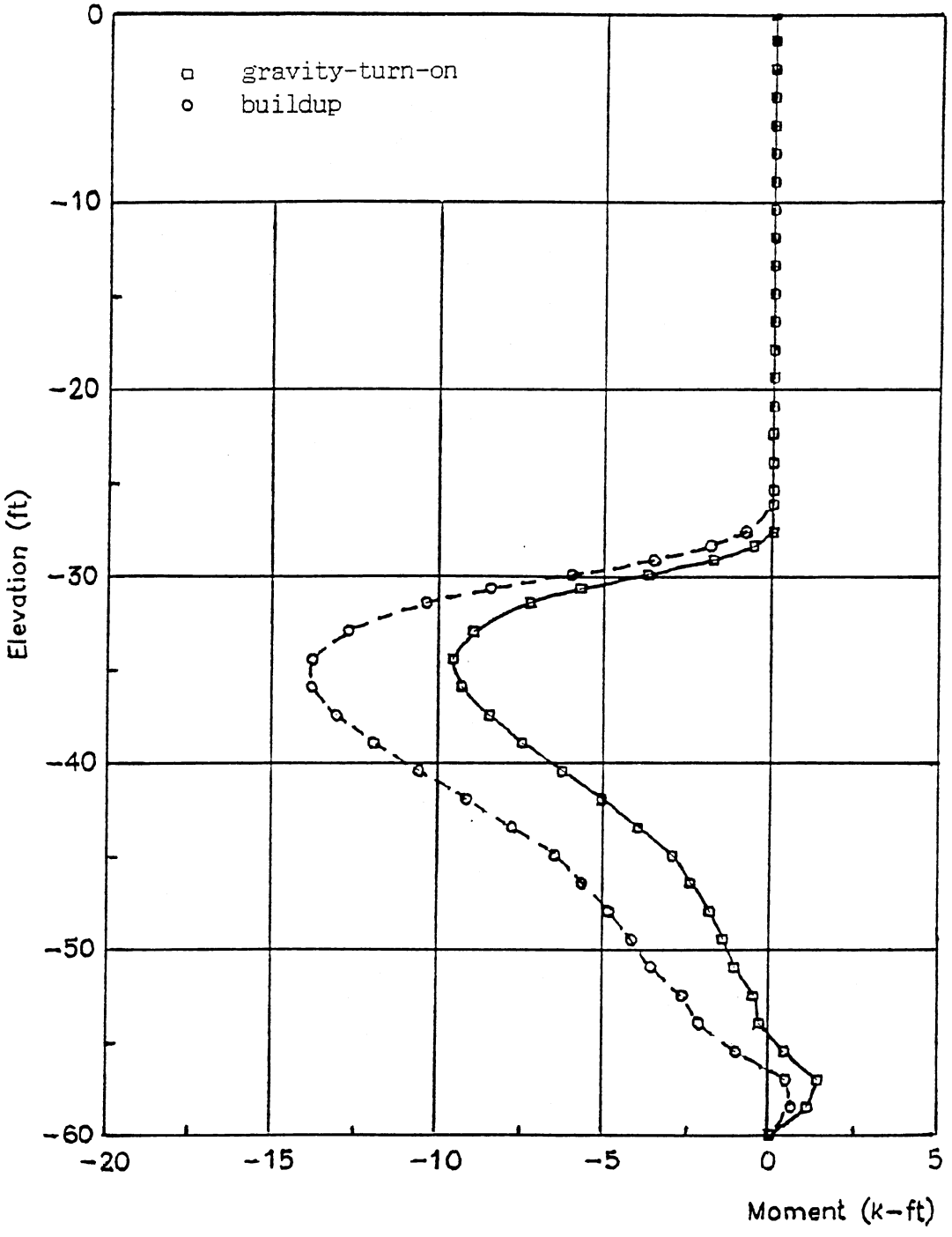

Figure 24. Bending moments vs. Elevation. Cu = 1600 psf. Depth of penetration = 30 ft.

gravity-turn-on solution. Because of that, the soil matrix, for the gravity-turn-on case, carries a larger portion of the total load (weight of the soil) thus resulting in smaller moments in the wall.

Lateral Displacement

Fig. 25 shows the lateral displacements for the same typical case analyzed before (Cu = 1600 psf, 30 ft penetration). It is clear from the figure that the displacements are higher for the buildup case. Because the effective stiffness of the soil is higher for the gravity-turn-on case, the resulting displacements are lower.

Net Soil Pressure

Fig. 26 shows the net soil pressure on the pile. The net pressure above the natural ground surface is larger for the buildup case. Furthermore, the figure shows that the tension crack is deeper for the gravity-turn-on case thus resulting in a smaller moment arm. These two reasons are mainly responsible for the higher moments observed in the buildup case. It is also interesting to note that for the lower 20 feet of the pile, the net pressure distributions are almost identical for the gravity-turn-on and buildup cases.

The difference between the gravity-turn-on and buildup solutions serves to underscore the fundamental significance of the stress-strain path due to the nonlinear nature of the soil. It also emphasizes the importance of initial stresses and/or strains in determining the behavior of the system. However, it is worth noting that the difference between the gravity-turn-on and buildup solutions is only quantitative in nature i.e., the only difference is in magnitude and not in the

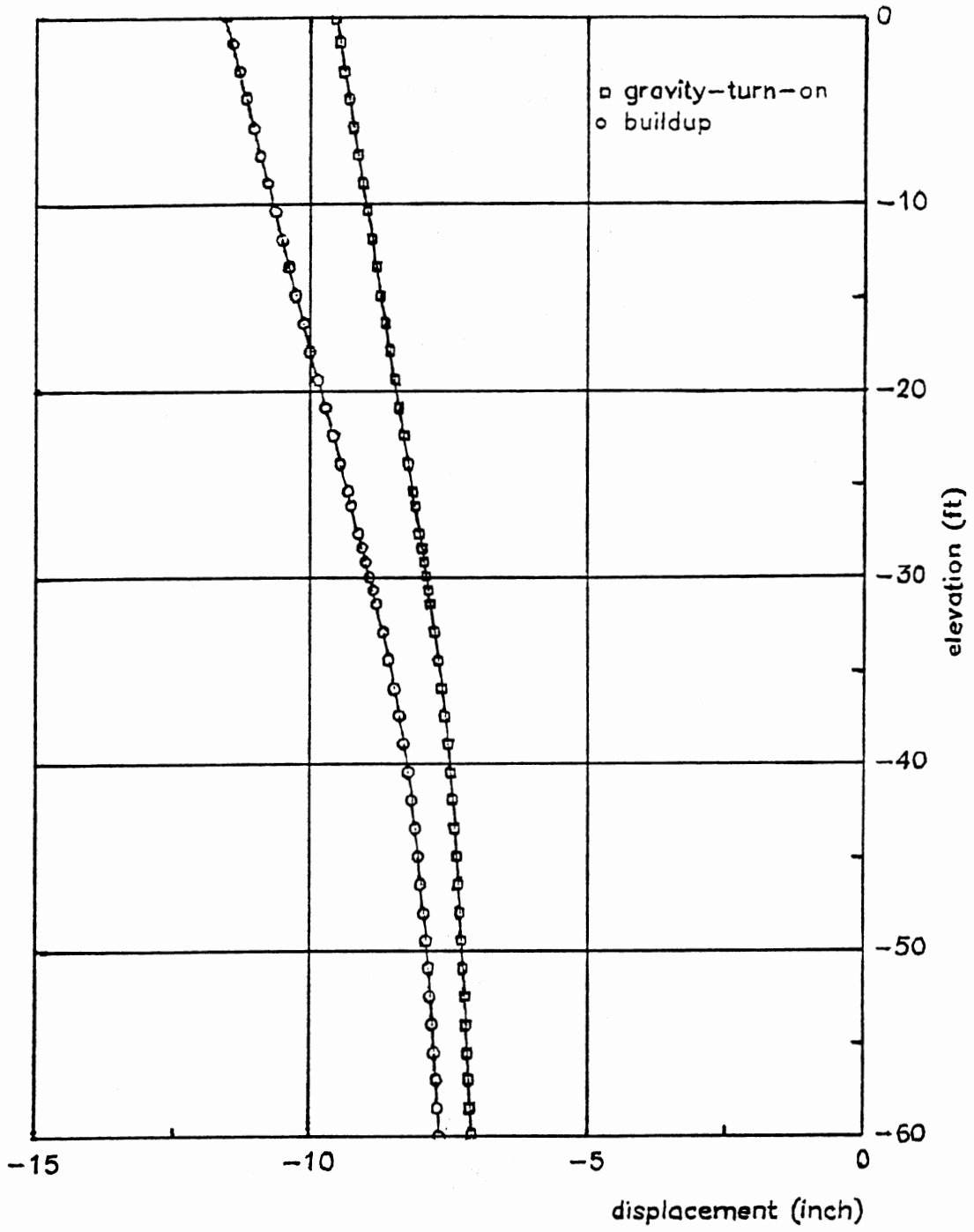

Figure 25. Pile deflection vs. Elevation. Cu = 1600 psf. 30 ft pile penetration.

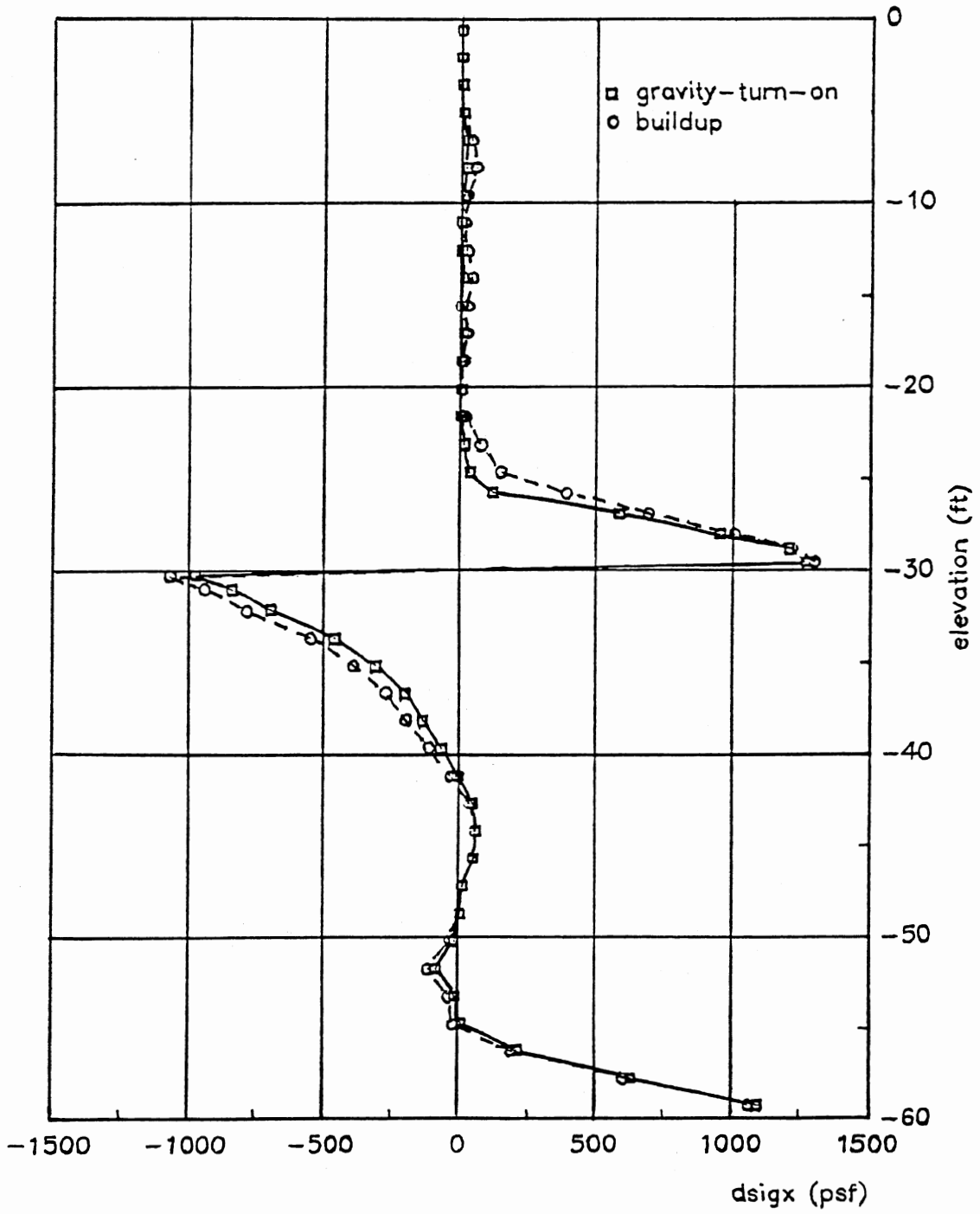

Figure 26. Net stress profile on the pile. Cu = 1600 psf. 30 ft pile penetration.

general behavior. For that reason, in what follows usually the gravity-turn-on solution is referred to unless otherwise specified.

The rest of the discussion focuses on the following points:

1. Analysis of some aspects of the general behavior obtained from the finite element solutions.
2. Analysis of some aspects of the SSI solutions.
3. A comparison between the finite element and the SSI results. This includes using the FE solutions to investigate some of the underlying assumptions of the SSI method.

The general aspects of behavior obtained from the FEM are:

1. Stress contours: vertical, horizontal, shear, and f contours.
2. Stress paths for critical locations along the pile.
3. The effect of varying the soil cohesion (Cu).
4. The effect of varying the penetration depth.

Stress Contours

Horizontal Stress Contours

The horizontal stress contours can be used to determine whether active or passive behavior is taking place at the wall. Under geostatic conditions, these contours are horizontal. The stress contours dip downward if the soil is exerting active pressure on the wall. By the same token, if these stress contours move upward, the soil is exerting passive pressure on the wall.

Figs. 27-28 show typical horizontal contours in the soil mass. These contours are obtained from a gravity-turn-on analysis and correspond to Cu = 1000 psf and 1300 psf and 30 ft penetration depth.

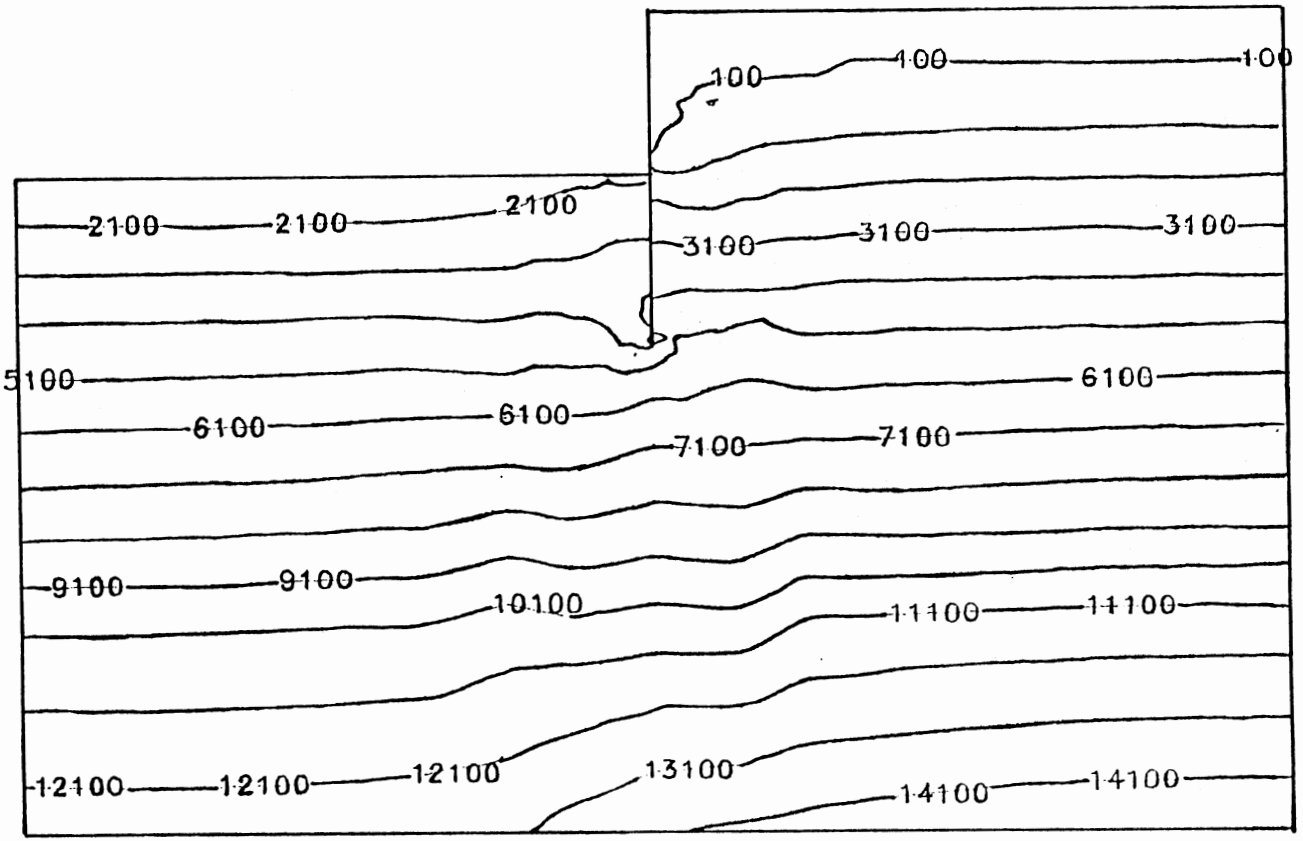

Figure 27. Horizontal stress contours from gravity-turn-on analysis.
Cu = 1000 psf, 30 ft pile penetration.

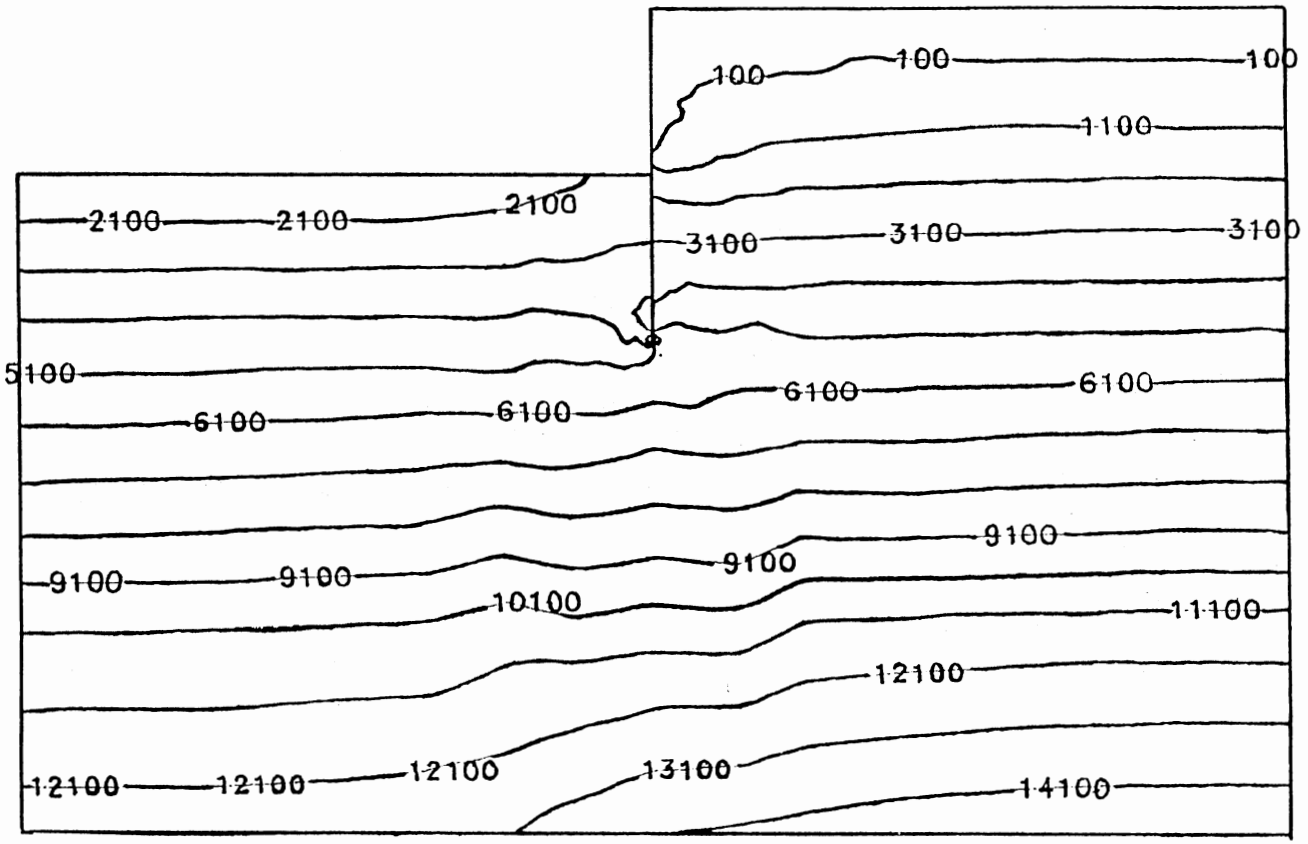

Figure 28. Horizontal stress contours from gravity-turn-on analysis.
Cu = 1600 psf, 30 ft pile penetration.

It is apparent that the retained soil is in an active condition where the horizontal stress contour drops sharply near the top surface. This sharp drop decreases when moving downward (up to 10 ft below the original ground surface). At this elevation, soils on both sides of the wall have the same stress magnitude. This observation includes all the soil between elevation -45 ft to -55 ft in the 30 ft penetration case. This resulted in an idle pressure zone in the sense that the net pressure exerted on the pile is near zero.

The soils in front of the wall, from the original ground surface to a zone extending 10 ft below, are in a passive state. Also, a region of stress concentration exists around the pile tip.

The above-described behavior was observed for all the cases analyzed in this study.

Vertical Stress Contours

Typical vertical stress contours are shown in Figs. 29-30 for Cu = 1600 psf, and 1000 psf and an embeddment depth of 30 ft. As expected, the vertical stress on the right is higher than that on the left. The transition from right to left is most severe near the tip of the pile (high stress concentration) and it becomes smoother with increased depth. One particular location of interest is at the tip of the tension crack in the retained soil where a sharp drop in vertical stress is observed. At that location, the soil column above is moving away clockwise thus reducing the vertical stress. Close to the bottom of the wall, the vertical stress increases (compared to geostatic stresses) on the right side and decreases on the left side due to incompressibility.

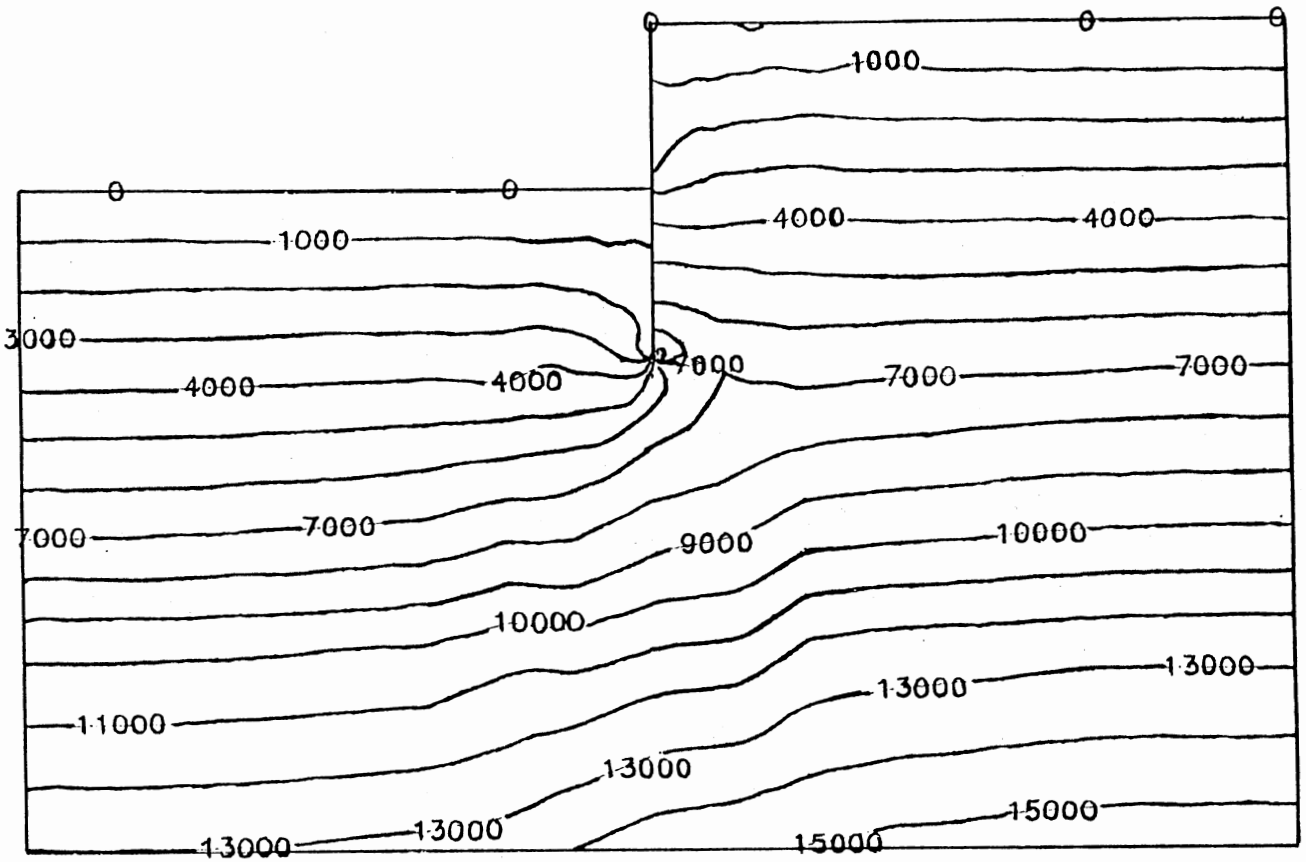

Figure 29. Vertical stress contours from gravity-turn-on analysis.
Cu = 1600 psf, 30 ft pile penetration.

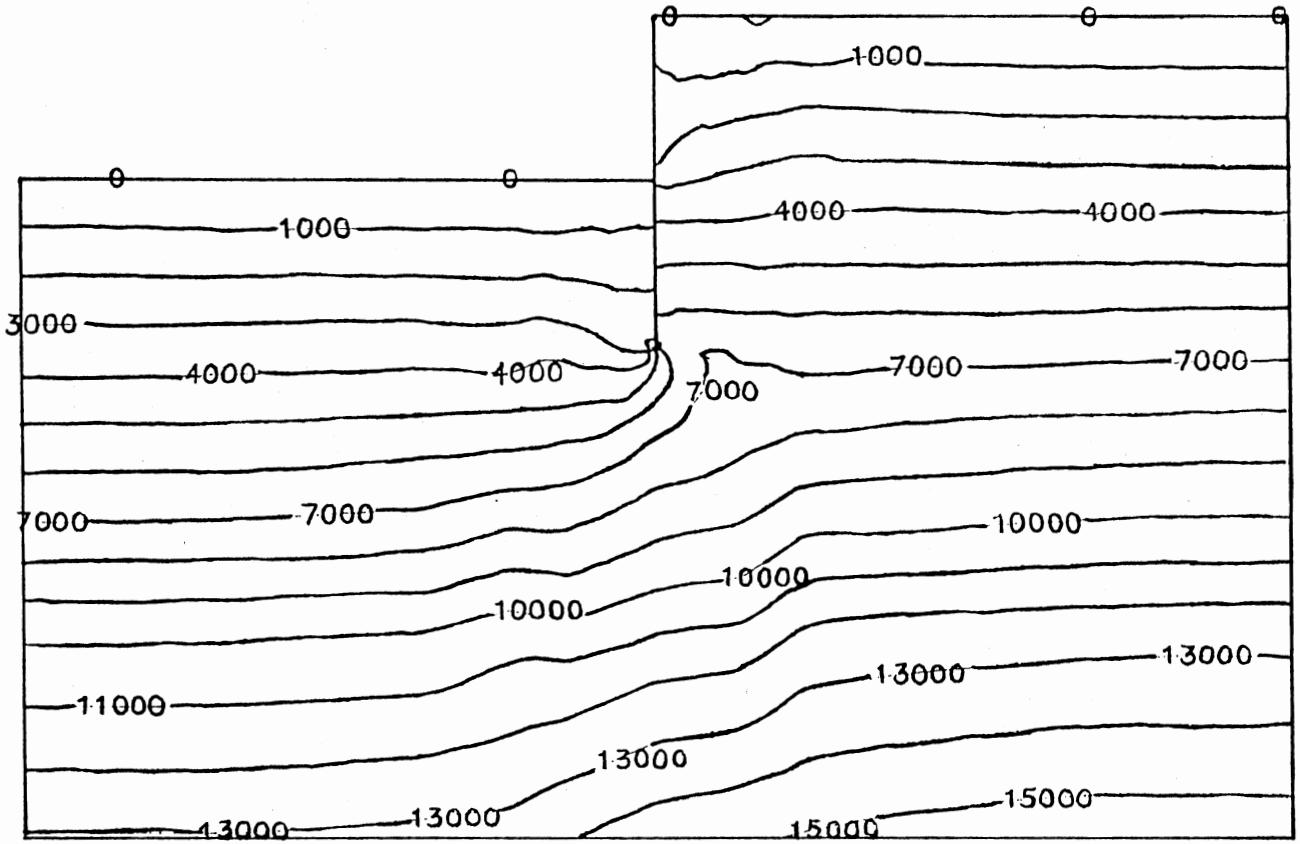

Figure 30. Vertical stress contours from gravity-turn-on analysis.
Cu = 1000 psf, 30 ft pile penetration.

This is best illustrated by buildup analysis for Cu = 1000 psf and penetration depth = 30 ft. A plot of horizontal versus vertical stress is shown for two elements to the left of the wall (Figs. 31,32). The points labelled 1 on both plots represent the original soil layer under geostatic conditions. It is clear that while the other soil layers were being added, the vertical pressure decreased considerably. A minimum value was reached when the third layer was added. At this stage, the vertical stress started to recover some of its original value. However, the final vertical stress level is smaller than the value under geostatic conditions. This decrease in vertical stress is due to the upheave resulting from the incompressibility of the soil. On the other hand, some soil elements on the right side experience an increase in vertical stress.

The behavior described above is common to all the cases investigated in this study.

Shear Stress Contours

Typical shear stress contours are shown in Figs. 33-34 for the 30 ft penetration case and Cu = 1000 and 1600 psf respectively. As in the case of the vertical and horizontal stresses, the tip of the pile is an area of high shear stress gradient. In the region extending from the tip of the tension crack to the soil surface, negative shear values are observed. This is due to the clockwise motion of the retained soil. At a sufficient depth, the shear contours become almost vertical indicating that the shear becomes constant with depth. The near symmetry of the shear stress contours indicates that the pile did not affect the general state of stress except at some sensitive locations in

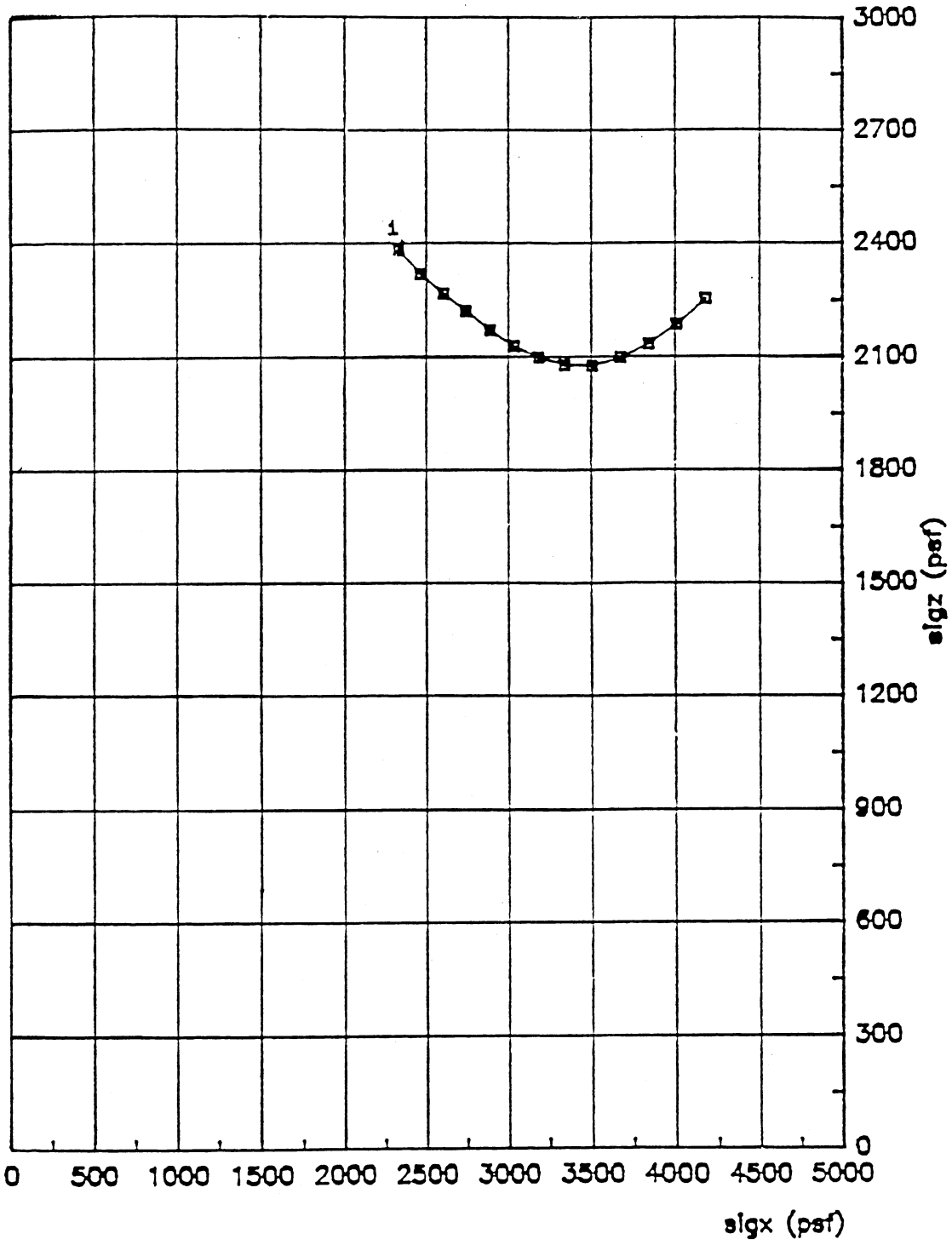

Figure 31. Horizontal vs. vertical stress at point D (Elev.= -50 ft) Buildup analysis; Cu = 1000 psf; 30′ penetration.

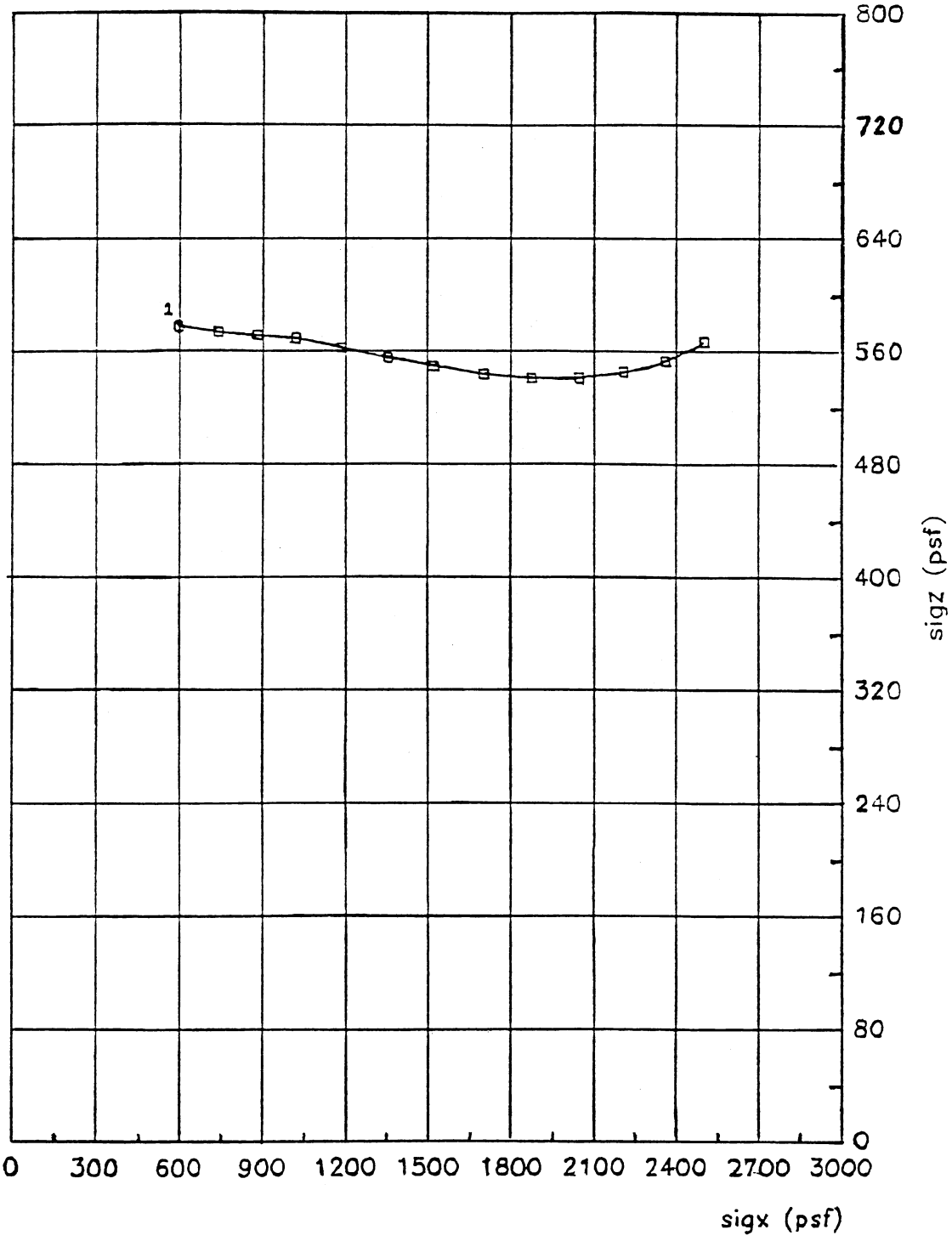

Figure 32. Horizontal vs. vertical stress at point F (Elev.= - 37 ft) Buildup analysis; Cu = 1000 psf; 30 ft penetration.

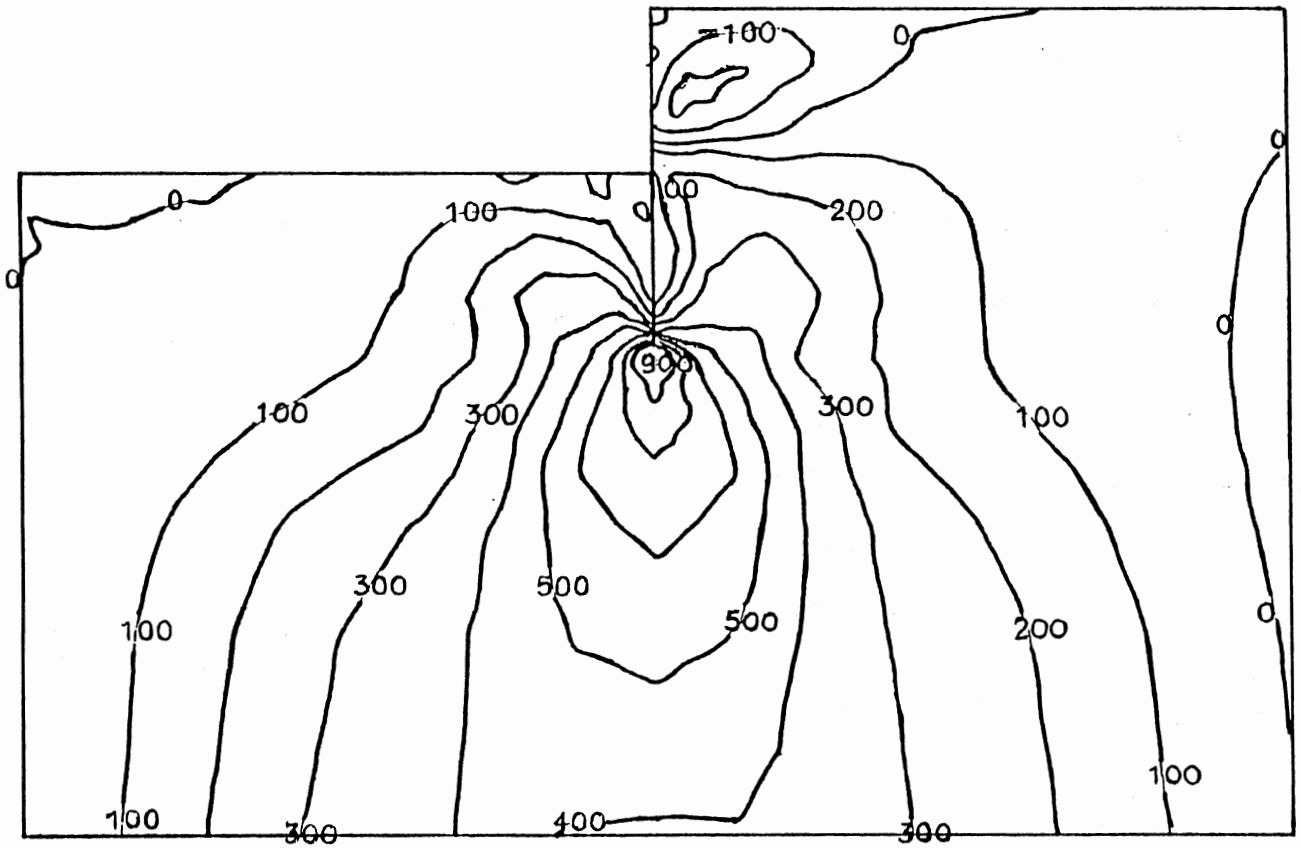

Figure 33. Shear stress contours from gravity-turn-on analysis.
Cu = 1000 psf, 30 ft pile penetration.

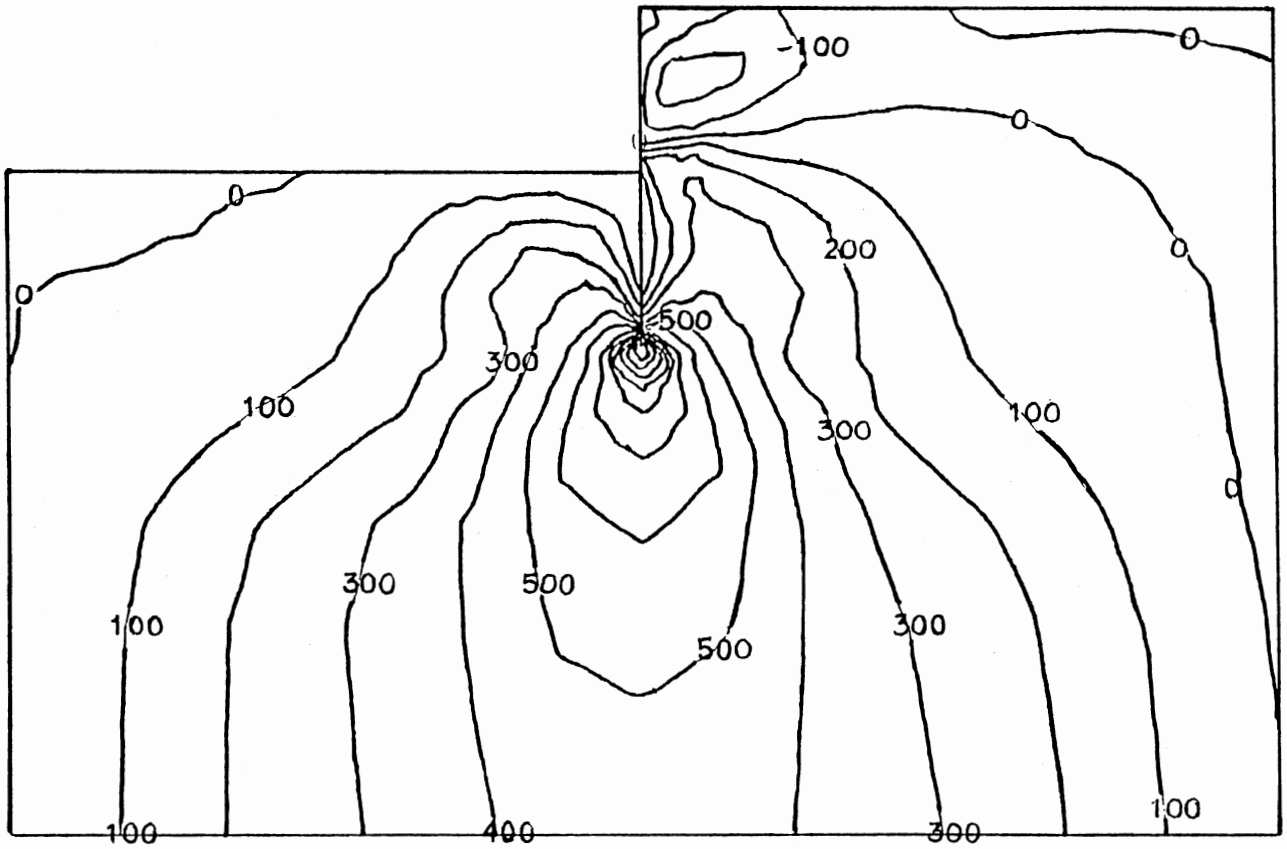

Figure 34. Shear stress contours from gravity-turn-on analysis.
Cu = 1600 psf, 30 ft pile penetration.

its vicinity.

The same behavior was observed for all the cases analyzed in this study.

Degree of Mobilization Contours

The degree of mobilization is a very effective way to describe the proximity of the soil elements to failure. It is a nice luxury that is exclusive to the finite element method. It offers a global picture of the overall behavior of the system. Figs. 35-36 are contour plots for the degree of mobilization for Cu = 1000 and 1600 psf and 30 ft penetration depth for the gravity-turn-on case. From the figures, the following observations can be made:

1. In the retained soil, the degree of mobilization increases going downward towards the original ground surface. It starts at about 10 % at zero elevation and increases to about 70% for the Cu = 1000 psf case and to 50 % for the Cu = 1600 psf case in the region around the tip of the tension crack.

2. The soil to the left of the wall at the level of the original ground surface is in a passive state. The degree of mobilization in that region is about 80% for Cu = 1000 psf and 70% for Cu = 1600 psf. In general, the passive area to the left of the wall is at a degree of mobilization of about 75% . On the other hand, the soil to the right of the wall is in an active state and the degree of mobilization is about 80% for Cu = 1000 psf and 60% for Cu = 1600 psf.

3. The area around the tip of the pile is the area with the highest degree of mobilization ($\approx$ 95 %) for all cases. This is due to the stress concentration in that region.

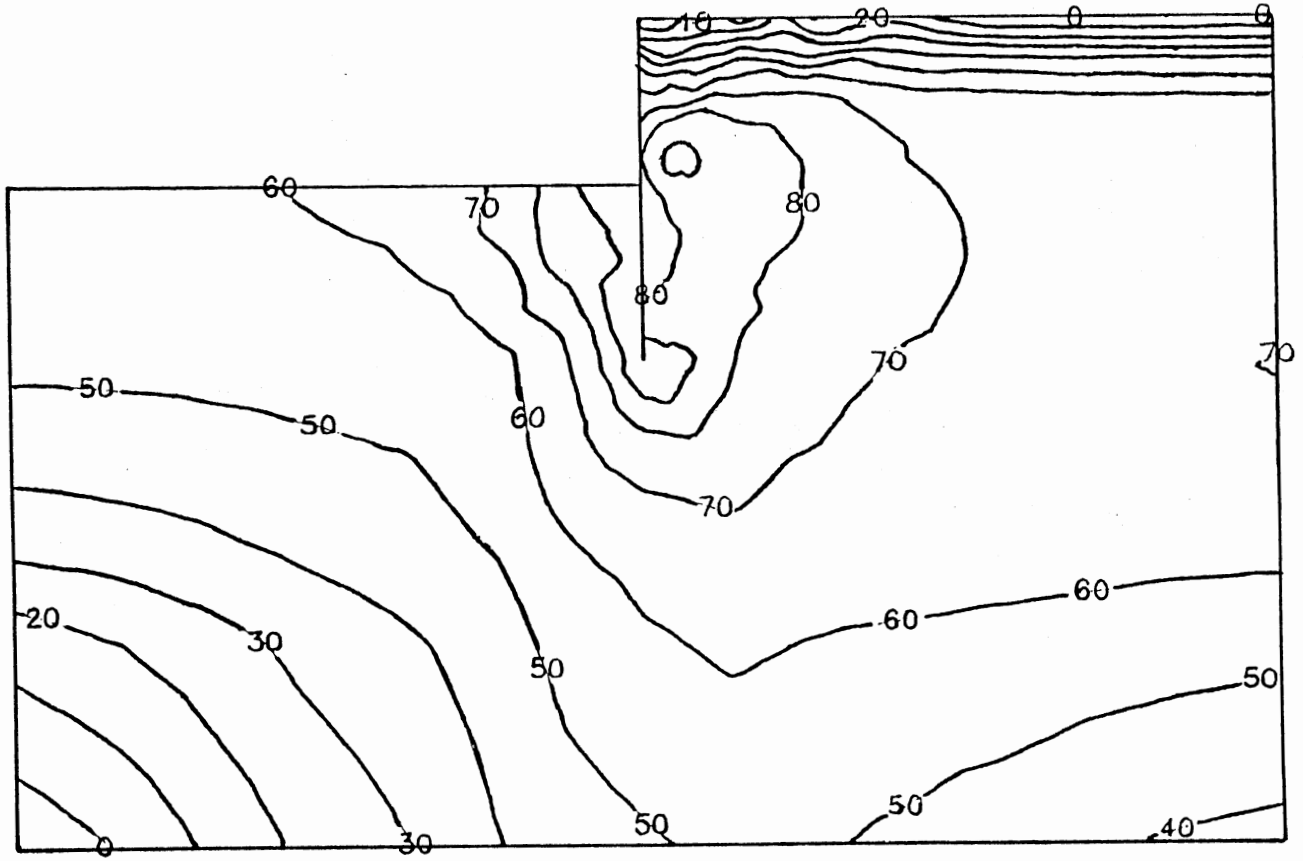

Figure 35. f contours from gravity-turn-on analysis.
Cu = 1000 psf, 30 ft pile penetration.

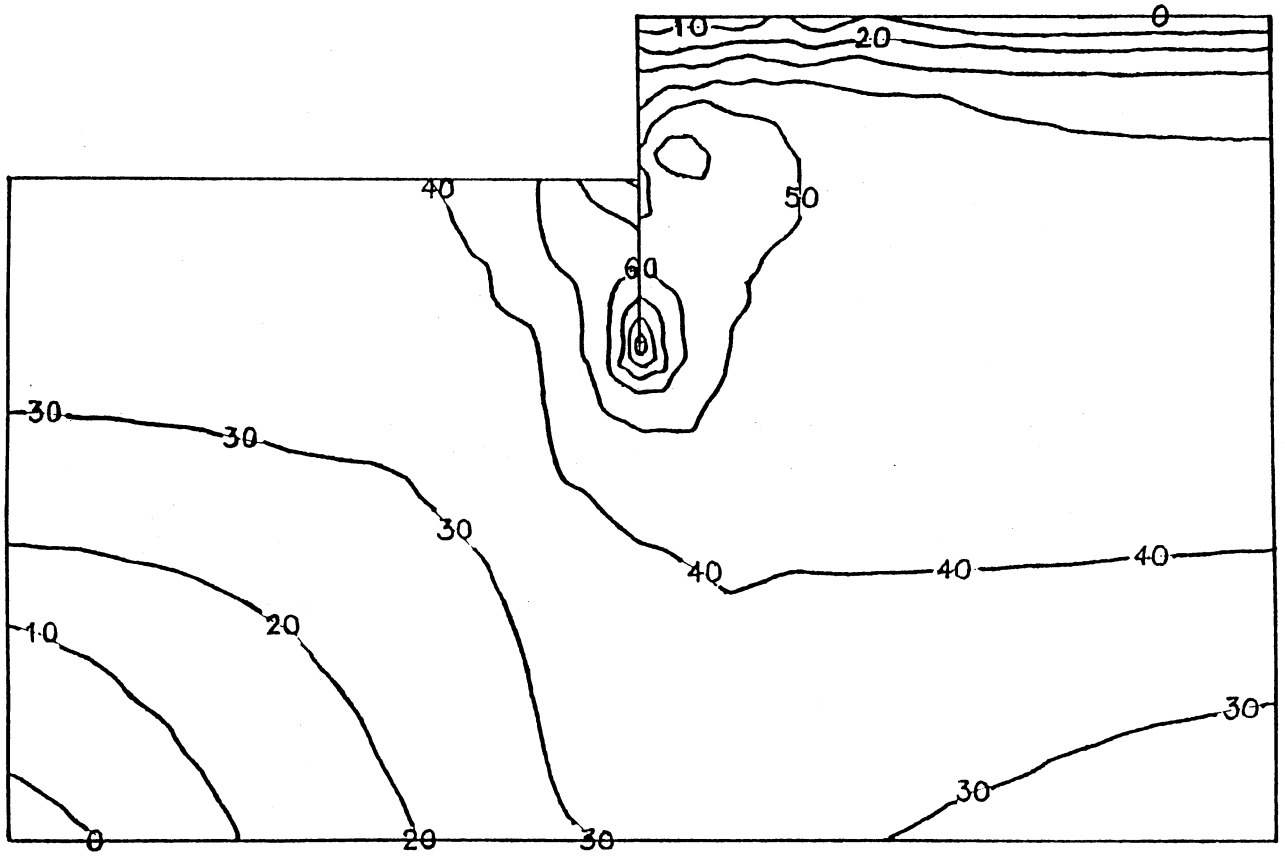

Figure 36. f contours from buildup analysis, Cu = 1600 psf. 30 ft pile penetration.

It is clear from Figs. 35-36 that the level of stress and hence the f values increase as the value of Cu decreases. However, that the behavior is the same qualitatively. The only discernible difference is that the f-contours are higher at all the locations for the lower Cu case with the exception of the area around the tip of the pile where the degree of mobilization is around 1 for both cases. Furthermore, the rate of change of the f-contours is much faster for the lower Cu case since more soil elements are getting progressively closer to failure.

The degree of mobilization contours show clearly that for this class of problems local failure can occur in some soil elements without causing the overall failure of the retaining wall.

Stress Paths

Stress-path diagrams shed light on the general behavior of the soil particularly at certain locations of interest. The stress path represents the locus of the top points on the Mohr circles. It represents the states of stress that the element goes through during its loading history. A stress path is also known as a p-q diagram where p and q are defined as follows:

$$p = (\sigma_1+\sigma_3)/2, \quad q =(\sigma_1-\sigma_3)/2$$

As can be easily seen, p represents the abscissa of the center of Mohr's circle and q is the radius of the circle and it is also the value of the maximum shear stress that is experienced by the particular soil element. Stress-path diagrams were made for different soil elements for the different cases studied. For convenience, the q values were plotted

as negative values when the soil element is experiencing a passive state of stress. On the other hand, the q values were left positive for the active state. In the classical theory, the active and passive pressures were always assumed to be principal stresses which can, at times, cause some confusion in interpreting the horizontal stress on the wall as being active or passive since it is usually not a principal stress. This is especially true in areas of high shear stress and high stress concentrations. One important line of interest on any stress-path diagram is the K_f line which goes through the highest points on all failure Mohr circles, i.e., circles that are tangent to the Mohr-Coulomb failure envelope. This K_f line for the p-q diagram is equivalent to the envelope in a Mohr-Coulomb type formulation. For all the cases studied, the K_f line is a horizontal line whose ordinate is $\pm$ Cu because of the ϕ = 0 condition. The distance between the point representing the state of stress and strain and the K_f line is a measure of the proximity of that element to failure and is another indication of the degree of mobilization.

Fig. 37 is a stress-path for an element located at 4 ft below the original ground surface (location H in Fig. 11) for 30 ft penetration depth and Cu = 1300 psf. The element referred to is located to the left of the wall and it is in a passive state as expected (negative q values). The final point on the graph is still far from failure (K_f line).

Another stress path for an element about 7 ft below the original ground surface to the right of the wall (location E in Fig. 11) is shown in Fig. 38. This figure indicates that the element is in active (q is positive). Furthermore, this element is still far from the

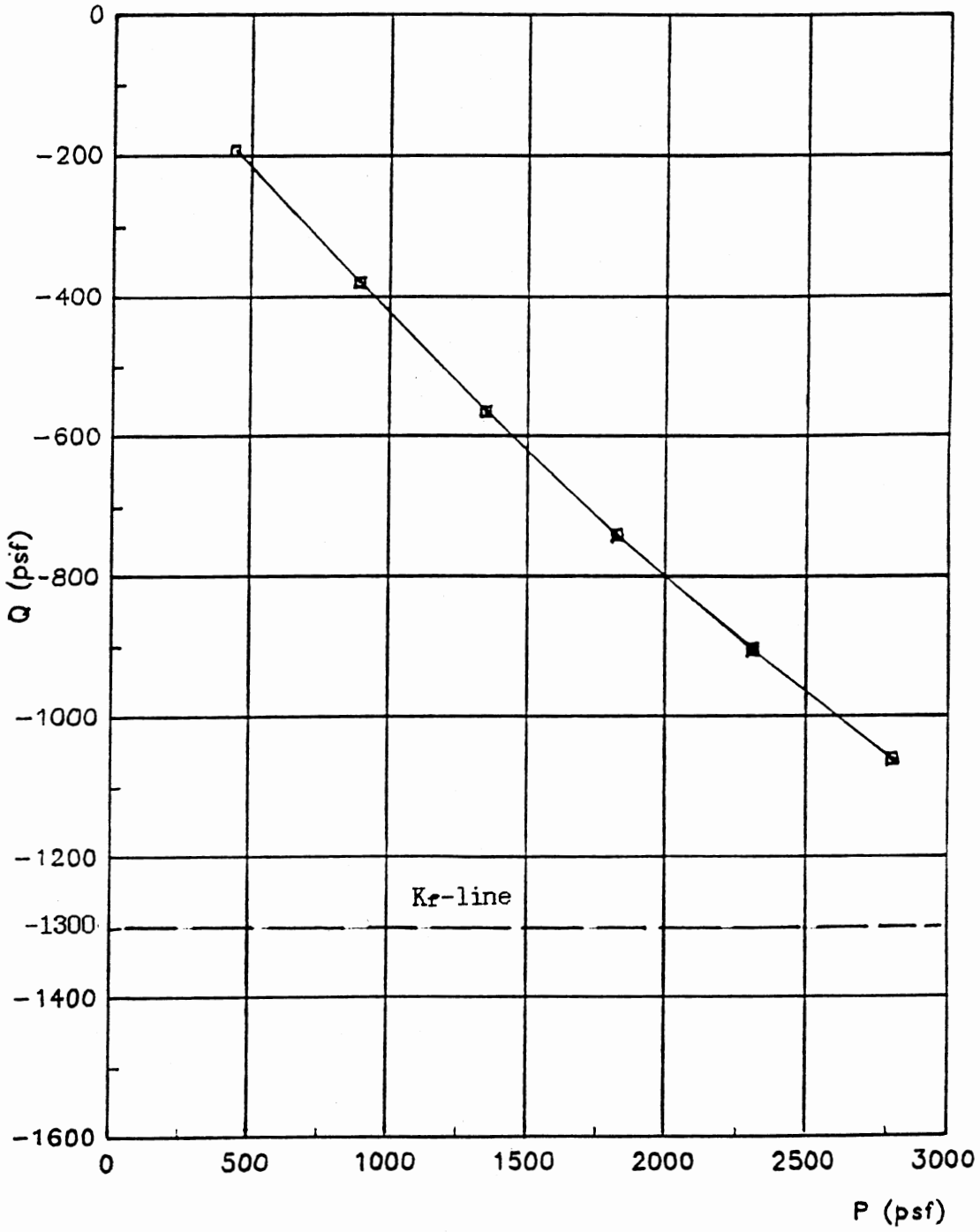

Figure 37. Stress path at point H (Elev.=-34 ft); gravity-turn-on. Cu = 1300 psf, 30 ft pile penetration.

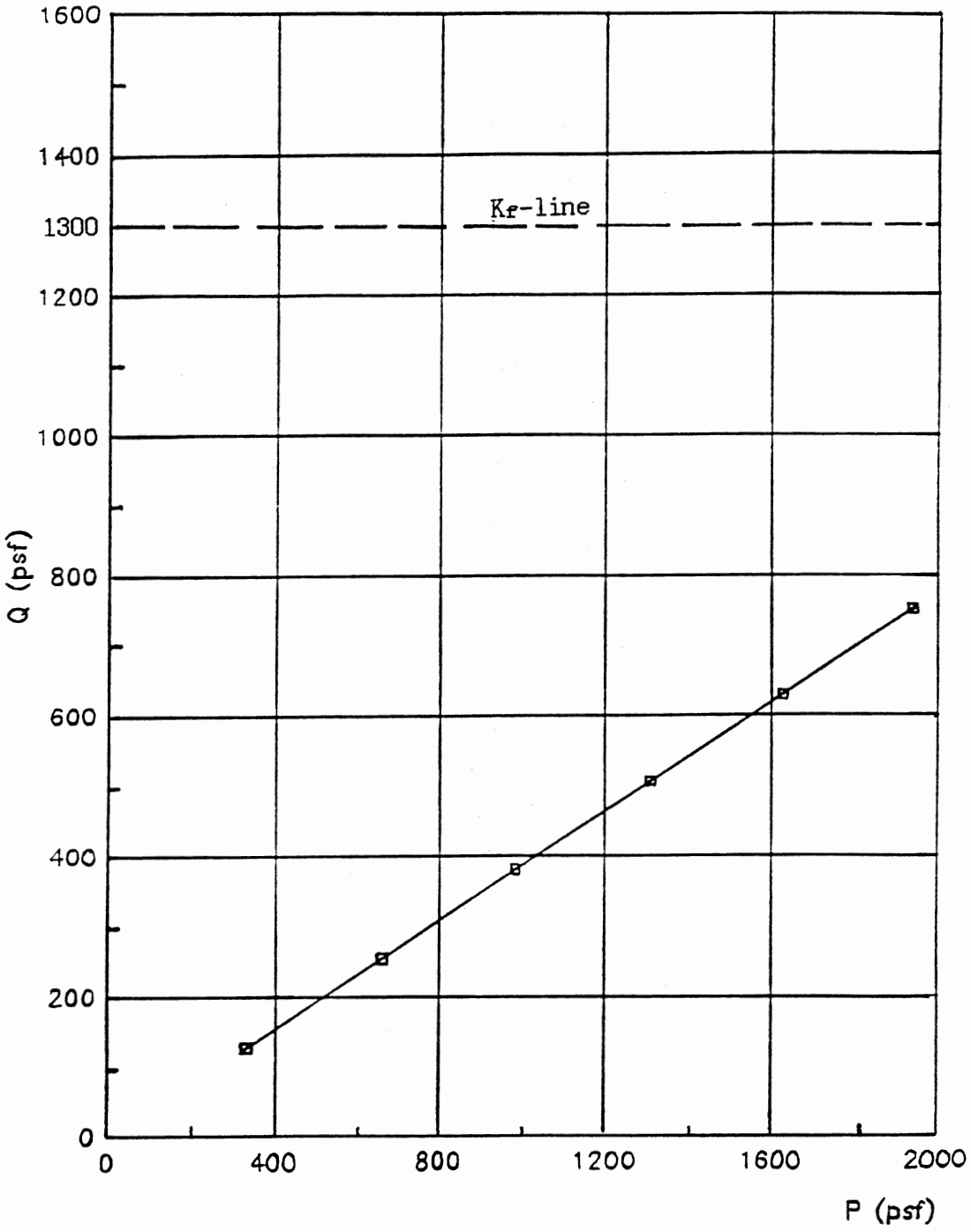

Figure 38. Stress path at point E (Elev.=-37 ft); gravity-turn-on. Cu = 1300 psf, 30 ft pile penetration

failure envelope (q = 1300 psf). An interesting observation is that the p-q diagram is almost linear which means that the major principal stress, σ_1, varies linearly with the minor principal stress, σ_3. The linear variation suggests that K_a, for that particular element, is constant throughout the loading stages.

Figs. 39-40 show the stress paths near the tip of the pile (points A & B). It is clear from Fig. 39 that the soil to the left of the pile tip is in a passive state and very close to failure (proximity to K_f line). Similarly Fig. 40 demonstrates that the soil to the right of the pile tip is in an active state and very close to failure as well. This proximity to failure on either side of the wall near the tip was observed for all the analyzed cases and is probably due to the high stress gradient in that vicinity.

Effect of Soil Cohesion

Increasing Cu in both the gravity-turn-on and the sequential construction analyses resulted in a reduction in the moments and displacements (Figs. 41-46). This is because as Cu increases, the soil stiffness increases. Therefore, the soil elements carry a bigger share of the total load (weight of the soil) and the moments and displacements of the pile decrease.

As Cu increases, the active pressure on the wall from the retained soil does not change, but the passive pressure on the wall from the left side soil increases (about five feet below the original ground surface). This has the net effect of decreasing the maximum moment developed in the sheetpile. The above mentioned behavior is best depicted by the net pressure diagrams for different values of Cu (Figs. 45,46). For

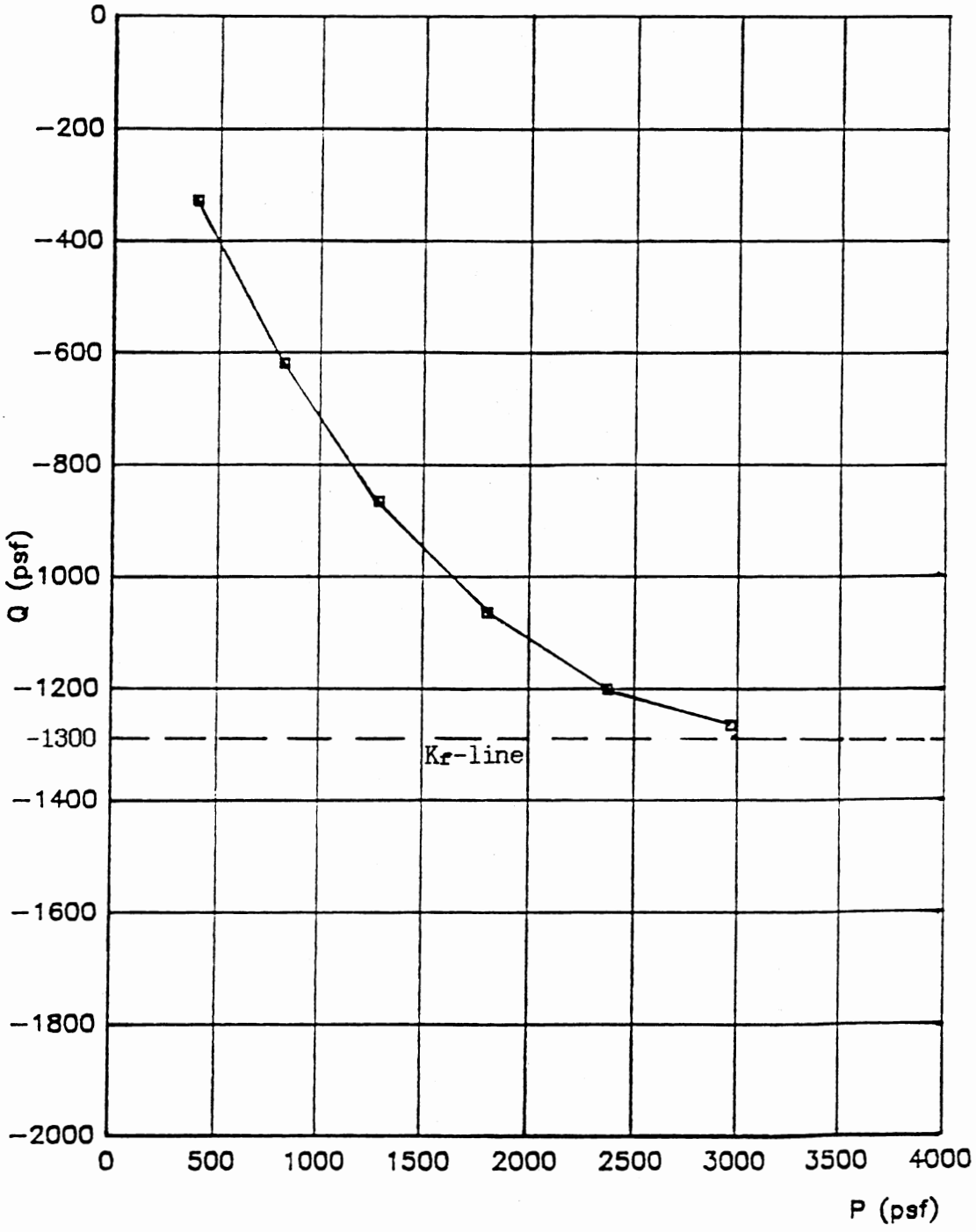

Figure 39. Stress path at point B (Elev.=-58 ft) ; gravity-turn-on. Cu = 1300 psf, 30 ft pile penetration.

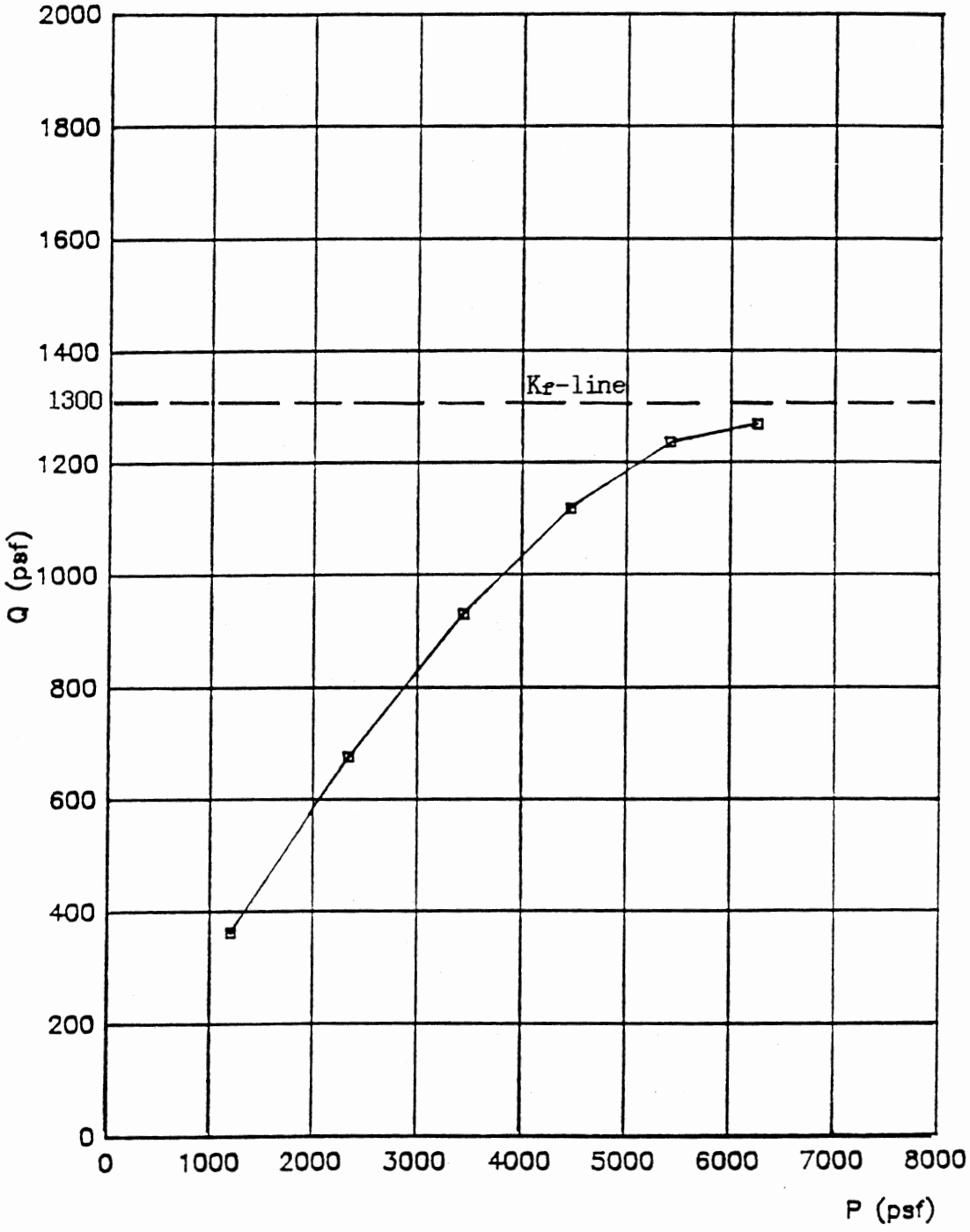

Figure 40. Stress path at point A (Elev.=-58 ft); gravity-turn-on Cu = 1300 psf, 30 ft pile penetration.

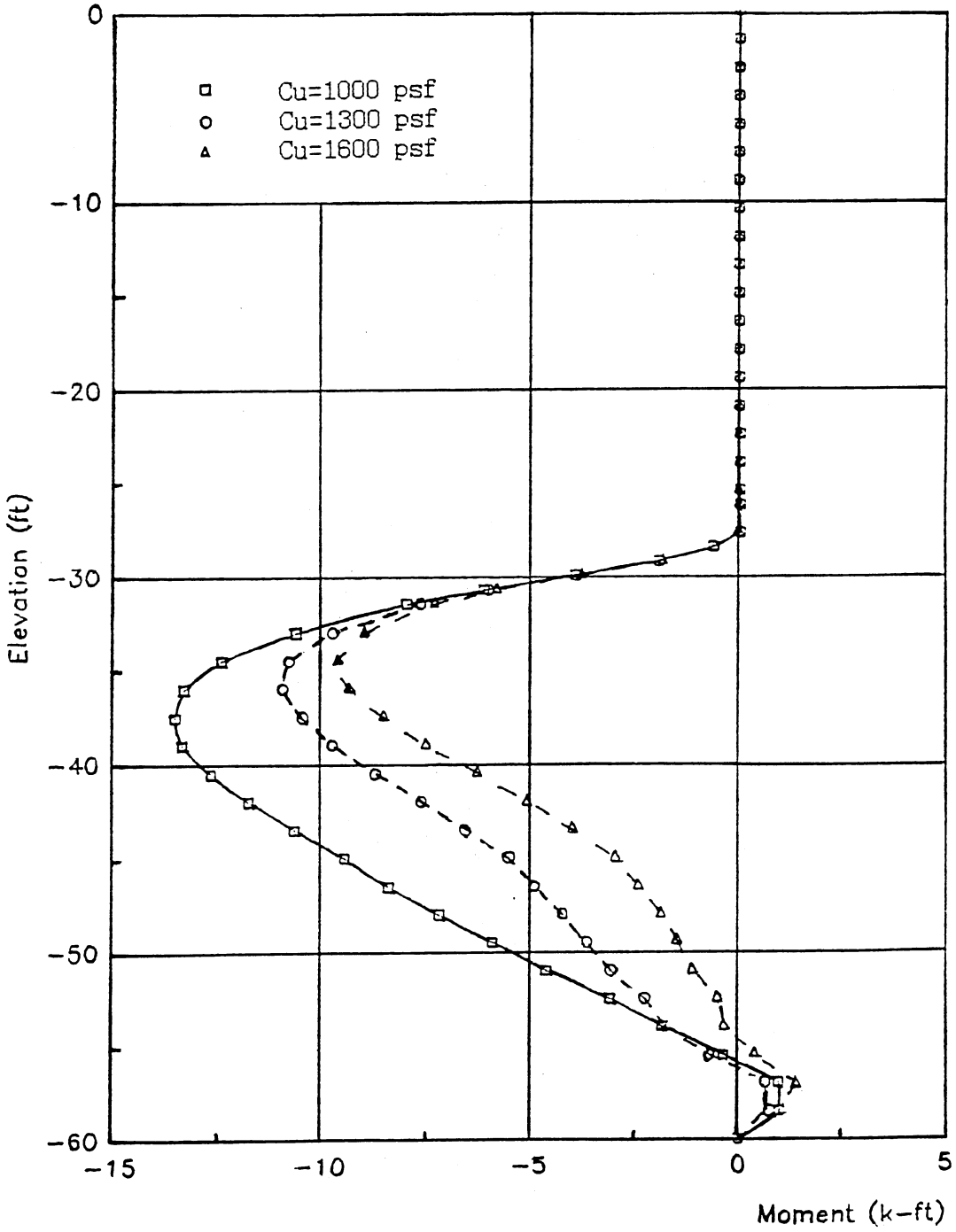

Figure 41. Bending moment profiles for different values of Cu. Gravity-turn-on analysis; 30 ft pile penetration.

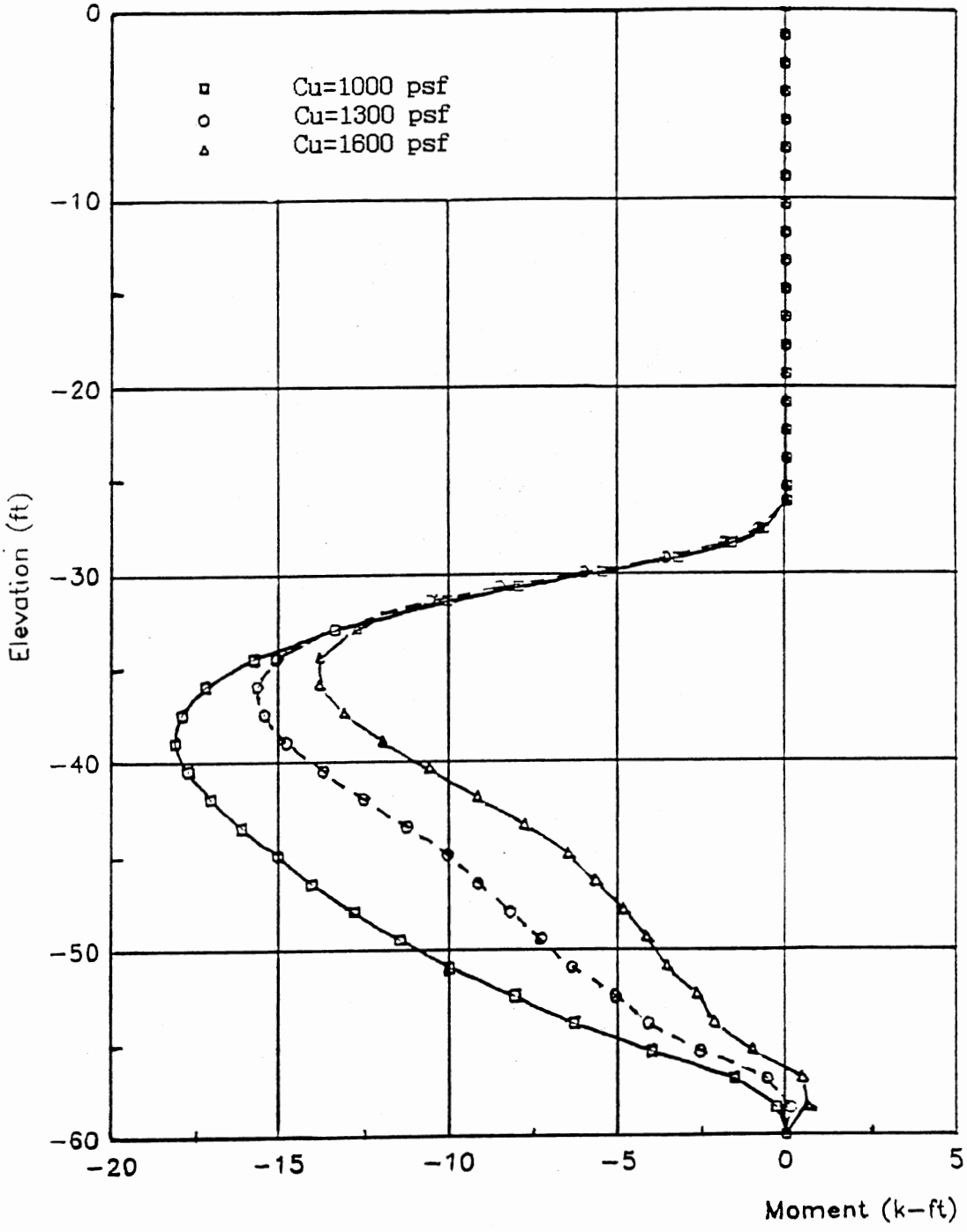

Figure 42. Bending moment profiles for different values of Cu. Buildup analysis; 30 ft pile penetration.

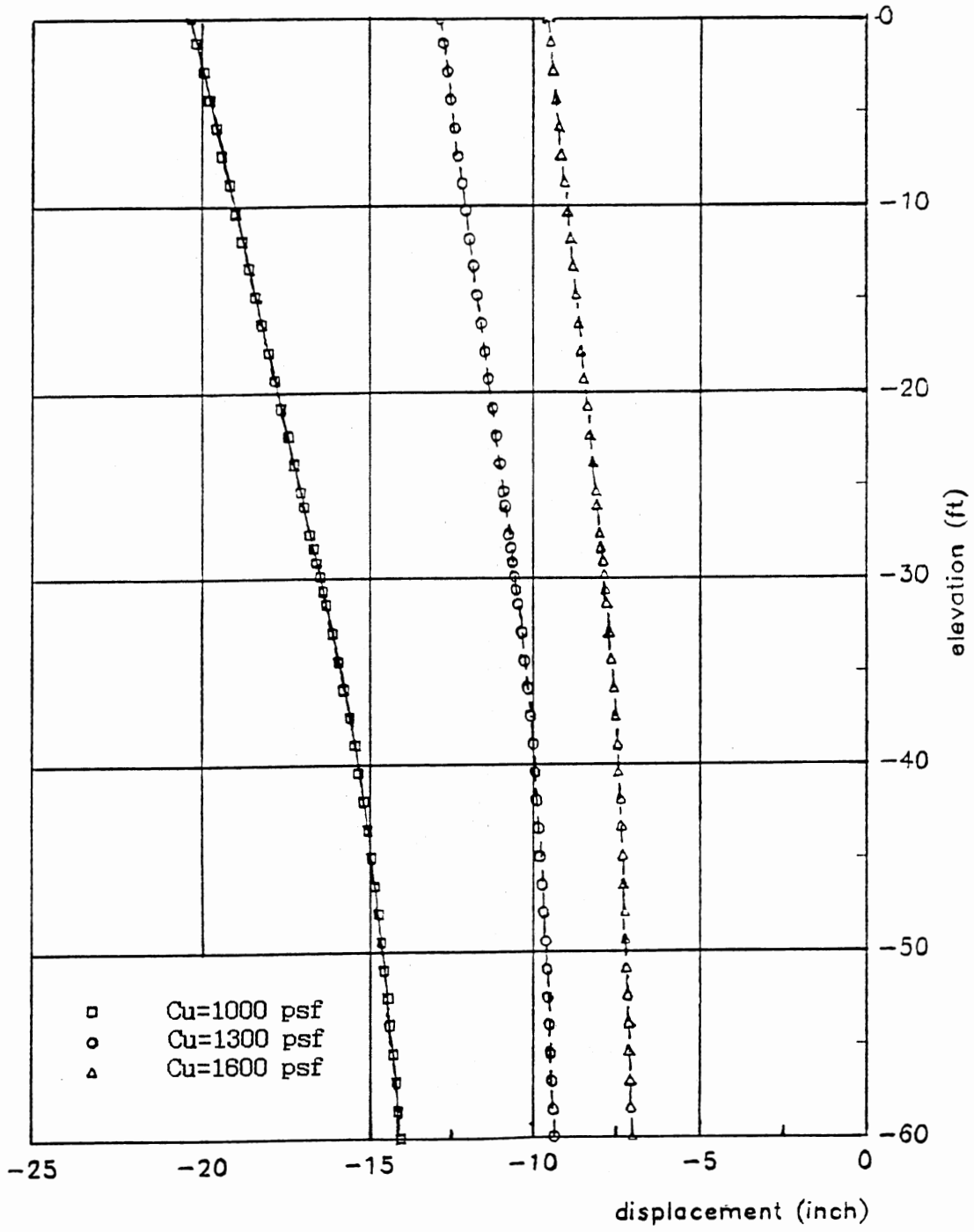

Figure 43. Pile deflection profiles for different values of Cu. Gravity-turn-on analysis; 30 ft pile penetration.

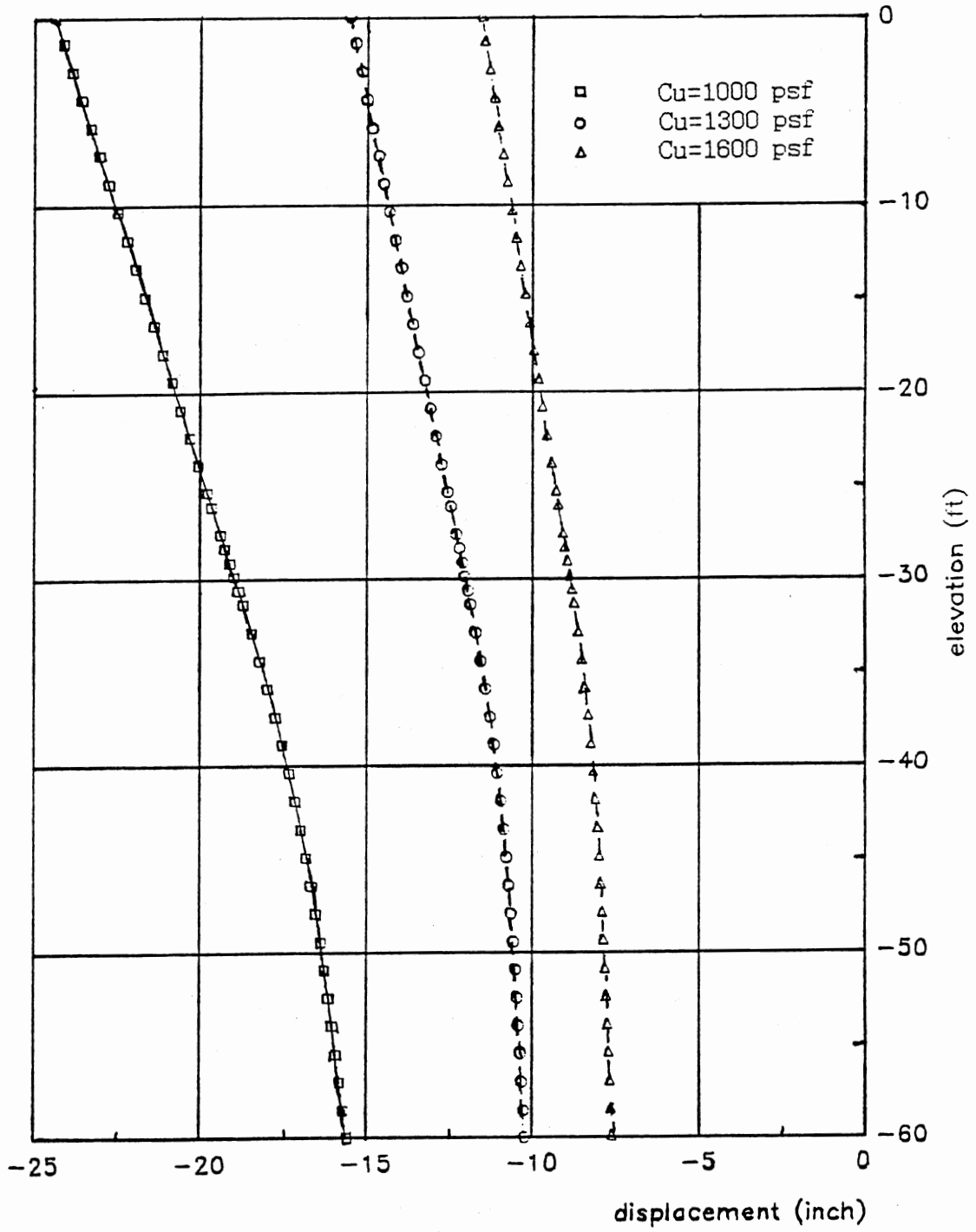

Figure 44. Pile deflection profiles for different values of Cu. buildup analysis; 30 ft pile penetration.

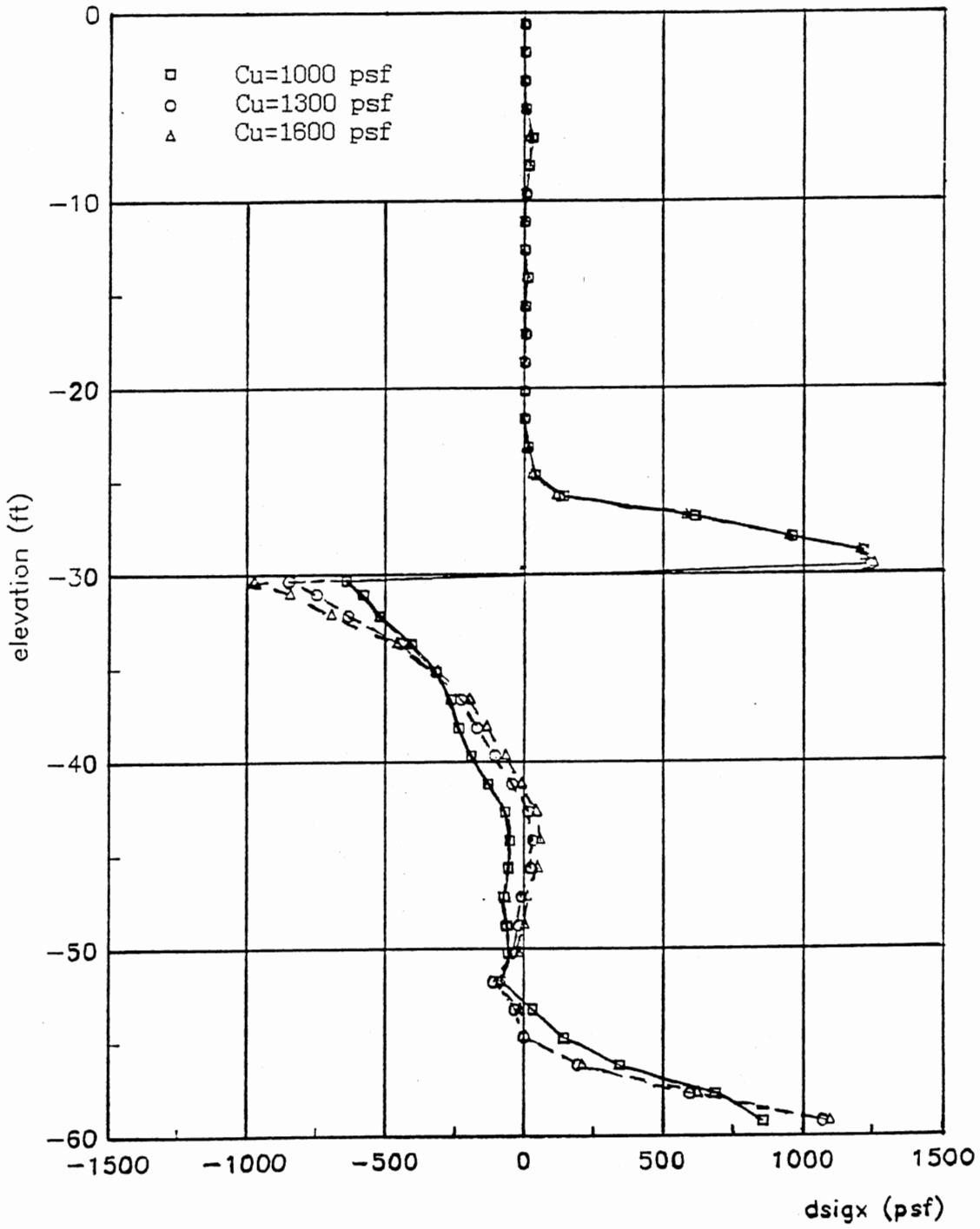

Figure 45. Net stress on the pile for different values of Cu. Gravity-turn-on; 30 ft pile penetration.

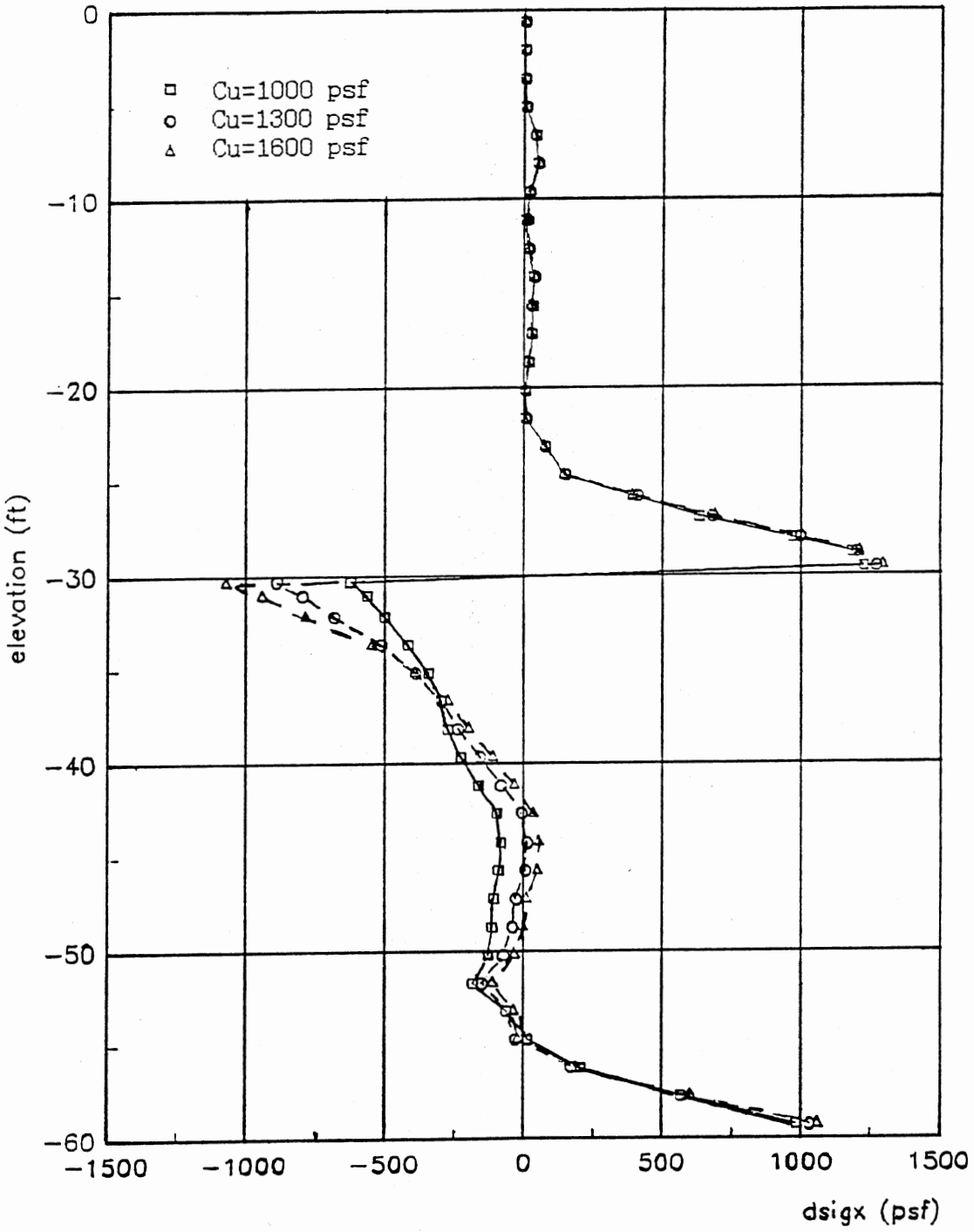

Figure 46. Net stress on the pile for different values of Cu. Buildup analysis; 30 ft pile penetration.

example, for Cu = 1000 psf and Cu = 1300 psf in the gravity-turn-on case (Figs. 45,46), little change is noticeable in the retained soil, but a definite increase is seen for the soil to the left of the wall under the original ground surface. Figs. 45-46 show a zone of zero net pressure in the middle third of the embedded depth.

Also, varying Cu did not have any effect on the depth of the tension crack (Figs. 45,46).

Effect of Depth of Penetration

Three different embeddment depths of penetration were studied (30, 20, 15) at the same Cu (1300 psf). The results are rather surprising in a way because the effect of embeddment depth was not as prominent as initially expected. As the results in Table II show, the moment location for the three cases from gravity-turn-on analysis is almost the same (@ about 5 ft below the original ground surface). Also, the magnitudes were not very far apart, especially for the 20 ft and 15 ft penetration cases. Furthermore, the soil pressures in the retained soil are almost the same in the three cases.

It is also interesting to note that the net force on the wall crosses from left to right at 5 ft above the pile tip in the three cases (Fig. 49). The displacement of the wall for the 15 ft embeddment depth is slightly lower than that for the 20 ft case. However, the net displacement, that is the difference between top and bottom displacement, for all practical purposes is the same for the two cases. This suggests that the only difference between these two cases is in the amount of rigid-body displacement.

For the 30 ft case, the displacements are slightly higher than for

the 20 ft and 30 ft penetration cases. In general, the moments increased and the total displacements decreased as the embeddment depth decreased. The increase of displacement with embeddment depth seems to be caused by the increase in contact area between the wall and the soil. In short, the following conclusions can be reached about the effect of embeddment depth.

1. In general, total displacements vary very slightly with the depth of penetration (Fig. 47). This suggests that the pile floats in the soil matrix (soil displacements prevail).

2. The increase in embeddment depth reduces the stiffness of the wall and the corresponding bending moments (Fig. 48). The reason is that the stiffness of the wall is inversely proportional to its length.

3. The soil pressures decreased slightly as the embeddment depth increased. An interesting observation is that for all cases, the transition of net pressure from left to right occurred at 5 ft above the pile tip (Fig. 49). Furthermore, for the 30 ft embeddment depth and for all Cu values, the portion of the wall between elevations -45 ft and -55 ft was almost stress-free, which suggests that sometimes increasing the penetration depth will be ineffective and does not increase the factor of safety.

4. The embeddment depth seems to have little effect on the general behavior. This is evident from the f-contours for the different values of embeddment depth which show no appreciable difference in the degree of mobilization at the same critical locations. An interesting point that can be made here is that the finite element solution in some cases predicts a small positive moment near the bottom of the pile. The above behavior was noticed only for the 30 ft embeddment depth but not

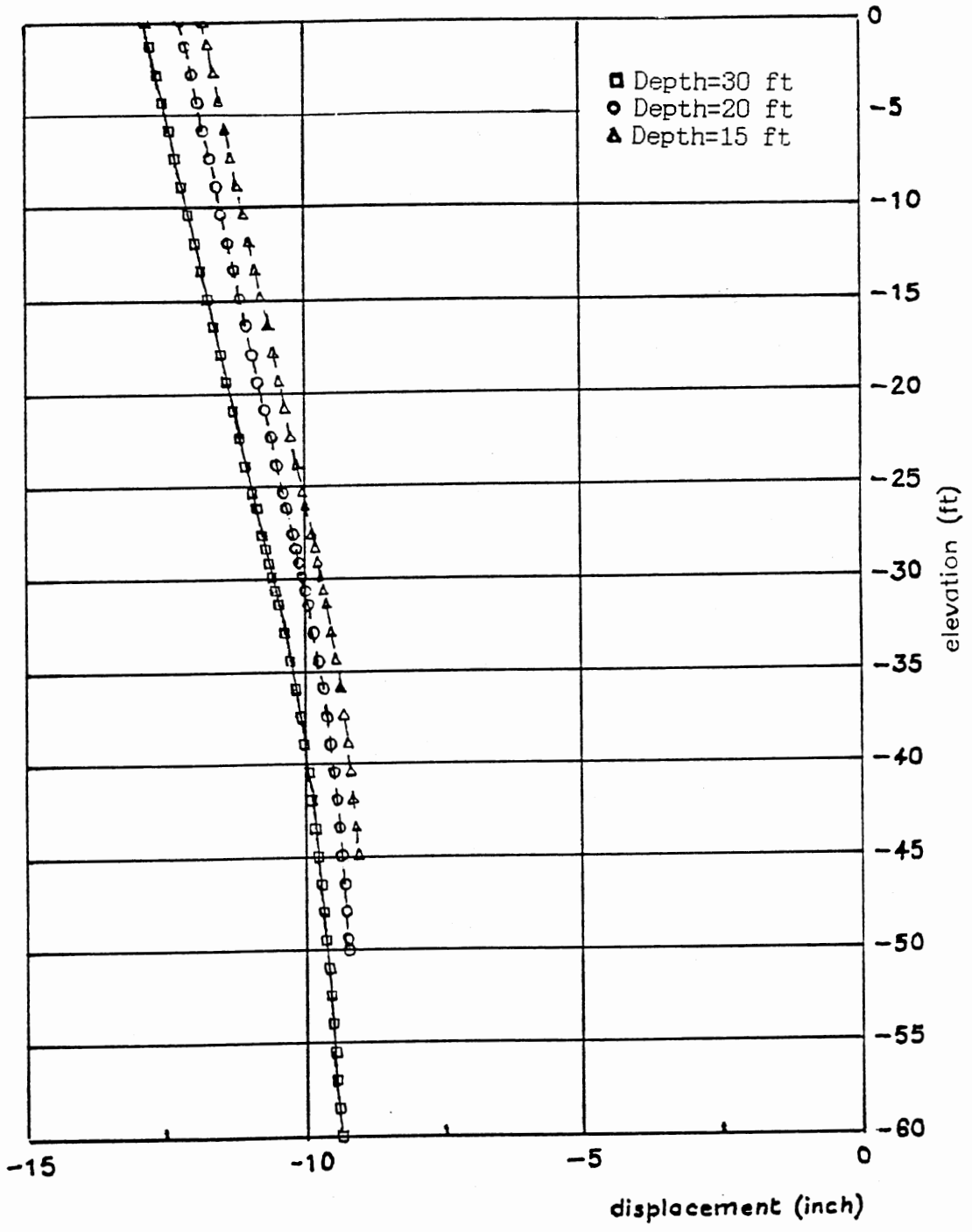

Figure 47. Pile deflections for different embeddment depths. Gravity-turn-on; Cu = 1300 psf.

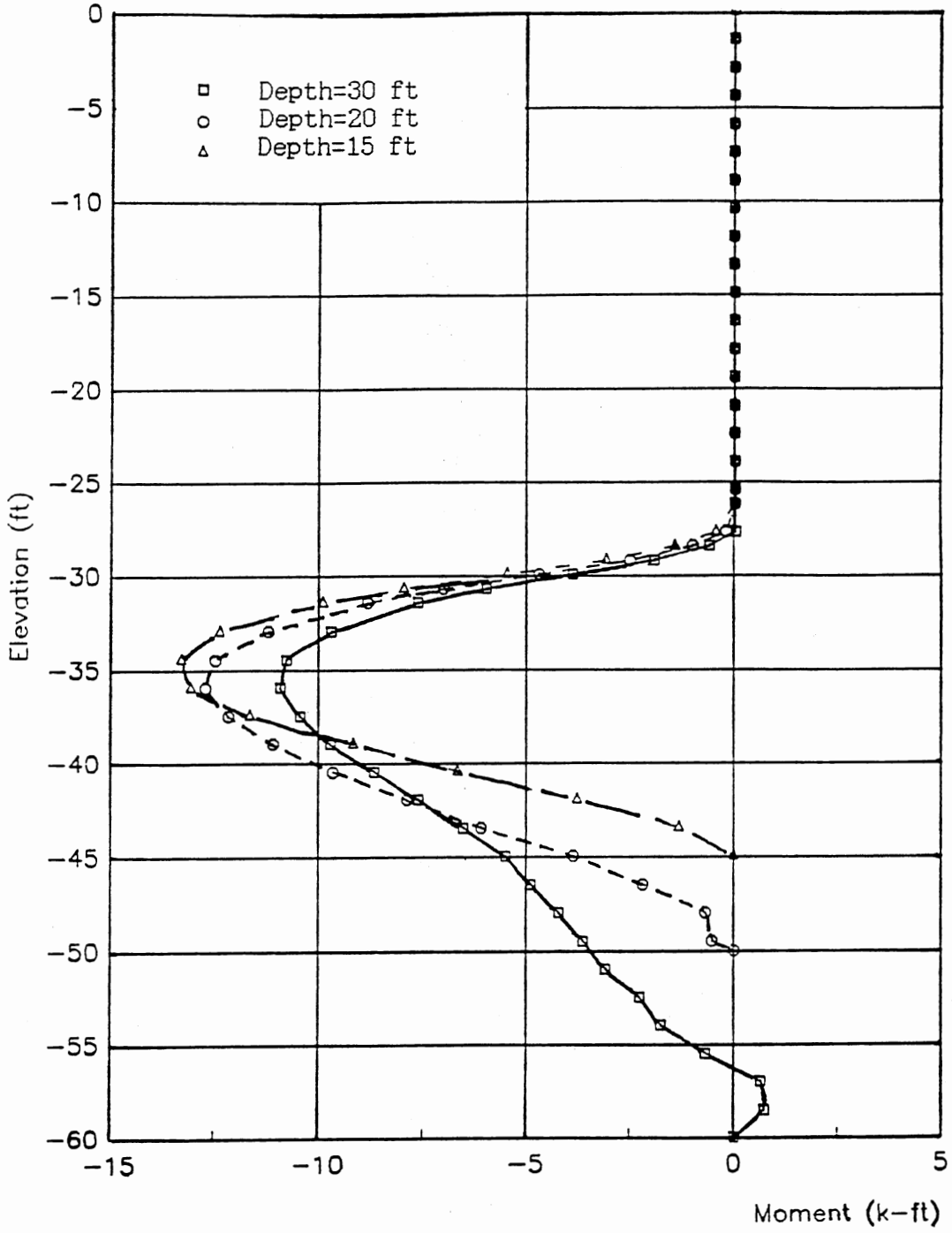

Figure 48. Bending moments profiles for different embeddment depths. Gravity-turn-on; Cu = 1300 psf.

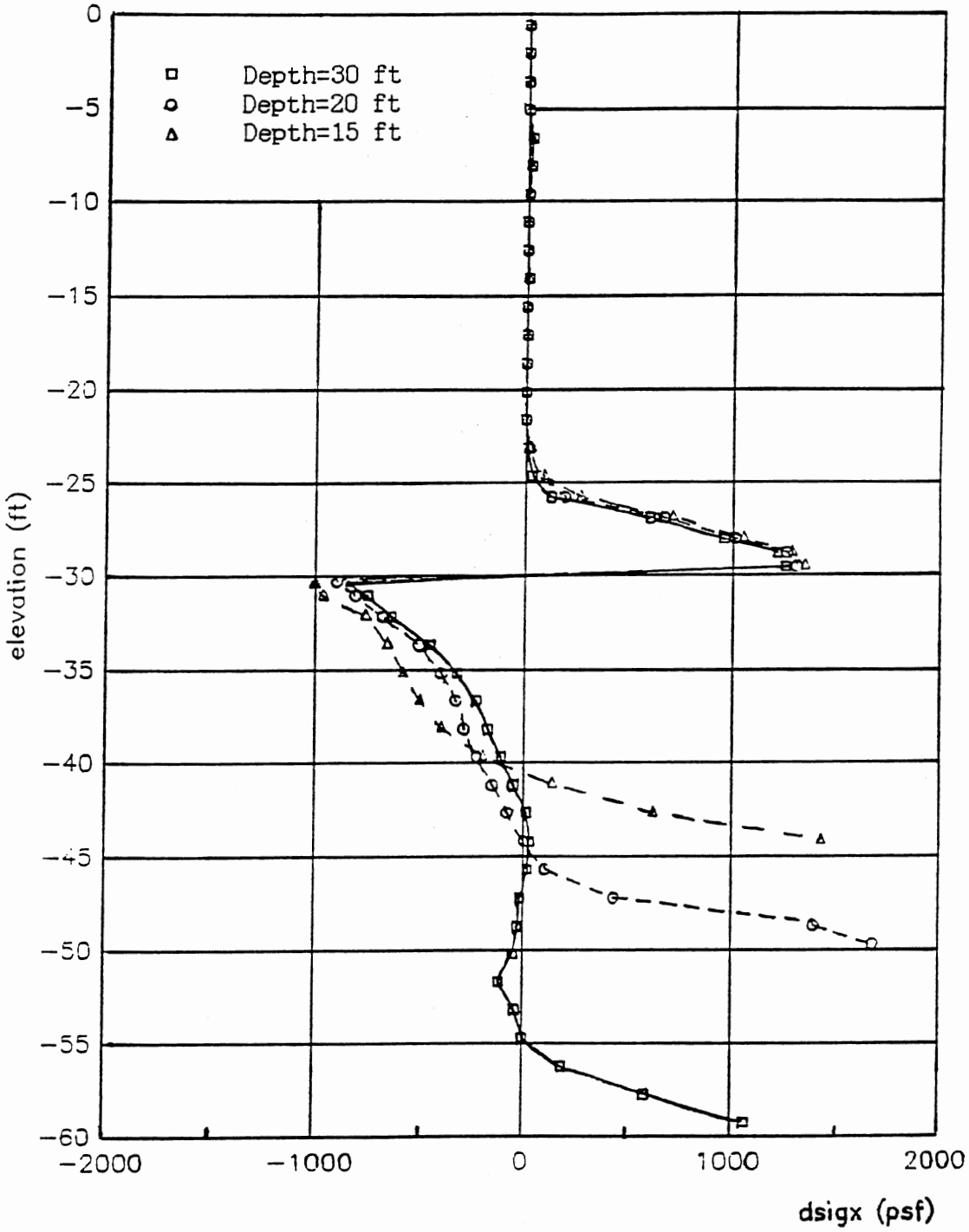

Figure 49. Net stress on the pile for different embeddment depths. Gravity-turn-on; Cu = 1300 psf.

for the 15 ft and 20 ft embeddment depth cases. A possible explanation is that the longer pile has a lower relative stiffness and also displaces more soil. This results in a high drag force at the tip of the pile (from left to right) causing contra-flexure and positive moment. (Similar findings were made in Reference (20) for a levy in ϕ = 0 clay for the high penetration case into a weak soil layer). Whether this behavior happens in nature or is the result of the finite element modelling of the continuum is unclear and is open to debate.

SSI Method

The concept of interaction distance, D, is of paramount importance in the SSI method. The soil modulus value (E_s) at each point along the pile depends in its determination on the value of D at that particular location. Furthermore, a systematic approach must be developed to ensure that the assumed values of D are compatible with the resulting solution, i.e., to establish the convergence of the SSI solution. With that in mind the following points were investigated:

1. The concept of interaction distance, D, and its influence on the behavior.
2. An iteration procedure to ensure convergence of the SSI solution.

Interaction Distance

A very vague point in SSI theory is the concept of interaction distance (D). It is supposed to reflect the extent of the effectively-stressed soil and it resembles the concept of a pressure bulb under a footing. The only suggestions found in the literature (Refs.11,12,19)

for a cantilever sheetpile wall are (1) to take the height of the retained soil as the interaction distance above the original ground surface, and (2) to take the embedded depth as the interaction distance for the soil beneath the original ground surface (Fig. 50). Also, the concept of interaction distance is based on the idea of a rigid structural member pressing against the soil. Therefore, the interaction distance qualitatively is more consistent with a passive-type situation rather than an active-type one when the wall is moving away from the soil. Furthermore, since the interaction distance depends on the stressed area, it is expected to vary along the pile.

The most difficult aspect of comparing the SSI results with the finite element solution is that the researcher or designer is completely in the dark when it comes to determining the interaction distance for various locations along the wall. Since the interaction distance affects the values of E_s no matter which formulation is used (Terzaghi's or Skempton's), it becomes extremely important to find a way to choose values of D in order to obtain a reliable solution.

Using the suggested values for the initial interaction distance (Fig. 50), analyses were made for different Cu values, and some of the results are shown in Figs. 51-56 for Cu = 1300 psf and 30 ft penetration depth. The maximum moment values are shown in Table 3. These values are two to three times larger than those obtained from the finite element analysis. Rowe (Ref.40) observed that moments which are too high are also obtained when the classical method is used.

Table III reveals a serious inconsistency. The maximum moment obtained (26.4 K-ft) when Cu = 1300 psf was found to be less than the maximum moment (35.2 k-ft) obtained when Cu = 1600 psf. This

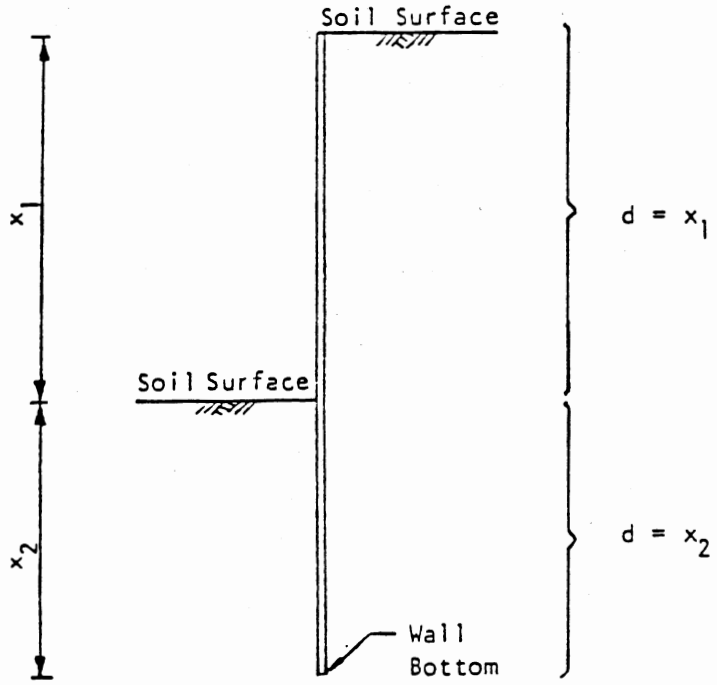

a. Cantilever walls

Figure 50. Initial estimates of interaction distance.

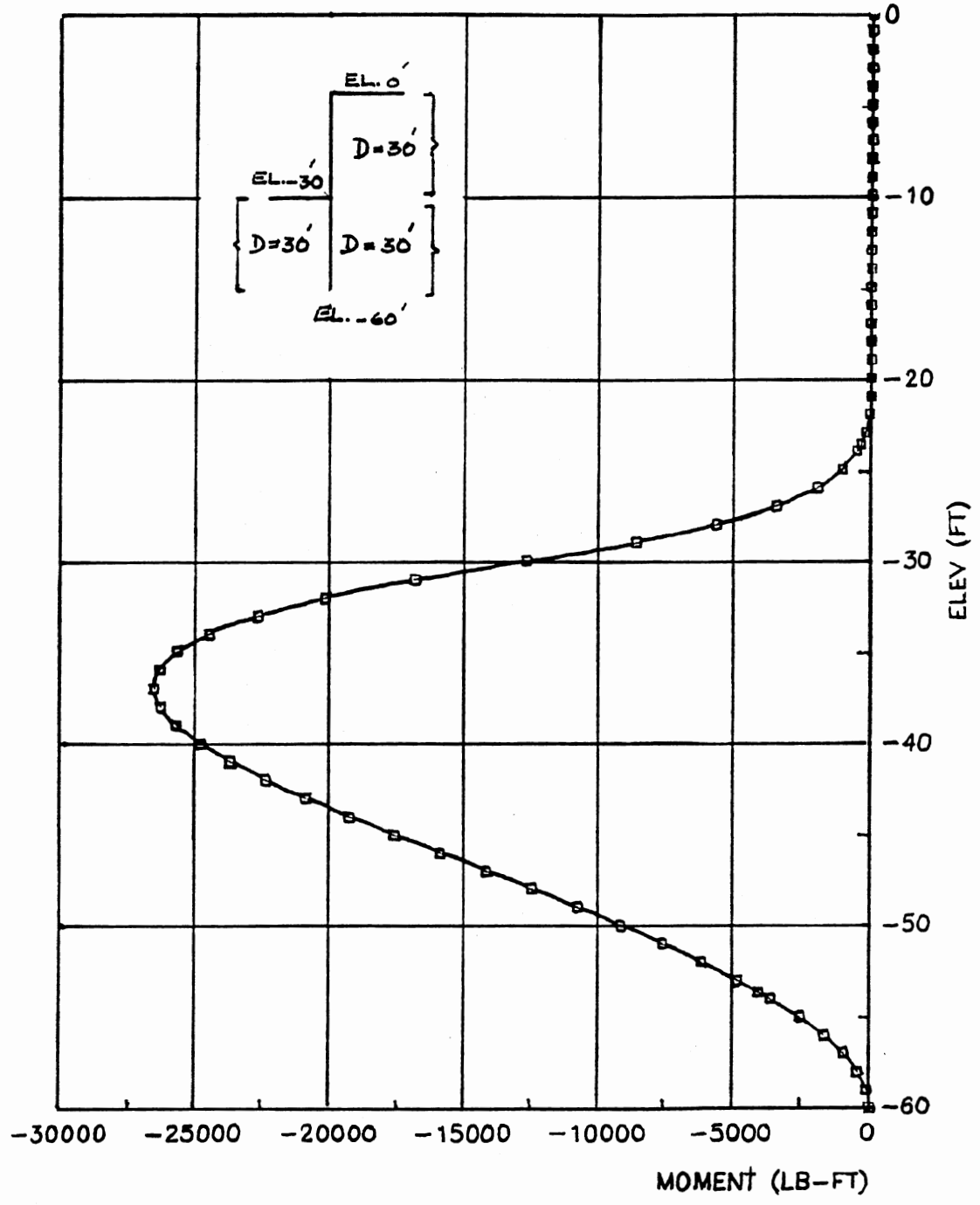

Figure 51. Bending moments from SSI analysis using Skempton's method. Cu = 1300 psf; Interaction Dist.: right(30'), left(30').

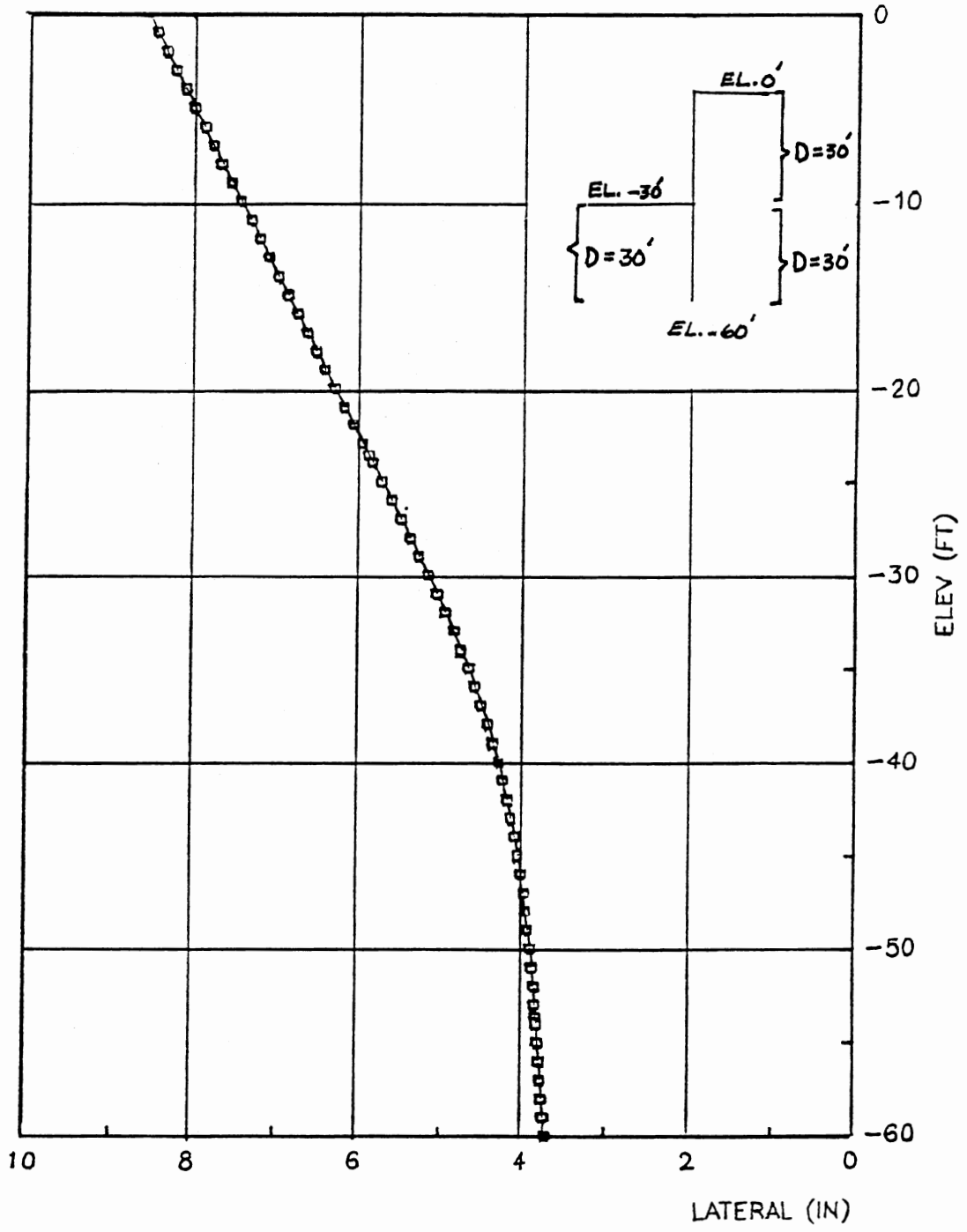

Figure 52. Pile deflections from SSI analysis using Skempton's method. Cu = 1300 psf; Interaction Dist.: right(30'), left(30').

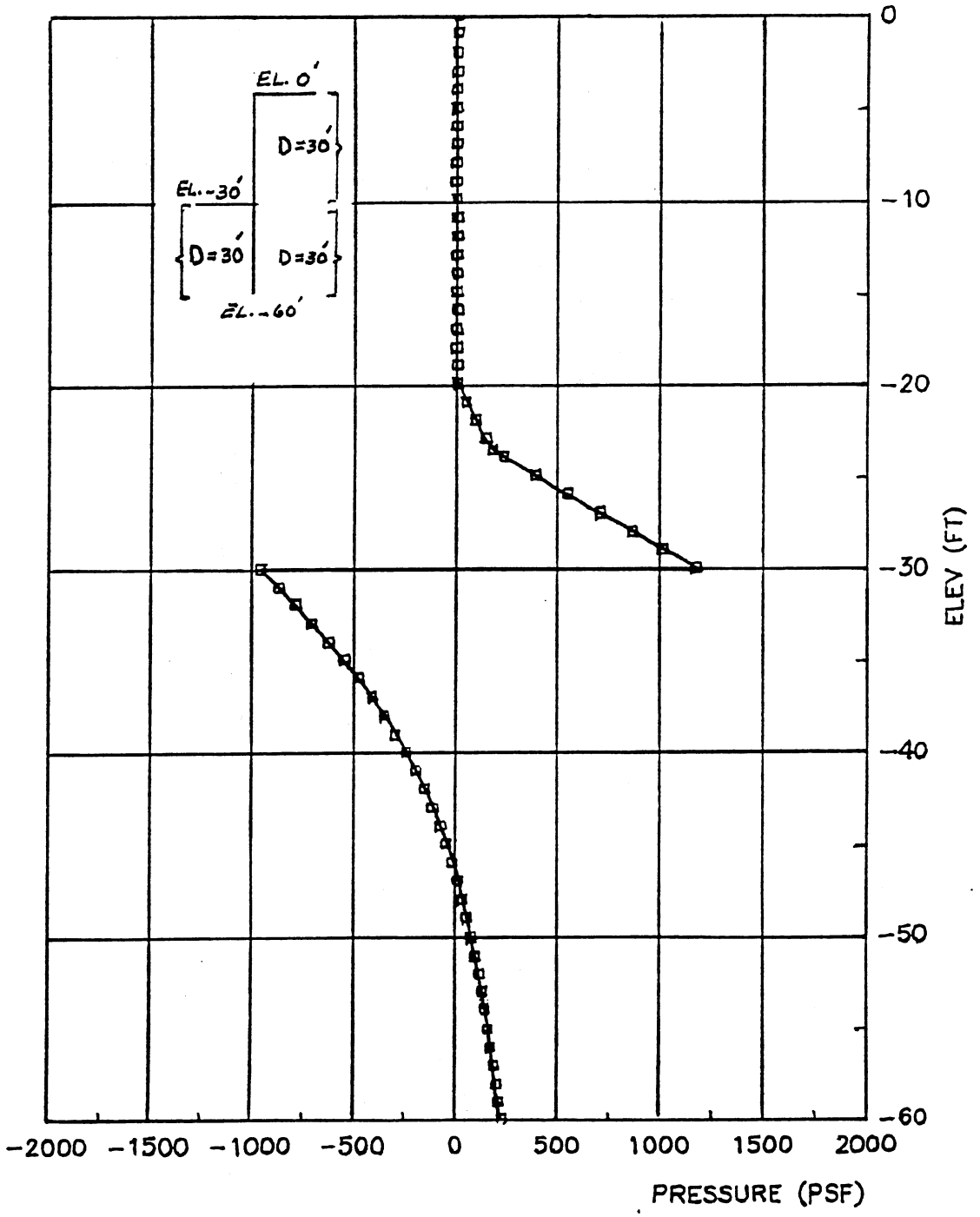

Figure 53. Net stress on the pile from SSI analysis; Skempton's method. Cu = 1300 psf; Interaction Dist.: right(30'), left(30').

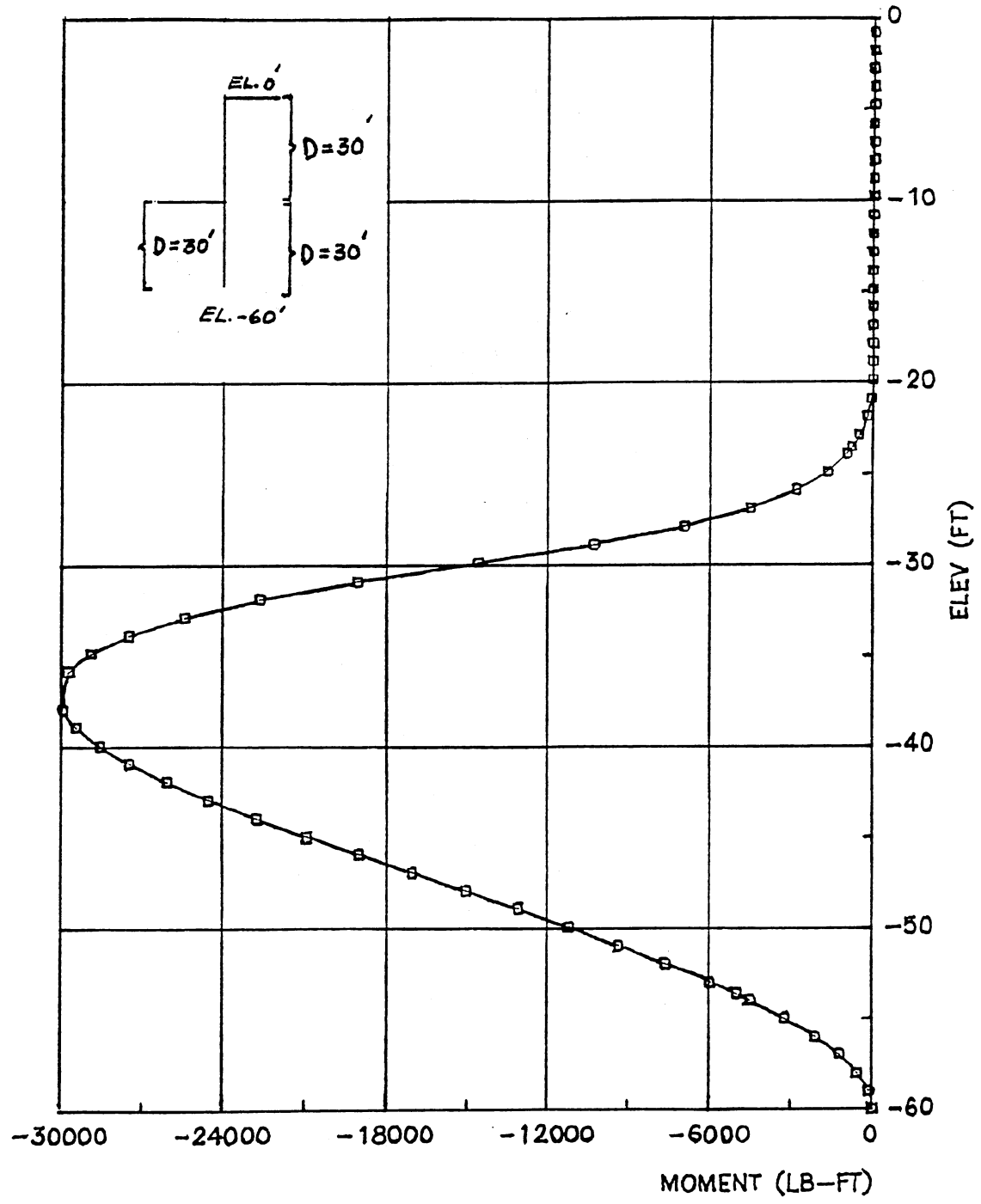

Figure 54. Bending moments from SSI analysis using Terzaghi's method. Cu = 1300 psf; Interaction Dist.: right(30'), left(30').

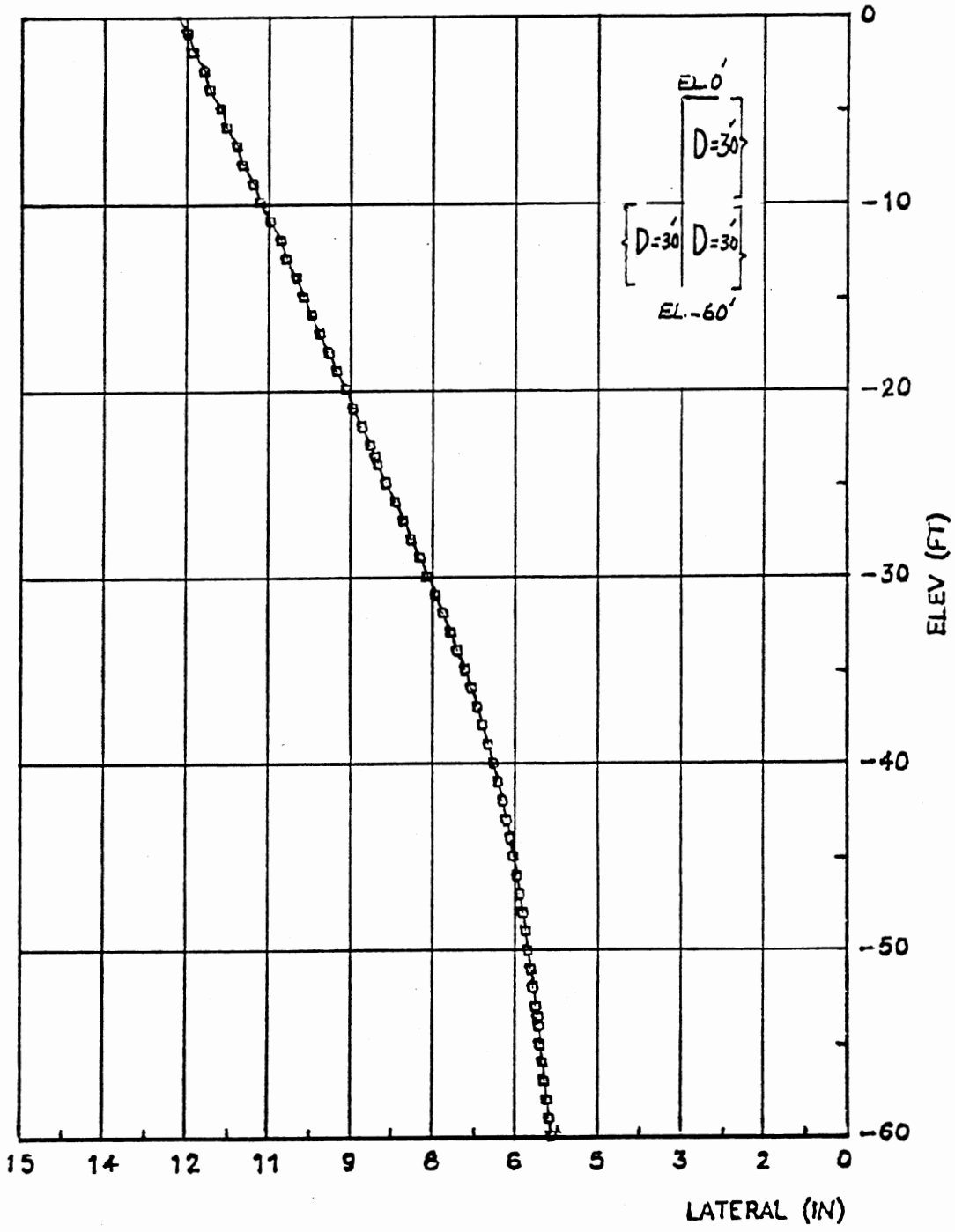

Figure 55. Pile deflections from SSI analysis using Terzaghi's method. Cu = 1300 psf; Interaction Dist.: right(30'), left(30').

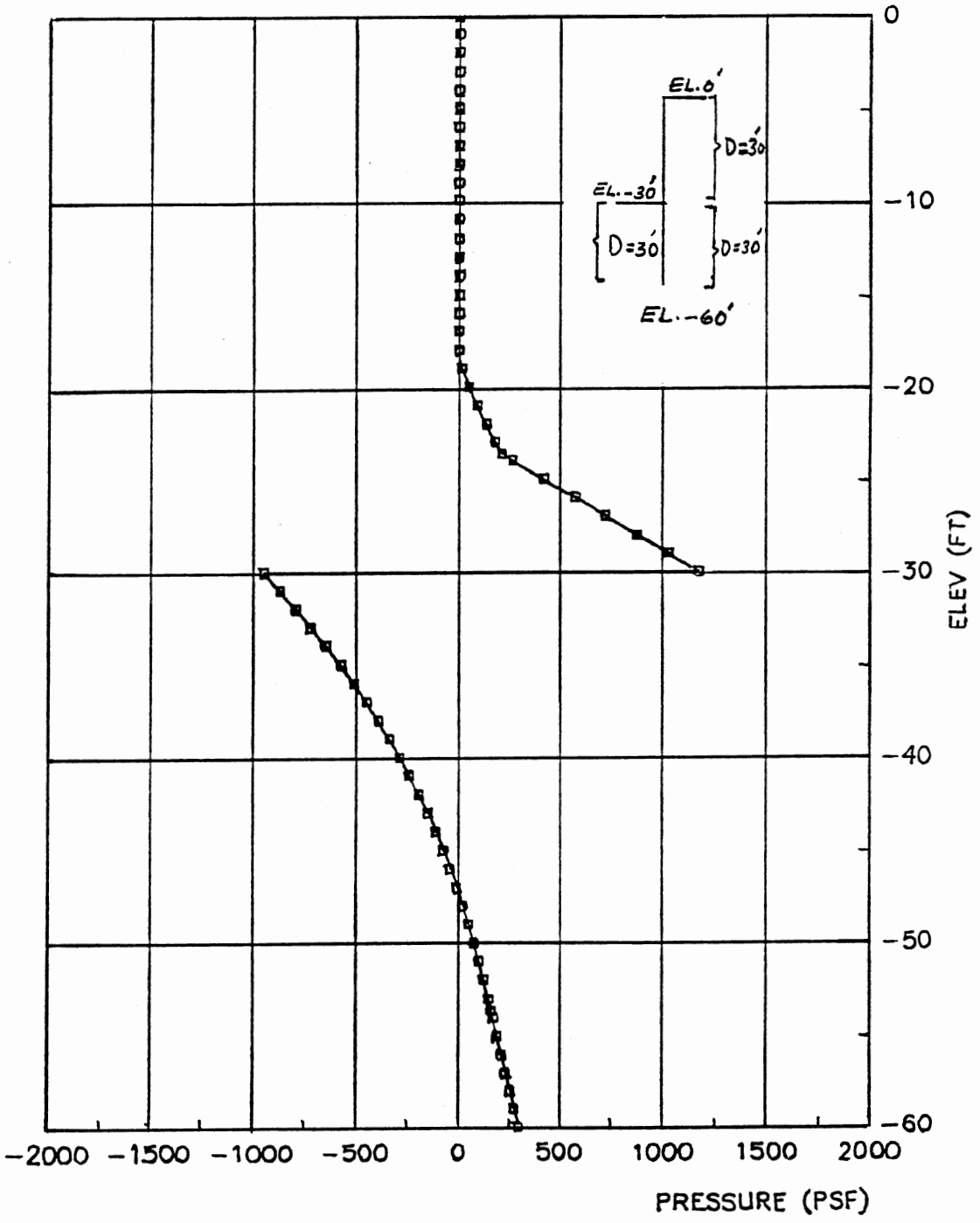

Figure 56. Net stress on the pile from SSI analysis; Terzaghi's method. Cu = 1300 psf; Interaction Dist.: right(30'), left(30').

TABLE III

COMPARISON OF SUGGESTED AND MODIFIED SSI SOLUTIONS

Description	*SSI Suggested Maximum -ve Moment (K-ft)	Elev. (ft)	*SSI Modified Maximum -ve Moment (K-ft)	Elev. (ft)
Cu = 1000 psf 30′penetration	≈ 73	-41.0	≈ 73	-41.0
Cu = 1300 psf 30′penetration	26.5	-36.9	9.4	-34.4
Cu = 1300 psf 20′penetration	26.7	-34.0	8.4	-34.0
Cu = 1300 psf 15′penetration	28.9	-33.5	7.7	-33.0
Cu = 1600 psf 30′penetration	35.2	-36.0	6.2	-35.5

*SSI analysis was done using Skempton′s method.
N.B: For Cu = 1000 psf, the recommended and modified SSI solutions are almost the same due to proximity to failure.

contradicts with the FEM results where higher moments develop in the wall as Cu decreases.

Another inconsistency in the SSI method is that in the active zone, the concept of interaction distance becomes unjustifiable. This is because the SSI theory, as stated earlier, interprets the interaction distance to be of the same nature as the " pressure bulb" under a footing. When the soil is in an active state, the above concept becomes invalid.

Furthermore, in most SSI references it is mentioned that the value chosen for interaction distance, for the active soil in general and the retained soil above the original ground surface in particular, does not affect the solution. This premise was investigated in this study and the results found contradict the above-mentioned belief. For example, two separate SSI runs were made for the 30 ft wall with 20 ft embeddment depth. In the first run, the suggested values for interaction distance were used, as in Reference (12), i.e., 30 ft for the retained soil and 20 ft for the soil under the original ground level. In the second run, all the parameters were kept constant except the interaction distance for the retained soil which was lowered to 8 ft. From the results (Figs. 57-59), the interaction distance of the retained soil did affect the results considerably. In the first case, the maximum negative moment obtained was 26.7 K-ft whereas in the second case it was only 8.55 K-ft. The reason for the decrease in moment is that reducing the interaction distance made the soil much stiffer. This in turn, resulted in smaller bending moments and deflections in the pile. This point was tested further using different values of penetration distances and soil properties.(For example, for cu = 1300

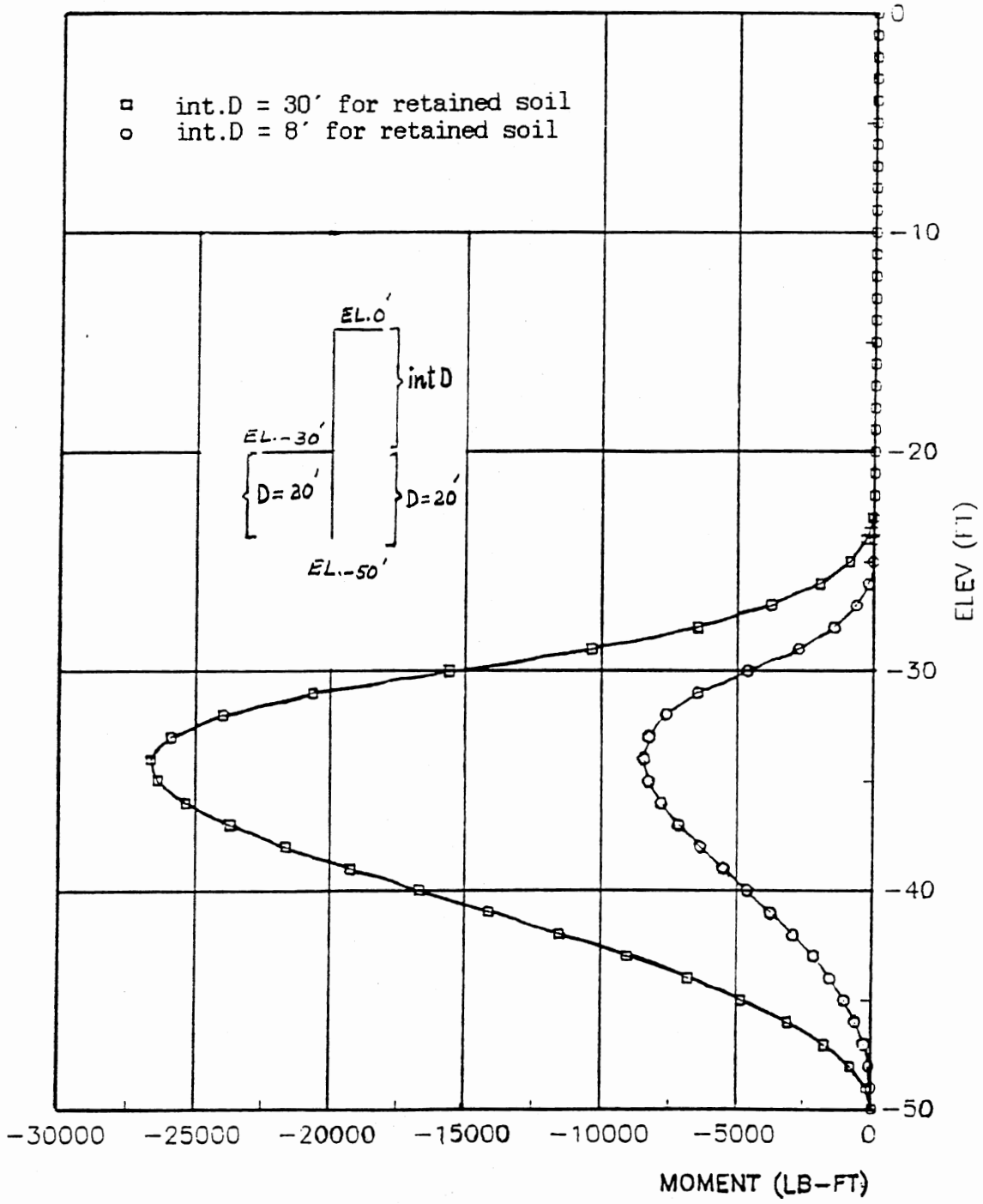

Figure 57. Bending moments from SSI analysis using Skempton's method. Cu = 1300 psf, D = 20 ft below zero elevation.

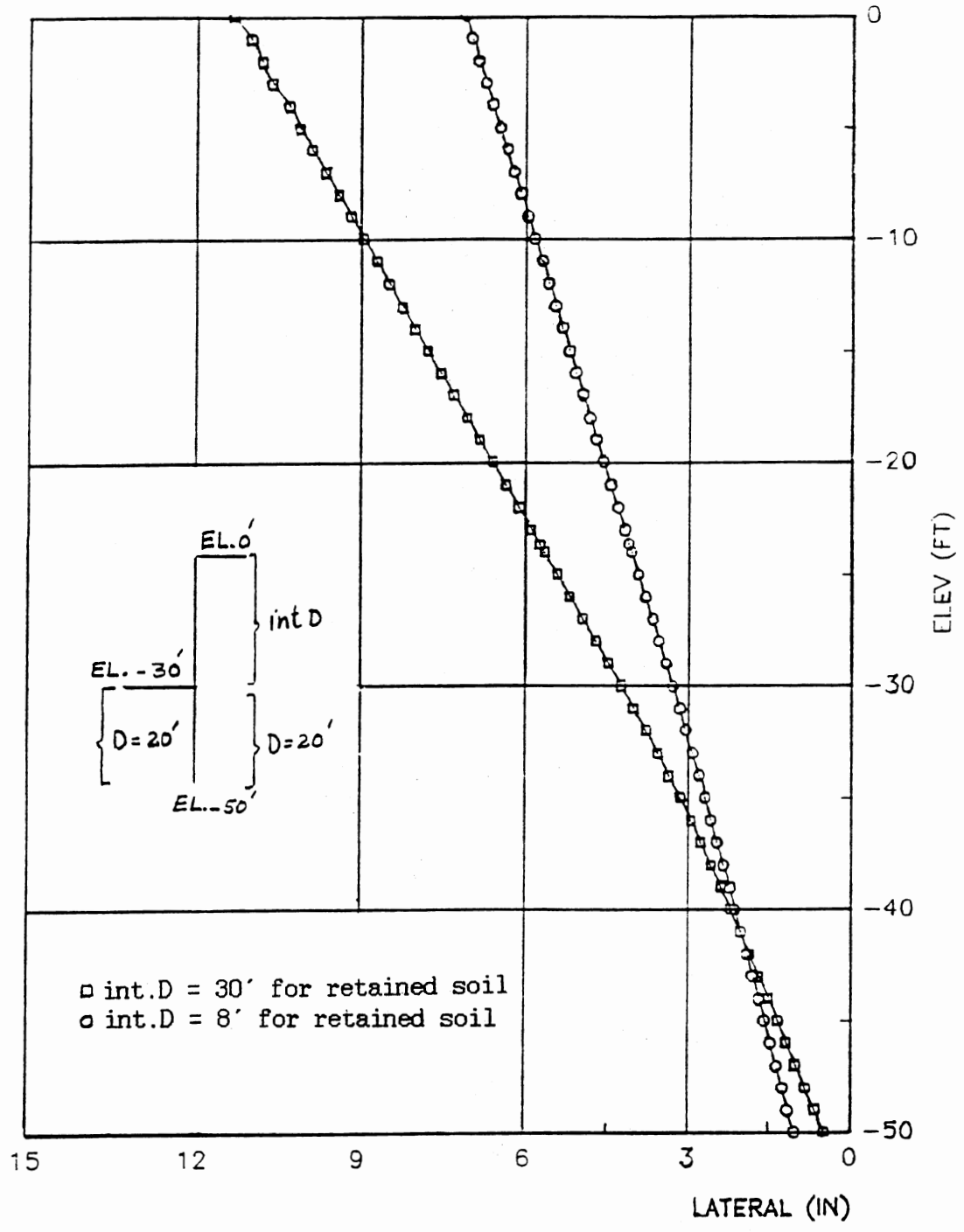

Figure 58. Pile deflections from SSI analysis using Skempton's method. Cu = 1300 psf, D = 20 ft below zero elevation.

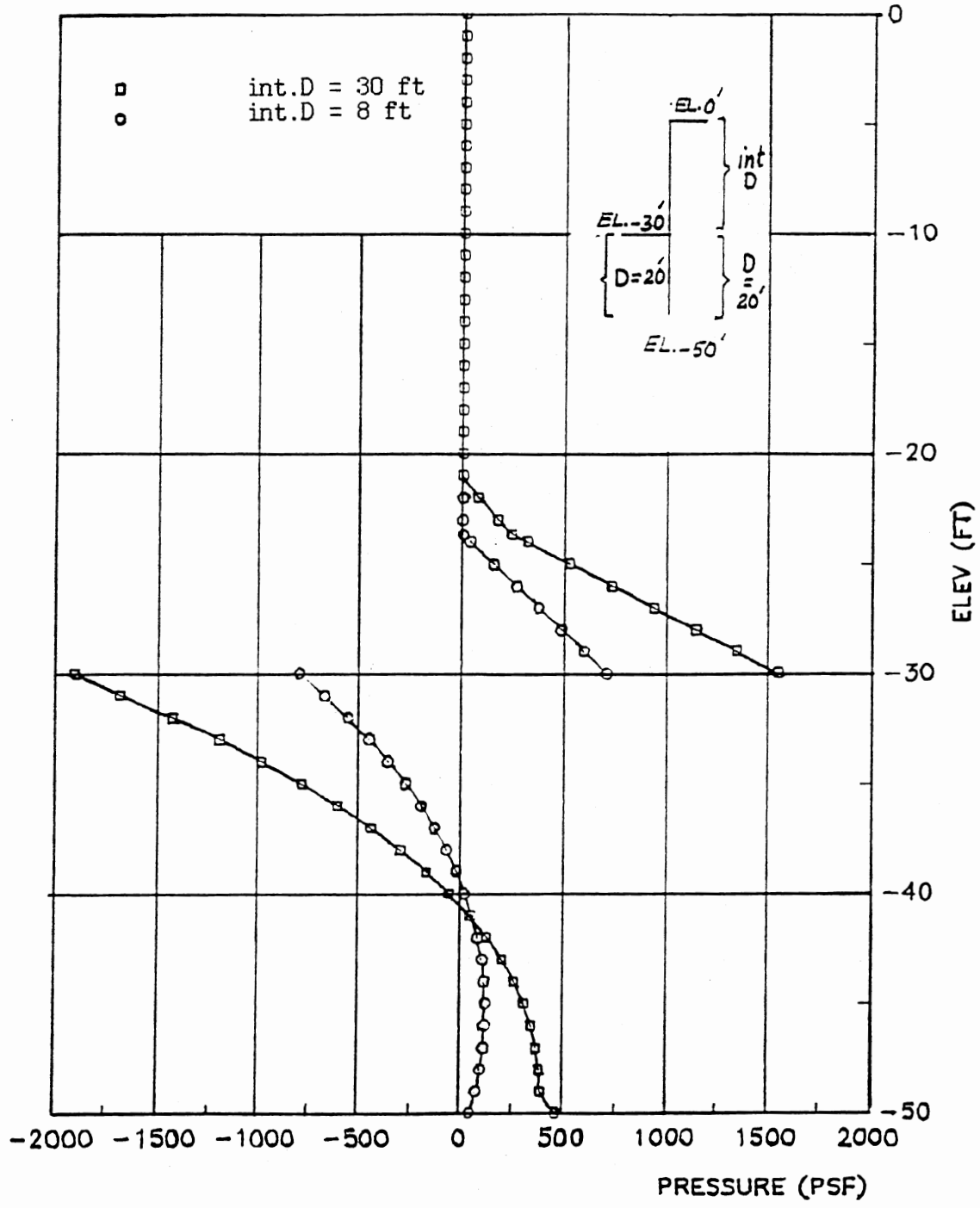

Figure 59. Net stress on the pile from SSI analysis using Skempton's method. Cu = 1300 psf, D = 20 ft below zero elevation.

psf and 15 ft penetration depth). One SSI run was made with an interaction distance of 30 ft for the retained soil above the original ground surface and 7 ft for the soil to the right of the wall beneath the original ground level, while an interaction distance of 8 ft was assigned for the soil to the left of the wall beneath the original ground level. In the second run, the interaction distance for the retained soil was changed to 6 ft and everything else was kept the same. As shown in Figs. 60-62, the maximum moment with D = 30 ft was found to be equal to 45 K-ft whereas it was only 7.69 K-ft for D = 6 ft.

These results confirm beyond doubt that the value of interaction distance is as important for active zones as it is for passive zones.

SSI Iteration Procedure

In the preceding section, many discrepancies and uncertainties were encountered when deciding on the values of interaction distance to be used. If the SSI approach is to have any real reliability for the types of problems discussed here, a consistent scheme has to be devised. The original idea was to base the trial values of interaction distance on the passive zone on either side. However, a quick inspection shows that in most cases, the wall will deflect in such a way that the displacement at every point will be to the left. Hence, almost invariably, the left side under the original ground surface will be in a passive state while the right side will be in an active state. Therefore, if the determination of interaction distance was to be based on the depth of the passive zone on either side, the same initially suggested values will have to be used. This assumption, as illustrated before, yields excessively high moments.

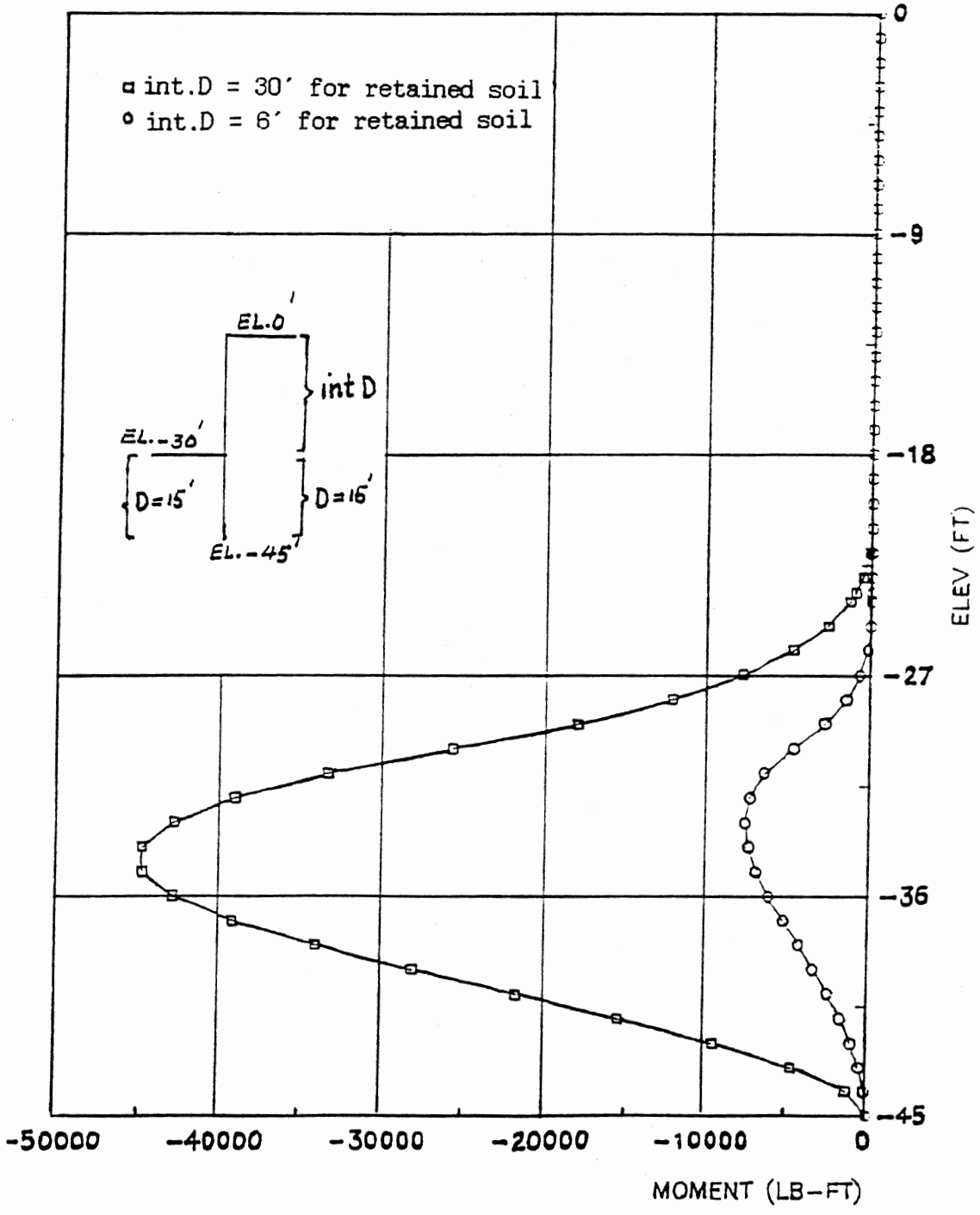

Figure 60. Bending moments from SSI analysis using Skempton's method. Cu = 1300 psf, D = 15 ft below zero elevation.

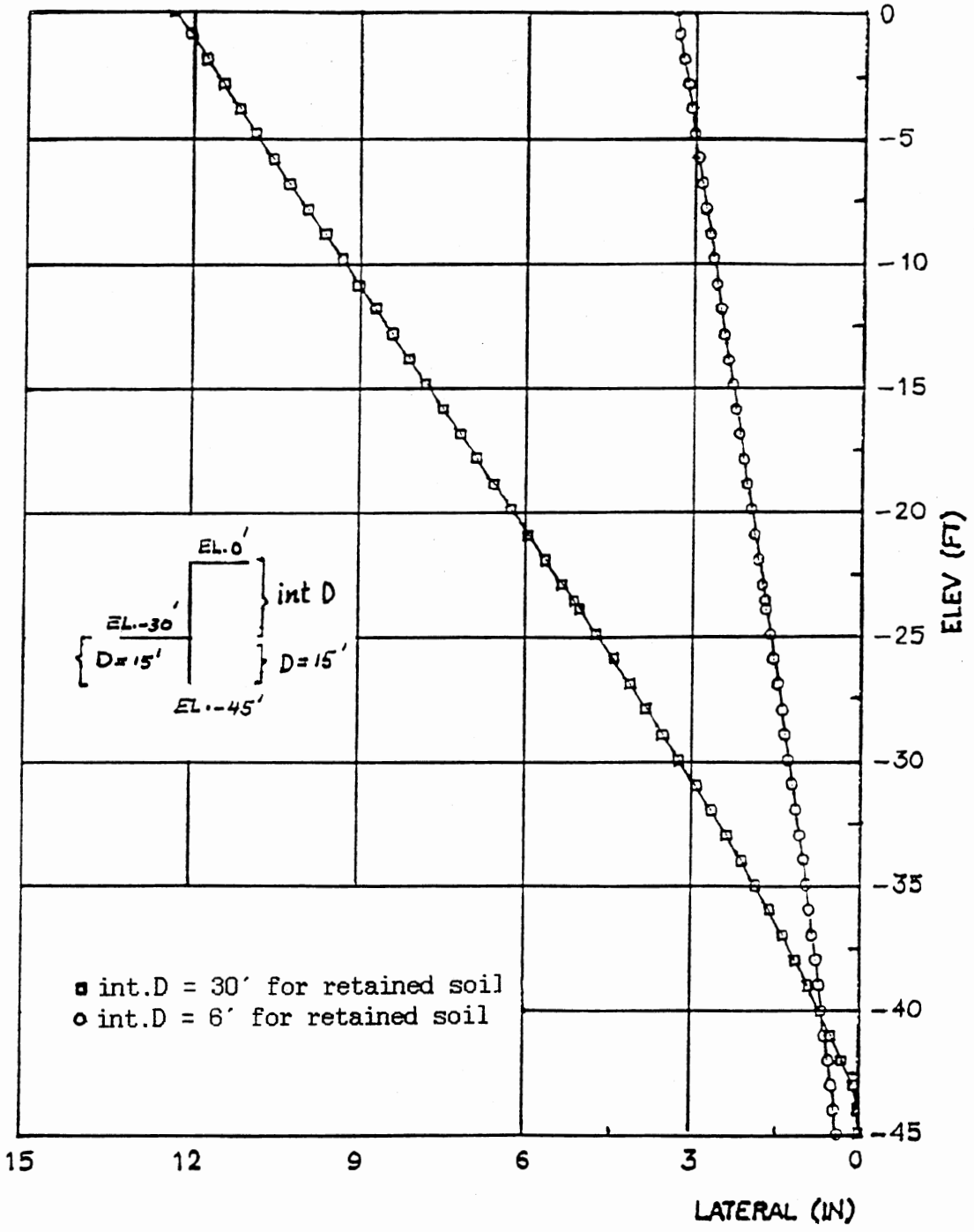

Figure 61. Pile deflections from SSI analysis using Skempton's method. Cu = 1300 psf, D = 15 ft below zero elevation.

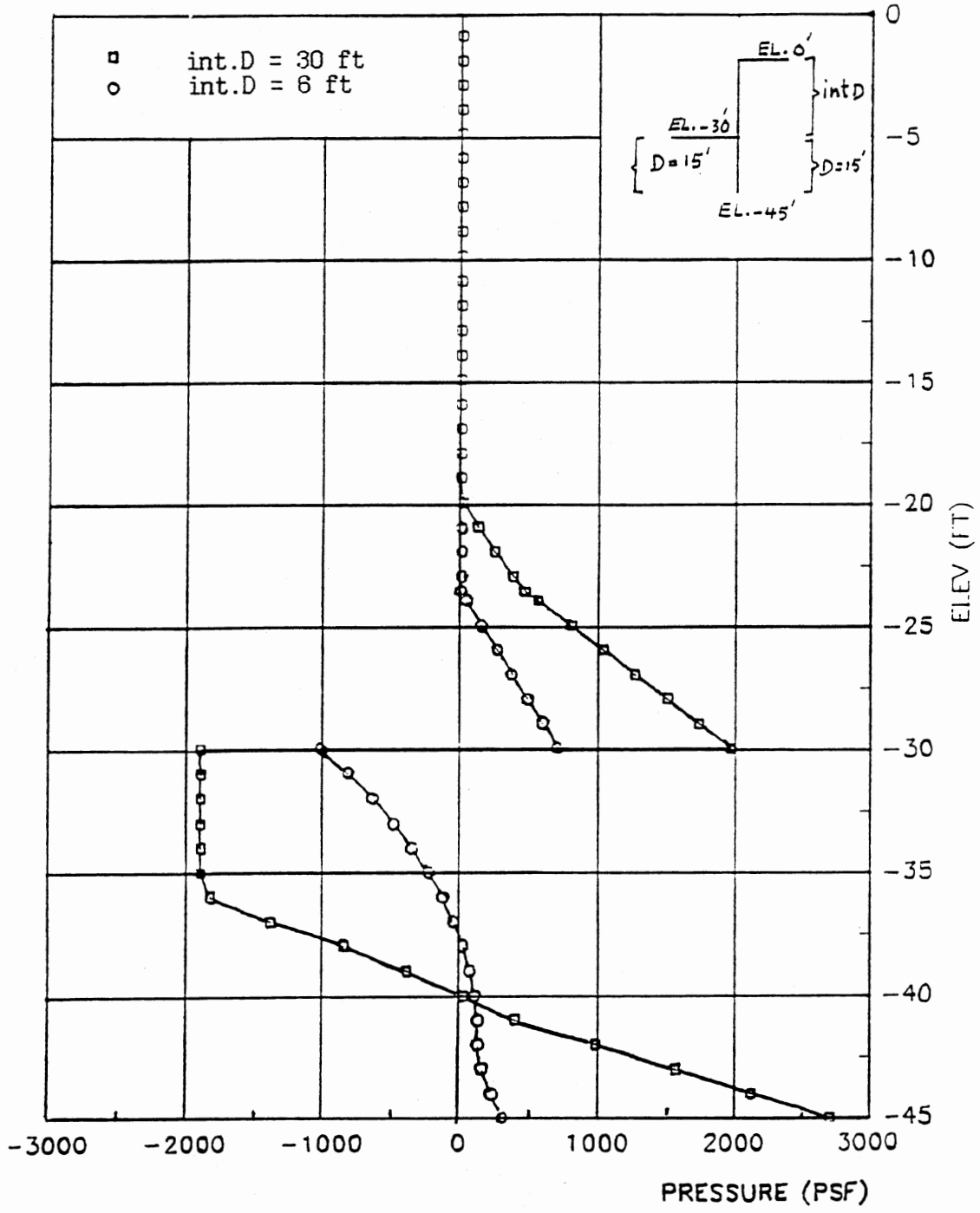

Figure 62. Net stress on the pile from SSI analysis using Skempton's method. Cu = 1300 psf, D = 15 ft below zero elevation.

It was found that even if the soil is in an active state, the interaction distance is still important. This suggested an alternate way of evaluating the interaction distance. The average depth that is responsible for the net pressure on either side is taken as the interaction distance on that side. For the retained soil above the original ground surface, the interaction distance is chosen as the distance through which the wall and soil are still in contact. This assumption, in spirit, is analogous to the "pressure bulb" assumption. This leads to a more reliable scheme that ensures convergence as follows:

1. An SSI run is made using the suggested values for interaction distance: Height of the retained soil for the soil above the original ground surface and the embeddment depth of the pile for the soil below that surface.

2. The values of the interaction distance are modified using the output from step 1. The easiest way to do that is to plot the net pressure versus elevation. From this generated graph, the net height of the retained soil that is still in contact with the wall is readily found and subsequently used as the interaction distance in that zone. Similarly, on either side below the original ground surface, the average distance through which the soil is predominant, as far as net pressure is concerned, is determined and used as interaction distance in the next run.

3. With the interaction distances found from step 2, a new SSI solution is carried out and another pressure versus elevation plot is obtained. The same process as in step 2 is repeated until the values of interaction distance used in a specific run and the values obtained

from the corresponding pressure versus elevation plot are the same or within a very small tolerance. When that happens, this is taken as the final SSI solution for that particular problem.

The above scheme was used in this study and it was found to converge in all the cases studied. It yielded very good and consistent results as far as moments are concerned. Of course, the SSI approach will always yield smaller displacement values than the finite element solution. This is due to the fact that the rigid body displacements obtained, if any, from the SSI method are always less than those found from the finite element method especially in the $\phi = 0$ case.

One example of putting this technique to work is for the Cu = 1600 psf case where Height = Depth = 30′. The solution was achieved as follows:

A value of E_s/ft of interaction distance is found from Skempton's formula using Terzaghi's value for Pult (5.7 Cu)

$$E_s = 5.7Cu/(5.\epsilon_{50}.D) = 5.7x1600/5x0.01x1/(12)^3 = 105.55 \text{ pci/ft of D}$$

1. An SSI run was made using 30 ft as the interaction distance for soil above and below the original ground surface. Figs. 63-65 show the results of this run. From the pressure versus elevation plot shown in Fig. 65, the depth of the tension crack is about 18 ft, and so an interaction distance of 12 ft will be used for the retained soil in the next run. For the soil below the original ground surface, the net pressure diagram crosses the elevation axis (y-axis) almost at mid-depth and therefore, in the next run, a value of 15 ft will be used as the interaction distance for the soil on both sides below the original

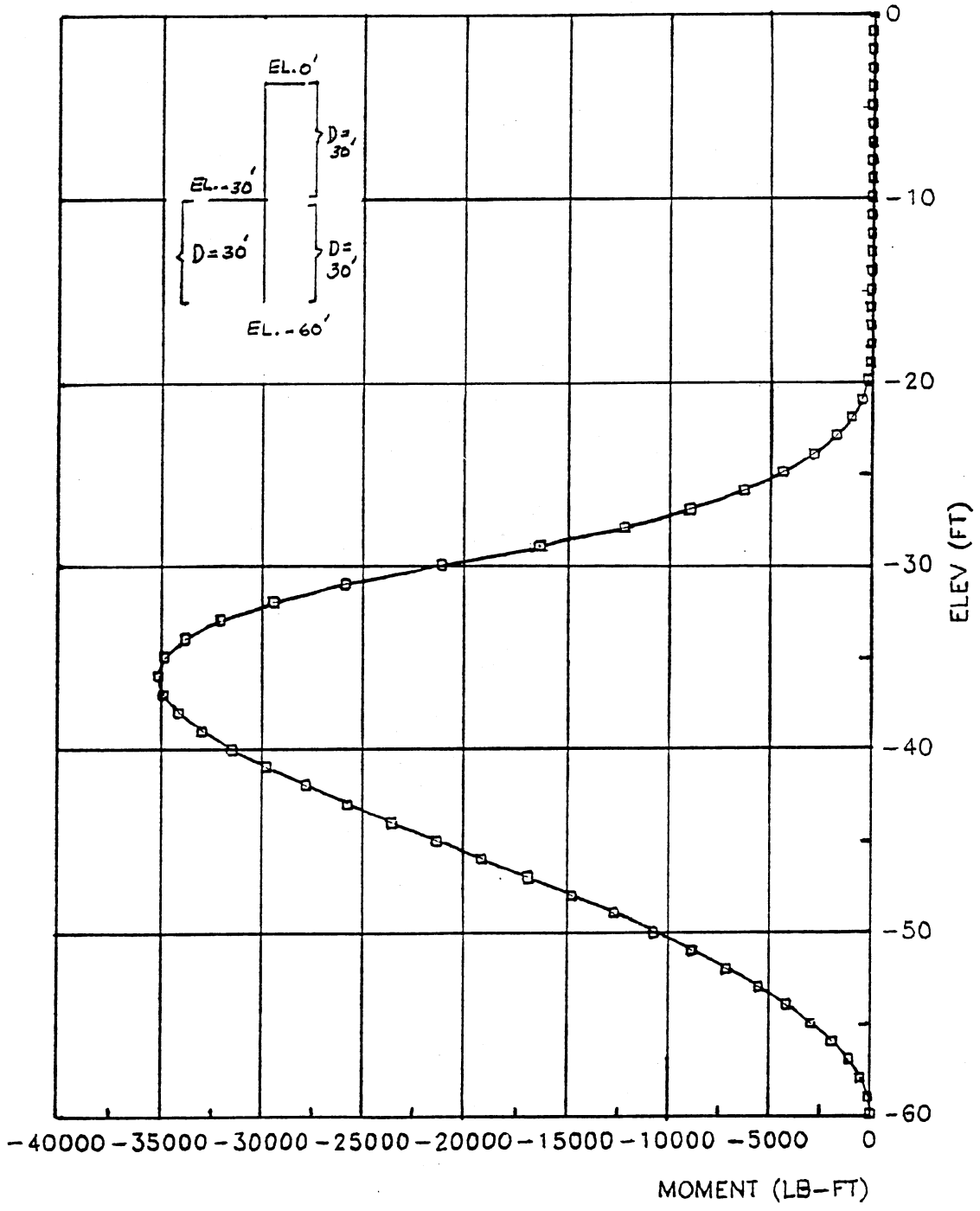

Figure 63. Bending moments from SSI analysis using Skempton's method. Cu = 1600 psf; Interaction Dist.: right(30'), left(30').

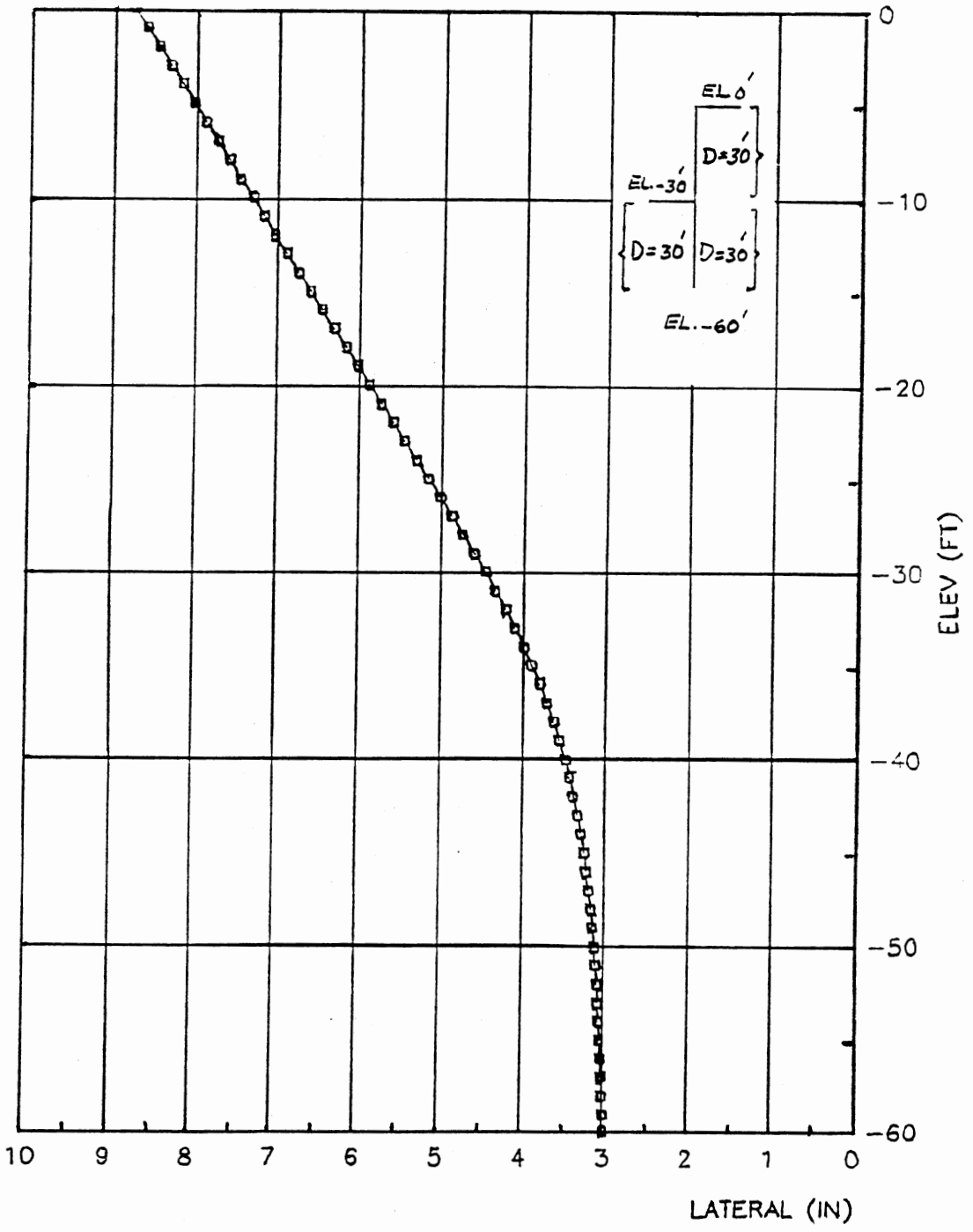

Figure 64. Pile deflections from SSI analysis using Skempton's method. Cu = 1600 psf; Interaction Dist.: right(30'), left(30').

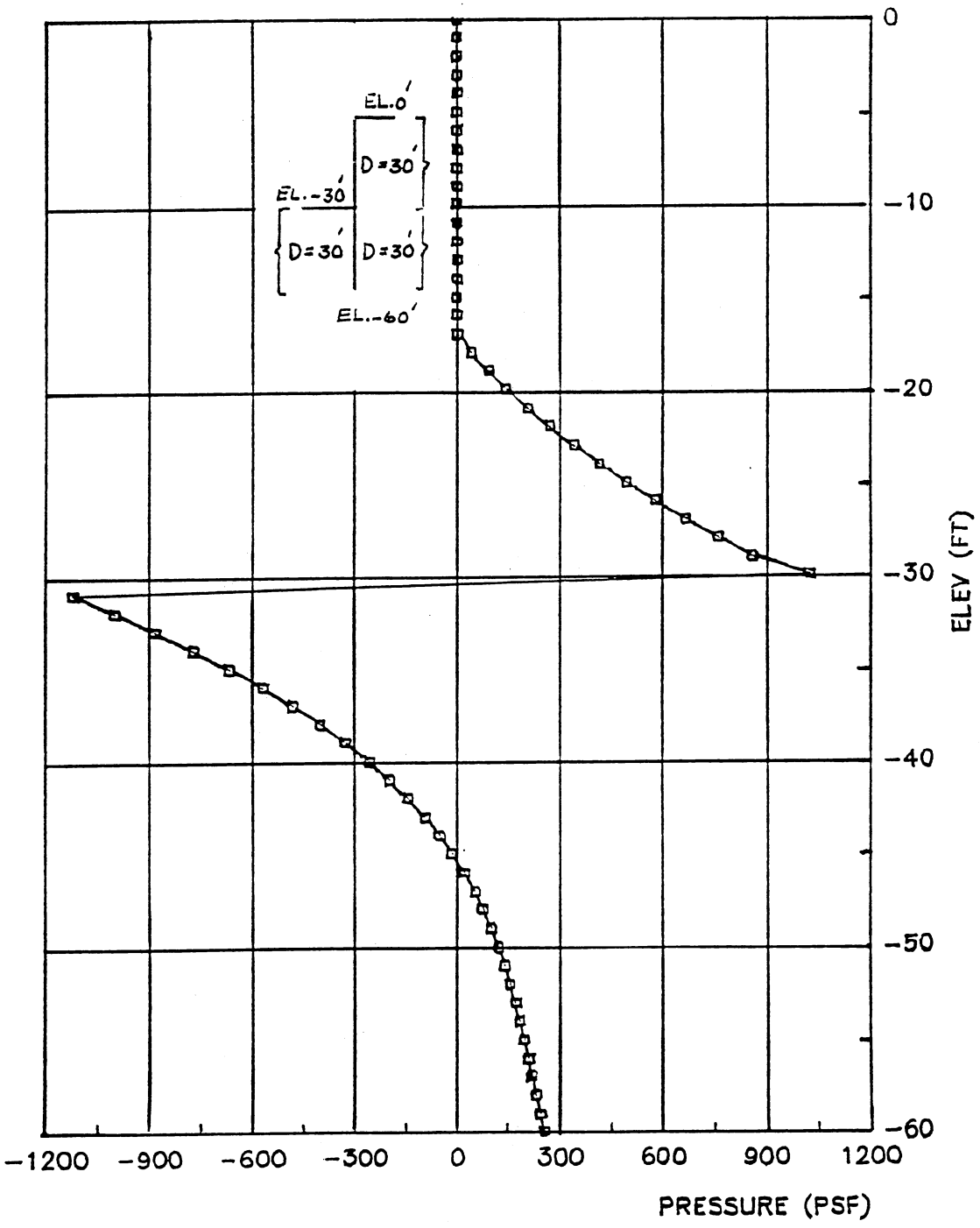

Figure 65. Net stress on the pile from SSI analysis; Skempton's method. Cu = 1600 psf; Interaction Dist.: right(30'), left(30').

ground surface.

2. A new SSI run using the values determined in step 1 was made. The results were plotted in Figs. 66-68. From the pressure versus elevation graph (Fig. 68), the depth of the tension crack is about 21 ft and the net pressure crosses the vertical-axis at 14 ft below the original ground surface. Therefore, an interaction distance of 9 ft will be used for the retained soil, 14 ft and 16 ft for the left and the right side below the original ground surface respectively.

3. A new SSI solution is performed with the values calculated (Figs. 69-71) shows very little change from the previous one. Therefore, this final run is deemed satisfactory since convergence has been achieved. The value of maximum negative moment obtained is 6.22 K-ft located at -35.50 ft elevation.

If Terzaghi's method was used to estimate E_s/ft of interaction distance, the solution can be improved even further. This is because the average value of E_s, as obtained from Terzaghi's method, is smaller than its counterpart from Skempton's method. For the above case, Terzaghi's method gives the following value for E_s:
from Reference (19), average E_{s1} = 87 pci, and minimum E_{s1} = 58 pci
thus:

E_s(average) = 0.67 x 87 x (1 ft/D ft) ≈ 58 pci/ft of int.distance
and,

Es(minimum) = 0.67 x 58 x (1 ft/D ft) ≈ 39 pci/ft of int.distance

A very interesting and convenient observation is that in most cases, the above iteration procedure does not need to be repeated when using Terzaghi's value, but the final values of interaction distance can be used directly with the new value of E_s. Such an analysis was done

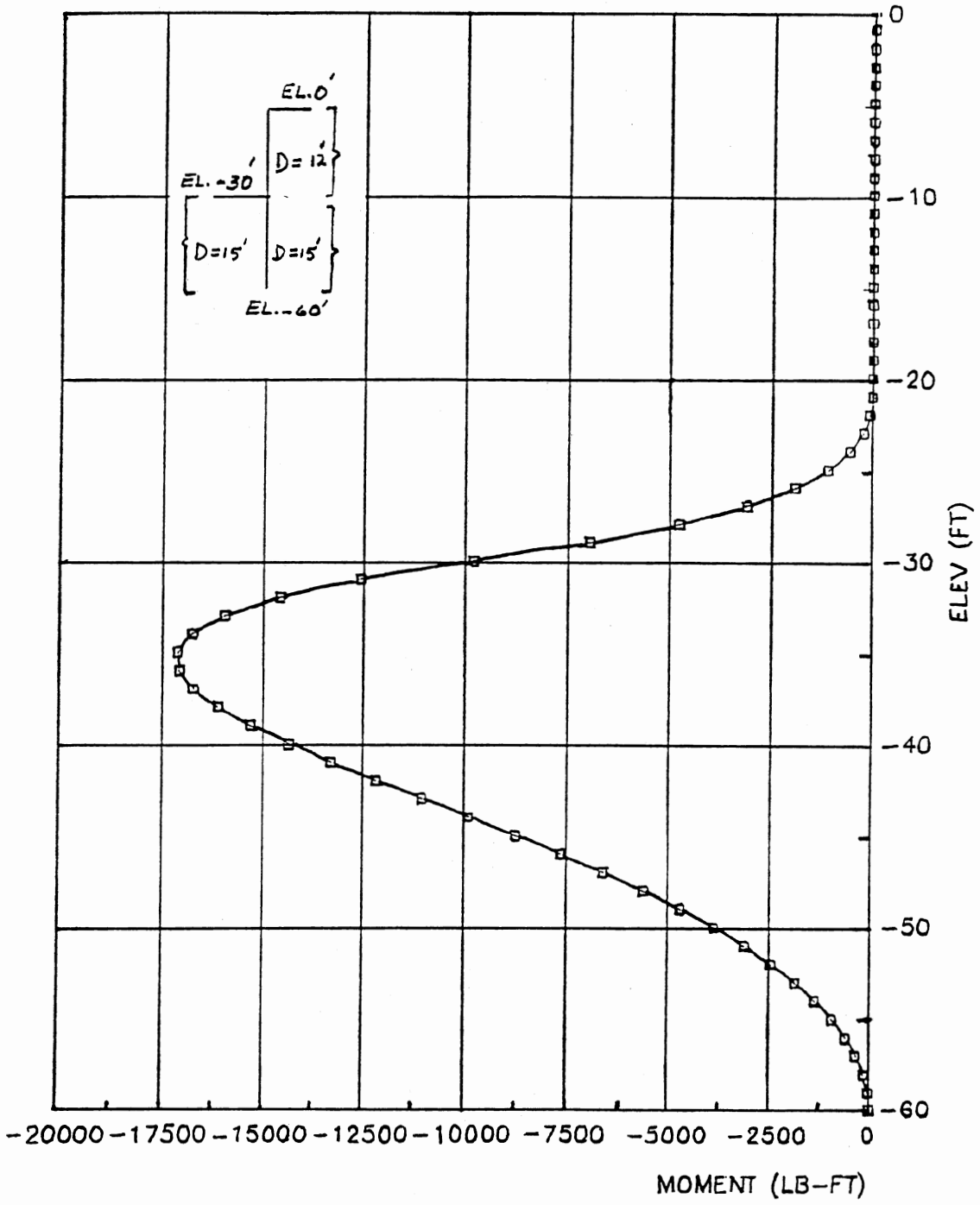

Figure 68. Bending moments from SSI analysis using Skempton's method. Cu = 1600 psf; Interaction Dist.: right(12,15),left(15)

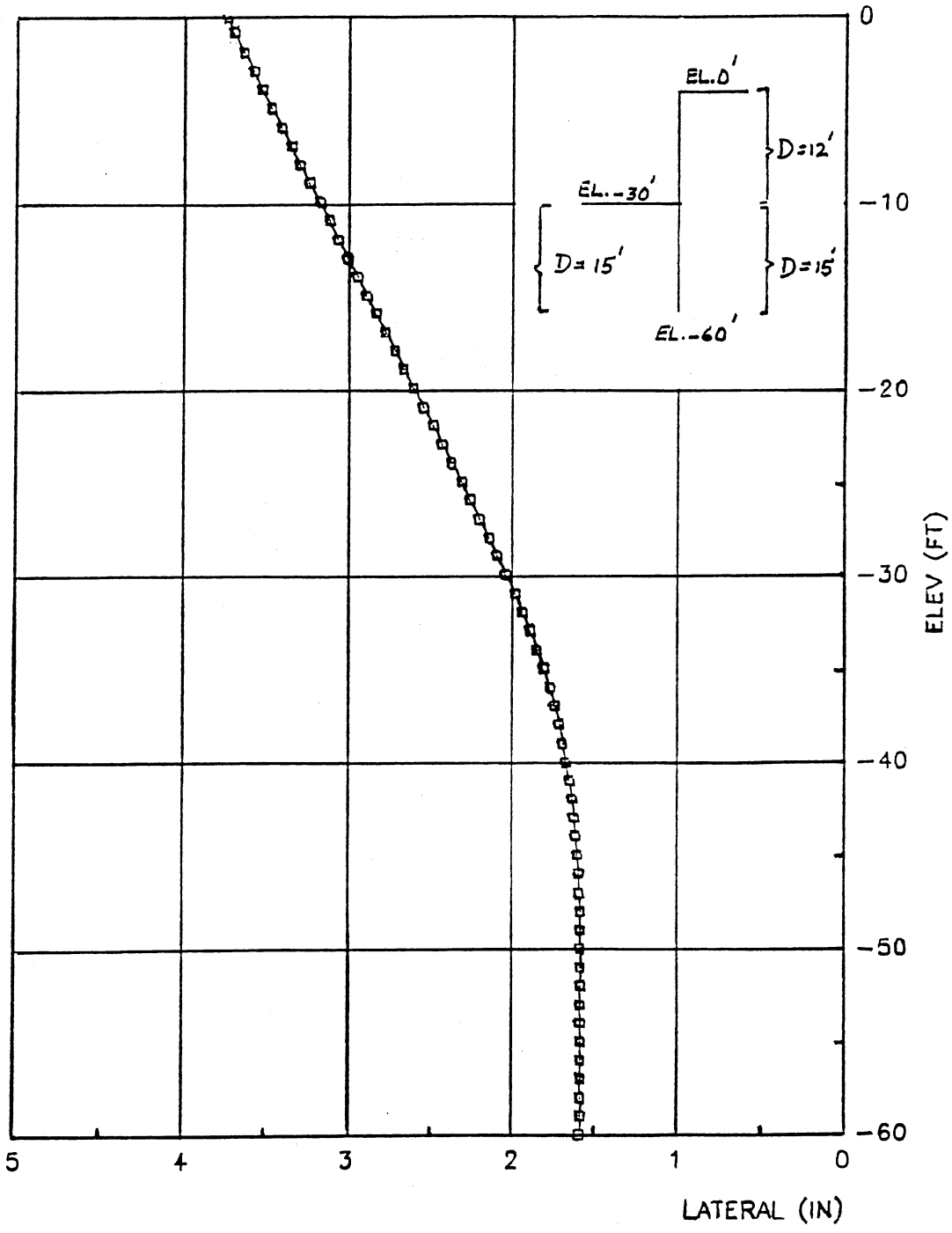

Figure 67. Pile deflections from SSI analysis using Skempton's method. Cu = 1600 psf; Interaction Dist.: right(12,15),left(15)

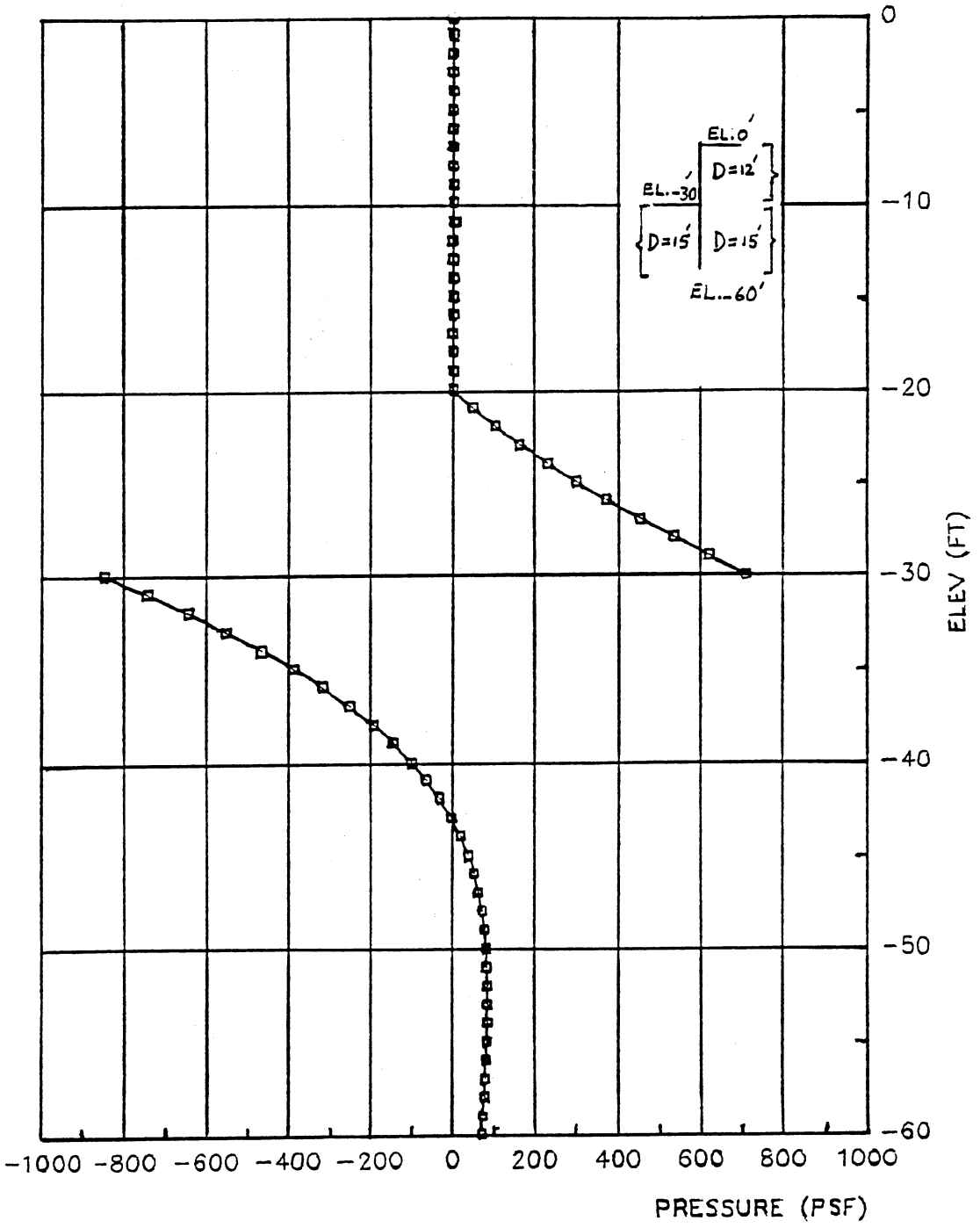

Figure 68. Net pressure from SSI analysis using Skempton's method. Cu=1600 psf;Interaction Dist.: right(12,15),left(15)

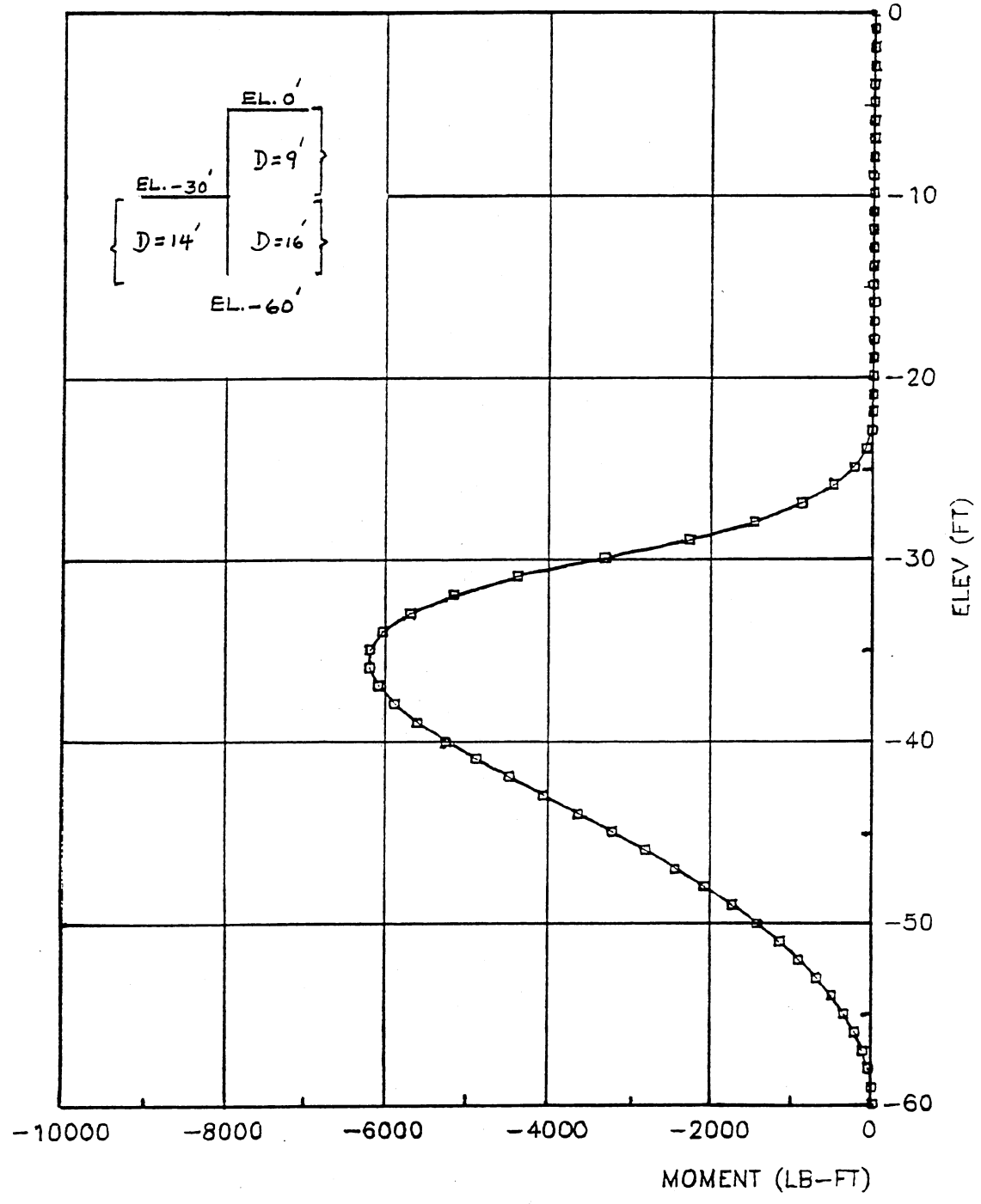

Figure 69. Bending moments from SSI analysis using Skempton's method. Cu = 1600 psf; Interaction Dist.: right(9,16),left(14)

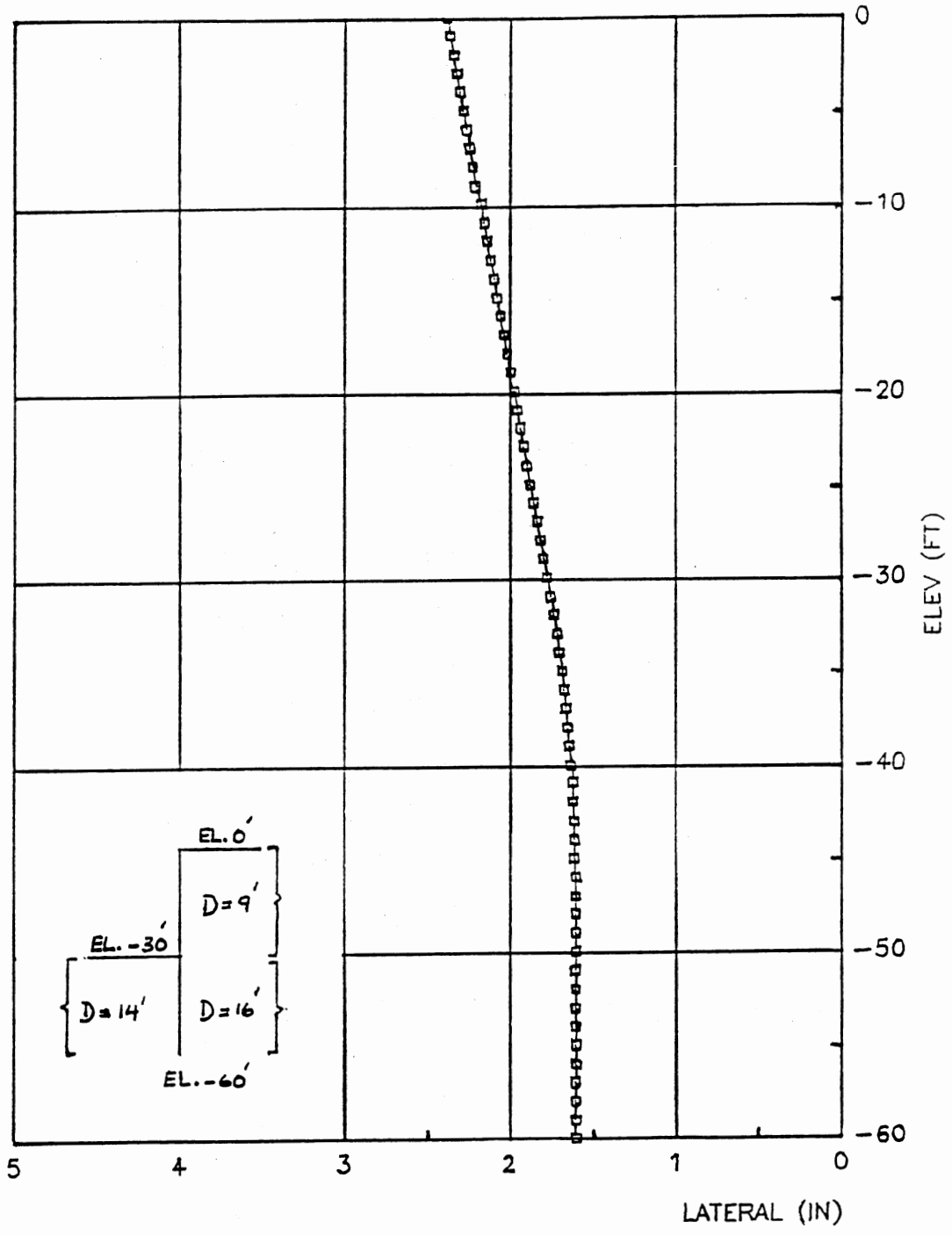

Figure 70. Pile deflections from SSI analysis using Skempton's method. Cu = 1600 psf; Interaction Dist.: right(9,16),left(14)

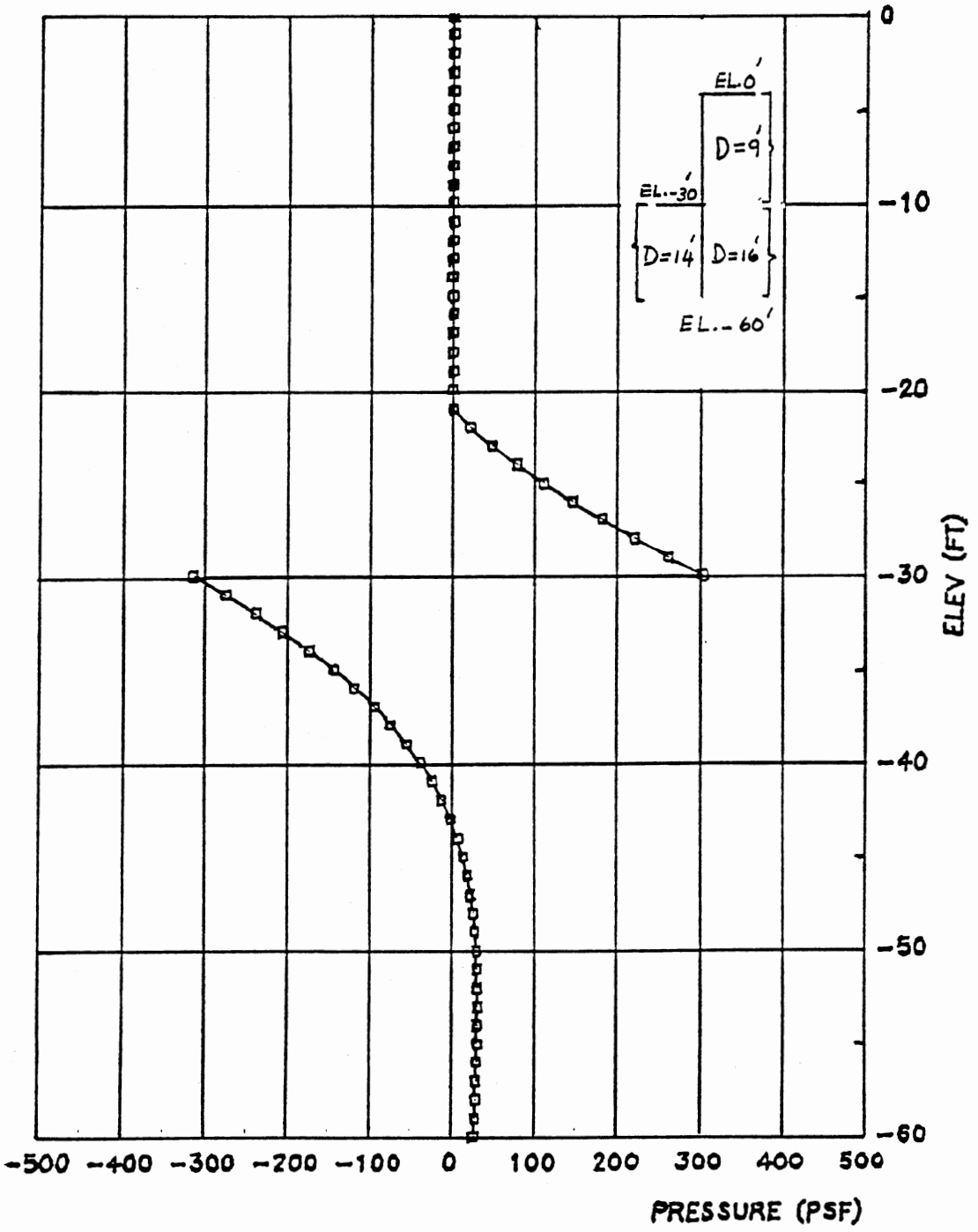

Figure 71. Net pressure from SSI analysis using Skempton's method. Cu=1600 psf; Interaction Dist.: right(9,16),left(14)

for the same case (30 ft penetration, Cu = 1600 psf). The results were plotted in Figs. 72-74. The maximum negative moment is 8.15 K-ft at -36 ft elevation using the average Terzaghi value, and 9.57 k-ft at -36.5 ft elevation based on the lower bound of Terzaghi's table.

All the remaining cases were analyzed in the same way and convergence was obtained in every case. It is also interesting to note that for 30 ft penetration depth with Cu = 1300 psf, contra-flexure was obtained and convergence was achieved by taking the average value of the two segments for which the left-side soil was the predominant factor in determining the net soil pressure.

Comparison between SSI and FE Solutions

From the results of the SSI and finite element solutions, the following assumptions and aspects of behavior can be compared:

1. Comparison between the moments and displacements in the SSI and FE approaches.
2. The variation of soil stiffness, E_s, with depth for homogeneous clay under $\phi = 0$ conditions.
3. The stiffness variation between the active and passive limits (i.e., the shape of the force vs. displacement curves).
4. A comparison of the FE plateau values (i.e., at or near failure) with the full-active and full-passive limit equilibrium values from the classical theory ($\sigma_v \pm 2Cu$).
5. The depth of propagation of the tension crack.
6. The lower bound of Cu for which failure or instability ensues.
7. Soil stress profile on the retaining wall.

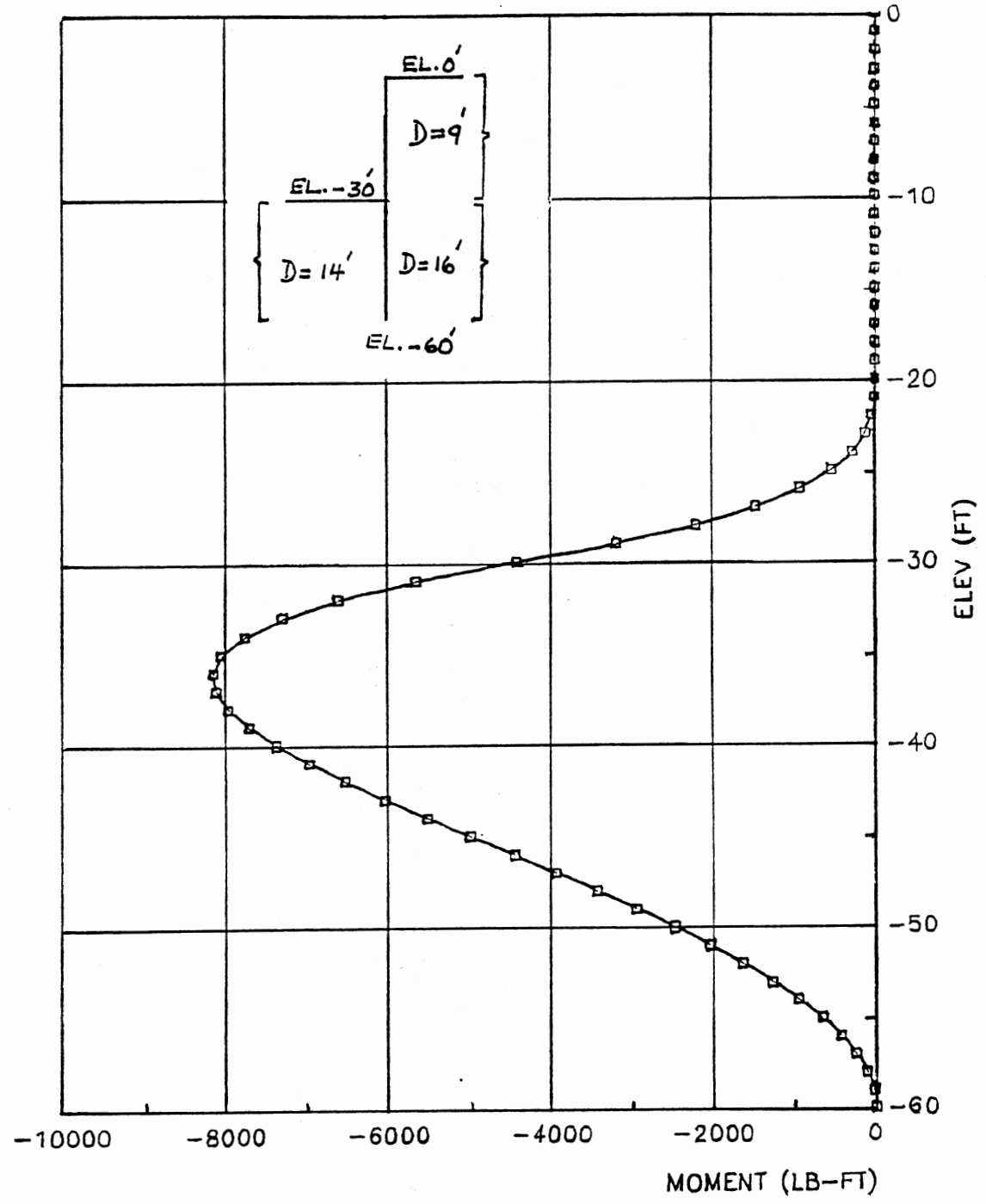

Figure 72. Bending moments from SSI analysis using Terzaghi's method. Cu = 1600 psf; Interaction Dist.: right(9,16),left(14)

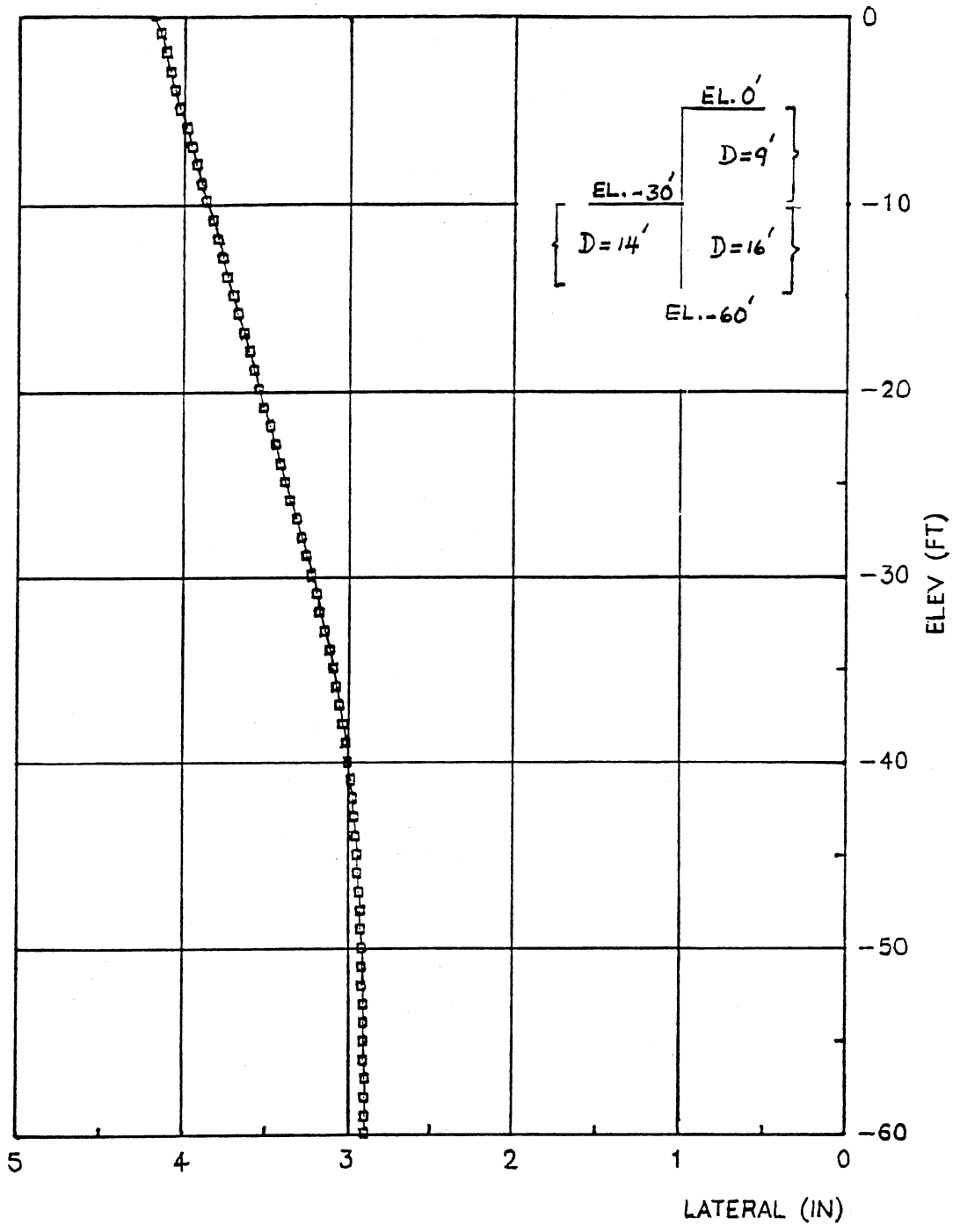

Figure 73. Pile deflections from SSI analysis using Terzaghi's method. Cu = 1600 psf; Interaction Dist.:right(9,16),left(14)

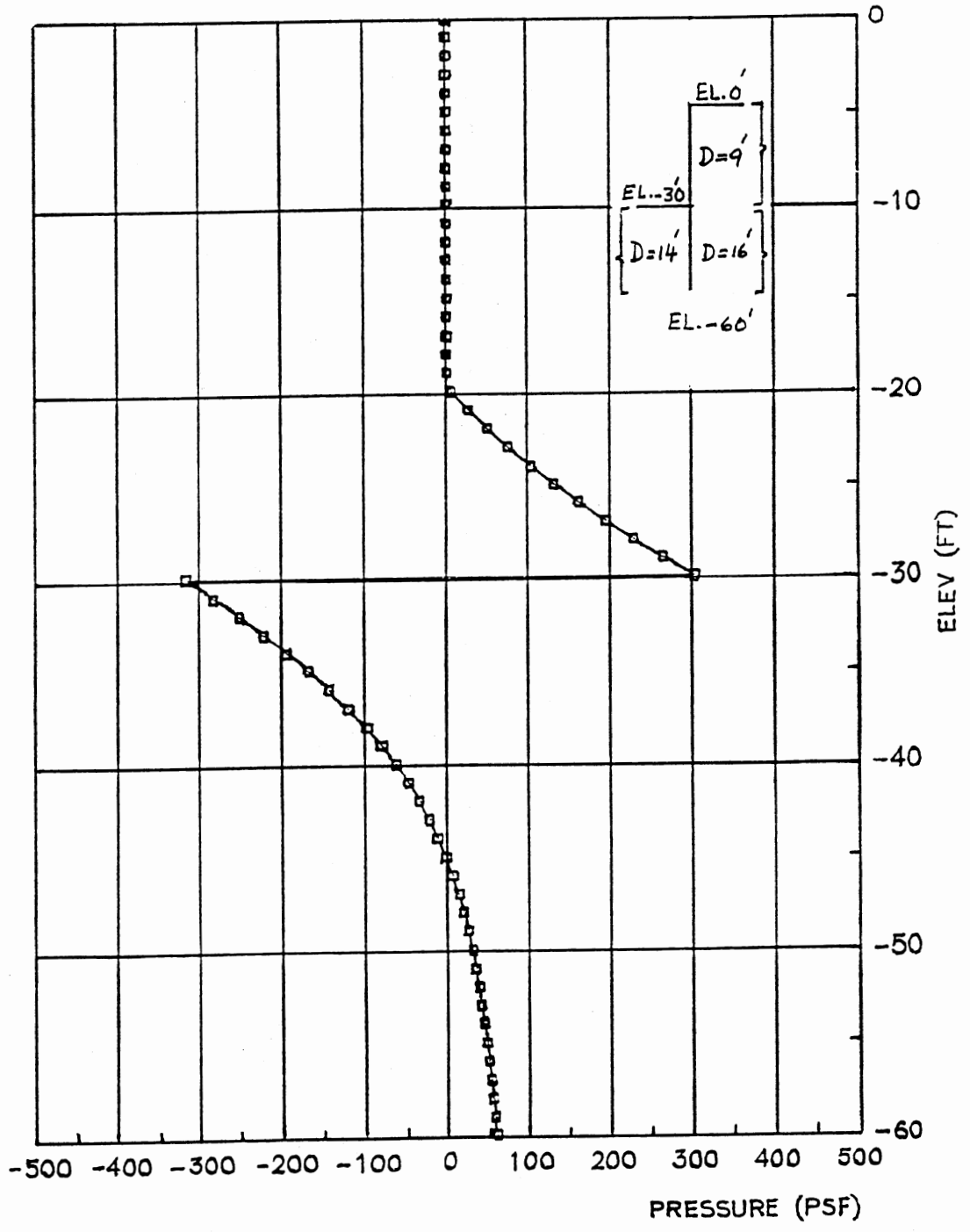

Figure 74. Net pressure from SSI analysis using Terzaghi's method. Cu = 1600 psf; interaction Dist.:right(9,16),left(14)

Moments and Displacements from FE and SSI Methods

Figs. 75-76 show the moment and displacement diagrams for a typical case (Cu=1600 psf, 30 ft penetration). The maximum negative moment is higher when Terzaghi's values for soil stiffness are used. This is because the E_s values obtained from Terzaghi's table are smaller than those calculated using Skempton's equation. Furthermore, the lower Terzaghi values for E_s result in moments that are in excellent agreement with those obtained from the FE gravity-turn-on analysis. For example, for the above analyzed case (Cu=1600 psf, 30 ft penetration), the maximum negative moment based on the minimum Terzaghi values was 9.57 k-ft at -36.50 ft elevation compared to 9.5 k-ft at an elevation of -34.9 ft obtained in the gravity-turn-on case. However, as Fig. 75 shows, the FEM predicts a small positive moment near the tip of the pile which is not obtained in the SSI case. The reason is that the FEM can account for a high tip reaction which is absent in the SSI case. As for displacements (Fig. 76), Terzaghi's values lead to higher displacements especially when the lower limit is used. However, these displacements are lower than those predicted by the FEM. This is due to the relatively large rigid-body displacements especially for the $\phi = 0$ case.

Soil Stiffness Variation

It is frequently assumed in SSI analyses that for homogeneous clay the value of soil modulus E_s (per ft of interaction distance) does not vary with depth for a certain layer. The assumption is implicit in the way E_s is calculated. If Skempton's method is used, E_s depends on Cu and ϵ_{50}. On the other hand, if Terzaghi's method is used, E_s depends only on the consistency of soil.

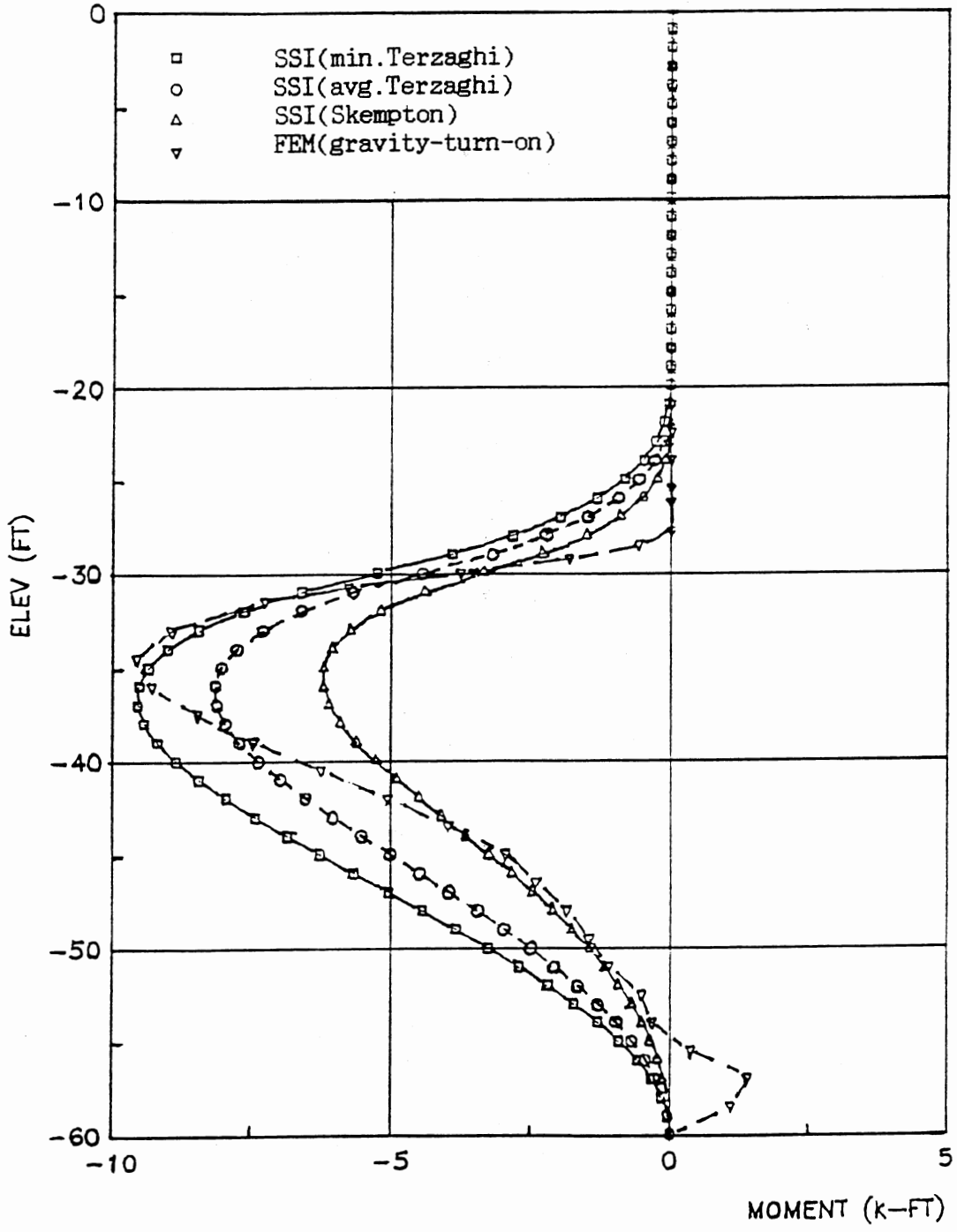

Figure 75. Bending moments vs. Elevation; Cu = 1600 psf. Depth of penetration = 30 ft.

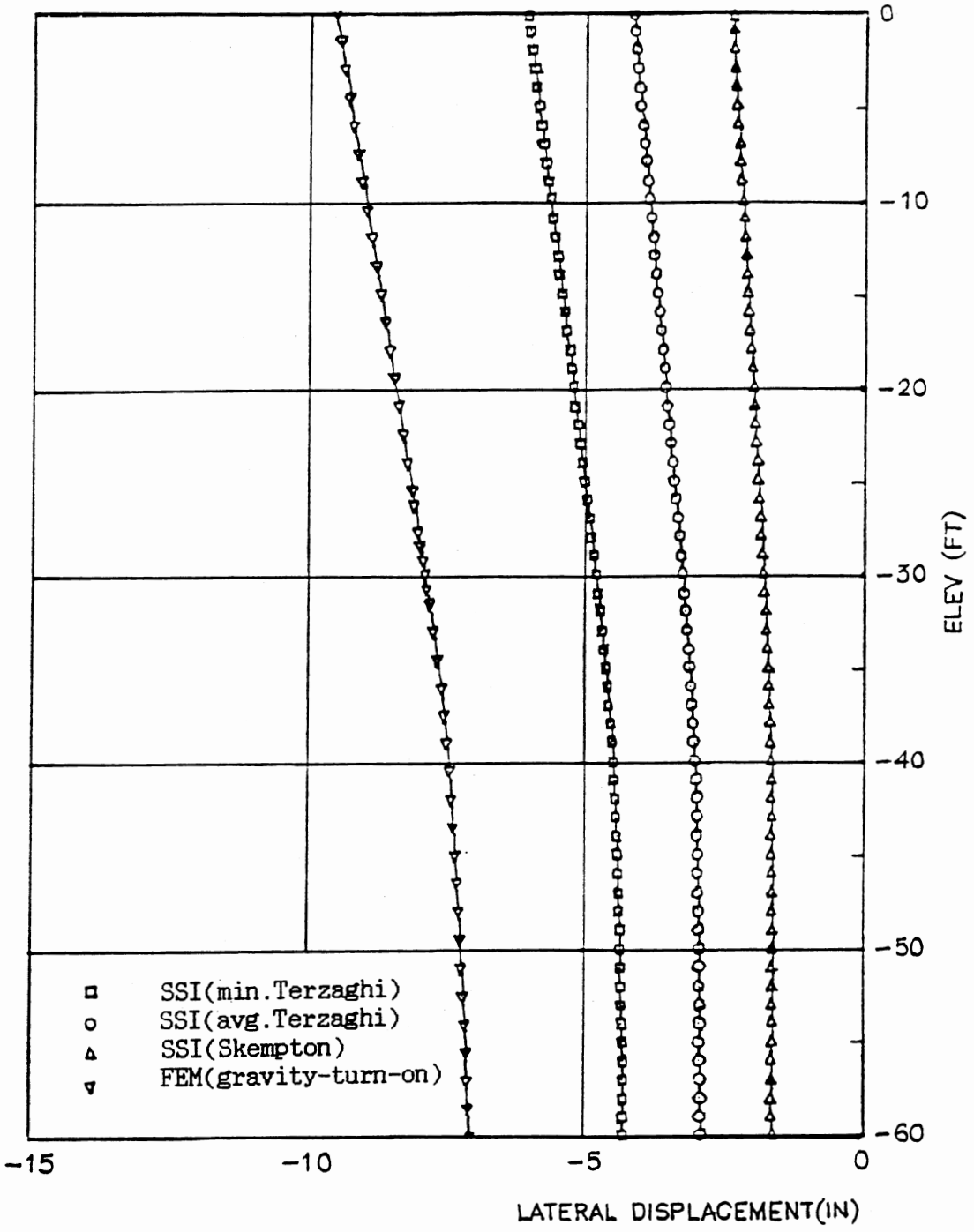

Figure 76. Pile deflections vs. Elevation; Cu = 1600 psf. Depth of penetration = 30 ft.

To investigate whether or not E_s varies with depth, some selected values of E_s are calculated at different stations along the pile for different finite element runs. Since the force-displacement curves found from the finite element analysis have the effect of D embedded in them, the variation of E_s was studied for stations expected to have roughly the same interaction distance according to SSI theory. In all of these calculations the secant modulus at the endpoint is calculated, i.e., the slope of the line joining the first and last points on the force-displacement plot. This secant modulus was chosen because the final state of the system was found to be very close for the gravity-turn-on and buildup cases. It is also independent of the number of substeps needed to ensure convergence in either method. This secant modulus will make it easier to compare various results.

Typical force vs. displacement curves were shown in Figs. 18-23. Some values of the soil modulus, E_s, were tabulated for Cu = 1600 psf and 30 ft penetration depth (Table I). The corresponding values of D were found by dividing Skempton's values of soil modulus (per ft of interaction distance) by the secant modulii obtained from the FEM solution. The resulting D values were tabulated along with the corresponding E_s values (Table IV) for the gravity-turn-on case. The values of E_s and D vary with depth, as easily seen from Table IV for Cu = 1600 psf and 30 ft penetration. In particular, the interaction distance, D, was found to decrease with depth while the soil modulus, E_s, was found to increase with depth (Figs. 77-80). At the same location along the pile, it is evident that the soil element in passive has a higher value of E_s, and therefore a lower value of D. Furthermore, the value of D around the pile tip is almost equal to the

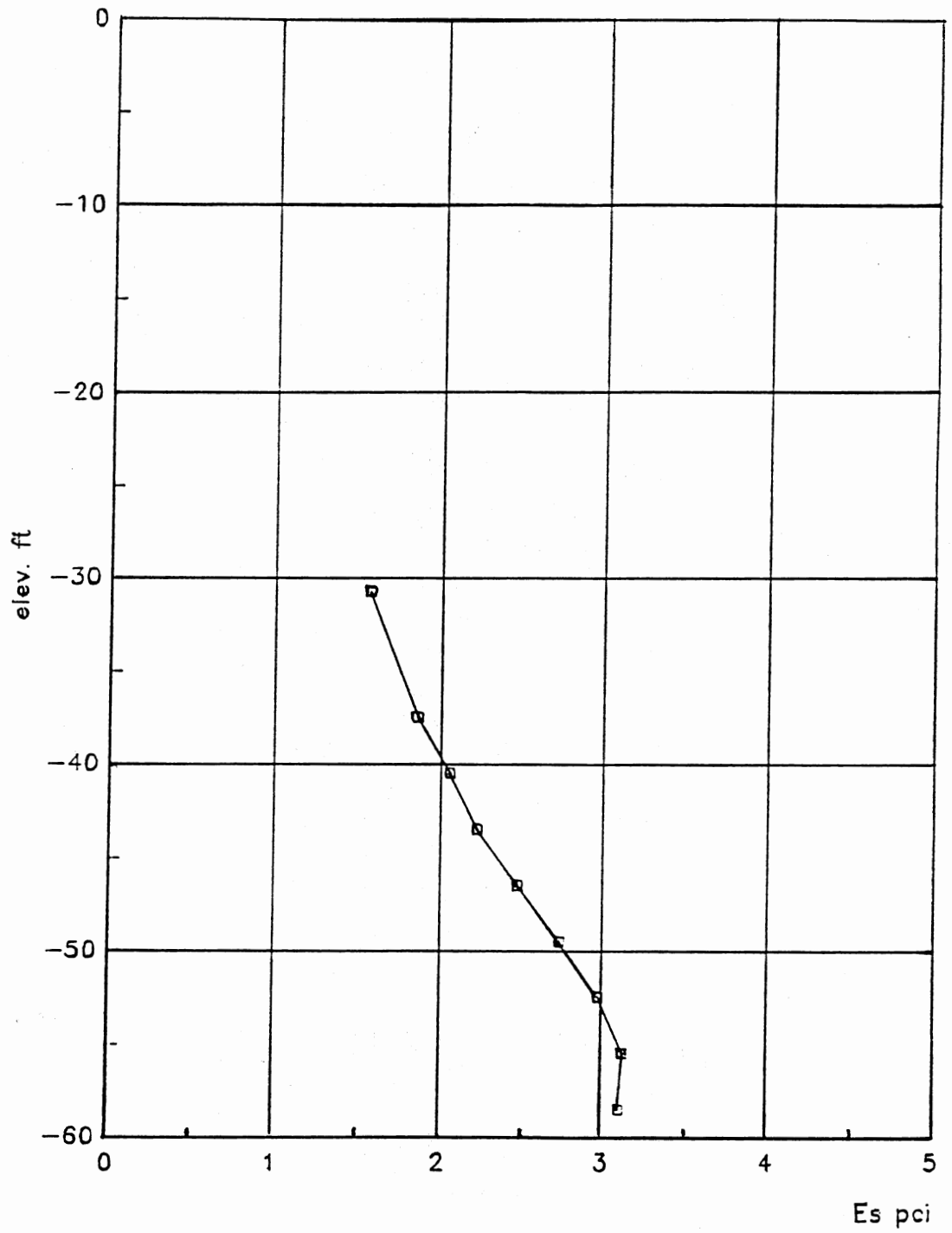

Figure 77. Soil Modulus (E_s) vs. Elevation (leftside); Cu = 1600 psf
Gravity-turn-on analysis; 30 ft penetration depth.

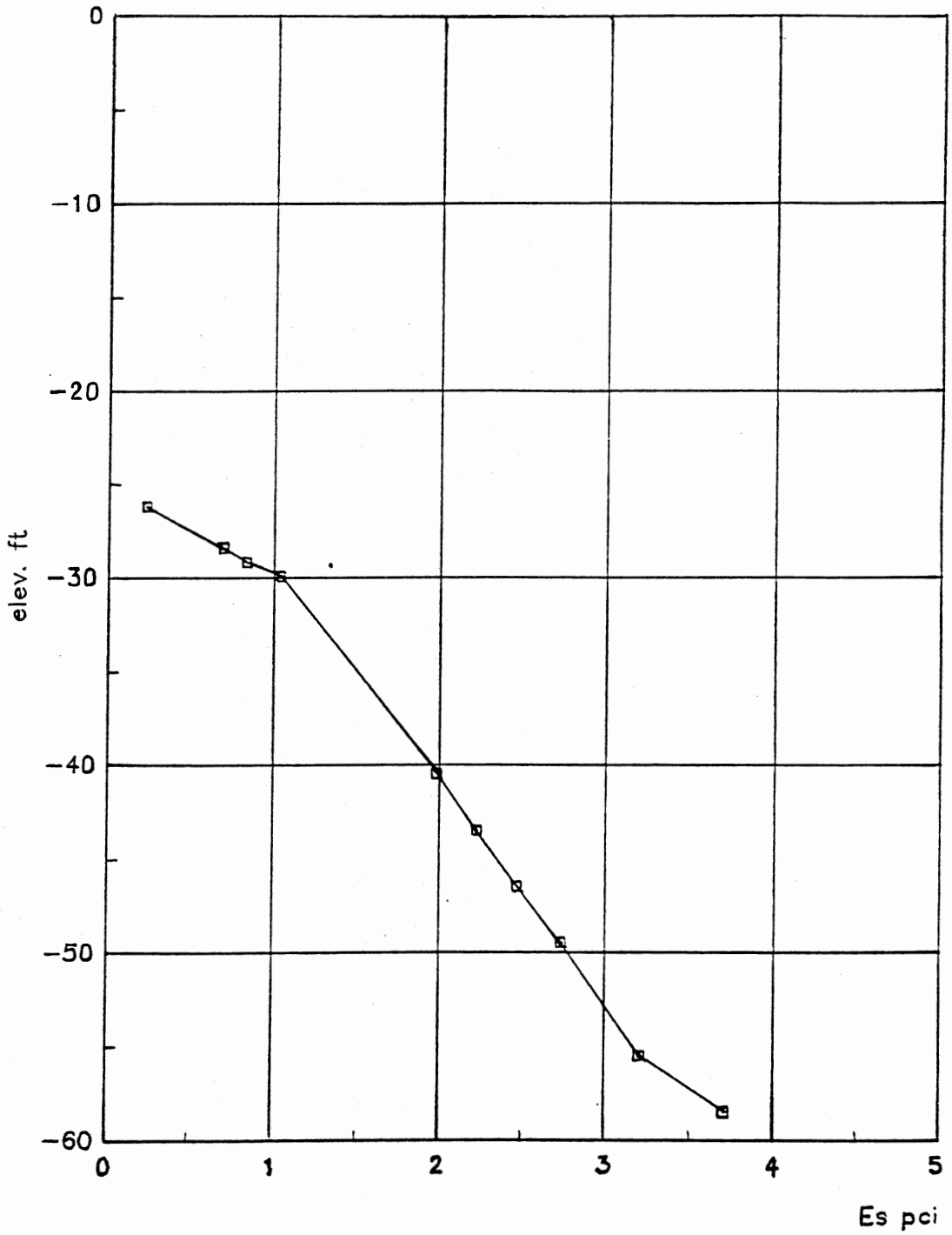

Figure 78. Soil Modulus (E_s) vs. Elevation (rightside); Cu = 1600 psf Gravity-turn-on analysis; 30 ft penetration depth.

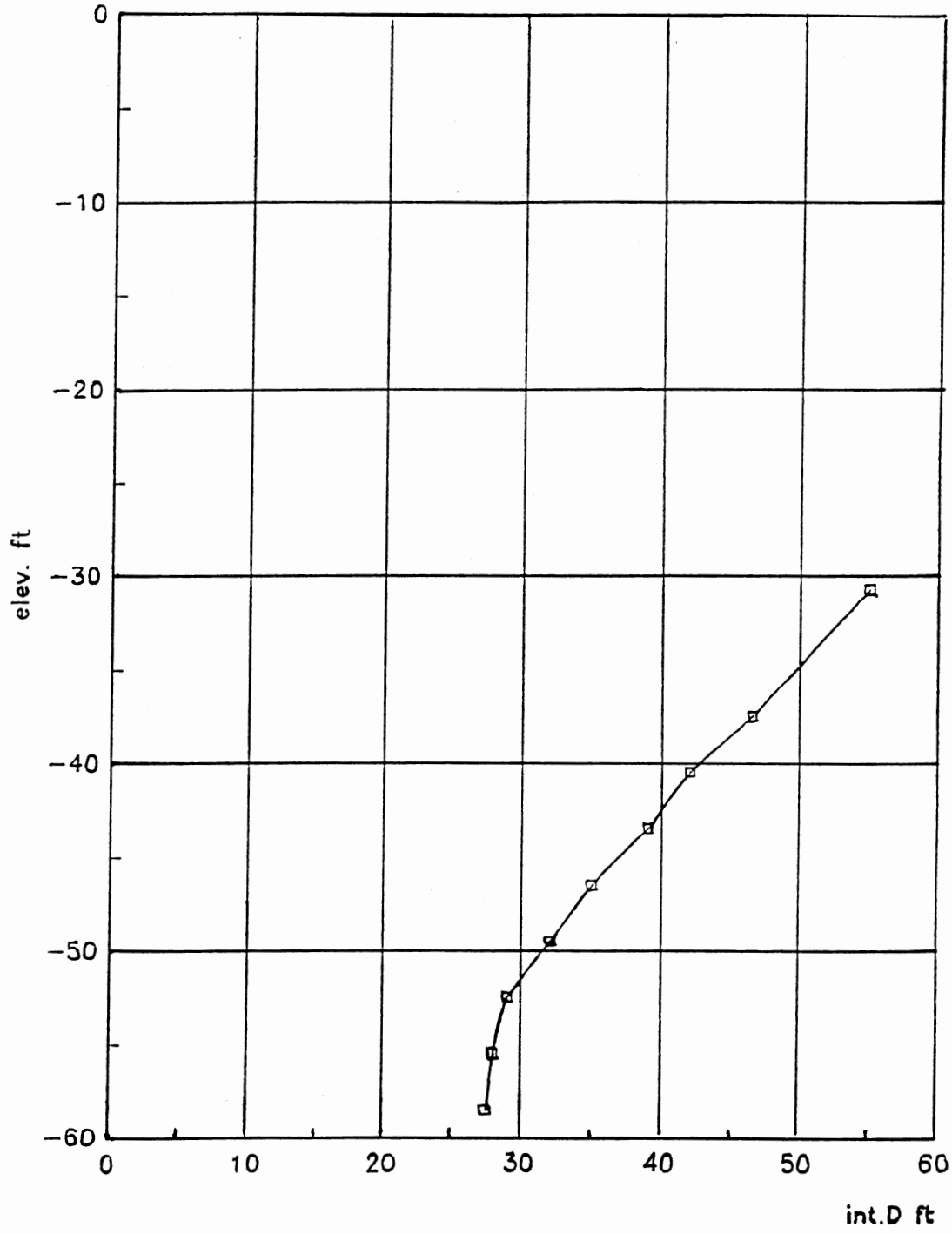

Figure 79. Interaction Dist.(D) vs. Elevation (leftside); Cu = 1600 psf Gravity-turn-on analysis; 30 ft penetration depth.

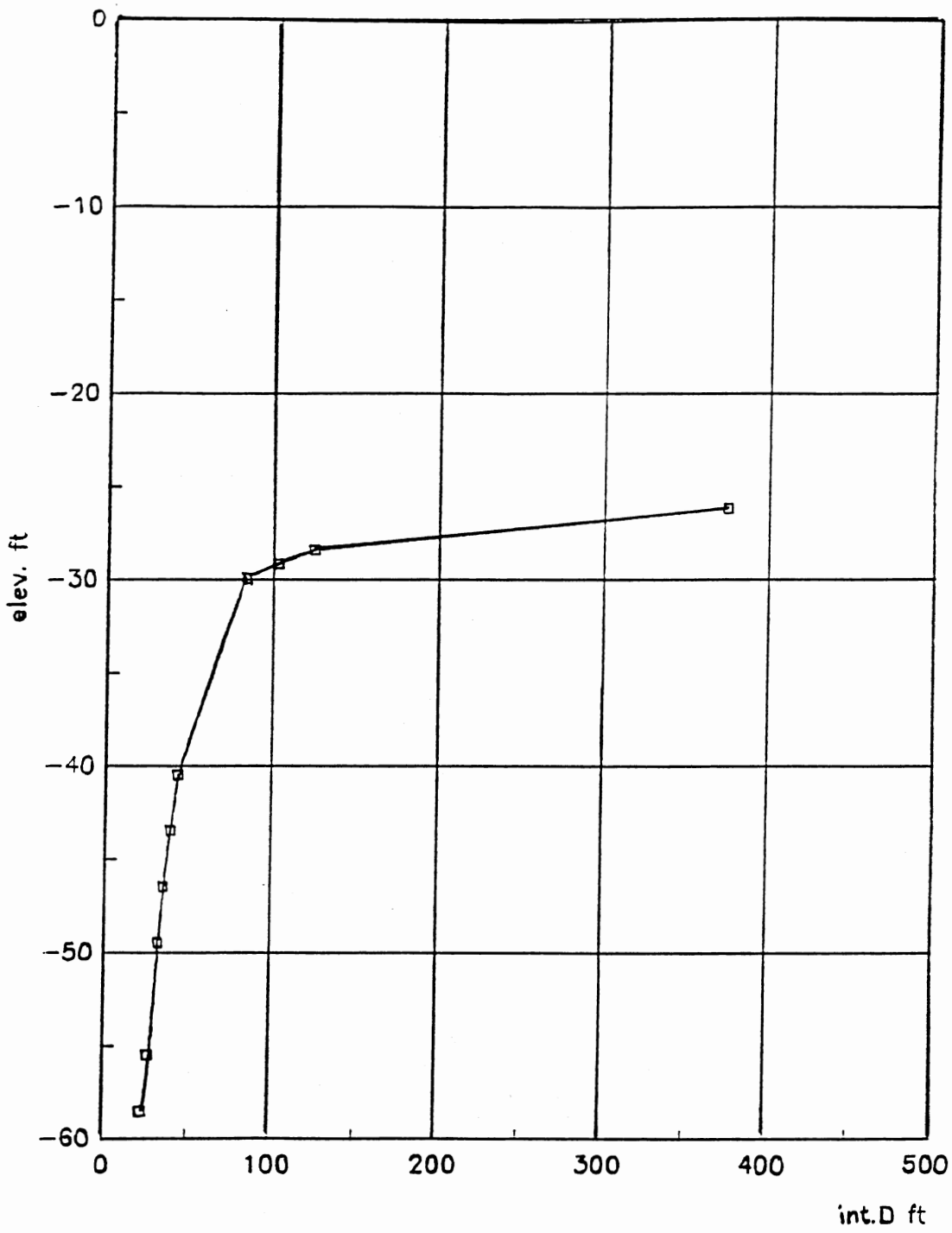

Figure 80. Interaction Dist.(D) vs. Elevation (rightside);Cu = 1600 psf
Gravity-turn-on analysis; 30 ft penetration depth.

TABLE IV

SOIL MODULUS AND INTERACTION DISTANCE
GRAVITY-TURN-ON; Cu=1600 PSF; 30 FT PENETRATION

	Left		Right	
Elev.(ft)	E_s(pci)	D(ft)	E_s(pci)	D(ft)
-58.5	3.10	28	3.7	23
-55.5	3.12	27.5	3.2	27
-52.5	2.97	29	2.94	29
-49.5	2.73	32	2.73	32
-46.5	2.47	35	2.47	35
-43.5	2.22	39	2.22	39
-40.5	2.05	42	1.98	43
-30.75	1.56	55	1.04	83
-29.25			0.83	103
-28.5			0.70	124
-26.25			0.23	374

* Gravity-turn-on; Cu = 1600 psf, 30 ft penetration depth.
N.B: The actual values of E_s are higher than the tabulated values and by the same token the actual values of D are lower; this is due to the rigid body displacement that should be subtracted from the total displacement when the effective values of E_s and D are calculated.

value of the embeddment depth (30′). It starts to increase when moving upward and reaches a very high value in the active zone, above the original ground surface.

For clay under undrained conditions, a relatively large portion of the total displacement is a rigid-body displacement that accounts for no stresses whatsoever. Therefore, when the value of E_s were calculated from the finite element method, the values used for displacement had embodied in them a rigid-body displacement. Consequently, smaller values of E_s were obtained. For the undrained case, depending on the relative stiffness of the wall to the soil, the soil can be the predominant factor. In this case, the wall would be merely `floating′ in the soil matrix. This observation was also found to govern the behavior of floodwalls, as the study in Reference (20) demonstrated. Therefore, the SSI assumption that the wall moves and by doing so triggers a soil response, is a very simplistic one and can be erroneous at times.

Although the values of E_s, as shown in Tables I and IV, are on the low side as explained above, yet it is logical to assume that the rigid-body portion of the displacement is uniform. Therefore, the variation of E_s with depth is still valid, at least in a qualitative sense. The amount of this rigid-body displacement is roughly the displacement of the tip of the pile.

Variation between Active and Passive

From the force displacement curves obtained from the finite element analysis, it is clear that, in general, the stress-displacement curves are not linear (e.g., Figs. 18-23). However, when the stress level is

relatively low, the resulting curves are linear. This is almost analogous to moving along the initial tangent to the stress displacement curves. Therefore, it seems likely that more accurate SSI results would be obtained if the general shape is taken into consideration. The characteristic shape of these stress-displacement curves is of the same nature as the stress-strain curves used in the soil model.

Stress Limits

An important assumption in the SSI method is that the maximum passive and the minimum active pressures are the limiting equilibrium values ($\sigma_v \pm 2Cu$ for $K_a = Kp = 1$). To investigate this crucial assumption, the closest that could be done for regular runs would be to choose soil elements that are close to local active and passive failure, and then check the validity of this assumption.

However, that problem was tackled from a different angle. Unlike an SSI run that can only provide information about the final state of stress and strain, the finite element solution (gravity-turn-on or buildup) can be used to shed some light on the whole process from beginning to end. It also shows at what level of load the system becomes unstable.

With this in mind, a finite element solution was obtained for a 30 ft x 30 ft wall with Cu = 700 psf, thus making sure the soil elements are stressed to failure (it was established earlier that progressive failure was observed at Cu = 725 psf).

Fig. 81 shows the progress of net displacement (top less bottom displacement) with the loading increments. It is clear that failure by instability (excessive wall displacements) starts at about 70% of the

total load.

Figs. 82-83 show typical stress-displacement curves. From these curves, two modes of soil behavior at the ultimate level are observed:

1. The response curve at failure is not exactly horizontal but has a slightly upward slope (residual strength) as shown in Fig. 82.
2. The force-displacement diagram reaches a maximum value and then decreases with the commencement of failure for the gravity-turn-on case and levels off for the buildup case as shown in Fig. 83.

The first type was observed for all elements below the original ground surface whether they are in active or in passive. The reason why the soil elements continue to pick up stress is inherent in the soil model. This is because the constrained modulus is not set to zero at failure. The second type occurs exclusively in the retained soil. This type of behavior was also noticed for other Cu values. This clarifies the mechanism of propagation of the tension crack. In the early loading stages, the poisson effect is more dominant than the tendency of the retained soil to move away from the wall. When the latter effect prevails (at higher loads), the confining stress starts decreasing as shown in Fig. 84. Eventually, the confining stress will diminish for those elements along the tension crack.

An interesting observation can be made about the limit values of active and passive pressures. The limit value reached in active condition is invariably smaller than (σ_v-2Cu), as predicted in the classical theory, and the limit value for passive state is always larger than (σ_v+2Cu). This is illustrated in Table V. The reason for this apparent discrepancy is that the effective value of at-rest

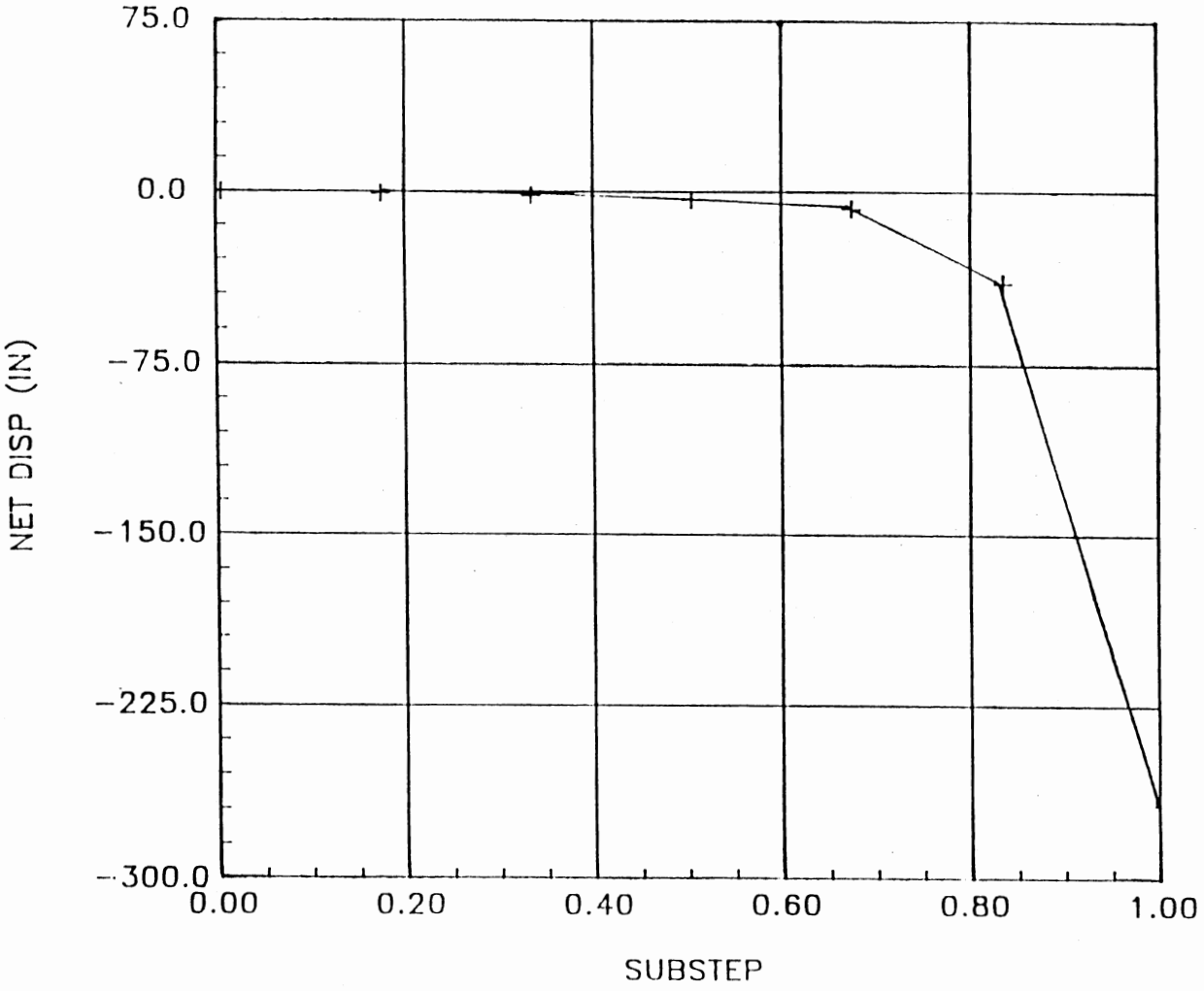

Figure 81. Net displacement vs. load; Cu=700 psf; gravity-turn-on 30 ft penetration depth.

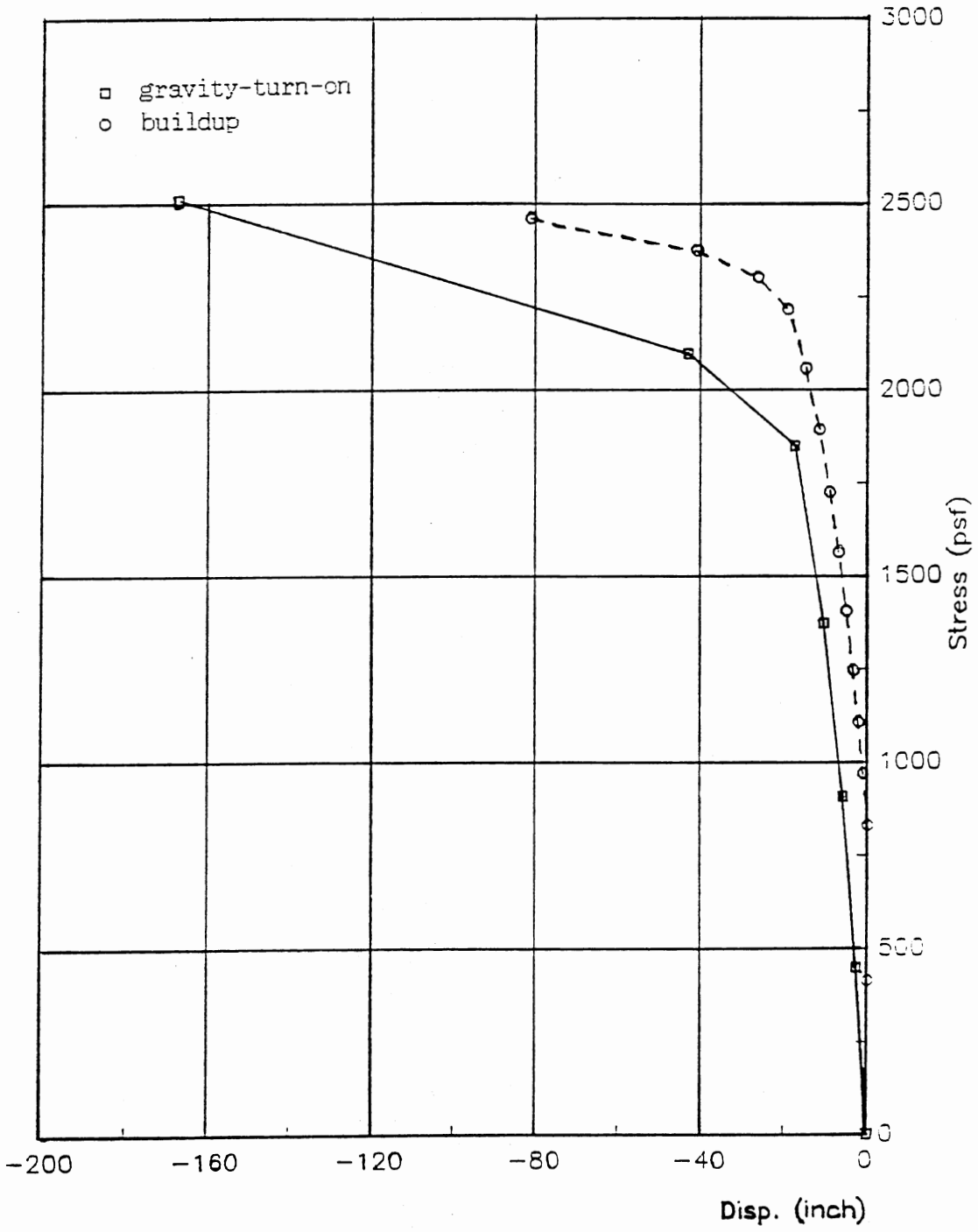

Figure 82. Soil-Response curves for point E at Elev. = -37 ft. Cu = 700 psf; 30 ft penetration depth.

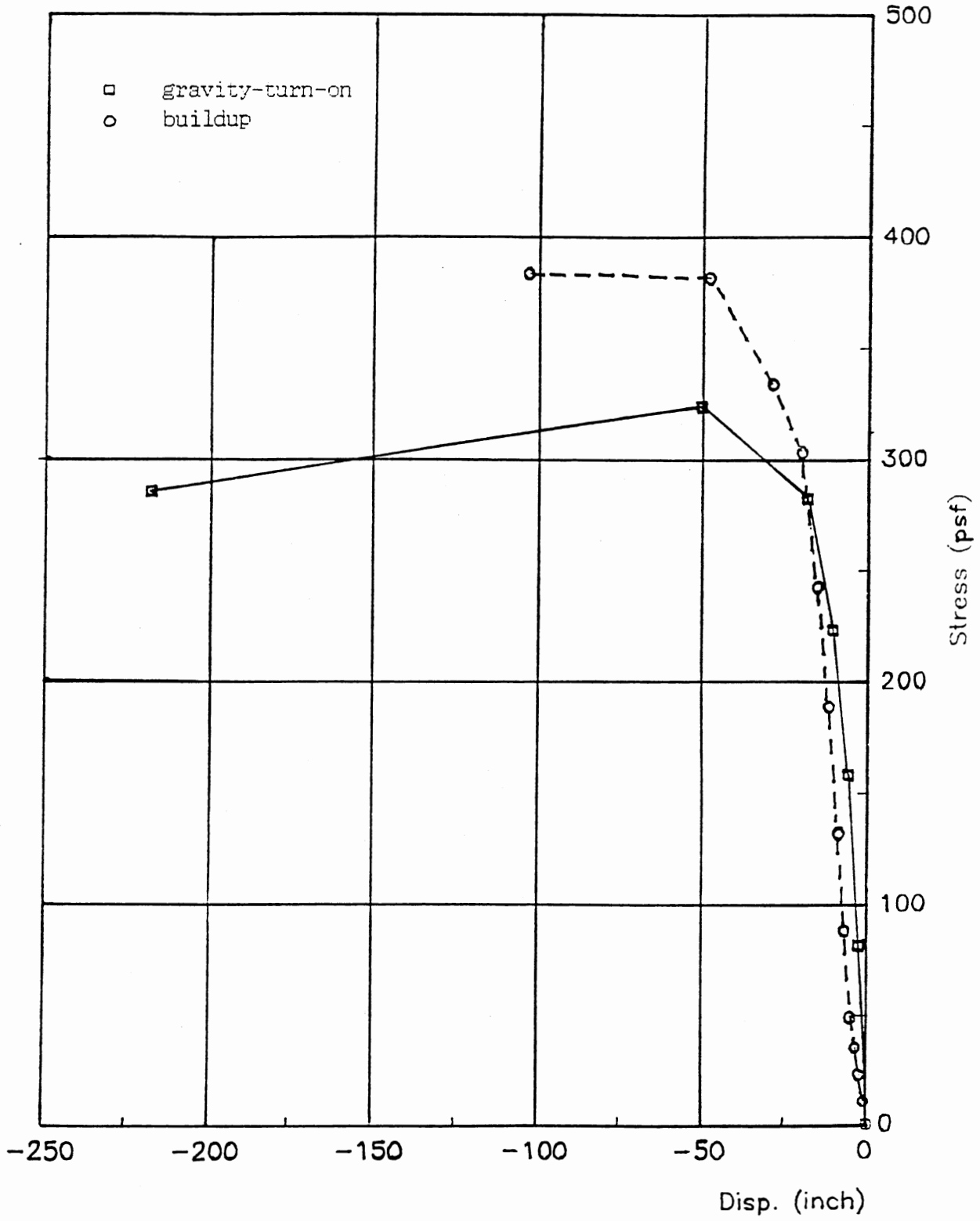

Figure 83. Soil-Response curves for point I at Elev. = -26 ft. Cu = 700 psf; 30 ft penetration depth.

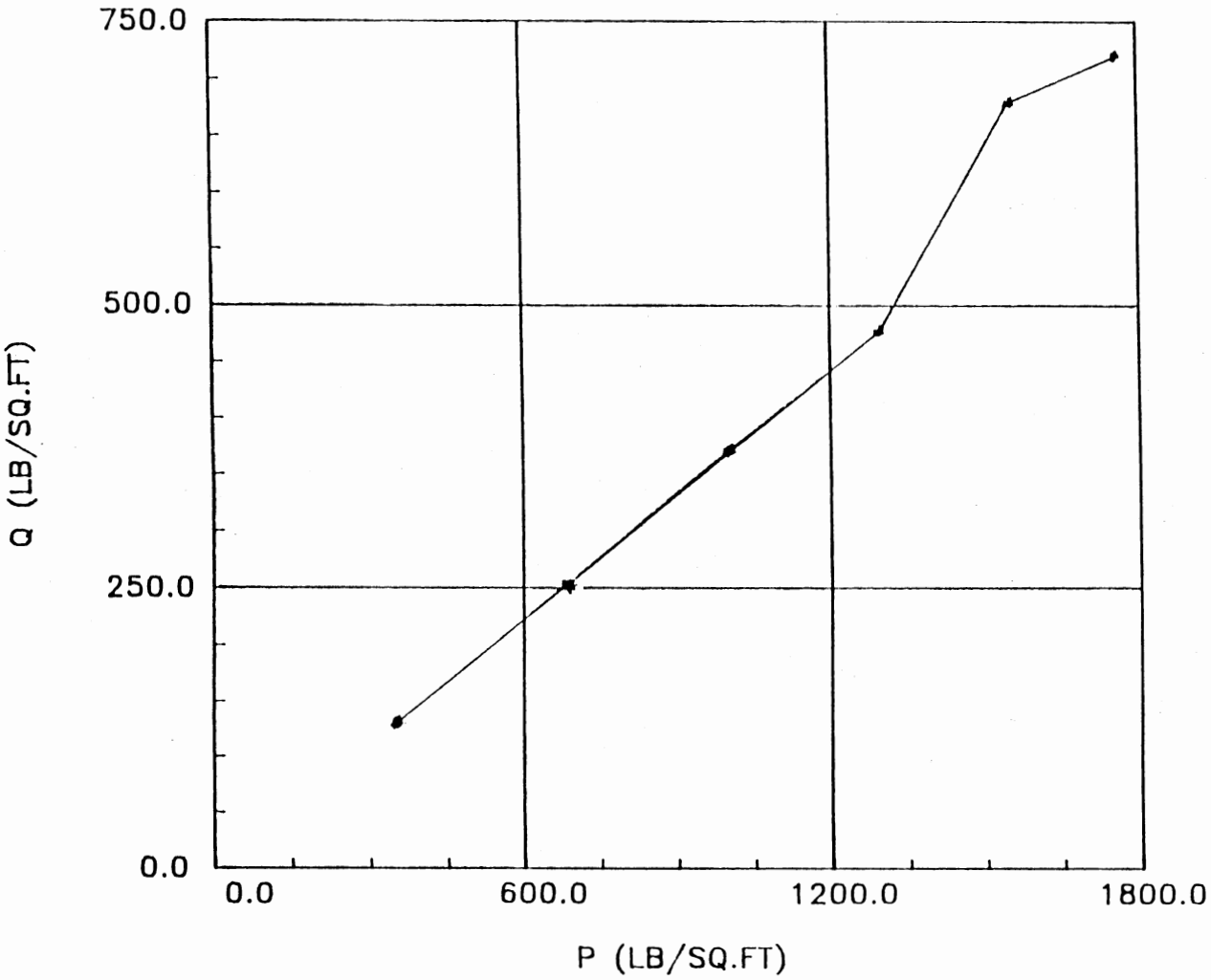

Figure 84. Stress path at elevation=-28 ft; Cu=700 psf
Gravity-turn-on; 30 ft pile penetration.

TABLE V

COMPARISON OF σ_a & σ_p BETWEEN FEM & CLASSICAL THEORY

	Finite Element		Classical Theory	
Elev. ft	σ_{ult}(right) psf	σ_{ult}(left) psf	σ_v-2.Cu psf	σ_v+2.Cu psf
-46.5	3300	3450	3715	3215
-43.5	2900	2900	3385	2885
-40.5	2700	2800	3055	2555
-37.5	2300	2500	2725	2225
-34.5	1850	2150	2395	1895
-29.25	1150		1817	
-28.5	1050		1735	
-27.75	675		1653	

* Comparison of σ_a and σ_p near failure (FEM) with limit equilibrium values from the classical theory. Gravity-turn-on case; Cu = 700 psf; depth of penetration = 30 ft.

pressure coefficient (K_o) is around 0.96 rather than one. This is because a value of K_o = 1 necessitates a Poisson's ratio of 0.5 resulting in numerical problems and instability of the FE solution. By the same token, the effective values of K_a and K_p are 0.91 and 1.08 respectively. When these values are used to determine the limit values from the classical theory, the results are skewed favorably in the direction of the FE solution.

Depth Of Tension Crack

Another finite element aspect of behavior that is in contradiction with the classical and SSI theories, is the depth of the tension crack in the soil. According to the classical theory of soil mechanics, a tension crack will be formed in clay because the tension that clay can carry allows the soil to stand on its own without the need of any supporting structural element. Once again, relying on the Coulomb-Rankine equation for active stress, the depth of the crack, $h_c = 2.Cu/\gamma$.

For Cu = 1000 psf, h_c = 18.18 ft

for Cu = 1300 psf, h_c = 23.64 ft

for Cu = 1600 psf, h_c = 29.10 ft

The depth of the tension crack predicted by SSI analyses does not only depend on Cu and γ, but is also affected by other factors, e.g., displacements, height, interaction distance, etc... However, the maximum depth of the tension crack is that predicted by the classical theory, i.e., $hc=2Cu/\gamma$. To illustrate why for the SSI method, the depth of the crack can be less than the value predicted by the classical theory, a hypothetical case with γ = 100 pcf, Cu = 400 psf will be used

for demonstration purposes. In this case, the classical theory estimates the depth of the tension crack to be 8 ft.

Referring to Fig. 85, the force-displacement curve (1), is the curve at a depth of 8 ft. All the curves below it (2 and 3) correspond to points whose depth is less than 8 ft. The curves above (4 and 5) correspond to points along the pile whose depths are more than 8 ft and this is why active pressure developed there. The distance, x, to the left and right corresponding to full-active and full-passive pressures can be easily found as follows:

$$x = 2Cu/E_s = 800/E_s$$

The range of behavior for points whose depths are less than 8 ft lies in the triangular sector ABC (Fig. 85). If the displacement in that region happens to be larger than the "v-intercept" for a particular location, then the force on the wall will be zero at that point. Unless this is the case for every point between the surface and a depth of 8 ft, some pressures will be exerted on the wall and so the depth of the crack will be less than 8 ft.

On the other hand, in the finite element analysis, the depth of the tension crack is almost the same for all values of Cu ($h \approx 23$ ft), regardless of whether a gravity-turn-on or buildup analysis was performed. This is readily apparent in Figs. 45-46 for soil pressures on the wall obtained from FE analysis. The reason for this discrepancy is that while the wall-soil system displaced to the left, the retained soil moved clockwise away from the wall (Figs. 86-88), thus aggravating the formation of the crack. The net pressure distribution

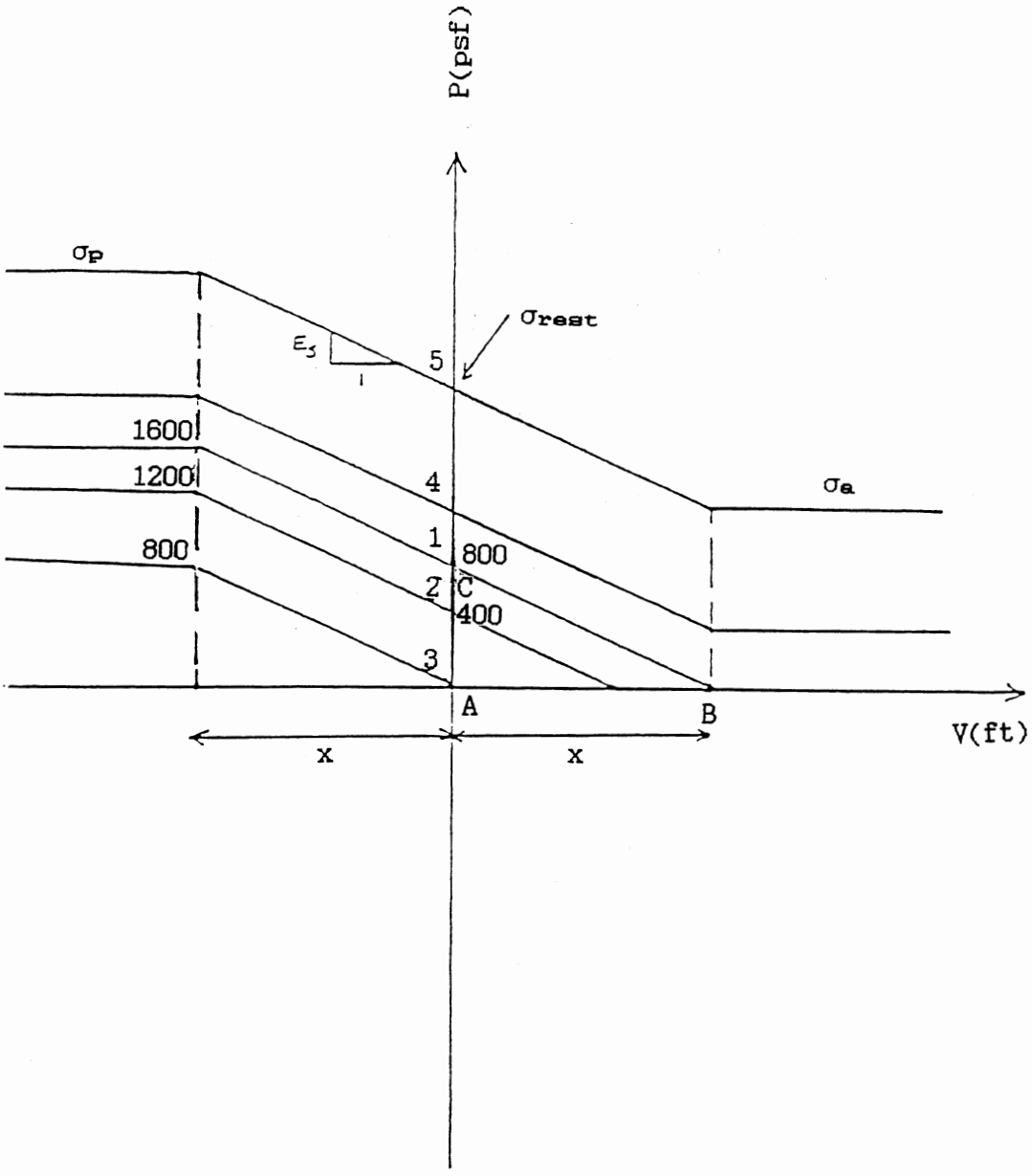

Figure 85. SSI Soil-Response curves near tension crack.

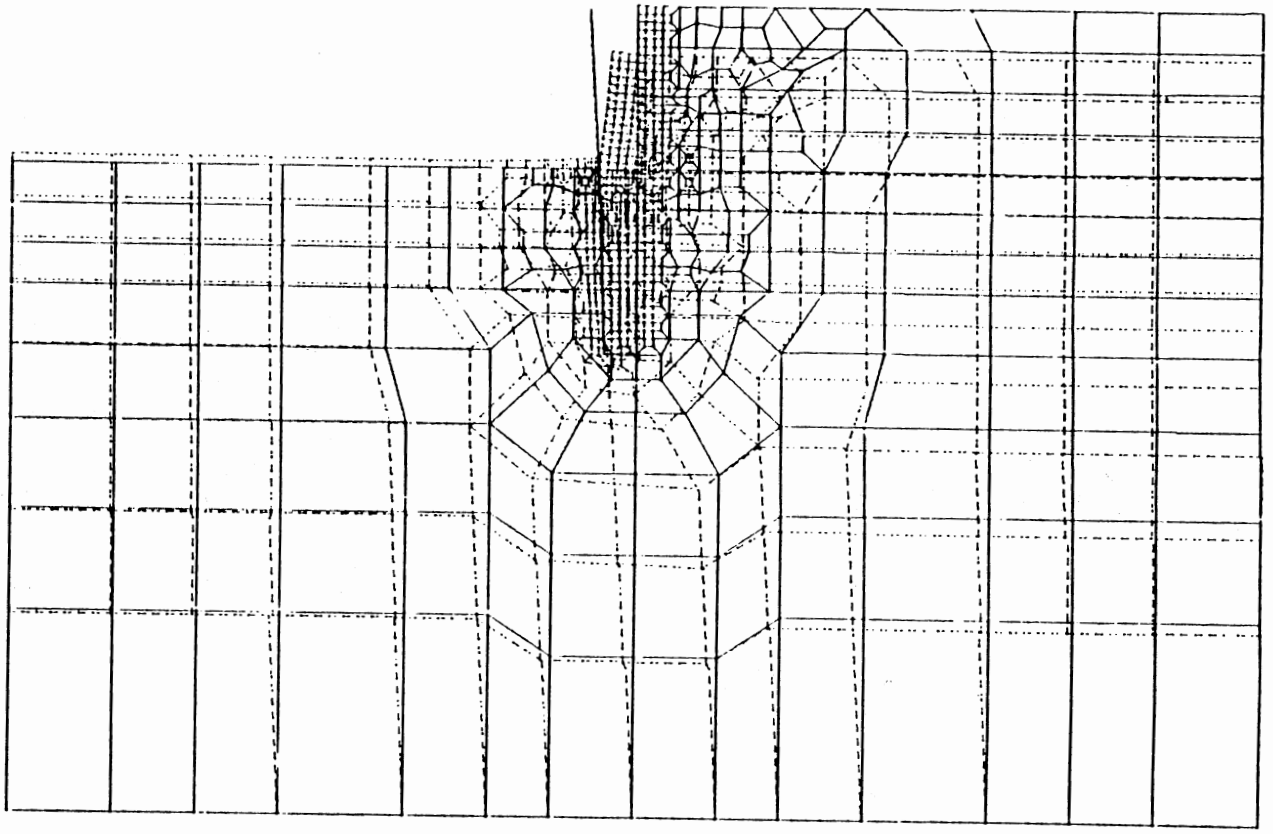

Figure 86. Deformed shape from gravity-turn-on analysis.
Cu = 1300 psf; 30 ft penetration depth.

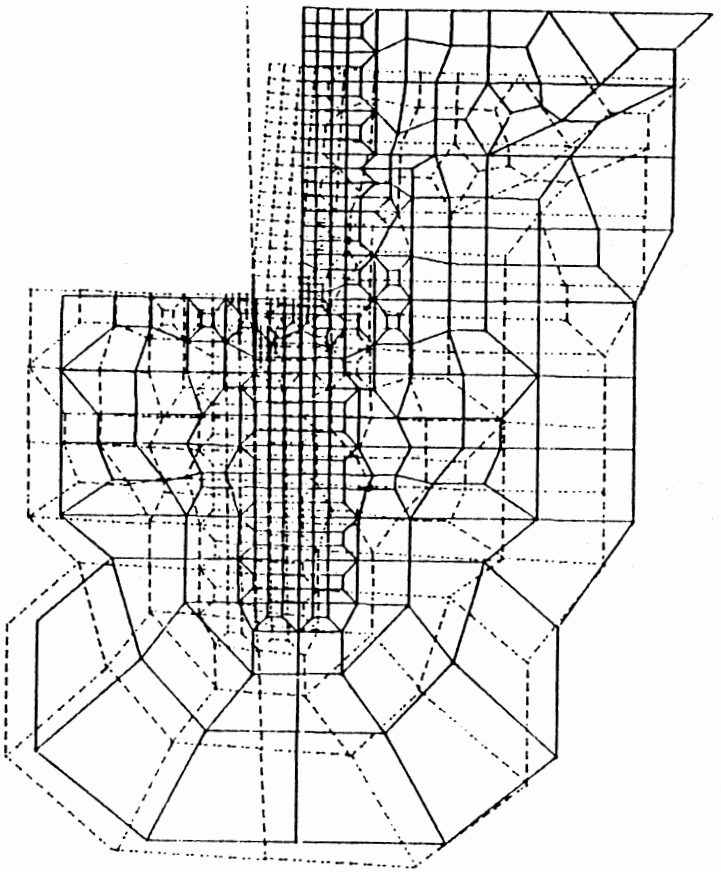

Figure 87. Deformed shape in the vicinity of the pile; Cu = 1000 psf
Gravity-turn-on analysis; 30 ft penetration depth.

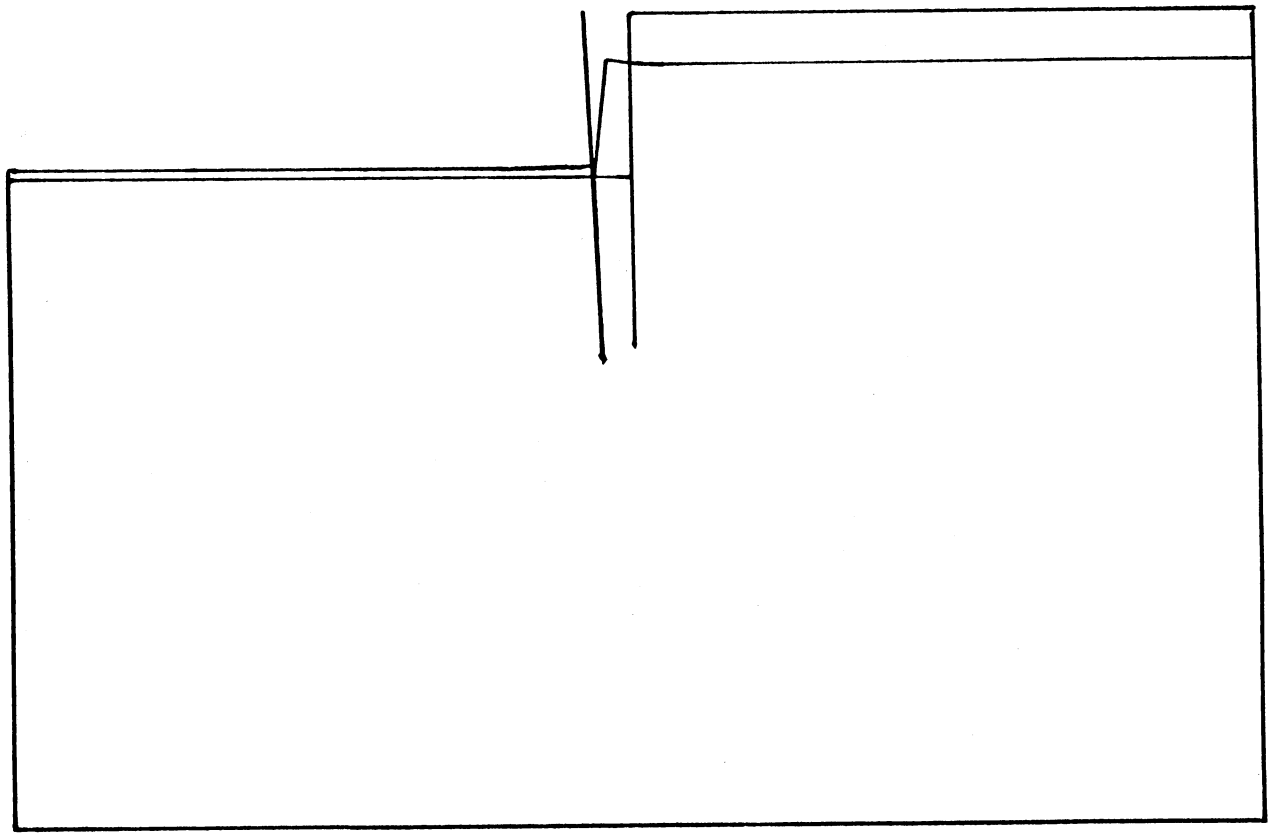

Figure 88. Deformed shape for the pile and boundaries; Cu = 1000 psf Buildup analysis; 30 ft penetration depth.

above the tension crack is zero because of the complete separation between the interface and the wall. However, the little irregularities in the pressure distribution in this region are the result of the method by which these pressures were calculated. The net pressures were found at the centroids of the soil elements just adjacent to the wall. These stresses are obtained from the average of the stresses at the four Gaussian integration points within the element and are not exactly zero.

Lower Bound of Soil Strength at Failure

The lower bound of Cu for which the 30 ft by 30 ft wall became unstable was investigated. For Cu = 1000 psf, the classical method predicted that the wall is almost in a state of limit equilibrium with full-active and passive pressures mobilized (Appendix A). Similarly, the SSI analysis predicted failure at Cu = 975 psf. At Cu = 1000 psf, the solution became stable. However, the moments and displacements became insensitive to any changes in the soil stiffness or interaction distance. This is because the forces in the nonlinear springs were always at the plateau level due to the large displacements triggered by the proximity to failure. The SSI results (Figs. 89-91) correspond almost exactly to the results obtained using the classical design method (Appendix A). The value of maximum moment ($\approx$ 72.4 K-ft) and its location ($\approx$ 9 ft below the original ground surface) were almost the same in both methods.

The finite element results for the same problem (Cu=1000 psf) are shown in Figs. 92-94. The maximum negative moment was found to be 13.3 K-ft from the gravity-turn-on analysis and 18.3 K-ft from the build-up case. These values are considerably lower than those obtained

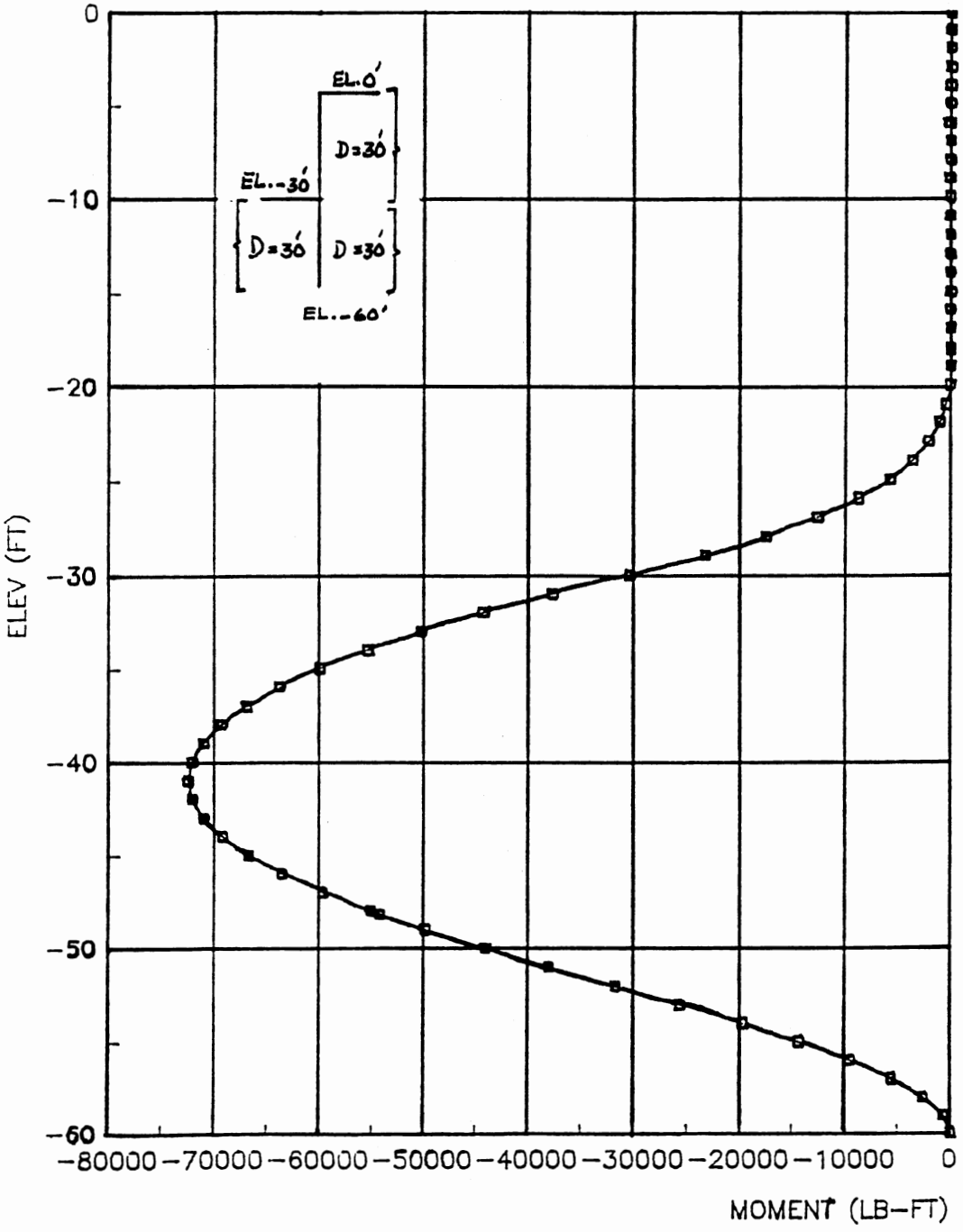

Figure 89. Bending moments from SSI analysis using Terzaghi's method. Cu = 1000 psf; 30 ft penetration depth.

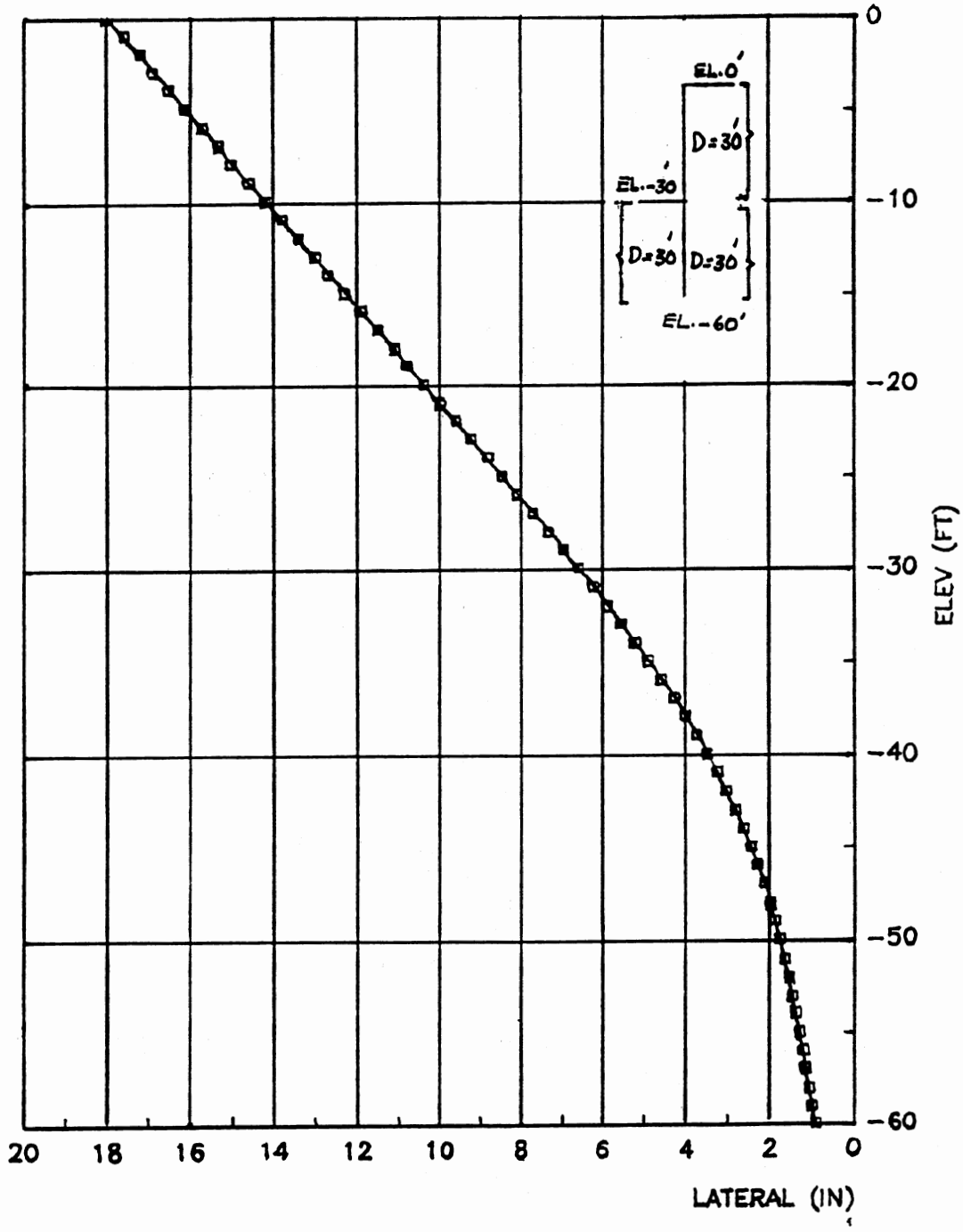

Figure 90. Pile deflections from SSI analysis using Terzaghi's method. Cu = 1000 psf; 30 ft penetration depth.

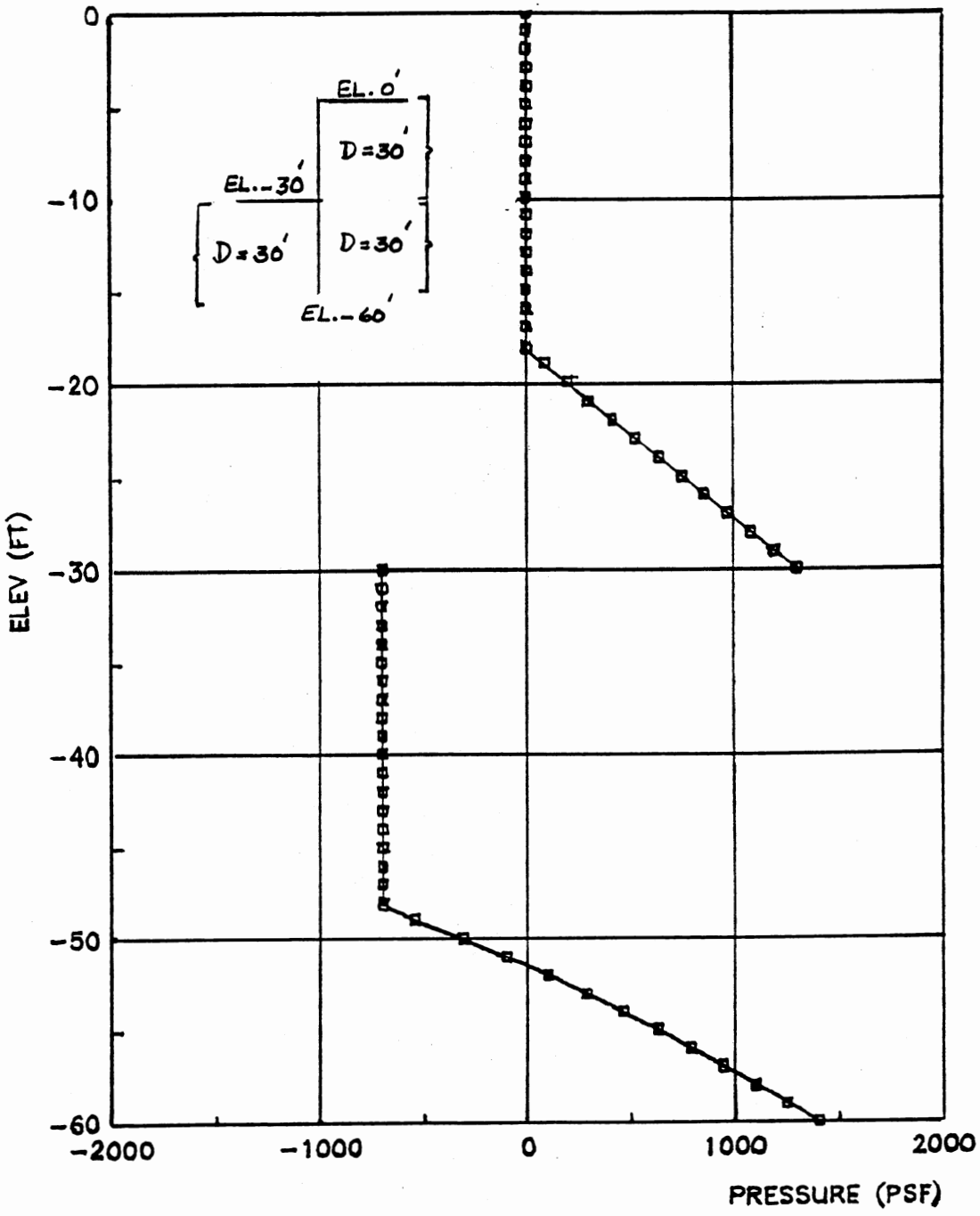

Figure 91. Net pressure from SSI analysis using Terzaghi's method. Cu = 1000 psf; 30 ft penetration depth.

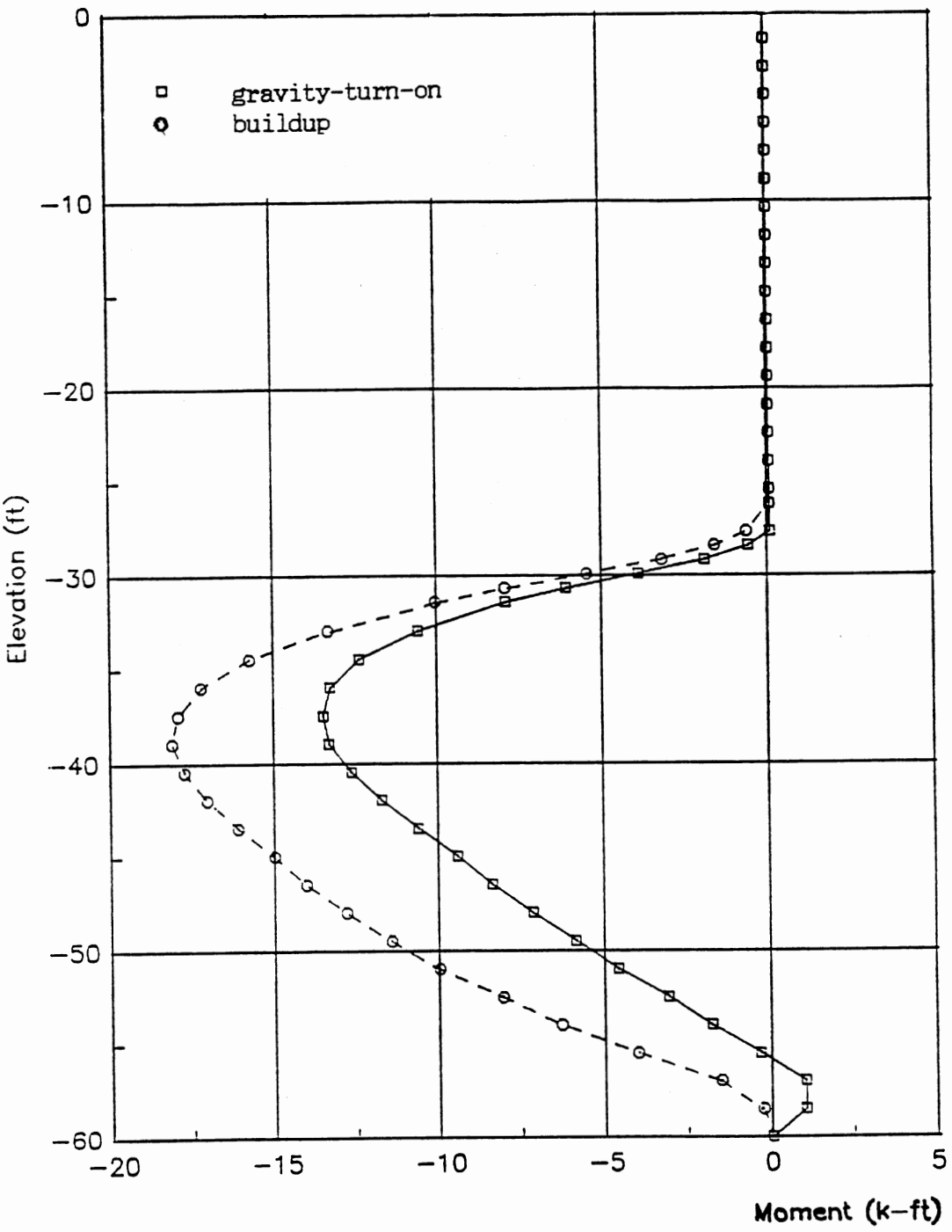

Figure 92. Bending moments vs. Elevation from FEM; Cu = 1000 psf. 30 ft penetration depth.

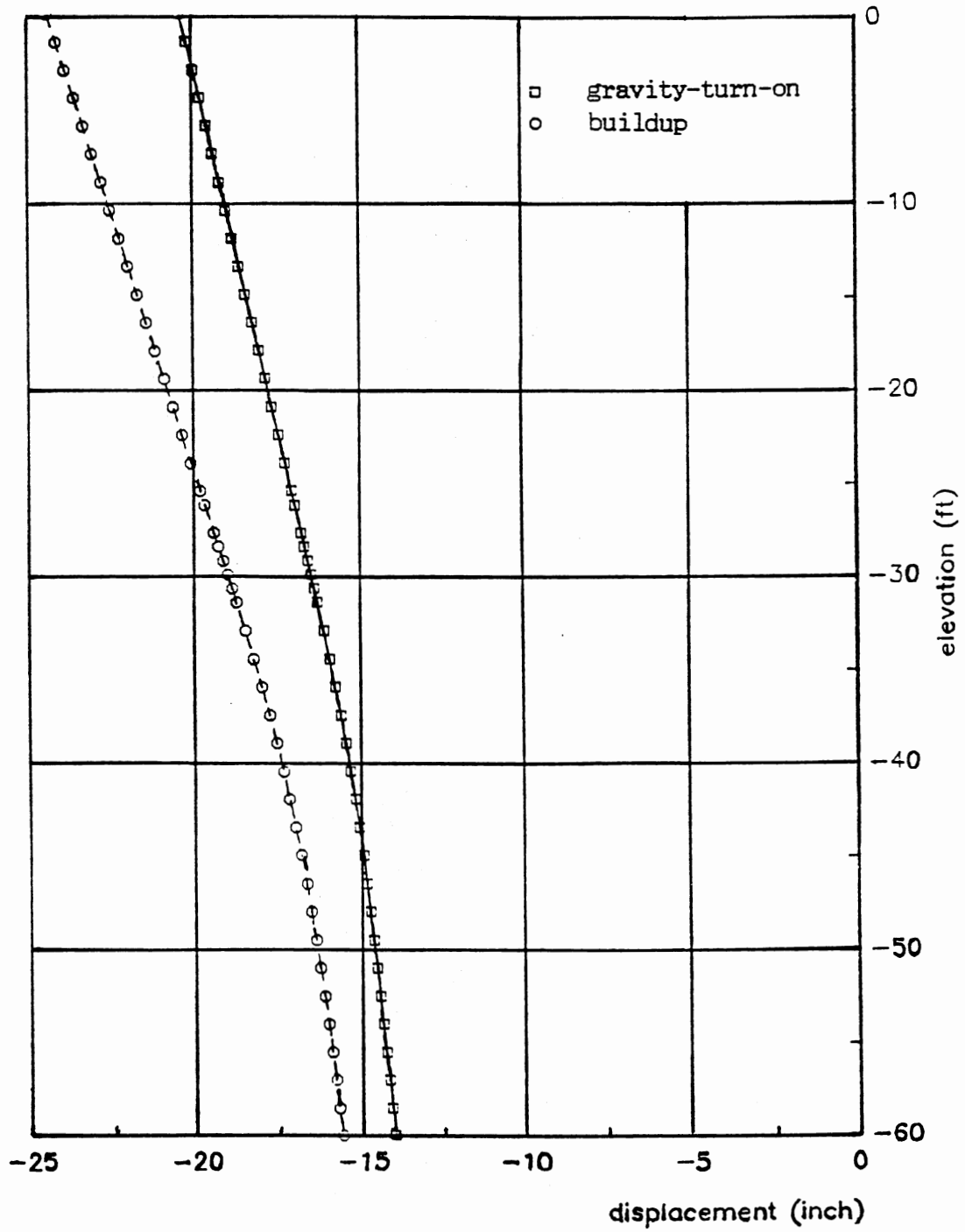

Figure 93. Pile deflections vs. Elevation from FEM; Cu = 1000 psf. 30 ft penetration depth.

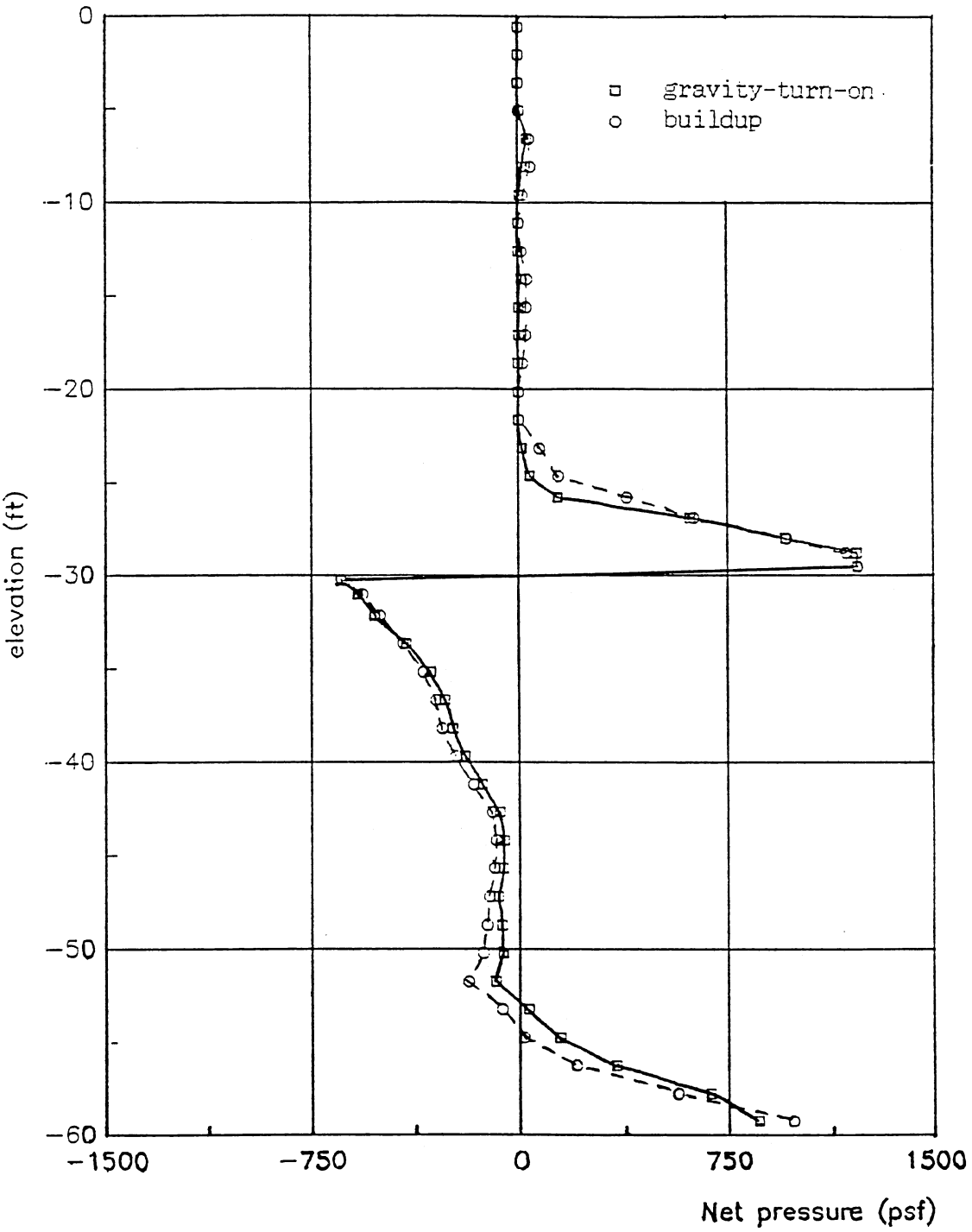

Figure 94. Net pressure vs. Elevation from FEM; Cu = 1000 psf. 30 ft penetration depth.

from the classical and SSI methods. The pressure values (Fig. 94) obtained from the finite element analysis were lower than those predicted by the classical and SSI methods. Furthermore, the finite element method predicted failure at a much lower Cu value (Cu = 725 psf). This is because the solution obtained from the finite element method is slightly stiffer. Also, the finite element method allows some stress redistribution to take place. Once local failure of some soil elements occurs, subsequent additional stresses will be carried by neighboring non-failing elements and the structure remains relatively stable. Local stress failure is apparent from Fig. 35 where the degree of mobilization is close to 1. Furthermore, the soil model used in the finite element program accounts for some post-failure strength for $\phi = 0$ condition. This is because, as stated earlier, the bulk modulus is not set to zero at failure.

Another point worth mentioning is that the classical design method predicts that for a certain cantilever wall height, there is a value of Cu below which the wall cannot be built in clay regardless of the embeddment depth. This conclusion is implicit in Eq. 6.1 from reference (3):

$$Z = (D'(4Cu-q)-R)/4Cu \qquad (6.1)$$

where R is the resultant of the active soil pressure above the original ground surface, D′ is the embeddment depth, q is the pressure at the original ground surface, and Z is the transition distance. From Eq. 6.1, it is clear that for Z to be determinate the quantity (4Cu-q) has to be positive. This leads to the following equation:

$$4Cu > \gamma . H \qquad (6.2)$$

where H is the height of the retained soil, and γ is the soil density. Therefore, if Eq. 6.2 is not satisfied a stable wall cannot be constructed in such clay regardless of the value of depth of penetration. In the problem at hand, the critical value of Cu = 825 psf was found from Eq. 6.2.

Quantitatively, the above hypothesis is obviously questionable since the finite element method predicts that failure will occur at Cu $\approx$ 725 psf. However, as will be seen later, it is true that for the ϕ = 0 case, the embeddment depth does not affect the stability of the problem to a large degree. This is because the wall is not the most dominant stiffness element in the system as the classical theory assumes; In most cases, the wall floats in the soil mass.

Soil Stress Profile on the Pile

For all the analyzed cases, Figs. 95-100 show the stress profile on the right and left of the wall. It can be seen that the stress profiles in the vicinity of the pile tip ($\approx$ 5 ft above the pile tip) undergo a sharp change in curvature. The soil pressure on the leftside decreases and the corresponding pressure on the rightside increases. The above behavior is more pronounced for the stiffer cases and for embeddment depths of 20 ft and 15 ft. This behavior, at first glance, seems consistent with the classical theory which assumes a transition from net active on the left side to net passive on the right side; the sharp change on the right can be interpreted as going towards a passive type failure while the left side is going in the active

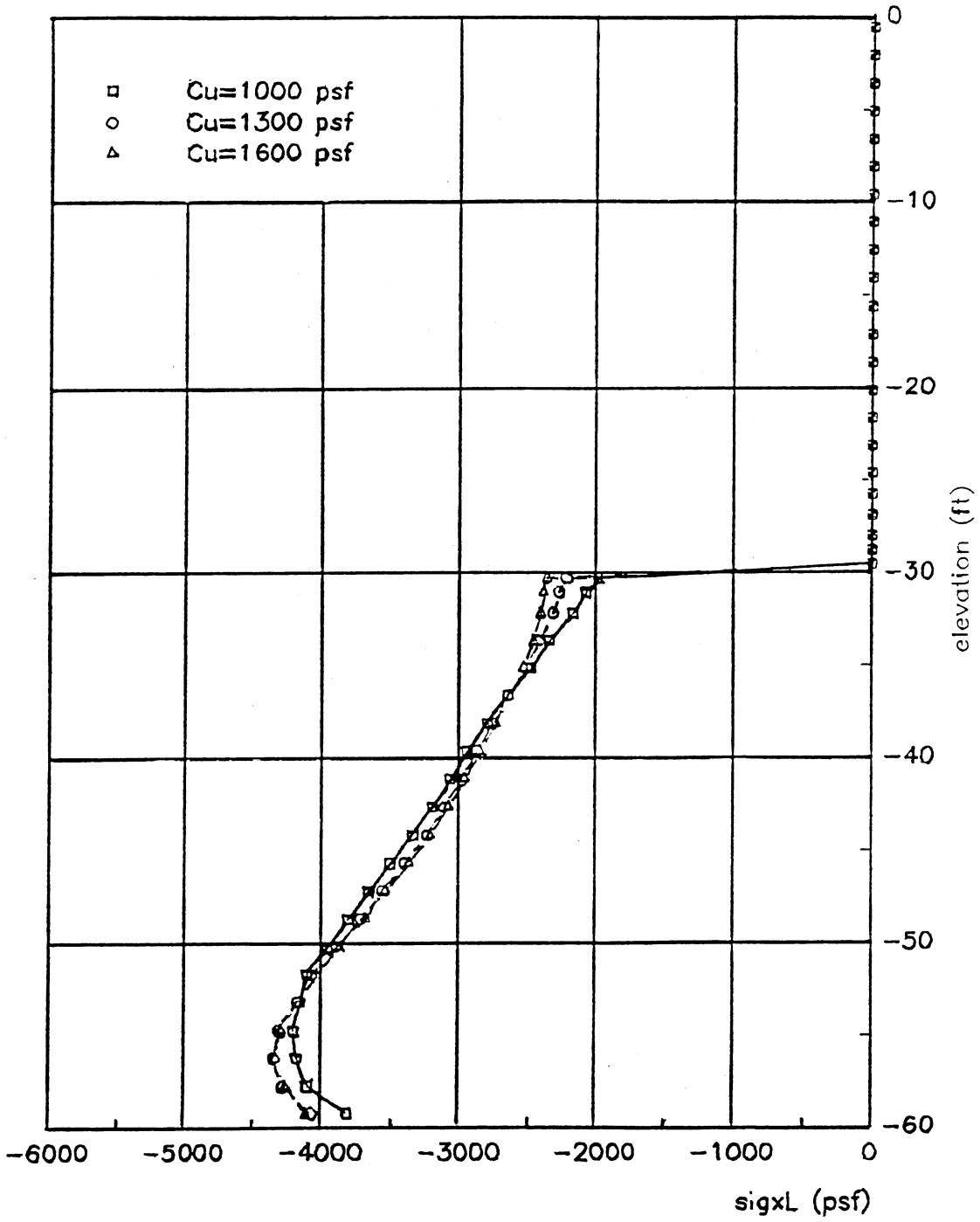

Figure 95. Pressure profile on the pile from leftside soil. Gravity-turn-on analysis; 30 ft penetration.

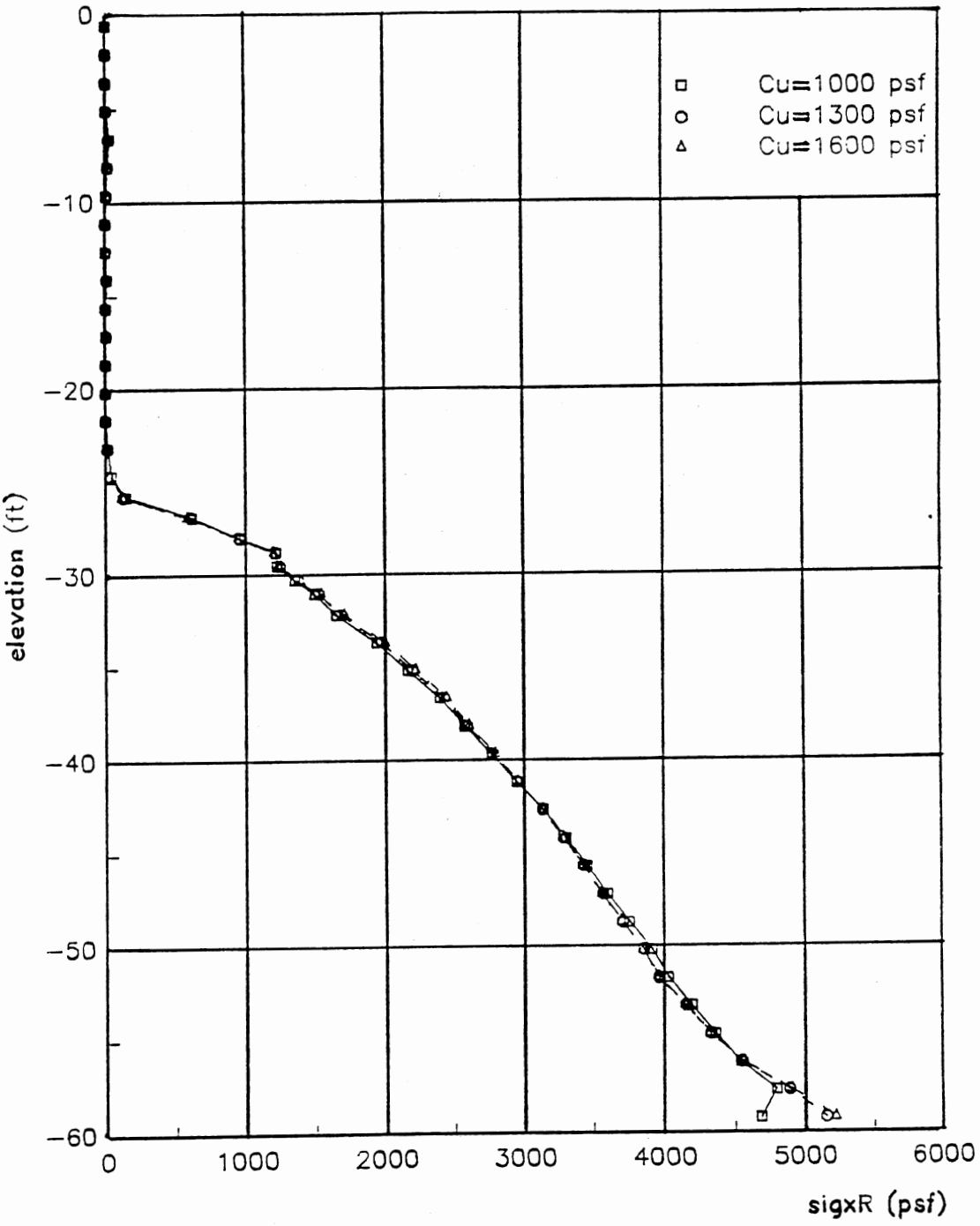

Figure 96. pressure profile on the pile from rightside soil. Gravity-turn-on analysis; 30 ft penetration.

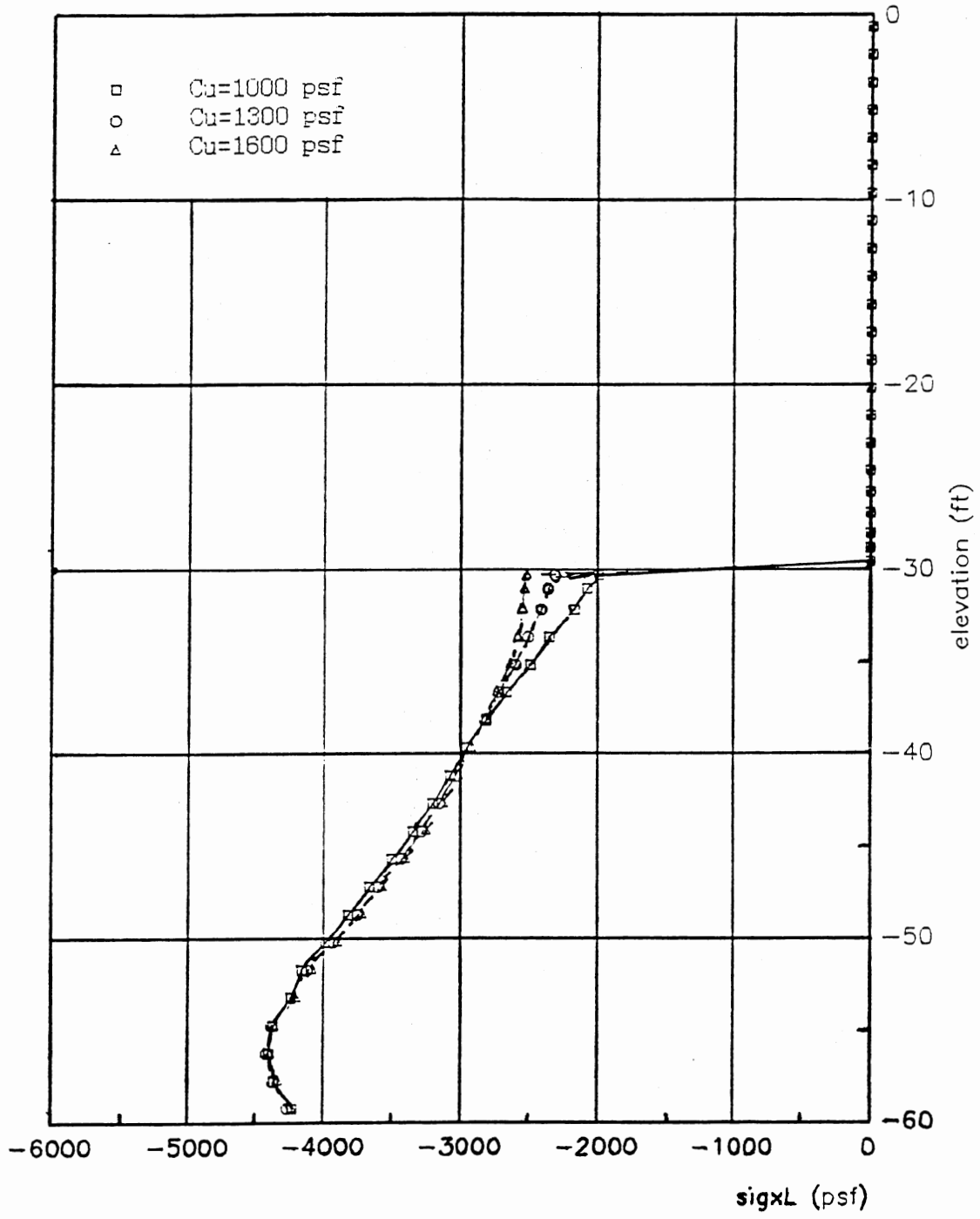

Figure 97. Pressure profile on the pile from leftside soil. Buildup analysis; 30 ft penetration.

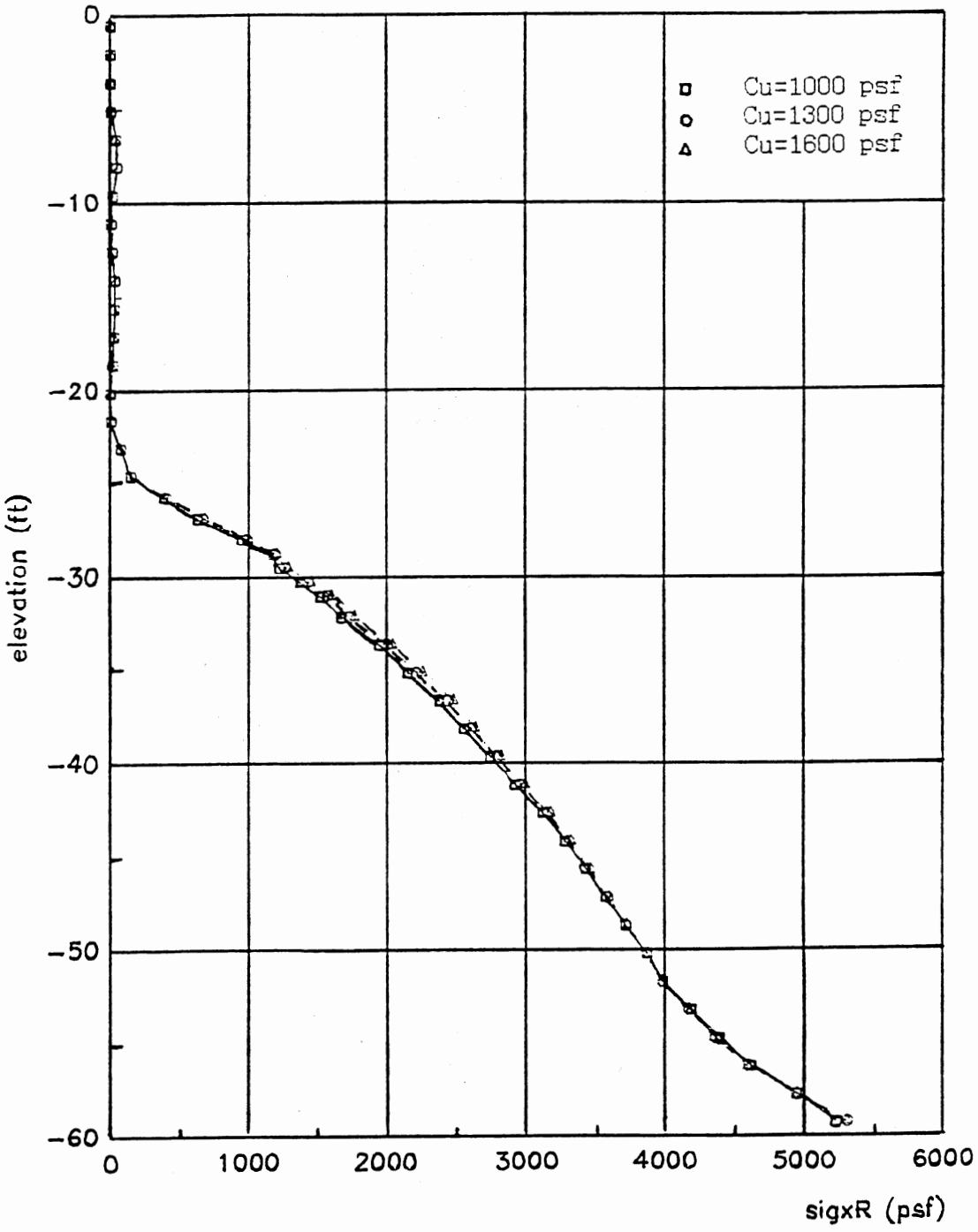

Figure 98. Pressure profile on the pile from rightside soil. Buildup analysis; 30 ft penetration.

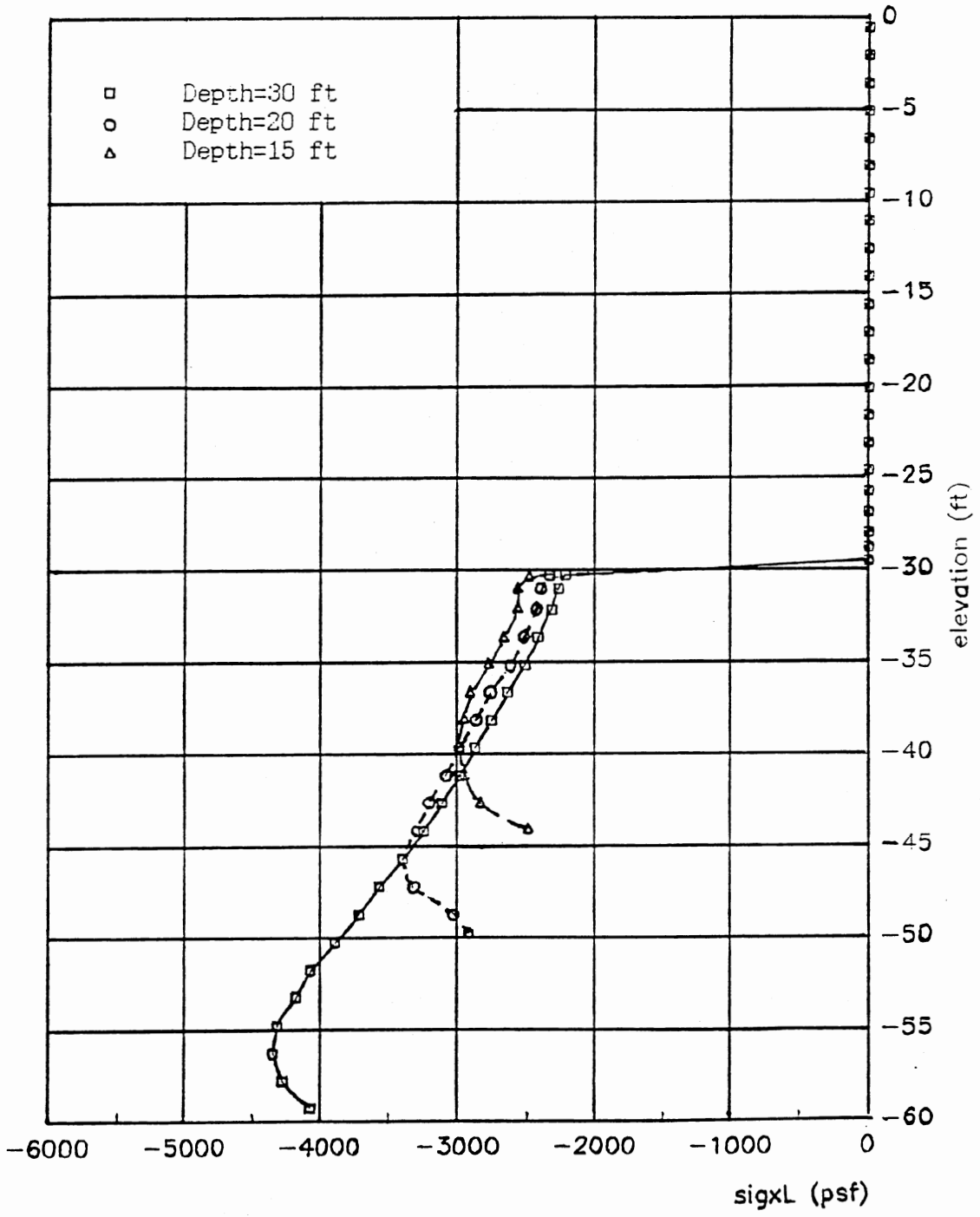

Figure 99. Pressure profile on the pile from leftside soil. Cu = 1300 psf; Gravity-turn-on analysis.

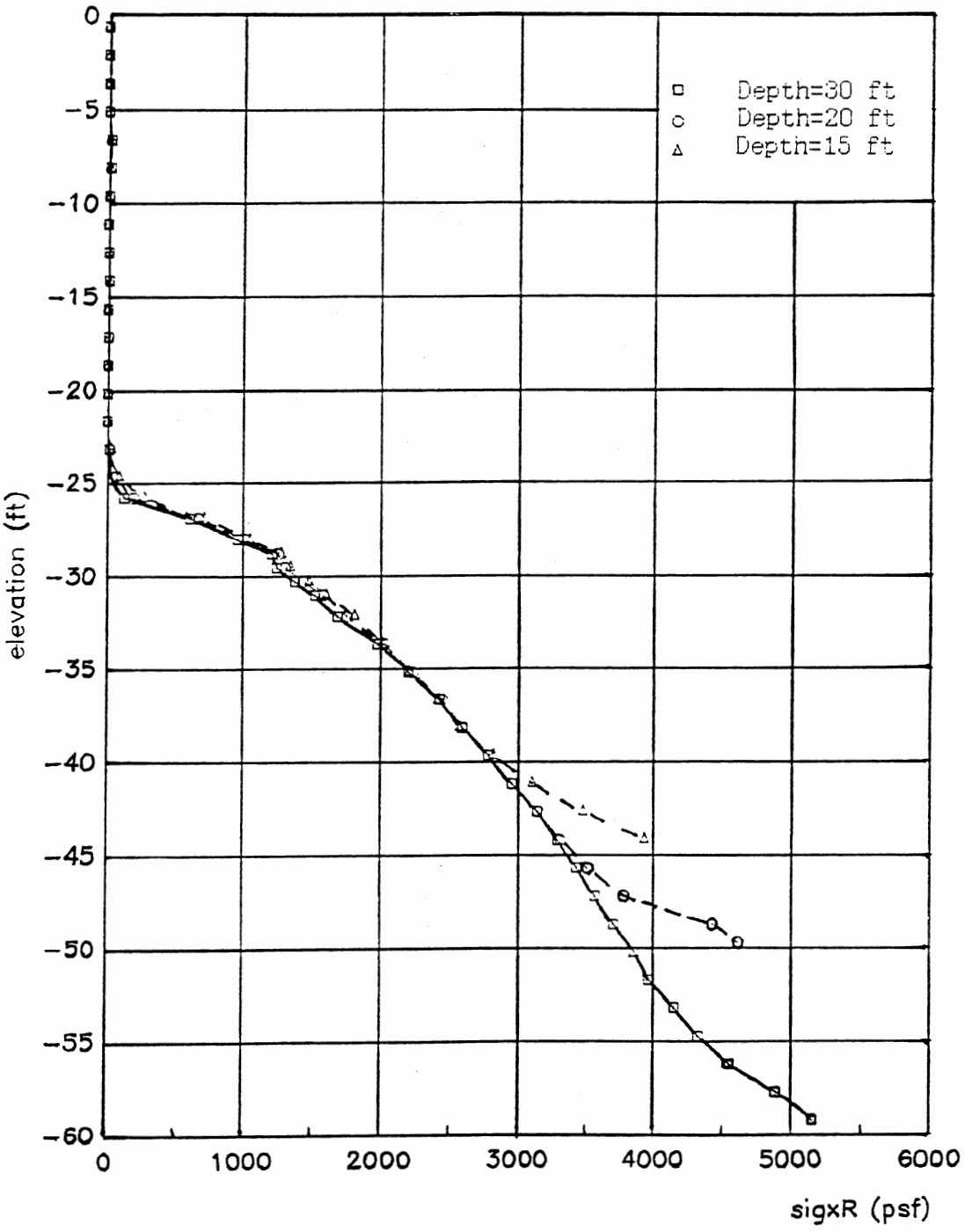

Figure 100. Pressure profile on the pile from rightside soil. Cu = 1300 psf; gravity-turn-on analysis.

direction. However, the finite element solutions predict that the rightside soil is in an active state while the leftside soil is in a passive state. This was seen earlier from the soil stress paths. Also, SSI analyses confirmed the same conclusion since all the pile nodes displaced to the left. Furthermore, it was shown earlier that the soil on either side of the wall in the vicinity of the tip is near failure. Also, the magnitude of the active soil pressure is larger than that of the passive pressure (Figs. 95-100). At first glance, one might jump to the erroneous conclusion that the above observation is in contradiction with limit equilibrium theory according to which the limit passive pressure from the left should be greater than the limit active pressure from the right. For example, for Cu = 1000 psf and 30′ ft penetration depth, the classical theory gives:

at the bottom of the wall on the right side:

$\sigma_a(ult) = 60 \times 110 - 2(1000) = 4600$ psf

at the bottom of the wall on the left side:

$\sigma_p(ult) = 30 \times 110 + 2(1000) = 5300$ psf

As contradictory as these values seem with the finite element results, a possible explanation is found from the facts that the vertical stress in the soil mass to the right of the wall is greater than geostatic and is less than geostatic to the left due to incompressibility. This phenomenon is exacerbated near the tip of the

pile by the stress concentration on one hand, and the sudden abrupt change in vertical stress from the right side to the left side. Fig. 101 shows that many different vertical stress contours converge at the tip of the pile due to the high stress concentration there. From this figure, it can also be seen that just to the right of the tip, the vertical stress is ≈ 7000 psf which is larger than the geostatic stress (6600 psf) whereas it is ≈ 2000 psf to the left of the tip which is smaller than the geostatic stress (3300 psf). This increase in vertical stress on the rightside and decrease on the leftside tends to offset the discrepancy described earlier between limit active and limit passive pressures on the rightside and leftside respectively.

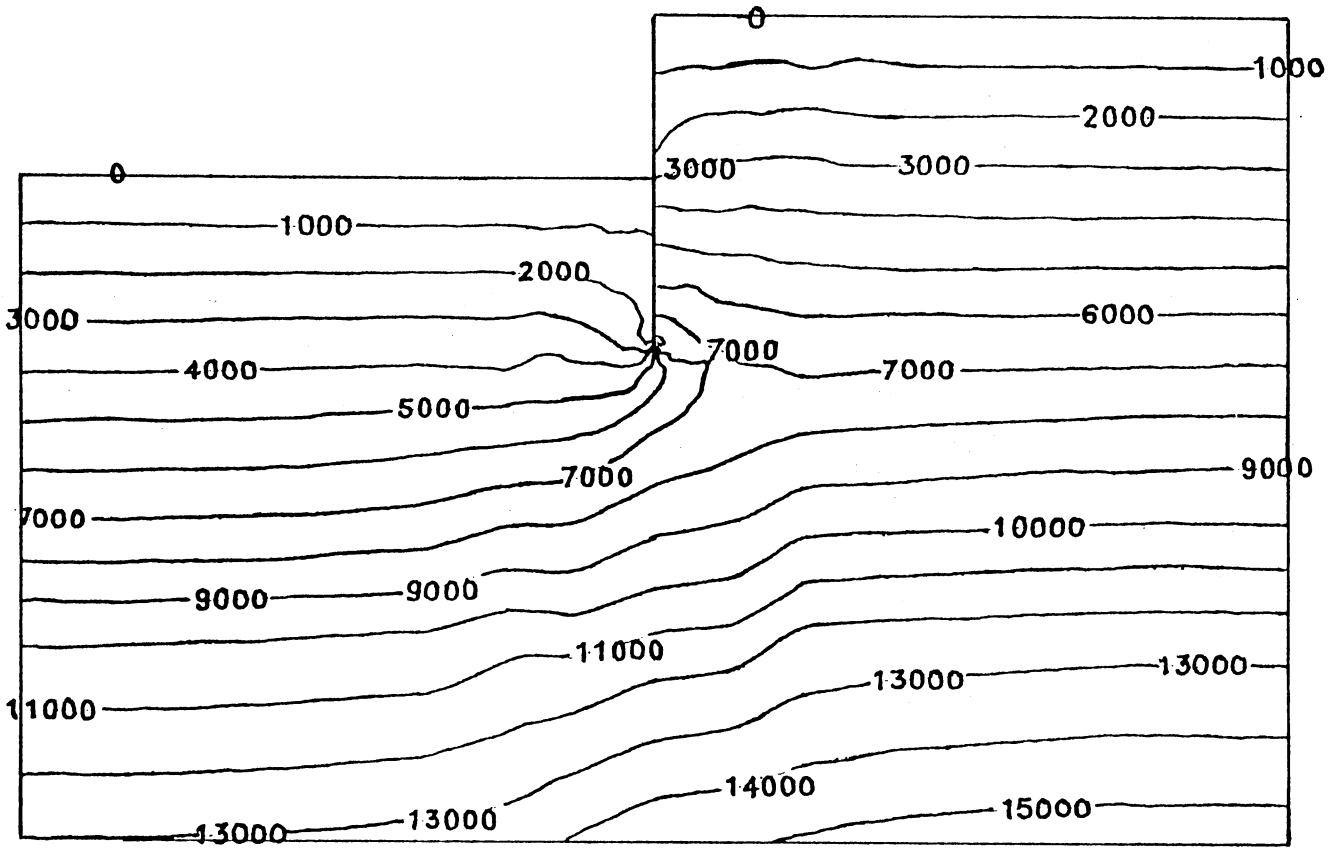

Figure 101. Vertical stress contours from buildup analysis.
Cu = 1000 psf; 30 ft penetration depth.

CHAPTER VII

CONCLUSION AND RECOMMENDATIONS

Finite element analyses using a gravity-turn-on and a sequential construction approach were carried out for a cantilever sheetpile retaining wall in saturated clay. The results were compared with the classical design theory as well as with the SSI approach. Some of the interesting findings in this work are:

1. The buildup procedure gives rise to higher deflections and moments in the pile as compared with the gravity-turn-on solution. This demonstrates the importance of the stress path on the final configuration of the system due mainly to the nonlinear behavior of the soil.

2. If the values of interaction distance suggested in various SSI references were used, the SSI moments are about two to three times higher than the actual values from the finite element solutions.

3. An iteration procedure can be used to ensure convergence of the SSI solution. The results obtained using this technique predict moments that are lower than those obtained from the finite element method, especially in the buildup case. Furthermore, best results are obtained when the lower limit of Terzaghi's values for soil stiffness is used.

4. The soil modulus for clay was not found to be constant as commonly assumed in the SSI theory, especially in the region close to the original ground surface and in the retained soil. Furthermore, the

value of interaction distance in the retained soil is extremely high resulting in lower soil stiffness in that area.

5. For the $\phi = 0$ case, the estimates for the interaction distance are as important in the active regions as in the passive ones, contrary to previous beliefs.

6. The finite element analysis predicts a large rigid-body displacement due to the incompressibility of the soil. This is because for normally consolidated saturated clay under undrained loading conditions, $v = 0.5$. This rigid body displacement is much higher than the one obtained from the SSI solution.

7. The soil on the right side of the wall rotates clockwise and displaces downward while the soil on the left side heaves upward. This gives rise to an increase in vertical stress on the right side and a decrease on the left side. This phenomenon is more pronounced around the pile tip due to the sudden change in vertical stress and the large stress-gradient in that vicinity.

8. The depth of the tension crack varies with Cu in the classical and SSI methods. However, the finite element method predicts the same value for all the cases analyzed.

9. The area with the highest stresses and degree of mobilization is near the original ground surface and the tip of the pile. Furthermore, the stresses obtained from the buildup solution are bigger than those from the gravity-turn-on case. This is especially pronounced in the region between the original ground surface and mid-depth of the pile. However, in the retained soil, the stresses are almost the same.

10. The moment values obtained from the finite element analysis were found to increase slightly with any decrease in embeddment depth.

However, the values of degree of mobilization were relatively insensitive to the embeddment depth. All this suggests that the pile is not predominant when compared to the soil and that in many cases, the pile acts as if it is floating in the soil.

11. The ultimate pressures obtained from the finite element method are higher in the passive case and lower in active than those from classical methods.

12. For the stress-displacement curves obtained in the finite element analysis, the variation is not linear but of the same general shape as the soil stress-strain curves.

13. For the large penetration depth (30 ft), a relatively large tip reaction is obtained which results in contra-flexure and a positive moment near the tip of the pile. Further research must be done to determine whether that effect is real or just a result of the finite element model used.

14. The finite element solution predicts failure for a lower value of Cu than the one obtained from either the classical method or the SSI solution.

15. The moments obtained from the SSI method were closer to the finite element solution when Terzaghi's values for E_s were used rather than when Skempton's values were used.

16. The values of E_s in the buildup case are much smaller than in the gravity-turn-on analysis. This is because the in-situ (initial) stresses are associated with zero displacements.

These are some of the points discussed in this study and they give rise to the following recommendations:

1. The finite element method is a powerful tool for research, but

it is too expensive and time consuming to be practical. Therefore, the SSI method has to be refined whenever necessary since it remains the more practical alternative.

2. When the SSI method is used for analysis or design, the moments obtained must be multiplied by a factor of safety (> 1) in order to stay on the safe side.

3. The comparison of the SSI method with the finite element solution has to be extended to include other situations; e.g., anchored bulkheads, different loading conditions, layered systems consisting of different soil types, and water loads.

4. The concept of interaction distance, specifically in the active regions, must be put on more solid grounds for different cases.

5. The SSI method cannot account for the soil layer that underlies the pile. Hence, a way must be found to incorporate the geometry into the global picture.

6. The variation from net active to net passive should take into account the general stress-strain behavior in a way similar to the curves developed by Matlock for offshore piles (Ref. 29).

To conclude, it is hoped that this work has helped clarify some aspects of the behavior of the class of problems discussed in this study. Only with thorough understanding of all the facets of this behavior can better modelling be achieved, resulting in more reliable use of the soil-structure interaction method for analysis and design.

BIBLIOGRAPHY

(1) Biot, M.A. Bending of an Infinite Beam on an Elastic Foundation. Journal of Applied Mechanics, ASME, Vol. 59, 1937, pp. A1-A7.

(2) Boussinesq, J. Applications des Potential A L'Etude de L'Equilibre et du Mouvement des Solides Elastiques, Gauthier-Villars, Paris, 1885.

(3) Bowles, J.E. Foundation Analysis and Design: McGraw-Hill, 1988, Fourth Edition.

(4) Cheung, Y.K. Beams, Slabs and Pavement. Numerical Methods in Geotechnical Engineering. G.S. Desai and J.T. Christian, Eds. New York: McGraw-Hill, 1977.

(5) Clough, G.W., and J.M Duncan. Finite Element Analysis of Port Allen and Old River Locks. Contract Report No. TE 69-3, USAEWES, Sept. 1969.

(6) Clough, G.W., and J.M. Duncan. Finite Element Analysis of Retaining Wall Behavior. Journal of Soil Mechanics and Foundations Divisions, ASCE, Vol. 97, No. SM 12, Dec., 1971, pp. 1657-1673.

(7) Clough, R.W., and R.J. Woodward. Analysis of Embankment Stresses and Deformations. Journal of the Soil Mechanics and Foundations Division, ASCE, Vol. 93, No. SM4, July 1967.

(8) Clough, R.W. Comparison of Three Dimensional Finite Elements. Proceedings, Symposium on Application of Finite Element Methods in Civil Engineering, American Society of Civil Engineers, 1969, pp. 1-26.

(9) Coulomb, C.A. Essai Sun Une Application Des Regiles Des Maximis et Minimis a Quelques Problemes de Statique. Member Academy R. Sci. Vol. 7, Paris, France, 1776.

(10) D'Appolonia, Poulos, and Ladd. Initial Settlement of Structures on Clay. Journal of the Soil Mechanics and Foundations Division, ASCE, Vol. 97, No. SM10, Oct., 1971, pp. 1359-1377.

(11) Dawkins, W.P. User's Guide: Computer Program for Analysis of Beam-Column Structures for Nonlinear Supports (CBEAMC). Instruction Report K-82-6, U.S. Army Engineer Waterways Experiment Station, Vicksburg, Miss., 1982.

(12) Dawkins, W.P. User's Guide: Computer Program for Soil-Structure Interaction Analysis of Sheetpile Retaining Walls (CSHTSSI). Report to ADD Center, U.S. Army Engineer Waterways Experiment Station, Vicksburg, Miss., 1982.

(13) Duncan, J.M., and C.Y. Chang, Nonlinear Analysis of Stress and Strain in Soils. Proceedings of The ASCE, Journal of the Soil Mechanics and Foundation Division, Vol. 96, SM5, Sept. 1970.

(14) Dunlop, P., J.M. Duncan, and H.B. Seed. Finite Element Analysis of Slopes in Soils. Contract Report S-68-6, U.S. Army Engineer Waterways Experimental Station, Vicksburg, Miss., May, 1968.

(15) Filonenko-Borodich, M.M. A Very simple Model of an Elastic Foundation Capable of Spreading the Load. Trans. Sb. Tr. Mosk. Elektro. Inst. Inzh., No. 53, 1945. (In Russian)

(16) Girijavallabhan, C.V., and L.C. Reese. Finite Element Method Applied to Some Problems in Soil Mechanics. Proceedings of the ASCE, Journal of Soil Mechanics and Foundation Division, Vol. 94, SM2, Mar. 1968.

(17) Goodman, R.E., R.L. Taylor, and T. L. Brekke. A Model for the Mechanics of Jointed Rock. Journal of the Soil Mechanics and Foundation Division, ASCE, Vol. 94, No. SM3, 1968, pp. 637-659.

(18) Haliburton, T.A. Numerical Analysis of Flexible Retaining Structures. Journal of the Soil Mechanics and Foundation Division, ASCE, Vol. 94, No. SM6, November, 1968, pp. 1233-1251.

(19) Haliburton, T.A. Soil Structure Interaction. School of Civil Engineering, Oklahoma State University, Stillwater, OK. September, 1979.

(20) Hallal, Issam. Analysis of the Nonlinear Behavior of Floodwall Structures. Ph.D. Dissertation Oklahoma State University, Stillwater, Ok, 1988.

(21) Hallal, Issam, M. Oner. Nonlinear Plane Strain Finite Element Program, Oklahoma State University, 1987.

(22) Hetenyi, M. Beams On Elastic Foundations. Ann Arbor: The University of Michigan Press, 1946.

(23) Janbu, N. Soil Compressibility as Determined by Oedometer and Triaxial Tests. Proc. European Conference on Soil Mechanics and Foundation Engineering, Vol. 1, Wiesbaden, 1963, pp. 19-25.

(24) King, I.P. Finite Element Analysis of Two-Dimensional Time-Dependent Stress Problems, Ph.D Dissertation University of California, Berkeley, 1964.

(25) Kodner, R.L., J.S. Zelzsko. A Hyperbolic Stress-Strain formulation for Sands. Proc. Second Pan-Am Conf., Soil Mechanics and Foundation Engineering, Vol. 1, Brasil, 1963.

(26) Kodner, R.L. Hyperbolic Stress-Strain Response: Cohesive Soils. Journal of the Soil Mechanics and Foundation Division, ASCE, Vol. 89, No. SM1, Feb., 1963, pp. 115-143.

(27) Kulhawy, F.H., J.M. Duncan, and H.B. Seed. Finite Element Analysis of Stresses and Movements in Embankments During Construction. Contract Report No. S-69-8, U.S. Army Engineer Waterways Experiment Station, Vicksburg, Miss., Nov. 1969.

(28) Marsal, R.J. Large Scale Testing of Rockfill Materials. Journal of the Soil Mechanics and Foundations Division, ASCE, Vol. 93, No. SM2, March, 1967, pp. 27-43.

(29) Matlock, H. Correlations for the Design of Laterally Loaded Piles in Soft Clay. Preprints, Second Annual Offshore Technology Conference, Houston, Texas, Vol. 1, 1970, pp. 577-594.

(30) Oner, M. and N. Janbu. Nonlinear Analysis of Foundation Vibrations. Proc. Second International Conference on Numerical Methods in Geomechanics. Blacksburg, Virginia, Vol. 2, pp. 1025-1037, 1976.

(31) Oner, M. and I. Hallal. Nonlinear Analysis of Floodwall Structures. Oklahoma State University, 1987.

(32) Pasternak, P.L. On a New Method of Analysis of an Elastic Foundation by Means of Two Foundation Constants. (Gosuedarstvennoe Izadatelstrvo Literaturi Po Stroitelsvu Arkhitekture.) Moscow, U.S.S.R., 1954. (In Russian)

(33) R.W. Clough, H.C. Martin, L.J. Topp and M.J. Turner. Stiffness and Deflection Analysis of Complex Structures. Journal of the Aeronautical Society, Vol. 23, 1956, pp. 805-823.

(34) Rankine, W.J.M. On the Stability of Loose Earth. Phil. Tans. Royal Society, London, 147, Part 1, pp. 9-27.

(35) Reese, L.C. and H. Matlock. Numerical Analysis of Laterally Loaded Piles. Proc., ASCE Second Structural Division Conferences on Electronic Computations, Pittsburgh, Penn., September, 1960.

(36) Rowe, P.W. Sheetpile Walls in Clay, PICE, Vol. 7, July, 1957, pp. 629-654.

(37) Ruser, R.J. and W.P. Dawkins. Application of the Three-Dimensional Finite-Element Method to Some Problems in Soil Mechanics. Ph.D Dissertation, The University of Texas at Austin, 1970.

(38) Skempton, A.W. The Bearing Capacity of Clays. Building Research Congress. Division I, Part 3, London, 1951, pp. 180-189.

(39) Terzaghi, K. Large Retaining Wall Tests. I. Pressure of Dry Sand. Engineering News Record, Vol. 3, Feb., 1934. pp. 136-140.

(40) Terzaghi, K. Evaluation of Coefficients of Subgrade Reaction. Geotechnique, Vol. 5, December, 1955, pp. 297-326.

(41) Vesic, A.B. Beams on Elastic Subgrades and the Winkler's Hypothesis. Proc., Fifth Intl. Conference on Soil Mechanics and Foundation Engineering, Paris, France, 1961, pp. 845-850.

(42) Vlasvo, V.Z. and N.N. Leont'ev. Beams, Plates and Shells on an Elastic Foundation. Jerusalem: Israel Program for Scientific Translations, 1966. (Translated from Russian)

(43) Winkler, E. On Elasticity and Fixity. Praque, 1867, p. 182.

APPENDIXES

APPENDIX A

CLASSICAL DESIGN METHOD

Definitions

Net active pressure is the active pressure on the right side of the wall less the passive pressure on the left side.

Net passive pressure is passive pressure on the right side of the wall less the active pressure on the left side.

In general,

$P_a = P_v - 2.\sqrt{K_a}.Cu$ (active pressure)

$P_p = P_v + 2.\sqrt{K_p}.Cu$ (passive pressure)

For $\phi = 0$ case, $K_a = K_p = 1$.

Referring to Fig. 102,

On the Right Side:

$P_a = \gamma.x - 2.Cu = 110.X-2000$ psf

$P_p = \gamma.x + 2.Cu = 110.X+2000$ psf

$P_a = 110.X-2000 = 0 \Rightarrow h_c = x = 18.18$ ft (Depth of tension crack)

Therefore, the actual active pressure starts from a depth of 18.18′ because the soil is not assumed to have any tensile strength.

Pa (at the original ground surface) = $(30 - 18.18)110 \approx 1300$ psf

P_p (at the bottom of the wall) = $(30 + D')110 + 2(1000)$ psf

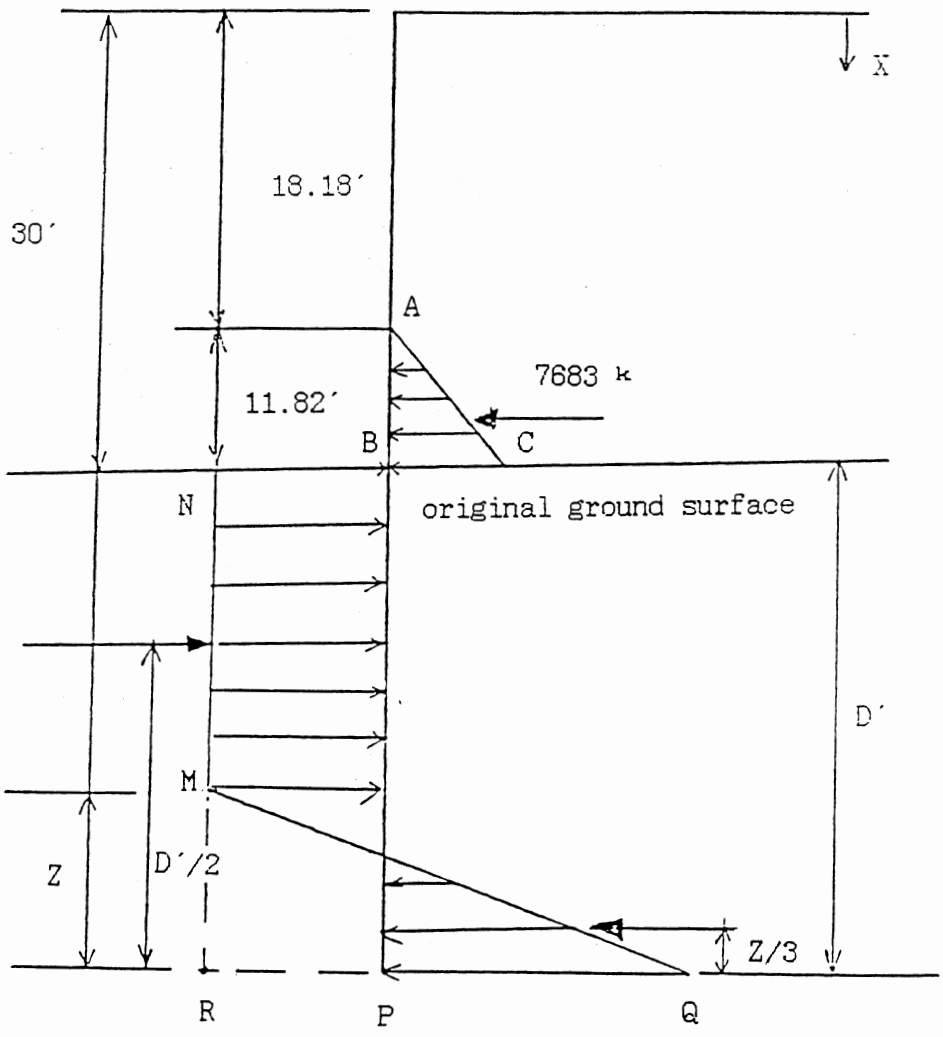

Figure 102. Pressure distribution from the classical theory.

On the Left Side:

P_p (at the original ground surface) = Pv + 2.Cu = 2000 psf

P_a (at bottom of wall) = Pv-2.Cu = 110.D′-2000 psf

Net Active = 110.X-2000-(110.Y+2000) = 110(X-Y)-4000 psf

At the original ground surface:

Net active = 110(30)-4000 = -700 psf

Net passive = 110(30+Y) + 2000-[110(Y)-2000] psf

At the bottom of the wall:

Net passive = 110(30)+4000 = 7700 psf

TABLE VI

NET FORCE AND BENDING MOMENTS
FROM CLASSICAL METHOD

Pressure Area	Net Resultant (lb)	Moment Arm (about bottom) (ft)	Moment (lb-ft)
ABC	7683	3.94 + D′	30271 + 7683 D′
BNRP	-700 D′	D′/2	-350 D'^2
QMR	4200 Z	Z/3	1400 Z^2

$\Sigma F = 0$ 7683-700.D′+1400.Z = 0 ==> Z = (700.D′-7683)/4200

$\Sigma Mt = 0$ 30271+7683.D′-350.D'^2+1400.Z^2 = 0

By trial and error, D′= 26.3 ft and Z = 2.55 ft

The maximum moment = 72.43 K-ft at 10.97 ft below the original ground surface .

APPENDIX B

CORRELATION BETWEEN THE F-MODEL AND THE HYPERBOLIC MODEL

The hyperbolic model is based on isotropic consolidation ($\sigma_1 = \sigma_2 = \sigma_3$), whereas the f-model is based on geostatic consolidation ($\sigma_2 = \sigma_3 = K_o.\sigma_1$).

Hyperbolic Model

$$E_i = KPa(\sigma_3/Pa)^n \qquad (B.1)$$

$$E_t = [1-R_f(\sigma_1-\sigma_3)/(\sigma_1-\sigma_3)_f]^2.E_i \qquad (B.2)$$

$$(\sigma_1-\sigma_3)_f=(2Cu.\cos(\phi)+2.\sigma_3.\sin(\phi))/(1-\sin(\phi)) \qquad (B.3)$$

f-Model

$$M_o = m.Pa(\sigma_1/Pa)^n \qquad (B.4)$$

$$G = G_o(1-f/1-f_o) \qquad (B.5)$$

$$G_o = M_o(1-K_o/2) \qquad (B.6)$$

$$G_i=G_o/(1-f_o) \qquad (B.7)$$

$$f_o = (1-K_o)/2\tan(\phi).\sqrt{K_o} \qquad (B.8)$$

$$f = \tan(\theta)/\tan(\phi) \qquad (B.9)$$

Under plane-strain conditions,

$$v_o = K_o/(1+K_o) \qquad (B.10)$$

f_o is the degree of mobilization at K_o conditions. G_o is the shear modulus at K_o conditions. M_o is the constrained modulus at K_o conditions.

For the $\phi = 0$ case, a simple correlation can be obtained as follows: Because $v = 1/2$, the volumetric strain equals 0.

$$dv/v = 0 \Rightarrow \epsilon_1+\epsilon_2+\epsilon_3 = 0$$

$$\epsilon_3 = -\epsilon_1/2$$

Referring to Fig. 103,

$$\gamma max/2 = (\epsilon_1-\epsilon_3)/2$$

And,

$$\gamma max = (\epsilon_1+\epsilon_1/2) = 3.\epsilon_1/2 \qquad (B.11)$$

At failure,

$$\tau max = (\sigma_1 - \sigma_3)/2 = Cu$$

$$G_t = d\tau max/d\gamma max = 2d\tau max/3d\epsilon \qquad (B.12)$$

Hence,

$$d\epsilon = 2.d\tau max/3.G_t$$

From the f-model,

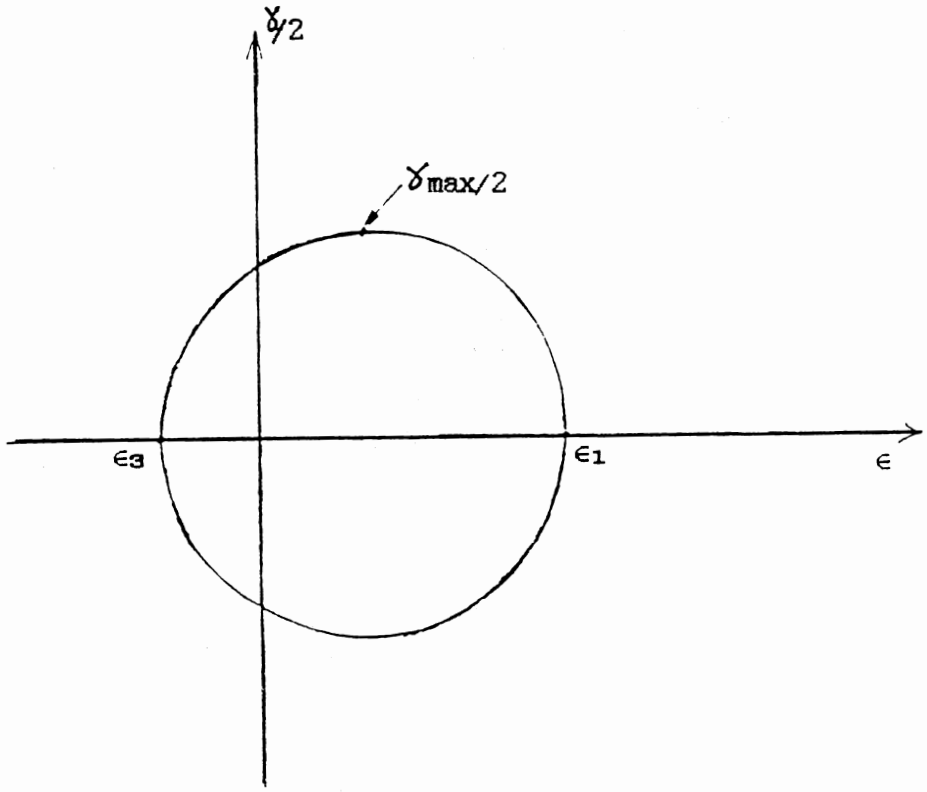

Figure 103. Mohr's strain circle.

$$G_t = G_1(1-f)$$

Therefore,

$$d\epsilon = 2d\tau max/3G_1(1-f) \qquad (B.13)$$

$$d\epsilon = 2Cu(df)/3G_1.(1-f) \qquad (B.14)$$

$$\int_0^{\epsilon} d\epsilon = 2Cu/3G_1 \int_0^{f} df/(1-f) \qquad (B.15)$$

$$\epsilon = (-2.Cu/3G_1).\ln(1-f) \qquad (B.16)$$

$$E_1 = 2.G_1(1+v_1)$$

$$\Longrightarrow G_1 = E_1/3$$

Therefore,

$$\epsilon = -2.Cu.\ln(1-\tau max/Cu)/E_1 \qquad (B.17)$$

At f=0.5,

$$\epsilon_{50} = -2Cu.\ln(1/2)/E_1 = 2Cu.\ln(2)/E_1 \qquad (B.18)$$

Also,

$$\epsilon_{50} = (\sigma_1 - \sigma_3)/2 = Cu/E_{50}$$

Therefore,

$$\epsilon_{50} = Cu/E_{50}=1/m \qquad (B.19)$$

Substituting into equation (B.18),

$$2Cu.\ln(2)/E_1 = Cu/E_{50}$$

$$E_1/E_{50} = 2\ln(2) = 1.386 \qquad (B.20)$$

Also, from (B.19),

$$2Cu.\ln(2)/E_1 = 1/m$$

$$E_1/m = 2Cu.\ln(2) \qquad (B.21)$$

For $\phi = 0$, $n = 0$, substituting into Eq. B.1,

$$K = 2.\ln(2).Cu.m/Pa \qquad (B.22)$$

VITA

MICHEL IBRAHIM NAJJAR

Candidate for the Degree of

Doctor of Philosophy

Thesis: ANALYSIS OF THE NONLINEAR BEHAVIOR OF CANTILEVER SHEETPILE RETAINING WALLS IN SATURATED CLAY

Major Field: Civil Engineering

Biographical:

Personal Data: Born in Beirut, Lebanon, December 17, 1958, the son of Mr. and Mrs. Ibrahim N. Najjar.

Education: Graduated from Bishmizzine High School, Bishmizzine Lebanon in June 1976; studied at the American University of Beirut, Beirut, Lebanon between 1976-1978; received the Bachelor of Science degree in Civil Engineering from Oklahoma State University in 1979; received the Master of Science degree in Civil Engineering from Oklahoma State University in December 1980; completed the requirements for the Doctor of Philosophy degree in Civil Engineering at Oklahoma State University in May, 1989.

Professional Experience: Structural Engineer, Civil Construction Establishment, Riyadh, Saudi Arabia, February 1981 to December 1983; Teaching Assistant, Department of Civil Engineering at Oklahoma State University, Fall 1980, and September 1983 to December 1985.

Professional Organizations: Civil Engineering Honor Society (Chi Epsilon), Phi Kappa Phi and National Dean's Honor Roll.